01 Jan 1970

Influence of ductility on the structural behavior of light-gage cold-formed steel members

A. K. Dhalla

George Winter

S. J. Errera

Dhalla, A. K., Errera, S. J., Winter, G. INFLUENCE OF DUCTILITY ON THE STRUCTURAL BEHAVIOR OF LIGHT-GAGE COLD-FORMED STEEL MEMBERS

CCFSS LIBRARY
22 1 * 176
1970

Dhalla, A. K., Errera, S. J., Winter, G. INFLUENCE OF DUCTILITY ON THE STRUCTURAL BEHAVIOR OF LIGHT-GAGE COLD-FORMED STEEL MEMBERS

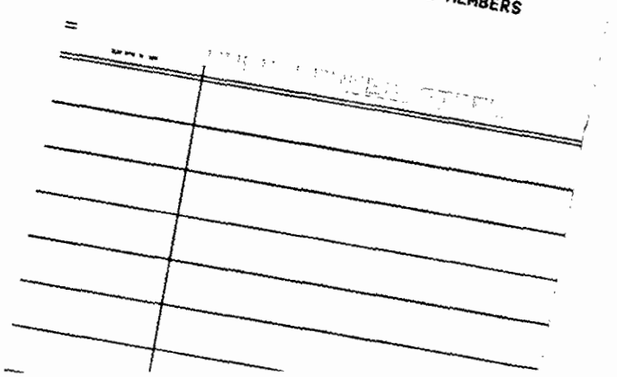

DEPARTMENT OF STRUCTURAL ENGINEERING

SCHOOL OF CIVIL ENGINEERING

CORNELL UNIVERSITY

INFLUENCE OF DUCTILITY ON THE STRUCTURAL BEHAVIOR OF LIGHT-GAGE COLD-FORMED STEEL MEMBERS

THIRD PROGRESS REPORT

by

A. K. Dhalla

S. J. Errera and G. Winter

Project Directors

A Research Project Sponsored by

The American Iron and Steel Institute

Ithaca, New York January 1970

TABLE OF CONTENTS

1. ABSTRACT

Ductility parameters defined in the second progress report were previously obtained by conducting tension coupon tests on specially produced A and S steels. In this report, tension coupon test results are presented for a 20 gage commercial low ductility steel, i.e. an ASTM Grade E steel, herein designated as steel B. Its behavior is compared with that of the specially rolled A and S steels to test the validity of conclusions arrived at in the second progress report. Test programs were set up to study the behavior of B steel under static tension loading, one program for single bolted connections and another for rectangular plates with holes. Here again the behavior of B steel is compared with A and S steels. A few connection tests were conducted on fully annealed A steel specimens to compare their behavior with low ductility A steel specimens.

In Appendix B the processing and metallurgical history for A, B and S steels is given.

2. MATERIAL PROPERTIES

2.1 Introduction

In order to determine the "suitability of steel"[1]* for cold formed construction one needs to know, in addition to the mechanical properties and the metallurgical history, performance characteristics like ductility, formability and weldability of the material. Ductility is the ability of a material to undergo large plastic deformations without fracture. The parameters necessary to define the ductility of steel under essentially static loading, were reported in the second progress report.[2] These parameters (percent elongation, percent reduction in area and tensile-yield ratio) were obtained from a standard tension coupon test wherein the coupons were prepared as per ASTM-E8-65T specifications.

There are two basic aims in conducting coupon tests on a material.

(a) To compare and distinguish various deformation and strength characteristics of different steels in a satisfactory manner. For this purpose material property investigations were made on a commercial low ductility high strength steel, i.e. an ASTM A 446 Grade E steel, herein designated as B steel.

(b) To correlate the results of coupon tests with structural behavior, such as in connections or in rectangular plates with stress raisers in them. (This area will be explored later in the report--Sections 3 and 4).

2.2 Coupon Test Procedure and Results

In the first[3] and second[2] progress reports, results of tension coupon tests on specially produced (A and S) steel

---

* S

were reported. In this report the results of six longitudinal and three transverse coupon tests on 20 gage B steel are reported. Load was applied parallel to rolling direction for longitudinal specimens and perpendicular to rolling direction for transverse specimens. The main purpose of material testing of commercial B steel was to test the conclusions arrived at in the second progress report. The testing procedure was the same as that described in the second progress report. In B steel fracture occurred after some necking at the weakest cross-section. It showed an inclined shear type of failure at the fractured cross-section, the same as was observed in the case of A and S steel.

In this report major emphasis will be placed on longitudinal specimens because of their practical importance, and conclusions arrived therein can then be easily applied to transverse specimens. If there is a significant difference in the behavior of transverse specimens as compared to the longitudinal ones, they too will be discussed.

The mechanical properties of B steel, such as 0.2% offset yield strength, tensile strength, percent elongation (after fracture) in 2 inch gage length, and percent reduction of area and thickness, are reported in Table 1. Ultimate tensile strength (σ_t) of longitudinal B steel is 82 ksi compared with 79 ksi for 12S (12 gage S steel), 72 ksi for 1205 (12 gage 5% elongation A steel), and 89 ksi for 1605 (16 gage 5% elongation A steel). Figure 1 shows the complete stress-strain curves for A, S and B steels (1205-L3, 1605-L2, 12S-L2, 20B-L5

and 20B-T2). The stress-strain plots of 16O5-L2, 1205-L3 and 12S-L2 are reproduced from Figures 1 and 2 of Reference 2. It can be observed in Figure 1 that the longitudinal B steel specimen was able to strain harden, while A and S steel do not show strain hardenability. From the same figure it can be seen that the transverse B steel specimen (20B-T2) has ultimate tensile strength of 99.0 ksi which is 20 percent higher, and shows an elongation in a 2 inch gage length of 1.54 percent which is 68% lower than that for longitudinal B steel specimen. Also B steel in the transverse direction does not show any strain hardening capacity.

Table 2 indicates percent elongation in different gage lengths as obtained from coupon tests of B steel. Typical longitudinal permanent strain distribution for B steel specimens is shown in Table 3. The longitudinal distribution of strain after fracture for typical A, B and S steel specimens is plotted in Fig. 2(b). Numerical values for A and S steel used in plotting strain distribution are taken from Table 4 of Reference 2. Since longitudinal B steel was able to work harden in the plastic range, a uniform strain of about 2.7% is observed along the length of the coupon except at the section where fracture took place. In contrast low ductility A and S, and transverse B steel showed a uniform strain of only 0.2 to 1.0 percent (for A and S steel, refer to Table 4 of Reference 2).

During the investigation of A and S steel it was observed that though the elongation in a 2 inch gage length was 5 to 8

percent, the elongation in a 1/4 inch gage length was 30 to 45 percent. Hence the measure of ductility was separated into two parts, one designated as local ductility and the other as overall ductility. The total percentage strain is given by the following equations[2].

$$e = K'L^{\alpha} \tag{1}$$

and

$$e = K\left(\frac{L}{A}\right)^{\alpha} \tag{2}$$

where e = Percent elongation in gage length L

A = Cross-sectional area of the coupon

K, K' and α are constants.

The advantage of the relationship represented in Equation 2 is that the constants K and α are independent of the size and shape of the specimen used. The numerical value of α is a measure of overall ductility of the material, while K (or K') is a measure of local ductility. K, K' and α can be obtained by plotting the test values of e, L and A as indicated in Eqs. (1) and (2) on a log-log scale. Figures 3 and 4 show the log-log plot for A, S and B steel. Numerical values of constants K, K' and α are presented in Table 4.

2.3 Discussion of Results of Longitudinal B, A and S Steel

Two characteristic features of longitudinal B steel in contrast with A or S steel that can be observed from complete stress strain curves shown in Fig. 1 are as follows:

(1) After yielding has occurred, A or S steel does not show any strain hardening capacity, while B steel does show some amount of strain hardening.

(2) For B steel the major portion (73%) of the total strain (percent elongation in 2 inch G.L.) is incurred before necking of the coupon. On the other hand corresponding strains incurred by 12S-L2, 1205-L3 and 1605-L2 before necking are 10%, 12% and 22%, respectively of the total strain. This behavior shown in Figure 1 indicates that B steel has less local ductility but more overall ductility than A or S steel.

Ductility parameters obtained for all three steels from a standard tension coupon test are presented in Table 5. It was mentioned in Reference 2 that the percent reduction in area, percent elongation in 1/4 inch gage length including fractured section, and K are the indicators of local ductility of the material, (i.e. the higher the local ductility the larger the algebraic values of the above quantities). On the other hand, tensile to yield ratio, percent elongation in 2 1/2 inch gage length excluding neck, and α are the indicators of overall ductility of the material (i.e. the higher the overall ductility, the larger the algebraic value of the above quantities). In discussing the complete stress-strain curves of A, B and S steel it was pointed out above that B steel has less local ductility but more overall ductility than A or S steel. We can arrive at the same conclusion by observing the algebraic values in Table 5. Comparing the average of six coupon values of 20 gage B steel with 12S-L3 the following observations can be made:

(3) For B steel, the indicators of local ductility, i.e.

the value of constant K, percent elongation in 1/4 inch and percent reduction in area viz. 20.5, 15.5, 56.1, respectively, are less than those for S steel viz. 45.0, 38.4, 65.2, respectively.

(4) On the other hand, the indicators of overall ductility, i.e. the algebraic value of α, percent elongation in 2 1/2 inch, and tensile to yield ratio viz. -0.58, 2.7, 1.08, respectively, are greater than those for S steel viz. -0.97, 0.3, 1.01, respectively.

Thus it can be seen that the ductility parameters mentioned in Table 5 are helpful to visualize the behavior of the material. The tensile to yield ratio along with percent reduction in area, qualitatively indicate the ductility of the material. This view is reinforced by the quantitative values of elongation in 1/4 inch and 2 1/2 inch gage lengths.

Sufficient local ductility in a material would wipe out the effect of stress concentration, while strain hardenability would distribute yielding to areas other than where yielding initiated (discussed in Section 3).

2.4 Conclusions

1. Ductility of a commercial low ductility steel (designated as B steel) can be characterized by the same parameters defined in the second progress report.

2. Comparison of B steel can be made with specially produced steel (designated as A and S steel) as shown in Table 5. Table 5 as well as Fig. 1 shows that longitudinal B steel has more overall ductility but less local ductility than A or S steel.

3. B steel in the transverse direction has 20 percent higher ultimate tensile strength and 68 percent lower elongation in 2 inch gage length, than in the longitudinal direction.

4. Stress strain curves drawn in Figure 1 indicate that in the longitudinal direction B steel has some strain hardening capacity while A and S steels, and B steel in the transverse direction do not. This fact is indicated by the tensile-yield ratios in Table 5, wherein the longitudinal direction B steel has a ratio equal to 1.08, while that for low ductility A and S steel is 1.00 and 1.01 respectively, and for B steel is transversely 1.00.

(5) Sufficient local ductility in a material will wipe out the effect of stress concentration, while strain hardenability will distribute yielding to areas other than where yielding initiated.

3. TENSION TESTS ON RECTANGULAR PLATES WITH HOLES

3.1 Introduction

The strength of a high ductility steel tension member under static load is not affected by the presence of stress raisers. For a rectangular plate with a central hole, the ultimate load is given by the equation:

$$P_{ult} = \sigma_t \ A_{net} \qquad (3)$$

where σ_t = Ultimate tensile strength of material

A_{net} = Net cross-sectional area of the member

But in the case of a brittle material Equation 3 is not valid.

As soon as σ_t is reached at the point of stress concentration, a crack forms which immediately propagates to the boundary. Hence one has to take into account the effect of a stress raiser in designing a brittle tension member. Fracture without much deformation is the failure mode of a tension member made of brittle material, while the failure of a high ductility steel tension member is generally due to excessive deformations. Performance of a limited or low ductility material (5 to 10% elongation in 2 inch G.L.) can be expected to lie between that of high ductility and brittle material behavior. The strength of limited ductility material may be as given by Equation 3, while the ability of the material to withstand extra stretching may be diminished considerably.

The results of tension tests conducted on low ductility S steel rectangular plates with a central hole were reported in the first progress report.[3] Therein it was observed that under static loading the ultimate load reached was given by Equation 3, but the ability of the entire member to elongate was diminished considerably as compared with high ductility steel. This report presents results of tension tests conducted on low ductility A and B steel plates with one, two or three holes in patterns as indicated in Table 6.

3.2 Purpose of Investigation

As an extension to the testing program presented in Reference 3 more than one hole in the longitudinal direction was drilled in the rectangular plates to study the following points.

(1) Longitudinal plastic strain distribution, after fracture.

(2) Comparison of local ductility of tension member with that obtained from the standard tension coupon test.

(3) Effects that overall ductility has on the deformation characteristics of a tension member.

(4) Indication of the increase in total member deformation by the introduction of extra holes in the longitudinal direction.

For a tension member with more than one hole in line of stress, one can expect yielding to be distributed around all the holes[4] if the material possesses overall ductility, i.e. the ability to work harden in the plastic range. Since B steel has more overall ductility but less local ductility than A steel, different elongation behavior for the members fabricated from these two different steels (A and B) can be expected.

3.3 Test Procedure and Results

Tension tests on rectangular plates were carried out on a Baldwin Southwark hydraulic testing machine. The specimens were scribed at 1/4 inch and 1/8 inch intervals as shown in Figs. 5a and 5b. The interval between the scribed lines at the hole is denoted by prefix H, and its approximate length is 1/8 inch. The interval between the scribed lines where there was no hole is denoted by prefix P, and its approximate length is 1/4 inch. These lines were read before and after the test under a travelling microscope (least count .0001 inch) along two longitudinal lines on each side of the hole. The difference between the reading taken before and after the test gave the longitudinal permanent strain in the specimen.

The nominal dimensions of the specimen along with the mechanical properties of the material are given in Table 6. Material property variables considered were (1) percent elongation in 1/4 inch G.L. including fractured portion, (2) percent elongation in 2 1/2 inch G.L. excluding fracture, (3) tensile and yield strength. Geometry of the cross-section was varied by using different thicknesses and $\frac{d}{s}$ ratios, where d is the diameter of the hole and s is the width of the specimen. In Table 6 specimens designated 1210-T-L1 to 1205-T-L5 and 12FA-T-L11 and -L12 were fabricated from A steel, while specimens 20B-T-L6 to 20B-T-L10 and 20B-T-T13 and T14 were fabricated from B steel. Ratio $\frac{d}{s}$ ranges from .044 to .263.

Results of the tension tests are reported in Table 7. Observing the ratio of tensile strength of the plate at ultimate load (σ_{tt}) to the tensile strength of coupon (σ_t) (Table 7--Column 9), it can be seen that all low ductility steel specimens were able to develop P_{ult} as given by Equation 3 except transverse B steel specimens, where failure load was about 6% lower than predicted value. Total deformation of the specimen as reported in Column 8 of Table 7 was measured (after fracture) in a gage length which was taken as the center to center distance between holes in longitudinal direction plus one inch.

Figure 5c shows the distribution of longitudinal permanent strain (after fracture) for specimens 1210-T-L2 (12 gage 10% A steel), 1205-T-L4 (12 gage 5% A steel), and 20B-T-L8 (20 gage B steel). Geometrical dimensions of these specimens

are the same, but the material has different local and overall ductility. Similar strain distribution curves for geometrically similar specimens 1210-T-L3, 1205-T-L5 and 20B-T-L9 are plotted in Fig. 5d. Appendix Tables A1 and A2 give the numerical values from which the distribution curves shown in Figs. 5c and 5d are plotted. Fractured A and B steel specimens are shown in Figures 6a and 6b respectively.

3.4 Observations on Longitudinal A, B and S Steel Specimens

(1) Strength of low ductility tension members fabricated from A and B steels with one or more holes in line of applied stress is given by Eq. 3; i.e. the ratio of net tensile strength, of plate with holes, at ultimate load (σ_{tt}) to the tensile strength of coupon (σ_t) is about 1.0 as shown in Table 7.

(2) For a plate with three holes in line of applied stress, initial yielding occurs at the weakest cross-section. If the material has even modest work hardening capacity (e.g. B steel) then yielding will also occur at some other hole and this process will continue until material around all the holes starts yielding. Thus for a material with noticeable overall ductility (say 2 to 5% elongation in 2 1/2 inch gage length, excluding the necked portion, as obtained from a tension coupon test) yielding will be distributed to other areas of stress concentration. Longitudinal stress distribution curves plotted in Figs. 5c and 5d are indicative of the above mentioned observation; e.g. for the specimens 1210-T-L2, 1210-T-L3, 20B-T-L8, and 20B-T-L9 the average longitudinal

zero. Here the crack, which one sees being formed at the hole, slowly propagates to the boundary and separation occurs when the load reaches zero (i.e. when complete unloading takes place). For low ductility longitudinal specimens, one does not see the crack being formed, but one can observe the necking of the weakest cross-section taking place after which the load drops rapidly, and fracture takes place around 0.6 P_{ult} (for A steel), and 0.8 P_{ult} (for longitudinal B steel). It is noted that the speed of testing was the same for all tension specimens.

(2) In transverse specimens of B steel, plastification or the necking of weakest cross-section before failure was not observed. This seems to indicate that the complete cross-section may not have plastified due to the lower local ductility of transverse B steel specimens.

(3) For all <u>longitudinal</u> low ductility specimens (plate with holes), inclined shear type of fracture was observed and the angle of failure was the same as that of the coupon. But in the transverse B steel specimens a transverse brittle type of failure was initiated near the point of stress concentration and as the fracture progressed towards the edge it became an inclined shear type of fracture. This means that due to the constraint against plastic flow, a brittle type of fracture was initiated at the stress concentration. As the crack propagated and when the plastic region was no longer constrained the crack inclined, hence at the edges an inclined shear type of fracture occurred. This observation and the one made in

the last paragraph seem to confirm that the behavior of B steel in the transverse direction approaches that of a semi-brittle material.

3.6 Conclusions

1. For longitudinal B and A steel under monotonically increasing static loading, it is possible to develop the full tension strength of a rectangular plate with a hole (stress raiser). That is, the ductility is sufficient to eliminate stress concentration by plastic redistribution.

2. For A, S, and B steel the local ductility parameter, i.e. percent elongation in 1/4 inch from coupon tests correlates satisfactorily with the local ductility of rectangular plates with holes.

3. Transverse B steel specimens have a tendency towards a brittle type of fracture.

4. In the specimens with three holes in line of stress, the yielding process starts at one of the holes (weakest cross-section). If the material shows even slight strain hardening capability (e.g. Steel B) then yielding will also occur at other holes. The ability to distribute yielding to other areas of stress concentration is characterized by the overall ductility of the material.

4. Increasing the number of holes in the longitudinal direction increases the total member deformation (or "member ductility") without sacrifice of strength. If two materials have the same local ductility but different overall ductility, then the material which possesses greater overall ductility

will show greater member ductility with the increase in number of holes drilled (in line of applied stress).

4. SINGLE BOLTED CONNECTIONS

4.1 Test Program

Tests on single bolted connections were conducted in order to gain information on the following points:

(1) Performance and behavior of commercial low ductility B steel.

(2) Interaction of tensile and bearing strength in a bolted connection.

(3) Effect of thickness on the bearing strength of the connected material.

(4) Behavior of low ductility A steel as compared with that of full annealed A steel.

Connection tests presented in this report are divided into three groups:

Group D - Specimens fabricated from B steel

Group E - Specimens fabricated from low ductility A and S steel

Group F - Specimens fabricated from full annealed A steel

Variables considered in the program in addition to the type of steel used were: edge distance e, bolt diameter d, sheet thickness t, plate width s, and coupon tensile strength σ_t.

Connection failures are divided into three main types:[5]

(i) Longitudinal shearing of plate along two practically parallel planes whose distance is equal to bolt diameter.

(ii) Bearing failure with considerable elongation of the hole and material "piling up" in front of bolt.

(iii) Transverse tension-tearing across the plate.

4.2 Test Procedure and Results

All connections were tested in tension on a Baldwin Southwark hydraulic testing machine of 400,000 lb. capacity. Nominal dimensions of Groups D, E, and F connection specimens are presented in Tables 8, 9 and 10 respectively. All holes over 3/16 inch in diameter were drilled 1/16 inch larger than the diameter of the bolt used. Completely threaded bolts were finger tightened with washers under head and nut. A few selected plates were scribed at 1/4 inch intervals, and were measured before and after the test under a travelling microscope, in order to obtain some information on the longitudinal permanent strain in the specimen after failure. Sketches of a connection and the lines scribed on one of the plates are shown in Fig. 7a and 7b respectively. All tests were conducted using an autographic recorder, wherein the gage distance used was equal to (2e + 1) inches. A few of these load deformation curves are presented in Figs. 8(a) to 8(c).

Results of the connection tests in groups D, E and F are reported in Tables 11, 12 and 13 respectively. In the first progress report, shear, bearing and tension type of failure of low ductility S steel were represented by the following equations:

$$P_{shear} = P_{sh} = 0.9\ e\ \sigma_t\ t \qquad (4)$$

$$P_{bearing} = P_b = 3.0\ \sigma_t\ d\ t \tag{5}$$

$$P_{tension} = P_t = (0.1 + 3\ \frac{d}{s})\sigma_t(A_{net}) \leq \sigma_t A_{net} \tag{6}$$

where A_{net} = net cross-sectional area of the plate through center of the hole.

σ_t = tensile strength of the material as obtained from the coupon test.

The remainder of the quantities used in the above equations were described earlier and are shown in Fig. 7a.

The predicted failure load for a connection fabricated from low ductility steel is the minimum of that given by Equations 4, 5 and 6. Equation 4 indicates that the shear strength of the connection increases in direct proportion with the increase in edge distance e. But there is an upper limit to this value of e at which bearing failure begins to govern the failure load. The upper limit of the e/d ratio is obtained by equating the right hand sides of Equations 4 and 5; i.e. equating P_b and P_s one finds;

$$(\frac{e}{d})_{max} = 3.33 \tag{7}$$

For e/d values greater than 3.33, failure would be governed by bearing rather than by shear. Equations 4 and 5 can be combined, to give failure load for predominantly bearing or combined bearing and shear failure as

$$P_c = 0.9\ e\ t\ \sigma_t \leq 3.0\ d\ t\ \sigma_t \tag{7a}$$

where P_c = failure load when predominantly bearing or

combination failure occurs.

A lower limit of the d/s ratio can be established below which the failure is by bearing and above which it is by tearing of the net cross-section. Equating Equations 5 and 6, we get;

$$\frac{P_b}{A_{net}} = \frac{P_t}{A_{net}} \tag{8}$$

or

$$\frac{3.0\ \sigma_t\ d\ t}{(s-d)\ t} = [0.1 + 3\ \frac{d}{s}]\ \sigma_t \tag{8a}$$

From Equation 8a we obtain;

$$(\frac{d}{s})_{min} = \frac{1}{6} = 0.167 \tag{9}$$

Below this limiting value of (d/s) bearing failure should occur before the tension failure load is reached.

As indicated by Equations 4 and 5, shear failure turns into a predominantly bearing failure when the e/d ratio is greater than 3.33. Therefore to put Equations 4 and 5 on the same graph, they are represented in a nondimensional form as;

$$\frac{\sigma_b}{\sigma_t} = 0.9\ (\frac{e}{d}) \leq 3.0 \tag{10}$$

In Fig. 9, the quantity $(\frac{\sigma_b}{\sigma_t})$ is plotted against e/d. The test values plotted therein indicate that $(\frac{\sigma_b}{\sigma_t})$ increases with increase in e/d value, according to Equation 10, until the limiting value of e/d is reached (Equation 7). After that, the scatter of test points (Fig. 9) increases somewhat and

the bearing failure load can be assumed not to increase further with the increasing e/d (Equation 5).

In Fig. 10 the ratio of net tensile stress at ultimate load (σ_{net}) to the tensile coupon strength σ_t, (i.e. σ_{net}/σ_t), is plotted against (d/s). Test points plotted in Fig. 10 give satisfactory agreement with Equation 6, except for the transverse test specimens fabricated from 20 gage B steel. Hence the tension failure load for longitudinal specimens of 20 gage B steel is adequately predicted by Equation 6 (compare σ_{net} and σ_{tt} in Table 11), but for transverse specimens this is not so. This lower strength of transverse B steel specimens, is due to lower local ductility (6% in 1/4 inch G.L.) than that for longitudinal ones (15% in 1/4 inch G.L.). That is, this lower transverse local ductility was not sufficient to wipe out stress concentration, hence transverse tearing of single bolted connection occurred in a brittle manner, i.e. fracture was horizontal instead of inclined shear type of fracture observed in other low ductility specimens.

The shear (τ_{sf}), bearing (σ_{bf}), and tensile (σ_{tt}), stresses can be calculated from the failure load observed in experiment, by the following equations;

$$\tau_{sf} = \frac{P_{fail}}{2\ e\ t} \tag{11a}$$

$$\sigma_{bf} = \frac{P_{fail}}{d\ t} \tag{11b}$$

$$\sigma_{tt} = \frac{P_{fail}}{A_{net}} \tag{11c}$$

The maximum shear, bearing or tensile stresses that can be developed in a connection specimen which are predicted by

Equations 4, 5 and 6 are as follows:

$$(\tau_s)_{max} = \frac{P_{sh}}{2e\ t} = 0.45\ \sigma_t \tag{12}$$

$$(\sigma_b)_{max} = \frac{P_b}{d\ t} = 3.0\ \sigma_t \tag{13}$$

$$(\sigma_{net})_{max} = \frac{P_t}{A_{net}} = (0.1 + 3\ \frac{d}{s})\ \sigma_t \leq \sigma_t \tag{14}$$

4.3 Alternate Graphical Representation of Failure Load For Low Ductility Steel Specimens

A study of test results represented by Equation 5 in Fig. 9, indicates that when the e/d ratio is between 3 and 4 the scatter of data points for low ductility steel specimens is more than that reported for high ductility steel.[5] This may be due to two factors:

(1) The thinner sheets of these low ductility steels may have lower bearing strength than reported for thicker ones in the first progress report.[3]

(2) Predominantly bearing or a combination of bearing, shear and tension type of failure may depend not only upon the e/d ratio but also upon the d/s ratio.

(A) Dimensional Analysis

The variables which affect the carrying capacity of a single bolted connection (Fig. 7a) were selected for dimensional analysis. The prediction equation for ultimate load would have to include the following quantities:

No.	Quantity	Description	Dimensional Units
1	P_{ult}	Predicted ultimate load	F
2	σ_t	Tensile strength of material	FL^{-2}
3	σ_b	Bearing strength of material	FL^{-2}
4	τ_s	Shear strength of material	FL^{-2}
5	t	Thickness of material	L
6	s	Width of specimen	L
7	e	Edge distance	L
8	d	Diameter of the bolt	L

F and L are the units of force and length respectively. Number of π terms required = Number of variables - Fundamental Dimensional Units = (8-2) = 6.

π terms will be formed as follows (for further details refer to Chapter 3 of Reference 6).

$$\left(\frac{P_{ult}}{\sigma_t d^2}\right),\ \left(\frac{\sigma_b}{\sigma_t}\right),\ \left(\frac{\tau_s}{\sigma_t}\right),\ \left(\frac{s}{d}\right),\ \left(\frac{e}{d}\right),\ \left(\frac{t}{d}\right)$$

The prediction equation for P_{ult} is formed as follows:

$$\pi_1 = f(\pi_2, \pi_3, \pi_4, \pi_5, \pi_6)$$

i.e.

$$\frac{P_{ult}}{\sigma_t d^2} = f\left(\frac{\sigma_b}{\sigma_t}, \frac{\tau_s}{\sigma_t}, \frac{s}{d}, \frac{e}{d}, \frac{t}{d}\right)$$

If one assumes that $\sigma_b = K_1\sigma_t$ and $\tau_{sh} = K_2\sigma_t$ for a given material, where K_1 and K_2 are constants then

$$\frac{P_{ult}}{\sigma_t d^2} = f\left(\frac{s}{d}, \frac{e}{d}, \frac{t}{d}\right)$$

The prediction equation is given as:

$$\frac{P_{ult}}{(t\ d)}\ \frac{(t\ d)}{\sigma_t d^2} = \frac{\sigma_b}{\sigma_t}\ (\frac{t}{d}) = f(\frac{s}{d},\ \frac{e}{d},\ \frac{t}{d}) \qquad (15)$$

At this stage it is difficult to say whether the right hand side of the prediction Equation 15 will be a sum or a product of the three π terms e/d, s/d and t/d. This will be discussed in the next section.

(B) Discussion of the Prediction Equation

Case I. Shear Failure (Type (i)) $[\frac{e}{d} \leq 2.25]$

Shear failure as explained in Section 4.1 can be characterized by longitudinal shearing of the plate but with no significant elongation of the hole; i.e., the bolt will not pile up the material in front of it as would be the case in a bearing type of failure. It was observed during testing that shear type of failure generally occurred when the e/d ratio was less than 2.25, and the tensile strength of the plate (as calculated on net section) was such that tension failure would not occur. Since longitudinal shearing will depend only upon the edge distance, the s/d ratio does not take any part in predicting the ultimate load. Therefore, Equation 15 can be rewritten as

$$\frac{P_{sh}}{\sigma_t d^2} = \frac{\sigma_b}{\sigma_t}\ (\frac{t}{d}) = f(\frac{e}{d},\ \frac{t}{d}) \qquad (16)$$

Here it can be said that P_{ult} increases in direct proportion with the increase in thickness of the specimen hence Equation 16 reduces to

$$\frac{\sigma_b}{\sigma_t} = f(\frac{e}{d}) \tag{17}$$

In Figure 9, the quantity $(\frac{\sigma_b}{\sigma_t})$ is plotted against e/d. Test points plotted in Figure 9 indicate that shear failure is predicted by

$$\frac{\sigma_b}{\sigma_t} = 0.9\ (\frac{e}{d}) \tag{17a}$$

$$P_{sh} = 0.9\ e\ t\ \sigma_t \tag{17b}$$

It is noted that Equation 17a is the same as Equation 10, and Equation 17b is the same as Equation 4.

Case II. Bearing or Combination of bearing, shear and Tension Failure (Type (ii) or Type (ii)+(i) or Type (ii)+(iii) or Type (i)+(ii)+(iii) Failures).

Bearing failure as explained in Section 4.1 can be characterized by excessive hole elongation, which is due to the bolt ploughing through the material and piling up the material in front of it. When transverse tearing or longitudinal shearing of the plate occurs after significant hole elongation, this is designated as a combination failure. It is noted that the resistance to the bolt ploughing through the material is provided by the material surrounding the bolt hole. Variables shown in the right hand side of Equation 15 can be combined in some form to predict the ultimate load for bearing or a combination type of failure. This was attempted by a trial

and error approach, since the conventional approach (outlined in Chapter 3 of Reference 6) requires a greater volume of test data than that gathered in this and in the first progress report. The graph plot that seemed to give the best fit for all the data points is $(\frac{\sigma_b}{\sigma_t})$ $(\frac{t}{d})$ plotted against $(\frac{e}{d} + \frac{s}{d} + 1)\frac{t}{d}$, which is shown in Fig. 11. In Table 14, values of $(\frac{e}{d} + \frac{s}{d} + 1)\frac{t}{d}$ and $(\frac{\sigma_b}{\sigma_t})\frac{t}{d}$ are shown in Columns 7 and 9. In that table test results of S steels (from the first progress report) along with low ductility A and B steels are presented for increasing $(\frac{e}{d} + \frac{s}{d})$ ratios. The prediction equation can be written as:

$$\frac{P_{ult}}{\sigma_t d^2} = (\frac{\sigma_b}{\sigma_t})\frac{t}{d} = C_1(\frac{e}{d} + \frac{s}{d} + 1)\frac{t}{d} + C_2 \qquad (18)$$

where C_1 is the slope of the line and C_2 is the intercept on the ordinate.

Values of C_1 and C_2 can be obtained from Fig. 11 by using method of least squares, and the final form of Equation 18 is:

$$(\frac{\sigma_b}{\sigma_t}) = 0.318(\frac{e}{d} + \frac{s}{d} + 1) - 0.026(\frac{d}{t}) \qquad (19)$$

I.e. the ultimate load for combination failure is given by:

$$P_c = 0.318\ (\frac{e}{d} + \frac{s}{d} + 1)\ t\ d\ \sigma_t - 0.026\ d^2\ \sigma_t \qquad (19a)$$

It will be noted in the next paragraph that there are certain limitations on the values of e/d and s/d for Equations 19 and 19a to be physically valid, since increasing e/d or s/d ratios can not increase the failure load indefinitely.

The upper limit on the e/d ratio is assumed to be 3.33, the same as the limit shown in Equation 7, wherein it was in-

ferred that beyond $(\frac{e}{d})_{max} = 3.33$, the bearing load does not increase. The upper limit on $\frac{s}{d}$ is assumed to be 6.0 (or $\frac{d}{s} = .167$, Equation 9), since it was observed during tests that beyond this value of the $\frac{s}{d}$ ratio there is no significant increase in the failure load. If in a test specimen the e/d and/or s/d ratios exceed the limiting values, then numerical values of 3.33 and 6.00 are substituted in Equations 19a instead of actual e/d and/or s/d ratios respectively, to arrive at the failure load.

Case III. Tension Failure (Type (iii) $[\frac{s}{d} \leq 3.33]$

It was observed during testing that transverse tearing type of failure occurred when the $\frac{s}{d}$ ratio was generally less than 3.33 (i.e., $\frac{d}{s} \geq 0.3$) and the shear strength of the plate was such that a longitudinal shear type of failure would not occur. Since tensile strength of the plate would depend only on the s/d ratio but not the $\frac{e}{d}$ ratio, Equation 15 can be rewritten as:

$$\frac{P_t}{\sigma_t \, d^2} = f(\frac{s}{d}, \frac{t}{d}) \qquad (20a)$$

Since the tension failure load would depend on the net cross-sectional area, instead of width s, the net width of the plate will be used. Also, tensile load will be directly proportional to the net cross sectional area of the plate. Hence Equation 20a could be written as

$$\frac{P_t}{\sigma_t \, d^2} = \frac{(s-d)}{d} \frac{t}{d}$$

i.e.

$$P_t = \sigma_t A_{net} \qquad (20b)$$

The above equation is valid for $\frac{s}{d} \leq 3.33$ (i.e., $\frac{d}{s} \geq 0.3$). This fact can be observed in Figure 10 (plot for Equation 6), where it can be seen that $\frac{\sigma_{net}}{\sigma_t}$ is equal to 1.0 for $\frac{s}{d} \leq 3.33$.

Summarizing the above three cases it can be said that for a single bolted low-ductility steel connection:

(1) Longitudinal shearing of the plate without significant elongation of bolt hole, occurs when $e/d \leq 2.25$. In that case the shear load, P_{sh}, is calculated from Equation 17b. But P_{sh} should be checked to see that it is not greater than P_t (Equation 20b).

(2) Bearing or a combination type failure occurs when e/d is greater than 2.25 and s/d is greater than 3.33 (i.e. $\frac{d}{s} < 0.30$). The failure load is given by Equation 19a.

(3) Transverse tearing of the plate without significant elongation of bolt hole occurs when $s/d \leq 3.33$ (i.e., $\frac{d}{s} \geq 0.30$). In that case, P_t is calculated from Equation 20b. But P_t should be checked to see that it is not greater than P_{sh} (Equation 17b).

4.4 Combination Failure in Low Ductility Steel Specimens

The ultimate load that a single bolted connection can carry, when e/d and s/d ratios are such that combination failure would occur, is given by Equation 7a or 19a. Since more variables are included in Equation 19a, the formula for the prediction of failure is rather complicated, hence the

preference to use Equation 19a over Equation 7a will have to be justified. Comparing the graphs of Equation 19a in Fig. 11 with that of Equation 7a in Fig. 9, it is observed that there is less scatter of experimental values plotted in Fig. 11, than in Fig. 9. The amount of scatter can be quantified by calculating the sum of the squared differences, and comparing the values obtained for the two prediction equations (7a and 19a). The difference used herein is obtained by subtracting predicted bearing stress (as per Equation 7a or 19a) from the actual bearing stress obtained from the experiments. Table 16 compares the sum of the difference squares for the two prediction equations. Therein it can be observed that the sum of the squared differences for prediction Equation 7a is greater (hence more scatter of test points) than for Equation 19a. Also the number of tests that fall more than 20% below the predicted value of bearing stress is higher for prediction Equation 7a than for Equation 19a.

In column 4 of Table 16,(for combination of bearing shear and tension failure), the ratio of the square root of the sum of difference squares, as obtained for the two prediction equations, is given. This ratio (i.e. square root of sum of difference squares for 7a to that for 19a) is equal to 1.27 which indicates that the prediction of failure load by Equation 19a gives on the average 27% less error than that by Equation 7a. Similarly, the ratio, for combination of shear and bearing failure, is equal to 1.31, which indicates that Equation 19a predicts the combination of shear and bearing

failure with about 31% less error than Equation 7a.

4.5 Deformation Behavior of Low Ductility B and A Steel

(1) Observing results of connection specimens in Tables 11 (20 gage B steel) and 12 (16 and 12 gage A steel), at first glance it seems that for the same $\frac{e}{d}$ and $\frac{d}{s}$ ratios, B steel developed less bearing strength than A steel specimens. But this difference may not be due to different ductility characteristics of the two steels, but to their different thicknesses. This variation in thickness is taken into account by Equation 19, which predicts predominantly bearing or combination type of failure. Test points shown in non-dimensionalized plot (Fig. 11) indicate that predominantly bearing failure is satisfactorily predicted by Equation 19, for low ductility A, B and S steel.

(2) A major difference observed in low ductility steel bolted connections was in transverse tearing failure [Type (iii)]. Here two identical specimens made from 20 gage B steel will be discussed, a longitudinal specimen 20B-L1 and a transverse specimen 20B-T10. Transverse tearing failure in the longitudinal specimen occurred at the load predicted by Equation 20b. But the transverse specimen 20B-T10 failed at a load 27% lower than predicted by Equation 20b (Table 11 Columns 7 and 9). Also an inclined fracture in specimen 20B-L1 occurred after the load had fallen to about 55% of ultimate load, while a horizontal fracture (as would be observed in a brittle material) occurred in specimen 20B-T11 after the load had fallen to about 92% of ultimate load.

This lower load carrying capacity in tension is because the local ductility of 20 gage B steel, in the transverse direction, was not sufficient to wipe out the stress concentration at the bolt hole, hence failure occurred before the net cross-section fully plastified. The local ductility parameter, i.e. elongation in 1/4" G.L., given in Table 2, column 6, shows that B steel has local ductility of about 6% in the transverse direction while in the longitudinal direction it is 15%.

(3) The difference in deformation behavior of the two types of steel (B and A) is brought out in tension type of failure. B steel specimens showed less local ductility (elongation in 1/4" G.L.) than those of A steel. This is seen from the typical permanent longitudinal strains recorded in a few single bolted connections after fracture as shown in Appendix Table A3. It can be observed that for longitudinal B steel connections which failed by transverse tearing, the maximum percent elongation in 1/4 inch gage length is 11.5%. The percent elongation in 1/4 inch in longitudinal tension coupons of B steel was 15.5% (Table 8, Column 10). Similarly for A steel connection specimens which failed by transverse tearing the percent elongation in 1/4 inch is between 21 and 26%, while that obtained in the tension coupon was between 22.6% and 27.6% (Table 9, Column 10). Both A and longitudinal B steel specimens which failed in tension showed an inclined shear type of fracture. As mentioned in Sections 2 and 3, this shear fracture was also observed in tension coupons as

well as in rectangular plates with holes. But transverse B steel connection specimens which failed by transverse tearing of the plate showed a horizontal fracture, the type one would observe in brittle material, although an inclined shear type of fracture was observed in transverse tension coupons of B steel.

The following two observations apply to all low ductility steel specimens except the B steel transverse specimen which showed type (iii) failure.

(4) Deformation characteristics of the connection specimens is illustrated in Table 15. When the specimen fails by shearing or transverse tearing of the plate, with some hole elongation, the net increase in hole size is limited to 0.2 to 0.4 inches. When $\frac{e}{d}$ and $\frac{s}{d}$ ratios are large enough to cause bearing failure the net elongation of the hole was observed to be greater than 0.5 inches.

(5) From Figs. 8(a) and 8(c) it can be seen that for a specimen which fails in tension the load reaches its maximum value and drops rather quickly. (Fracture load, not shown in the Figures, ranged from 60 to 80% of P_{ult}.) However, in a specimen which showed bearing failure, or a combination of tension and bearing or shear and bearing failure, the load after reaching its maximum value drops slowly. (Fracture load, not shown in the Figure is around 20% of P_{ult}.) Here it can be noted that the speed of testing was the same in all connection tests.

Thus a bolted connection made of low ductility steel, where transverse tearing or longitudinal shearing of the plate

occurs after excessive hole elongation, herein called combination failure, shows a ductile behavior.

(6) Figures 12a to 12f show different failure modes for low ductility steel specimens.

4.6 Performance of Full Annealed A Steel

A total of ten tests on full annealed A steel were conducted to compare its behavior with low ductility A steel. Nominal dimensions of the 16 and 12 gage specimens are presented in Table 10 and their results in Table 13. Here too, the failures were divided into three types, as described in Section 4.1; they are: shear, bearing and tension types of failure. The strength of these specimens is predicted by the same equations as those presented by Winter[5] for his earlier tests on high ductility steels. The following equations are reproduced from Reference 5.

$$P_{shear} = P_{sh} = 1.40\, e\sigma_y t \qquad (22)$$

$$P_{bearing} = P_b = 4.9\, \sigma_y dt \qquad (23)$$

$$P_{tension} = P_t = (0.10 + 3.0\, \frac{d}{s})\, A_{net}\, \sigma_t \leq A_{net}\, \sigma_t \qquad (24)$$

where σ_y = 0.2% offset yield strength obtained from tensile coupon tests. Failure load is the minimum of the three loads (shear, bearing or tension) given in the above equations. The corresponding maximum stresses that can be developed in a connection can be obtained from Equations 22, 23 and 24 as follows:

$$(\tau_s)_{max} = \frac{P_{sh}}{2e\, t} = 0.70\sigma_y \qquad (22a)$$

$$(\sigma_b)_{max} = \frac{P_b}{d\,t} = 4.9\sigma_y \qquad (23a)$$

$$(\sigma_{net})_{max} = \frac{P_t}{A_{net}} = (0.1 + 3\,\frac{d}{s})\,\sigma_t \leq \sigma_t \qquad (24a)$$

Testing procedure and reporting of the results is the same as that described earlier for low ductility specimens. Graphical representation of Equations 22 and 23 is shown in Fig. 13 and that for Equation 24 is shown in Fig. 14. In Fig. 8(c) a few typical load deformation curves are shown which were plotted by an autographic recorder. Figures 15a to 15d show different failure modes for full annealed A steel specimens. Permanent longitudinal strain, measured under a travelling microscope before and after the test, is presented in appendix Table A4. A sketch of a scribed specimen is shown in Fig. 7b.

4.7 Differences in the Behavior of High and Low Ductility A Steel

(1) In Table 12 of the First Progress Report the difference in the predicted shear strength for bolted connections of high and low ductility steel was pointed out. This difference will be briefly discussed herein.

Shear stress at ultimate load for type (i) failure is given by 0.7 σ_y (Equation 22a) for high ductility steel. If tensile-yield ratio of 1.35 is assumed, this means that $(\tau_s)_{max}$ for high ductility specimen is given by 0.52 σ_t. For low ductility steel the corresponding $(\tau_s)_{max}$ is 0.45 σ_t (Equation 12). This shows that the shear strength of low ductility steel in terms of σ_t is lower than that for high ductility steel.

(2) In high as well as low ductility steel specimens, the bearing pressure of the bolt is resisted by material surrounding the bolt hole. Resistance of this bolt pressure can be thought of as a "strut" and "string" type of action. That is to say that the "strut" is the material in compression, in front of the bolt e inches long but no longer than e = 3.33d, the "string" is the material in tension between the hole and the longitudinal edges and s inches long. In the case of low ductility steel significant yielding of the material surrounding the bolt hole does not occur. Hence, the bolt pressure is resisted by strut and string action in some proportion (i.e., $\frac{e}{d}$ and $\frac{s}{d}$ ratios) indicated by Equation 19a for predominantly bearing type of failure. On the other hand in high ductility material where a substantial part of the material surrounding the hole starts yielding, the bolt pressure is resisted mainly by strut type of action, i.e. the $\frac{e}{d}$ ratio will be of primary importance. For this reason a predominantly bearing type of failure as given by Equation 23 (Figure 13) for high ductility steel, takes into account the $\frac{e}{d}$ ratio but not the $\frac{s}{d}$ ratio.

4.8 Conclusions

(1) For low ductility single bolted connections (A, B and S steel), failure occurs either by longitudinal shearing (type (i)), or by considerable "piling up" of the material in front of the bolt (type (ii) bearing), or by transverse tearing of the plate (type (iii)), or by any combination of the above three types. Type of failure depends on the geometric

dimensions and tensile strength of the material (bearing and shear strength of the material are assumed to depend on the tensile strength, as mentioned in the dimensional analysis).

(a) Failure by longitudinal shearing occurs at a nominal shearing stress of 0.45 times the tensile strength of the sheet (Equation 12). This is likely when the $\frac{e}{d}$ ratio is less than 2.25.

(b) Failure by transverse tearing occurs when the tensile stress on the net cross-section exceeds the ultimate tensile strength of the material. This type of failure occurs when the $\frac{s}{d}$ ratio is greater than 3.33 (Equation 20b).

Above conclusion is valid only when local ductility of the material is sufficient to wipe out the stress concentration due to a concentrated force applied at the bolt hole. Hence for very low ductility steel (transverse 20 gage B steel) Equation 20b does not apply, since a horizontal brittle type of fracture was observed in type (iii) failure. This implies that the local ductility was not sufficient to plastify net cross-section before fracture.

(c) Type (ii) bearing failure or a combination of type (ii) and (iii) or type (ii) and (i) occurs when the $\frac{e}{d}$ ratio is greater than 2.25 and the $\frac{s}{d}$ ratio is greater than 3.33. In this case the ultimate load that a connection can carry is given by Equation 19a as:

$$P_c = 0.318 \left(\frac{e}{d} + \frac{s}{d} + 1\right) t\, d\, \sigma_t - 0.026\, d^2 \sigma_t \qquad (19a)$$

If e/d, s/d ratios in a specimen are greater than 3.33 and 6.0

respectively, then the limiting value of 3.33 will be substituted for e/d and 6.0 for s/d in above equation, irrespective of actual e/d, s/d ratios.

As a less accurate but simpler approximation, bearing failure can be predicted to happen at a bearing stress equal to 3 σ_t. For simplicity, therefore, Eqs. 4, 5, 6 in Sec. 4.2 are adequate for design purposes, though Eq. 19a is significantly more precise within the indicated range of e/d and s/d ratios.

(2) In regard to comparison of commercial B vs. special A and S steels, the following can be said:

B steel connection specimen behavior in longitudinal shearing or predominantly bearing type of failure was not significantly different from A and S steel specimens. In longitudinal and transverse B as well as in A and S steel connections where tensile strength of the plate (as calculated on net cross-section) was greater than the bearing strength of the plate (Equation 19) the bolt ploughed right through the material, piling it up at the end of the plate. The only difference in the behavior of longitudinal B steel and low ductility A and S steel is brought out in transverse tearing (type (iii)) failure. Here longitudinal B steel specimens showed less local ductility than those of A or S steel, since B steel possesses less local ductility than A or S steel as mentioned in the section on material properties.

(3) Strength of <u>high ductility</u> single bolted connections is satisfactorily predicted by the same equations as those

given by Winter, for his earlier tests, in Reference 5. Test results reported herein are for finger tight bolts, while those in Reference 5 were for hand torqued bolts. These equations reproduced in this report are Equations 22, 23, and 24 which predict shear, bearing and tension failures respectively.

(4) Shear stress at ultimate load for type (i) failure is given by 0.52 σ_t for high ductility specimens while the corresponding value for low ductility specimens is 0.45 σ_t. This indicates that the shear strength of low ductility steel is a lower multiple of ultimate strength than that for high ductility steel.

5. SUMMARY

The Commercial low ductility steel tested, i.e. an ASTM Grade E steel, (herein designated as steel B), in the transverse direction has 20% higher ultimate strength but 68% lower elongation in a 2 inch gage length than in the longitudinal direction. Different shapes of stress strain curves of low ductility A, S, and B steel (Figure 1) show that B steel in the longitudinal direction has the ability to strain harden, while A and S steel and B steel in the transverse direction do not. This ability to strain harden distributes yielding to areas other than where initial yielding occurred.

Tension tests of plates with holes showed that the local ductility of A, S and longitudinal B steel was adequate to wipe out the effects of stress concentration and the full tensile strength (as obtained in coupon) could be developed across the net section. However, B steel specimens in the

transverse direction did not possess sufficient local ductility to wipe out stress concentration due to a hole in center of the plate. Hence these specimens failed at 93% of the predicted ultimate load. In specimens with three holes in line of stress, yielding starts at one of the holes (weakest cross-section); B steel in the longitudinal direction, which showed slight strain hardening capacity was able to distribute yielding to areas of stress concentration other than where yielding was initiated (Figure 5).

For low as well as high ductility single bolted connections failure occurs either by longitudinal shearing (type (i)) or transverse tearing (type (iii)) of the plate, or by considerable piling up of the material in front of the bolt (type (ii), bearing), or by any combination of the above three types. A significant difference in the behavior of high and low ductility steel bolted connection specimens is due to large in-plane deformations occurring in high ductility steel after initial yielding. Also the shear stresses which cause failure are lower multiples of ultimate strength for the low ductility than for the high ductility material. A low ductility B steel single bolted specimen (20B-T10) in the transverse direction, which failed in tension (type (iii)), failed at 72% of the predicted tension failure load. This lower load carrying capacity in tension is because the local ductility of 20 gage B steel, in the transverse direction, was not sufficient to wipe out the stress concentration at the bolt hole, hence failure occurred before the net cross-section fully plastified.

REFERENCES

1. Light Gage Cold-Formed Steel Design Manual, American Iron and Steel Institute, 1968 Edition.

2. Dhalla, A. K.; "Influence of Ductility on the Structural Behavior of Light-Gage Cold-Formed Steel Members", Second Progress Report, Cornell University, Ithaca, N.Y., Oct. 1968.

3. Dhalla, A. K. and Errera, S. J.; "Influence of Ductility on the Structural Behavior of Light-Gage Cold Formed Steel Members", First Progress Report, Cornell University, Ithaca, N.Y., Feb. 1968.

4. Van Den Broek, J. A.; "Effect of Connections and Rivet Holes on Ductility and Strength of Steel Angles". Civil Engineering, Feb. 1940, Vol. 10, No. 2.

5. Winter, G., "Tests on Bolted Connections in Light Gage Steel", Proc. ASCE, Vol. 82, Paper No. 920, March 1956.

6. Murphy, G., "Similitude in Engineering", The Ronald Press Company, N.Y., 1950.

7. Timoshenko, S., "Strength of Materials" Part II. D. Van Nostrand Company, Inc., Princeton, N.J., 1956.

TABLE I

MECHANICAL PROPERTIES OF 20 GAGE B-STEEL
OBTAINED FROM STANDARD TENSION COUPON TESTS

Spec. Designation †	Thickness (in)	0.2% Offset Yield Strength σ_y (ksi)	Tensile Strength σ_t (ksi)	Tensile-Yield Ratio σ_t/σ_y	Elongation in 2" Gage Length %	Reduction in Thickness %	Reduction in Area %	Angle of Failure Degrees
20B-L1	0.039	81.0	86.6	1.07	4.57	54.6	54.9	22
20B-L2	0.039	70.9	78.0	1.10	4.86	55.0	55.3	20
20B-L3	0.039	72.1	78.5	1.09	4.25	58.5	59.0	20
20B-L4	0.038	74.4	81.0	1.09	4.10	52.0	52.4	22
20B-L5	0.039	72.3	79.5	1.10	4.35	58.0	59.0	22
20B-L6	0.039	82.4	86.6	1.05	4.18	55.4	56.0	25
Average	0.039	75.5	81.7	1.08	4.38	55.8	56.1	22
20B-T1	0.039	100.1	100.2	1.00	1.00	37.8	36.2	36
20B-T2	0.039	98.2	99.0	1.01	1.54	39.4	37.7	32
20B-T3	0.039	100.0	100.2	1.00	1.48	34.8	26.5	32
Average	0.039	99.4	99.8	1.00	1.34	37.3	33.5	33

† 20B-L specimens were taken from virgin material in longitudinal direction (i.e., parallel to direction of rolling)

20B-T specimens were taken from virgin material in transverse direction

TABLE 2

MAXIMUM PERCENT ELONGATION IN DIFFERENT GAGE DISTANCES FOR STANDARD TENSION COUPON TEST SPECIMENS (B-STEEL)

Spec. Designation	Elongation						Reduction in Area
	2 1/2" G.L. %	2" G.L. %	1" G.L. %	1/2" G.L. %	1/4" G.L. %	2" (Excluding ½" of necked portion) %	%
20B-L1	4.05	4.57	7.01	11.70	17.50	2.55	54.9
20B-L2	4.54	4.86	7.00	11.40	19.70	2.92	55.3
20B-L3	3.87	4.25	6.10	9.85	14.30	2.69	59.0
20B-L4	3.87	4.10	5.30	8.27	13.80	2.71	52.4
20B-L5	3.97	4.35	6.09	9.31	15.10	2.69	59.0
20B-L6	3.90	4.18	5.74	8.66	12.92	2.86	56.0
Average	4.03	4.38	6.21	9.86	15.55	2.74	56.1
20B-T1	0.88	1.00	1.67	3.00	5.58	0.45	37.8
20B-T2	1.07	1.54	2.70	4.65	7.10	0.45	39.4
20B-T3	1.14	1.48	2.72	4.80	5.60	0.55	34.8
Average	1.03	1.34	2.36	4.15	6.09	0.48	37.3

TABLE 3

LONGITUDINAL PERMANENT STRAIN DISTRIBUTION AFTER FRACTURE* IN 2 1/2" G.L. OF STANDARD TENSION COUPON TEST. (20 GAGE B STEEL)

Section No. ±	Distance From First Gage Line (in.)	Strain = $\frac{\text{Original G.L.-Final G.L.}}{\text{Original G.L.}}$ x 100			
		20B-L1 %	20B-L2 %	20B-L4 %	20B-T2 %
1	0.25	2.02	3.50	13.80	0.20
2	0.50	17.50	19.70	2.38	0.40
3	0.75	5.72	2.93	2.09	2.20
4	1.00	2.35	2.14	2.51	4.65
5	1.25	2.44	2.84	2.71	0.80
6	1.50	2.17	2.52	2.96	0.80
7	1.75	2.02	2.65	2.72	0.40
8	2.00	2.38	2.99	3.13	0.00
9	2.25	2.06	3.98	3.76	0.60
10	2.50	1.86	2.55	2.13	0.20

NOTE: * Gage distance measured before and after test under a travelling microscope.

± See Fig. 2(a) for a sketch of standard tension coupon.

TABLE 4

VALUES OF THE CONSTANTS K', K AND α

Spec. Designation	K'	K	α
20B-L1	7.28	27.5	-0.687
20B-L2	7.43	24.0	-0.577
20B-L3	6.60	20.5	-0.601
20B-L4	5.85	15.5	-0.489
20B-L5	6.55	18.5	-0.566
20B-L6	6.20	17.0	-0.556
Average	6.65	20.5	-0.579
20B-T1	1.75	8.3	-0.854
20B-T2	2.70	13.5	-0.809
20B-T3	2.60	15.0	-0.840
Average	2.35	12.1	-0.834

TABLE 5

COMPARATIVE STUDY OF DUCTILITY CHARACTERISTICS OF A, B AND S STEELS

Ductility Parameter	20B-L-Av. Long. B-Steel	20B-T-Av. Trans. B-Steel	12S*-L3 S-Steel	1205*-L2 A-Steel	1605*-L3 A-Steel	16FA*-L1 A-Annealed Steel
Elongation in 2" (%)	4.38	1.34	5.13	5.58	6.84	52.20
Reduction in Area (%)	56.10	33.50	65.20	69.40	59.00	83.80
Tensile/Yield Ratio	1.08	1.00	1.01	1.00	1.00	1.48
Elongation in 1/4" (including neck) (%)	15.55	6.09	38.40	44.40	35.20	85.60
Elongation in 2 1/2" (excluding neck) (%)	2.74†	0.48	0.33	0.40	1.28	38.00
K	20.50	12.10	45.00	46.00	45.00	120.00
α	-0.579	-0.834	-0.974	-0.983	-0.795	-0.335

* The values reported in these columns are taken from Table 7 of second progress report.

† This value is for percent elongation in 2", excluding neck.

TABLE 6

NOMINAL DIMENSIONS OF RECTANGULAR PLATES WITH HOLES
(A, S AND B STEEL)

Spec. Designation	GEOMETRIC PROPERTIES OF SPECIMENS						AV. MATERIAL PROPERTIES			
	Dia. of Hole d (in)	No. of Holes Long.	No. of Holes Transverse	Width of Plate S (in)	Thickness of Plate t (in)	$\frac{d}{s}$	σ_y (ksi)	σ_t (ksi)	Elong.in 1/4" G.L. (including fractured portion) %	Elong.in 2 1/2" G.L. (excluding neck) %
1210-T-L1	1/2	-	Two	3.50	0.107	0.263	76.2	76.9	-	-
1210-T-L2	1/2	Three	-	4.25	0.107	0.118	71.6	74.6	49.0	1.9
1210-T-L3	3/16	Three	-	4.25	0.107	0.044	71.6	74.6	49.0	1.9
1205-T-L4	1/2	Three	-	4.25	0.107	0.118	72.2	72.2	47.1	0.4
1205-T-L5	3/16	Three	-	4.25	0.107	0.044	72.2	72.2	47.1	0.4
20B-T-L6	13/16	One	-	2.52	0.038	0.323	75.5	81.7	15.5	2.74
20B-T-L7	9/16	One	-	4.25	0.038	0.133	75.5	81.7	15.5	2.74
20B-T-L8	1/2	Three	-	4.25	0.038	0.118	75.5	81.7	15.5	2.74
20B-T-L9	3/16	Three	-	4.25	0.038	0.044	75.5	81.7	15.5	2.74
20B-T-L10	1/2	-	Two	3.52	0.038	0.142	75.5	81.7	15.5	2.74
20B-T-T13	13/16	One	-	2.50	0.038	0.325	99.4	99.8	6.09	0.5
20B-T-T14	7/16	One	-	4.25	0.038	0.103	99.4	99.8	6.09	0.5
12FA-T-L11	3/16	Three	-	4.25	0.106	0.044	31.5	45.0	105.0	35.6
12FA-T-L12	1/2	One	-	4.25	0.107	0.118	27.4	43.9	102.0	-

TABLE 7

RESULTS OF TENSION TEST PERFORMED ON RECTANGULAR PLATES WITH HOLES
(A, S AND B STEEL)

1	2	3	4	5	6	7	8	9
		Av. Mat'l. Properties		Experimental Results				
Spec. Desig-nation	$\frac{d}{s}$	σ_t (ksi)	Elong. in 1/4" (%)	P_{ult} (kip)	σ_{tt} (ksi)	Elong. in 1/4" (%)	Total Member Deformation (in)	$\frac{\sigma_{tt}}{\sigma_t}$
1210-T L1	0.263	76.9	-	22.30	81.5	35.2	0.09	1.06
1210-T-L2	0.118	74.6	49.0	30.70	75.5	37.2	0.19	1.01
1210 T-L3	0.044	74.6	49.0	32.80	75.6	34.8	0.18	1.01
1205 T-L4	0.118	72.2	47.10	32.20	79.4	28.6	0.11	0.10
1205-T-L5	0.044	72.2	47.10	32.70	74.5	27.6	0.08	1.03
20B-T L6	0.323	81.7	15.5	5.28	81.2	21.7	0.06	0.99
20B-T L7	0.133	81.7	15.5	12.42	88.0	17.1	0.04	1.08
20B-T L8	0.118	81.7	15.5	12.80	90.0	12.9	0.06	1.10
20B-T-L9	0.044	81.7	15.5	13.70	88.8	11.5	0.05	1.09
20B-T-L10	0.142	81.7	15.5	8.90	95.6	14.3	0.03	1.17
20B-T-T13	0.325	99.8	6.09	6.02	93.8	6.4	0.05	0.94
20B-T-T14	0.103	99.8	6.09	13.58	93.5	3.2	0.03	0.94
		σ_y σ_t		P_y P_{ult}	σ_{ty} σ_{tt}			
12FA-T-L11	0.044	31.5 45.0	105.0	12.5 18.7	29.0 43.4	107.0	0.86	0.96
12FA T-L12	0.118	27.4 43.9	102.0	11.0 17.0	27.4 42.4	-	-	0.96

TABLE 8

NOMINAL DIMENSIONS OF LOW DUCTILITY SINGLE BOLTED CONNECTION SPECIMENS
(GROUP D, B STEEL)

Spec. Designation	Geometric Properties of Spec.					Av. Mechanical Properties of Mat'l.			
								ELONGATION	
	Edge Dist. e (in)	Bolt Dia. d (in)	Width of Plate s (in)	$\frac{e}{d}$	$\frac{d}{s}$	σ_y (ksi)	σ_t (ksi)	in 2" G.L. %	in 1/4" G.L. %
20B-L1	1.75	1/2-S.S.	1.50	3.50	0.33	75.5	81.7	4.38	15.5
20B-L2	1.00	1/2-S.S.	1.50	2.00	0.33	75.5	81.7	4.38	15.5
20B-L3	1.50	3/4-S.S.	2.50	2.00	0.30	75.5	81.7	4.38	15.5
20B-L4	2.25	3/4-S.S.	2.50	3.00	0.30	75.5	81.7	4.38	15.5
20B-L5	1.00	1/2-D.S.	2.50	2.00	0.20	75.5	81.7	4.38	15.5
20B-L6	1.50	1/2-D.S.	2.50	3.00	0.20	75.5	81.7	4.38	15.5
20B-L7	0.47	3/16-D.S.	2.00	2.50	0.09	75.5	81.7	4.38	15.5
20B-L8	0.66	3/16-D.S.	2.00	3.50	0.09	75.5	81.7	4.38	15.5
20B-L9	2.25	3/4-D.S.	2.50	3.00	0.30	75.5	81.7	4.38	15.5
20B-T10	1.75	1/2-S.S.	1.50	3.50	0.33	99.4	99.8	1.34	6.09
20B-T11	1.50	1/2-S.S.	2.50	3.00	0.20	99.4	99.8	1.34	6.09
20B-T12	0.66	3/16-S.S.	2.00	3.50	0.09	99.4	99.8	1.34	6.09
20B-T13	2.25	3/4-D.S.	2.50	3.00	0.30	99.4	99.8	1.34	6.09

(1) S.S. = Single Shear D.S. = Double Shear
(2) All holes drilled
(3) Finger tight bolts
(4) Washers under head of bolt and the nut

TABLE 9

NOMINAL DIMENSIONS OF LOW DUCTILITY SINGLE BOLTED CONNECTION SPECIMENS
(GROUP E, A AND S STEEL)

Spec. No.	Geometric Properties of Spec.					Av. Mechanical Properties of Mat'l.			
								ELONGATION	
	Edge Dist. e (in)	Bolt Dia. d (in)	Width of Plate s (in)	$\frac{e}{d}$	$\frac{d}{s}$	σ_y (ksi)	σ_t (ksi)	in 2" G.L. %	in 1/4" G.L. %
1605A-L1	2.25	3/4-S.S.	2.50	3.0	0.30	83.25	83.25	5.50	27.65
1605A-L2	2.25	3/4-D.S.	2.50	3.0	0.30	83.25	83.25	5.50	27.65
1605A-L3	1.50	3/4-D.S.	2.50	2.0	0.30	83.25	83.25	5.50	27.65
1605A-L4	1.50	1/2 D.S.	2.50	3.0	0.20	83.25	83.25	5.50	27.65
1605A L5	1.00	1/2 D.S.	2.50	2.0	0.20	83.25	83.25	5.50	27.65
1605A-L6	1.40	1/2-D.S.	5.00	2.8	0.10	87.60	87.60	8.18	22.60
1205A-L7	2.625	3/4-D.S.	3.75	3.5	0.20	81.60	81.60	4.28	27.65
1205A-L8	2.625	3/4-D.S.	3.00	3.5	0.25	81.60	81.60	4.28	27.65
1205A-L9	3.06	7/8-D.S.	3.50	3.5	0.25	81.60	81.60	4.28	27.65
1205A-L10	1.40	1/2-D.S.	5.00	2.8	0.10	80.50	80.50	4.70	27.00
1205A-L11	2.25	3/4 D.S.	2.50	3.0	0.30	80.50	80.50	4.70	27.00
7S-L31	1.50	1/2-D.S.	2.50	3.0	0.20	82.60	82.60	7.66	28.85
7S-L32	2.187	5/8-D.S.	3.00	3.5	0.21	82.60	82.60	7.66	28.85

(1) S.S. = Single Shear D.S. - Double Shear

(2) All Holes drilled

(3) Finger tight bolts

(4) Washers under head of bolt and the nut

TABLE 10

NOMINAL DIMENSIONS OF FULL ANNEALED SINGLE BOLTED CONNECTION SPECIMENS
(GROUP F, A STEEL)

Spec. Desig-nation	Geometric Properties of Specimen					Av. Mechanical Properties of Mat'l.			
								ELONGATION	
	Edge Dist. e (in)	Bolt Dia. d (in)	Width of Plate s (in)	$\frac{e}{d}$	$\frac{d}{s}$	σ_y (ksi)	σ_t (ksi)	in 2" G.L. %	in 1/4" G.L. %
16FAA-L12	2.25	3/4-D.S.	2.50	3.0	0.3	30.1	45.9	47.4	96.6
16FAA-L13	2.62	3/4-D.S.	2.50	3.5	0.3	30.1	45.9	47.4	96.6
16FAA-L14	1.25	1/2-D.S.	2.50	2.5	0.2	30.1	45.9	47.4	96.6
16FAA-L15	1.75	1/2-D.S.	2.50	3.5	0.2	30.1	45.9	47.4	96.6
16FAA-L16	1.75	1/2-S.S.	2.50	3.5	0.2	30.1	45.9	47.4	96.6
16FAA-L17	1.75	1/2 D.S.	5.00	3.5	0.1	30.1	45.9	47.4	96.6
12FAA-L18	2.25	3/4-D.S.	2.50	3.0	0.3	28.1	44.1	48.9	86.4
12FAA-L19	1.25	1/2-D.S.	2.50	2.5	0.2	28.1	44.1	48.9	86.4
12FAA-L20	1.75	1/2-D.S.	2.50	3.5	0.2	28.1	44.1	48.9	86.4
12FAA-L21	1.75	1/2-D.S.	5.00	3.5	0.1	28.1	44.1	48.9	86.4

(1) S.S. = Single Shear D.S. - Double Shear

(2) All holes drilled

(3) Finger tight bolts

(4) Washers under head of bolt and the nut

TABLE 11

RESULTS OF SINGLE BOLTED CONNECTION TEST ON LOW DUCTILITY B STEEL
(GROUP D)

1	2	3	4	5	6	7	8	9
Spec. Designation	$\frac{e}{d}$	$\frac{d}{s}$	P_{ult}	Mode of Failure	Stresses Predicted as Eqs. 12(τ_s), 13 (σ_b) and 14 (σ_{net})		Stresses Calculated from Ultimate Load as per Eqs. 11a (τ_{sf}) 11b (σ_{bf}) and 11c(σ_{tt})	
					Eq. No.	Stress (ksi)	Eq. No.	Stress (ksi)
			(kip)	(Type)*				
20B-L1	3.50	0.33	3.12	(iii)	12 **13** 14	36.8 245.5 81.7	11a 11b 11c	22.8 160.0 85.0
20B-L2	2.00	0.33	2.74	(ii)+(i) +(iii)	12 13 14	36.8 245.5 81.7	11a 11b 11c	35.1 140.4 74.7
20B-L3	2.00	0.30	4.20	(ii)+(i) +(iii)	12 13 14	36.8 245.5 81.7	11a 11b 11c	35.8 143.2 63.6
20B-L4	3.00	0.30	3.84	(ii)	12 13 14	36.8 245.5 81.7	11a 11b 11c	21.8 131.0 58.0
20B-L5	2.00	0.20	2.55	(ii)+(i)	12 13 14	36.8 245.5 57.2	11a 11b 11c	32.7 130.8 33.2
20B-L6	3.00	0.20	2.68	(ii)	12 13 14	36.8 245.5 57.2	11a 11b 11c	23.5 140.5 36.4

Table 11 (cont'd)

1	2	3	4	5	6	7	8	9
					12	36.8	11a	39.1
20B-L7	2.50	0.09	1.43	(i)	13	245.5	11b	192.0
					14	30.2	11c	30.2
					12	36.8	11a	29.2
20B-L8	3.50	0.09	1.50	(ii)+(i)	13	245.5	11b	206.0
					14	30.2	11c	21.2
					12	36.8	11a	28.6
20B-L9	3.00	0.30	4.88	(ii)+(iii)	13	245.5	11b	172.0
					14	81.7	11c	76.2
					12	44.8	11a	19.5
20B-T10	3.50	0.33	2.59	(iii)	13	299.5	11b	136.4
					14	99.8	11c	72.5
					12	44.8	11a	26.7
20B-T11	3.00	0.20	3.04	(ii)+(iii)	13	299.5	11b	160.2
					14	69.8	11c	41.4
					12	44.8	11a	40.0
20B-T12	3.50	0.09	1.85	(ii)	13	299.5	11b	260.0
					14	36.9	11c	27.0
					12	44.8	11a	28.7
20B-T13	3.00	0.30	4.90	(ii)+(iii)	13	299.5	11b	172.0
					14	99.8	11c	75.4

Underlining indicates critical values
Longitudinal shearing of plate is designated as Type (i) failure
Excessive hole elongation and material pile up in front of the bolt is designated as Type (ii) failure
Transverse tearing of the plate is designated as Type (iii) failure
Tension failure after excessive hole elongation is designated as Type (ii)+(iii) failure
Shear failure after excessive hole elongation is designated as Type (ii)+(i) failure

TABLE 12

RESULTS OF SINGLE BOLTED CONNECTION TESTS ON LOW DUCTILITY A AND S STEEL
(GROUP D)

1	2	3	4	5	6	7	8	9
Spec. Designation	$\frac{e}{d}$	$\frac{d}{s}$	Ultimate Load P_{ult}	Mode of Failure	Stresses Predicted as Eqs. 12(τ_s), 13 (σ_b), 14(σ_{tt})		Stresses Calculated from Ultimate Load as per Eqs. 11a (τ_{sf}), 11b(σ_{bf}), 11c(σ_{tf})	
					Eq. No.	Stress (ksi)	Eq. No.	Stress (ksi)
			(kips)	(Type)*				
1605A-L1	3.0	0.30	8.92	(iii)	12 13 14	37.50 250.00 83.25	11a 11b 11c	31.9 192.0 83.6
1605A-L2	3.0	0.30	9.40	(iii)	12 13 14	37.50 250.0 83.25	11a 11b 11c	33.9 203.5 90.0
1605-L3	2.0	0.30	7.54	(ii)+(i)+(iii)	12 13 14	37.50 250.00 83.25	11a 11b 11c	40.0 160.0 70.6
1605A-L4	3.0	0.20	5.80	(ii)	12 13 14	37.50 250.00 58.40	11a 11b 11c	31.2 187.0 48.2
1605A-L5	2.0	0.20	4.84	(i)	12 13 14	37.50 250.00 58.40	11a 11b 11c	36.2 157.0 40.5
1605A-L6	2.8	0.10	6.90	(ii)+(i)	12 13 14	39.50 263.00 33.30	11a 11b 11c	40.2 224.0 25.2

Table 12 (cont'd)

1	2	3	4	5 *	6	7	8	9
1205A-L7	3.5	0.20	20.0	(ii)+(i)		36.70 245.00 57.20	11a 11b 11c	36.0 252.00 63.2
1205A-L8	3.5	0.25	18.8	(ii)+(iii)		36.70 245.00 68.40	11a 11b 11c	33.8 236.0 81.0
1205A-L9	3.5	0.25	22.4	(iii)+(ii)		36.70 245.00 68.40	11a 11b 11c	34.4 242.0 82.0
1205A-L10	2.8	0.10	11.0	(ii)+(i)		36.20 242.00 32.20	11a 11b 11c	36.7 206.0 23.1
1205A-L11	3.0	0.30	13.7	(iii)		36.20 242.00 80.50	11a 11b 11c	28.6 172.0 75.5
7S-L31	3.0	0.20	20.3	(i)		37.20 248.00 57.80	11a 11b 11c	37.1 222.5 56.4
7S-L32	3.5	0.21	28.0	(ii)+(i)+ (iii)		37.20 248.00 60.40	11a 11b 11c	36.2 247.0 65.4

Underlining indicates critical values
Longitudinal shearing of plate is designated as Type (i) failure
Excessive hole elongation and material pile up in front of the bolt is designated as Type (ii) failure
Transverse tearing of the plate is designated as Type (iii) failure
Tension failure after excessive hole elongation is designated as Type (ii)+(iii) failure
Shear failure after excessive hole elongation is designated as Type (ii)+(i) failure

TABLE 13

RESULTS OF SINGLE BOLTED CONNECTION TESTS ON FULL ANNEALED A STEEL
(GROUP F)

1	2	3	4	5	6	7	8	9
Spec. Designation	$\frac{e}{d}$	$\frac{d}{s}$	Ultimate Load	Mode of Failure	Stresses Predicted as Eqs. 22a(τ_s), 23a (σ_b), 24a(σ_{tt})		Stresses Calculated from P_{ult} as per Eqs. 11a(τ_{sf}), 11b(σ_{bf}) 11c(σ_{tf})	
					Eq. No.	Stress (ksi)	Eq. No.	Stress (ksi)
			(kips)	(Type)*				
16FAA-L12	3.0	0.3	4.66	(iii)	22a 23a 24a	21.1 147.5 45.9	11a 11b 11c	16.45 98.80 43.00
16FAA-L13	3.5	0.3	4.68	(iii)	22a 23a 24a	21.1 147.5 45.9	11a 11b 11c	14.18 99.20 44.00
16FAA-L14	2.5	0.2	3.20	(i)+(ii)	22a 23a 24a	21.1 147.5 32.1	11a 11b 11c	20.30 101.60 26.20
16FAA-L15	3.5	0.2	5.10	(ii)+(iii)	22a 23a 24a	21.1 147.5 32.1	11a 11b 11c	23.10 161.80 41.60
16FAA-L16	3.5	0.2	4.80	(ii)+(iii)	22a 23a 24a	21.1 147.5 32.1	11a 11b 11c	21.80 152.20 39.30
16FAA-L17	3.5	0.1	4.28	(ii)	22a 23a 24a	21.1 147.5 18.4	11a 11b 11c	19.40 136.00 35.00

Table 13 (cont'd)

1	2	3	4	5*	6	7	8	9
					22a	19.6	11a	16.90
12FAA-L18	3.0	0.3	8.14	(iii)	23a	138.0	11b	101.20
					24a	44.1	11c	45.00
					22a	19.6	11a	24.05
12FAA-L19	2.5	0.2	6.44	(ii)+(i)	23a	138.0	11b	120.20
					24a	30.9	11c	31.00
					22a	19.6	11a	22.80
12FAA-L20	3.5	0.2	8.52	(ii)+(iii)	23a	138.0	11b	159.20
					24a	30.9	11c	41.00
					22a	19.6	11a	25.50
12FAA-L21	3.5	0.1	9.55	(ii)	23a	138.0	11b	178.40
					24a	17.7	11c	20.10

Underlining indicates critical values
Longitudinal shearing of plate is designated as Type (i) failure
Excessive hole elongation and material pile up in front of the bolt is designated as Type (ii) failure
Transverse tearing of the plate is designated as Type (iii) failure
Tension failure after excessive hole elongation is designated as Type (ii)+(iii) failure
Shear failure after excessive hole elongation is designated as Type (ii)+(i) failure

TABLE 14

SINGLE BOLTED CONNECTION TESTS REARRANGED IN INCREASING ORDER OF $(\frac{e}{d}+\frac{s}{d})$ RATIO. (TEST RESULTS OF 7 GA. AND 12 GA. S STEEL INCLUDED)

1	2	3	4	5	6	7	8	9	10
Spec. Designation	Dia.of Bolt (in)	$\frac{e}{d}$	$\frac{d}{s}$	$(\frac{e}{d}+\frac{s}{d})^*$	$\frac{t}{d}$	$[(\frac{e}{d}+\frac{s}{d})+1](\frac{t}{d})^*$	$\frac{\sigma_{bf}}{\sigma_t}$	$\frac{\sigma_{bf}}{\sigma_t}(\frac{t}{d})$	Mode of Failure (Type)
20B L2	1/2 S.S.	2.00	0.330	5.00	0.076	0.458	1.762	0.134	(i)+(ii)+(iii)
20B-L3	3/4-S.S.	2.00	0.300	5.33	0.051	0.323	1.805	0.092	(ii)+(i)+(iii)
1605A-L3	3/4-D.S.	2.00	0.300	5.33	0.083	0.525	1.950	0.162	(ii)+(i)+(iii)
20B L4	3/4-S.S.	3.00	0.300	6.33	0.051	0.374	1.650	0.084	(ii)
20B L9	3/4-D.S.	3.00	0.300	6.33	0.051	0.374	2.100	0.107	(iii)
20B-T13	3/4 D.S.	3.00	0.300	6.33	0.051	0.374	1.728	0.088	(ii)+(iii)
20B-L5	1/2-D.S.	2.00	0.200	7.00	0.076	0.607	1.620	0.123	(ii)+(i)
1605A-L1	3/4 S.S.	3.00	0.300	6.33	0.083	0.607	2.300	0.191	(iii)
1605A L2	3/4-D.S.	3.00	0.300	6.33	0.083	0.607	2.425	0.202	(iii)+(ii)
1605A L5	1/2 D.S.	2.00	0.200	7.00	0.124	0.993	1.880	0.233	(i)
1205A L11	3/4-D.S.	3.00	0.300	6.33	0.141	1.033	2.140	0.302	(iii)
7S L21	3/4 S.S.	3.20	0.300	6.53	0.244	1.835	2.235	0.546	(iii)
7S T5	3/4-S.S.	2.33	0.250	6.33	0.244	1.790	2.030	0.495	(i)+(ii)
20B-L6	1/2 S.S.	3.00	0.200	8.00	0.076	0.685	1.728	0.131	(ii)
20B-T11	1/2 S.S.	3.00	0.200	8.00	0.076	0.685	1.610	0.123	(ii)+(iii)
1605A L4	1/2 D.S.	3.00	0.200	8.00	0.124	1.117	2.245	0.278	(ii)
7S L31	1/2 D.S.	3.00	0.200	8.00	0.366	3.290	2.720	0.995	(i)+(ii)
12S L15	3/8 S.S.	3.99	0.247	7.38	0.283	2.375	2.642	0.750	(ii)+(iii)+(i)
7S-L32	5/8 D.S.	3.50	0.210	8.09	0.293	2.660	2.980	0.875	(ii)+(i)+(iii)
7S-L5	3/4-S.S.	2.50	0.200	7.50	0.244	2.075	2.435	0.594	(ii)+(i)+(iii)

TABLE 14 (cont'd)

1	2	3	4	5*	6	7*	8	9	10
1205A-L8	3/4-D.S.	3.50	0.250	7.33	0.141	1.172	2.900	0.409	(ii)+(iii)
1205A-L9	7/8-D.S.	3.50	0.250	7.33	0.121	1.009	2.960	0.358	(iii)+(ii)
12S-L17	5/8-S.S.	3.40	0.245	7.41	0.169	1.420	2.185	0.370	(ii)+(iii)+(i)
12S-L16	1/2-S.S.	3.50	0.245	7.41	0.212	1.785	2.865	0.608	(ii)
12S-L18	3/4-S.S.	3.53	0.247	7.38	0.141	1.182	2.090	0.295	(ii)+(iii)
12S-L19	7/8-S.S.	3.43	0.248	7.36	0.121	1.010	2.085	0.252	(iii)
1205A-L7	3/4-D.S.	3.50	0.200	8.33	0.141	1.317	3.085	0.435	(ii)+(i)
12S L26	3/4-S.S.	3.46	0.200	8.33	0.141	1.317	2.800	0.395	(ii)
12S-L13	5/8-S.S.	3.48	0.188	8.65	0.169	1.630	2.042	0.346	(ii)+(i)+(iii)
12S-L14	3/4-S.S.	3.46	0.191	8.57	0.141	1.350	3.960	0.560	(ii)+(iii)
12S-L12	1/2-S.S.	3.50	0.188	8.65	0.212	2.045	2.875	0.610	(ii)+(iii)
7S-L25	1/2-D.S.	3.00	0.152	9.00	0.366	3.660	2.865	1.048	(ii)+(i)
12S-L11	3/8-S.S.	3.97	0.187	8.67	0.282	2.730	2.920	0.824	(ii)+(i)
12S-L10	5/8-S.S.	3.37	0.152	9.33	0.169	1.750	2.780	0.470	(ii)+(i)
12S-L9	1/2-S.S.	3.50	0.147	9.33	0.212	2.195	3.635	0.770	(ii)
12S-L8	3/8-S.S.	4.00	0.148	9.33	0.282	2.920	3.340	0.942	(ii)
7S-L6	3/4-S.S.	5.00	0.200	8.33	0.244	2.280	3.705	0.905	(ii)+(iii)
20B-L7	3/16-D.S.	2.50	0.090	8.50	0.203	1.930	2.425	0.493	(i)+(ii)
1605A-L6	1/2-D.S.	2.80	0.100	8.80	0.124	1.215	2.540	0.316	(ii)+(i)
1205A-L10	1/2-D.S.	2.80	0.100	8.80	0.212	2.080	2.580	0.548	(ii)+(i)
12S-L7	1/2-D.S.	3.50	0.125	9.33	0.212	2.200	3.260	0.692	(ii)+(i)
7S-L24	1/2-D.S.	2.80	0.100	8.80	0.366	3.585	3.140	1.150	(ii)+(i)
20B-L8	3/16-D.S.	3.50	0.090	9.33	0.203	2.100	2.575	0.524	(ii)+(i)
20B-T13	3/16-S.S.	3.50	0.090	9.33	0.203	2.100	2.610	0.530	(ii)

* Upper limits on e/d and s/d ratios are 3.33 and 6.0 respectively; i.e., the limiting values are substituted even if the actual test specimen has higher e/d or s/d ratio than 3.33 and 6.0 respectively.

TABLE 15

DEFORMATION CHARACTERISTICS OF SINGLE BOLTED CONNECTIONS

1 Spec. Designation	2 $\frac{e}{d}$	3 $\frac{d}{s}$	4 P_{ult} (kips)	5 Mode of Failure (Type)*	6 Increase in Hole Size (in)	7 Deformation at P_{ult} ** (in)	8 Max. Long. Elong. in 1/4" G.L. (%)
				(Low Ductility B Steel Specimens)			
20B-L1	3.50	0.33	3.12	(iii)	0.20	——	12.4
20B-L2	2.00	0.33	2.74	(ii)+(i)+(iii)	0.49	0.50	14.3
20B-L3	2.00	0.30	4.20	(ii)+(i)+(iii)	0.54	——	——
20B-L4	3.00	0.30	3.84	(ii)	0.70	0.70	——
20B-L5	2.00	0.20	2.55	(ii)+(i)	0.65	0.35	——
20B-L6	3.00	0.20	2.68	(ii)	1.20	0.55	——
20B-L7	2.50	0.09	1.43	(i)	0.35	0.15	——
20B-L8	3.50	0.09	1.50	(ii)+(i)	0.55	0.15	——
20B-L9	3.00	0.30	4.88	(ii)+(iii)	1.10	0.60	11.5
20B-T10	3.50	0.33	2.59	(iii)	0.14	0.19	——
20B-T11	3.00	0.20	3.04	(ii)+(iii)	0.54	0.50	——
20B-T12	3.50	0.09	1.85	(ii)	0.80	0.35	——
20B-T13	3.00	0.30	4.90	(ii)+(iii)	0.56	——	——
				(Low Ductility A Steel Specimens)			
1605A-L1	3.0	0.30	8.92	(iii)	0.40	——	23.4
1605A-L2	3.0	0.30	9.40	(iii)	0.40	0.38	24.1
1605A-L3	2.0	0.30	7.54	(ii)+(i)+(iii)	0.45	0.43	21.4
1605A-L4	3.0	0.20	5.80	(ii)	0.50	0.33	11.9
1605A-L5	2.0	0.20	4.84	(i)	0.45	0.43	16.2
1605A-L6	2.8	0.10	6.90	(ii)+(i)	0.65	0.46	26.1
1205A-L7	3.5	0.20	20.0	(ii)+(i)	0.85	0.80	23.5
1205A-L8	3.5	0.25	18.8	(ii)+(iii)	0.65	0.67	——

Table 15 (cont'd)

1	2	3	4	5*	6	7**	8
1205A-L9	3.5	0.25	22.4	(iii)+(ii)	0.60	0.60	——
1205-L10	2.8	0.10	11.0	(ii)+(i)	0.45	0.45	——
1205A-L11	3.0	0.30	13.7	(iii)	0.35	0.35	29.1
(High Ductility A Steel Annealed Specimens)							
16FAA-L12	3.0	0.3	4.66	(iii)	0.55	0.45	——
16FAA-L13	3.5	0.3	4.68	(iii)	0.45	0.60	——
16FAA-L14	2.5	0.2	3.20	(i)+(ii)	0.74	0.53	43.5
16FAA-L15	3.5	0.2	5.10	(ii)+(iii)	0.64	0.65	50.0
16FAA L16	3.5	0.2	4.80	(ii)+(iii)	0.84	0.70	——
16FAA-L17	3.5	0.1	4.28	(ii)	1.20	0.75	——
12FAA L18	3.0	0.3	8.14	(iii)	0.50	0.60	131.0
12FAA-L19	2.5	0.2	6.44	(ii)+(i)	0.95	0.60	50.6
12FAA-L20	3.5	0.2	8.52	(ii)+(iii)	0.90	0.80	66.5
12FAA-L21	3.5	0.1	9.55	(ii)	1.30	0.80	——

* Longitudinal shearing of the plate is designated as Type (i) Failure. Excessive hole elongation and material pile up in front of bolt is designated as Type (ii) Failure.

Transverse tearing of the plate is designated as Type (iii) Failure. Tension failure after excessive hole elongation is designated as Type (ii)+(iii) Failure. Shear Failure after excessive hole elongation is designated as Type (ii)+(i) Failure.

** This deformation was recorded by an autographic recorder. It includes streching of the connection specimen over a gage length (2e+1) inches.

TABLE 16

COMPARISON OF PREDICTION EQUATIONS 7a AND 19a USING SUM OF DIFFERENCE SQUARES

Eq. No.	No. of Tests Where Experimental Value of Bearing Stress is below 80% of Predicted Value	Sum of Difference Squares	Ratio of Sq. Roots of sum of Diff. Sqs. of Eqs. 7a, 19a and 7b, 19b.	No. of Tests Where Experimental Value of Bearing Stress is below 80% of Predicted Value	Sum of Difference Squares	Ratio of Sq. Roots of sum of Diff. Sqs. of Eqs. 7a, 19a and 7b, 19b
	For Type (ii), (ii)+(i) and (iii) Failures (Total No. of Tests=34)			For Type (ii) and (ii)+(i) Failures (Total No. of Tests=25)		
7a	8	70,290	1.27	6	33,740	1.31
19a	2	43,790		2	19,670	
+ 7b	7	74,650	1.31	5	32,710	1.55
±19b	2	43,300		2	13,680	

\+ Equation 7b is a modified form of Equation 7a, where load for combination failure is given by

$$P_c = 0.9\ e\ t\ \sigma_t \leq \underline{2.7}\ d\ t\ \sigma_t \qquad (7b)$$

± Equation 19b is a modified form of Equation 19a, where load for combination failure is given by

$$P_c = 0.318\ \left(\frac{e}{d}+\frac{s}{d}+1\right)\ dt\sigma_t - \underline{0.050}\ d^2\sigma_t \qquad (19b)$$

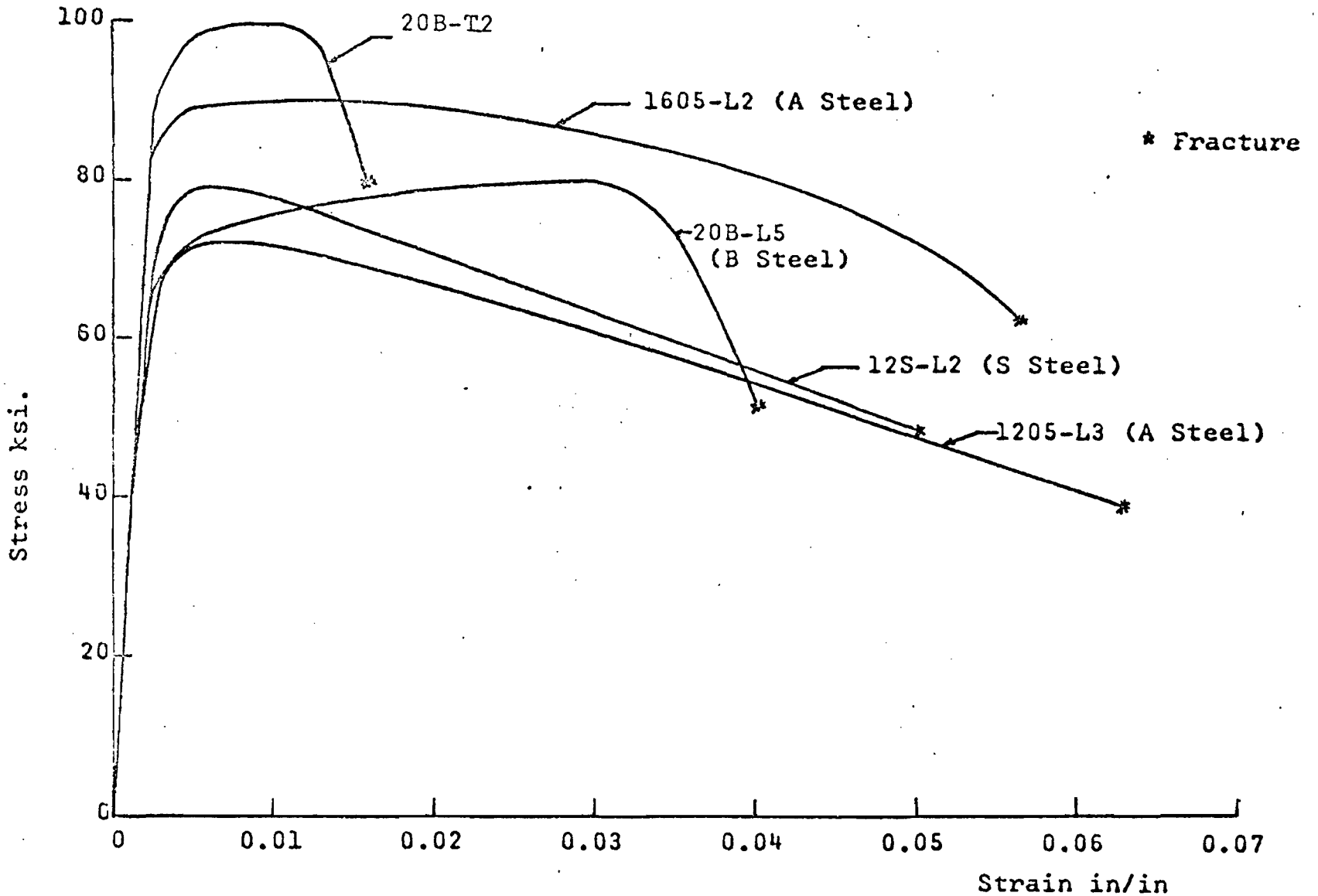

FIG. 1 COMPLETE STRESS STRAIN CURVES OF A, S AND B STEEL. (2" G.L.)

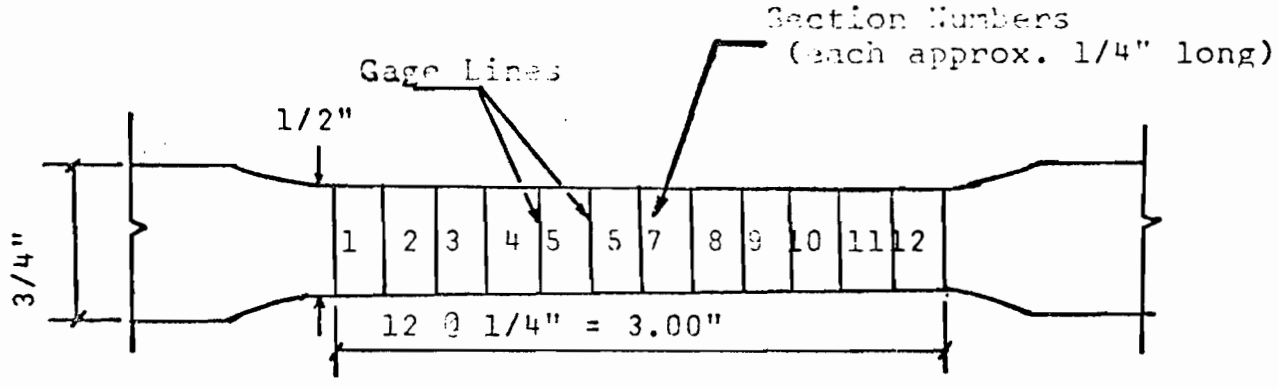

FIG. 2a. SKETCH OF A STANDARD TENSION COUPON

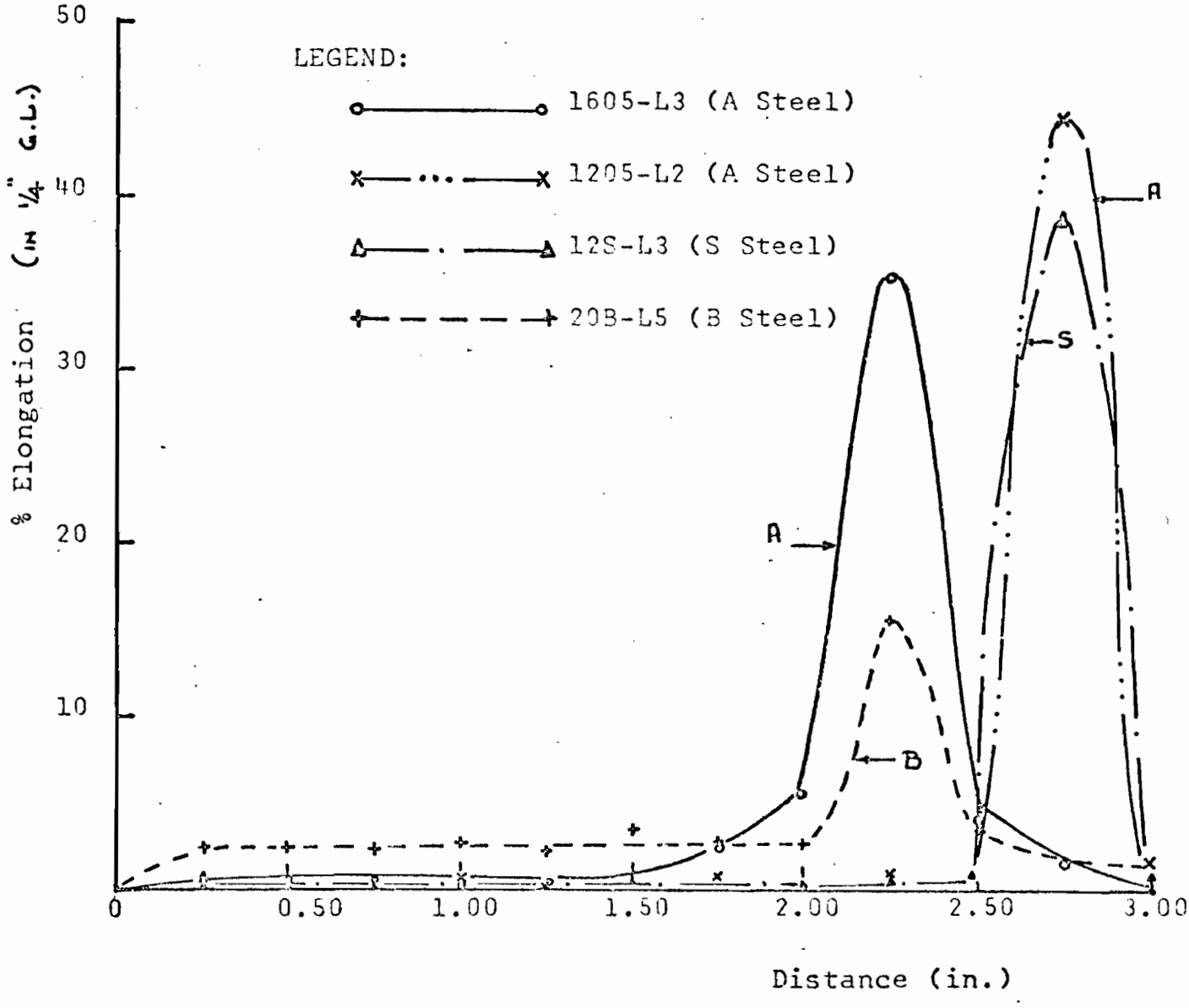

FIG. 2b. DISTRIBUTION OF LONGITUDINAL STRAIN IN TENSION COUPON (after fracture)

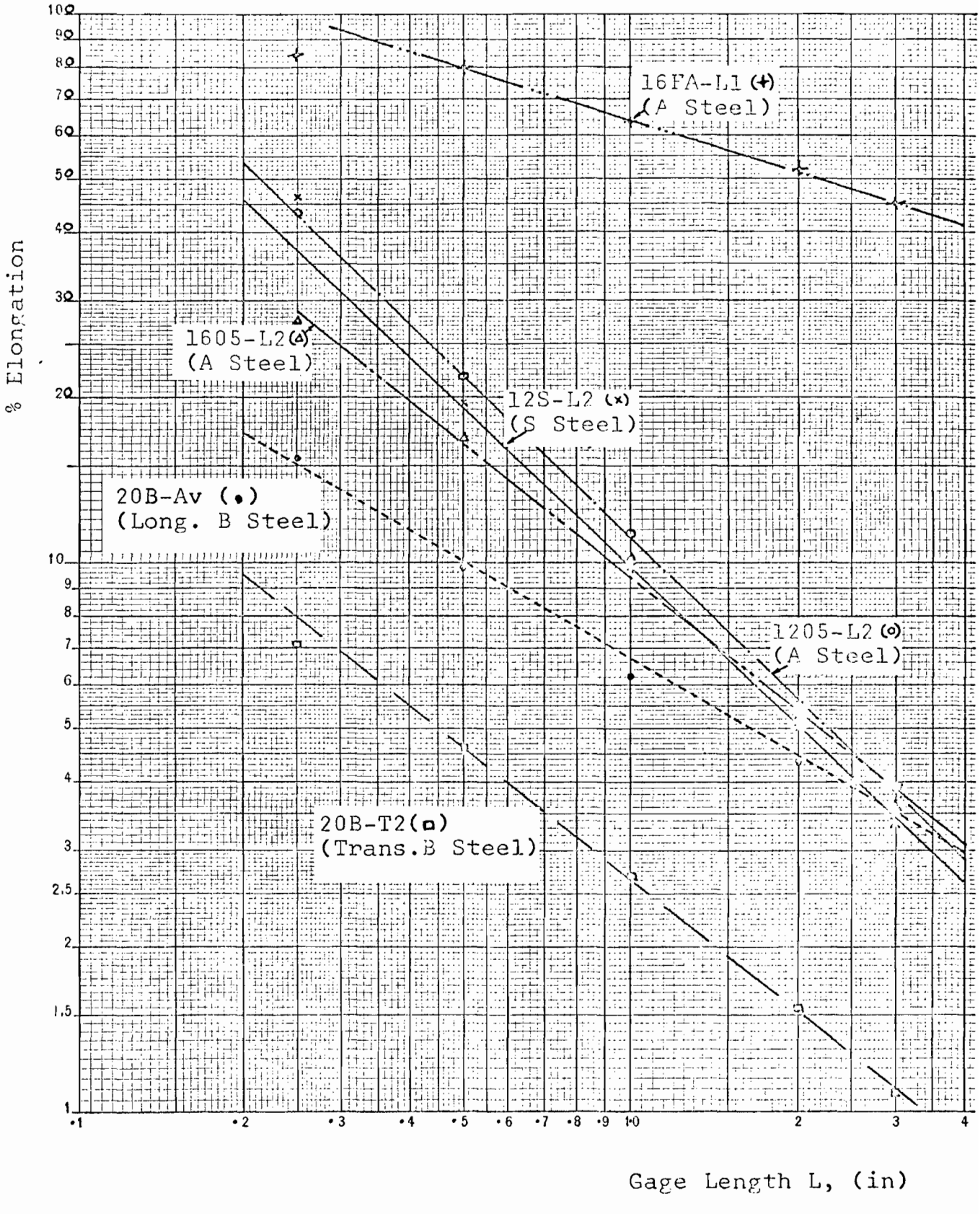

FIG. 3. LOGARITHMIC RELATIONSHIP BETWEEN ELONGATION AND GAGE LENGTH FOR A, S, AND B STEEL.

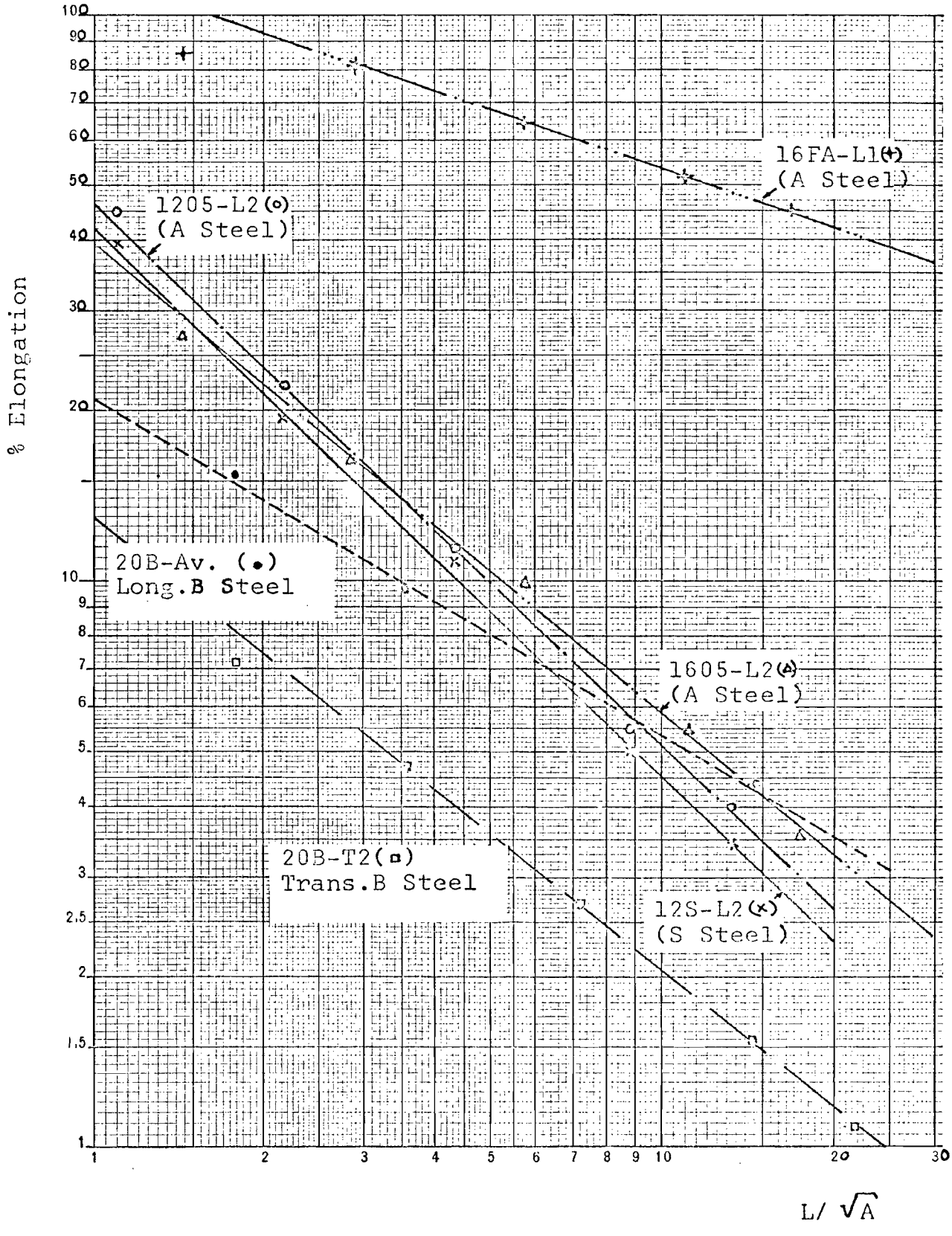

FIG. 4. LOGARITHMIC RELATIONSHIP BETWEEN ELONGATION AND L/ $\sqrt{A}$ FOR A, S AND B STEEL

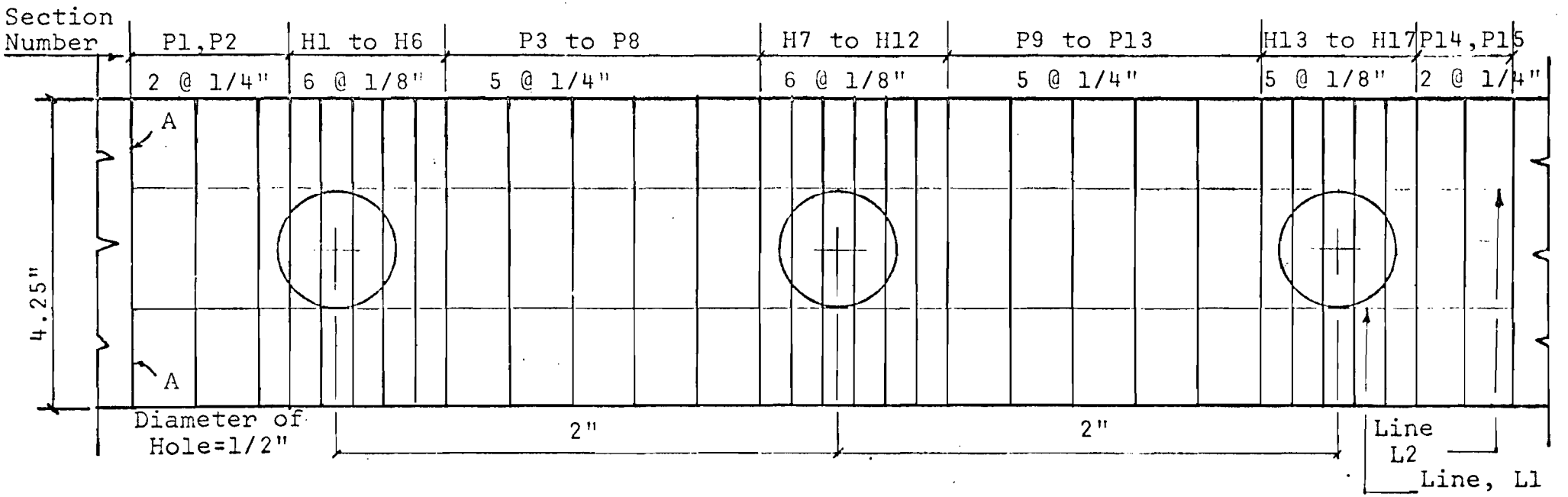

FIG. 5a. SKETCH OF A SCRIBED PLATE (d/s = 0.118)

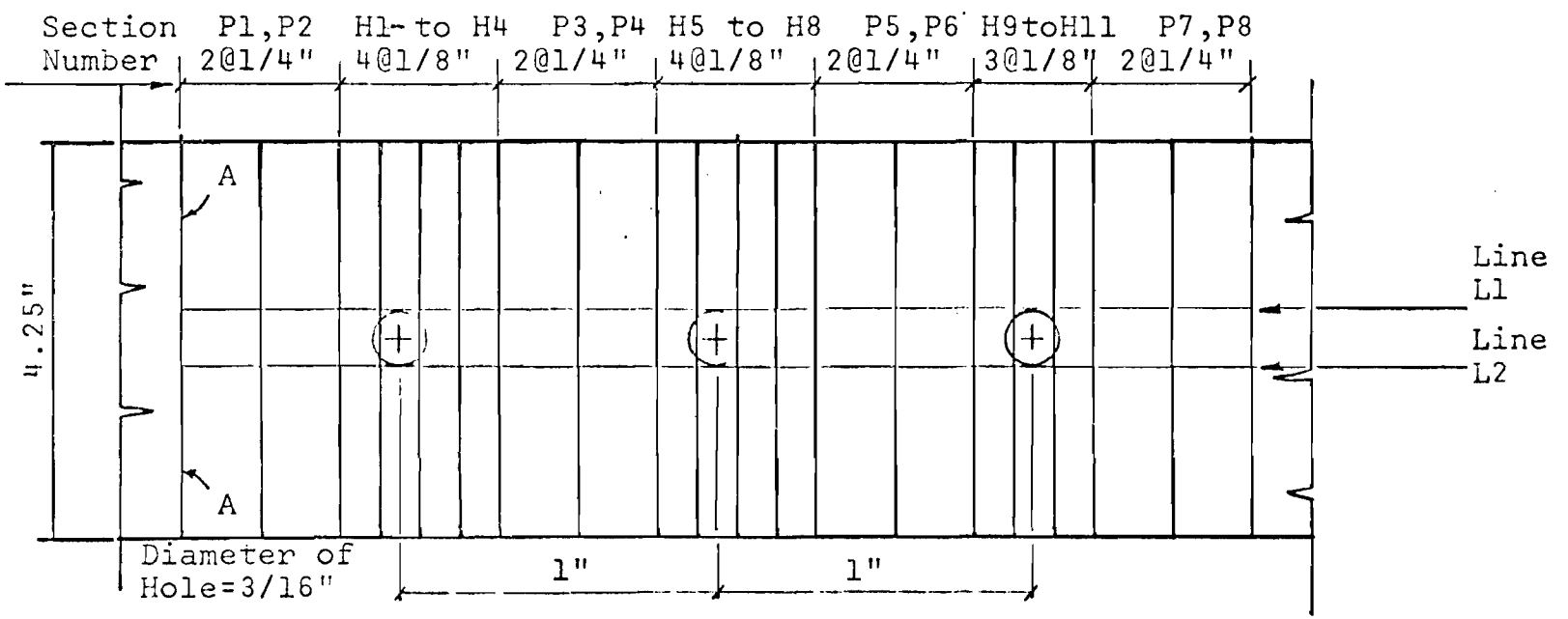

FIG. 5b. SKETCH OF A SCRIBED PLATE (d/s = 0.044)

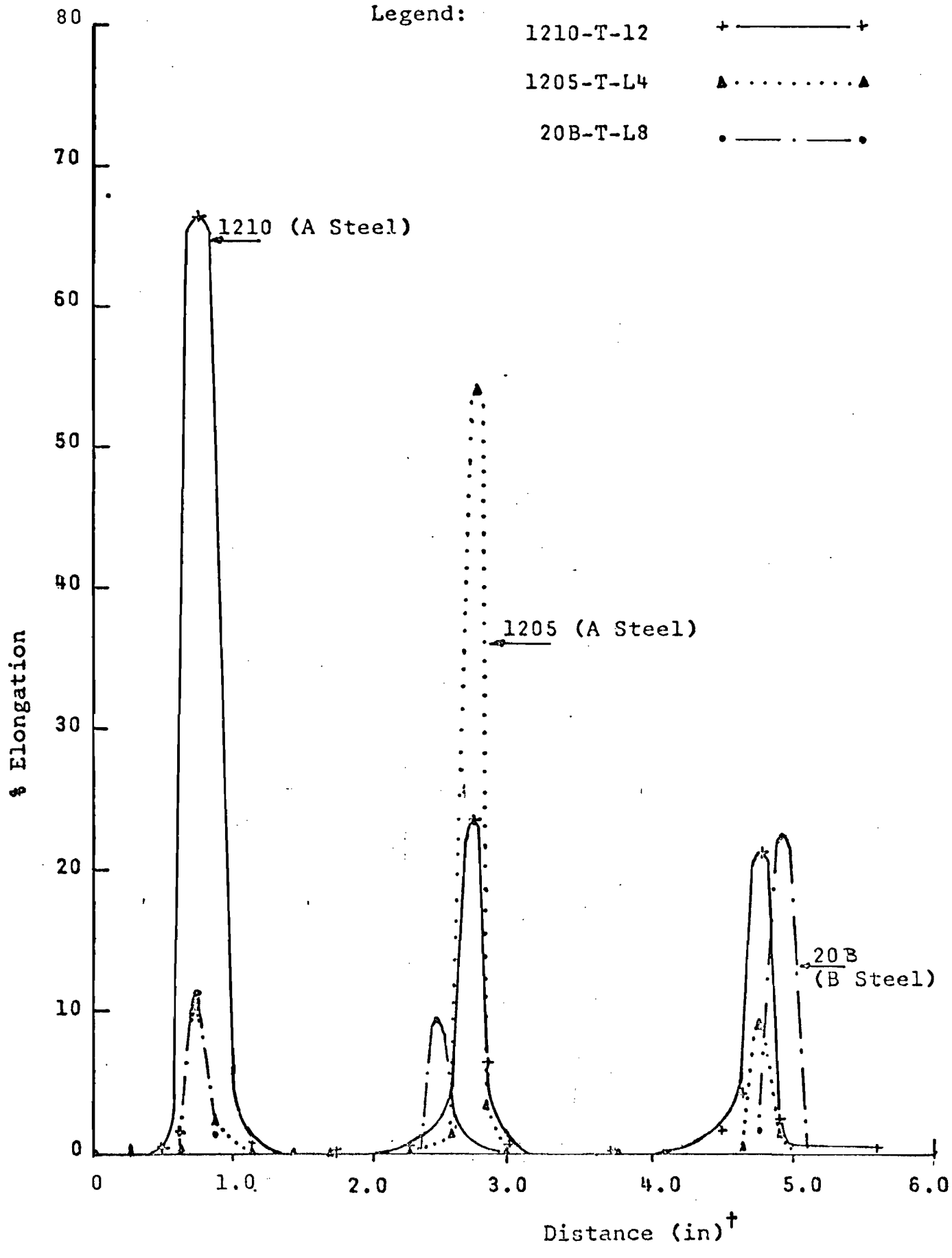

FIG 5(c) LONGITUDINAL STRAIN DISTRIBUTION (AFTER FRACTURE)

† Distance measured from Line A-A (Fig. 5a)

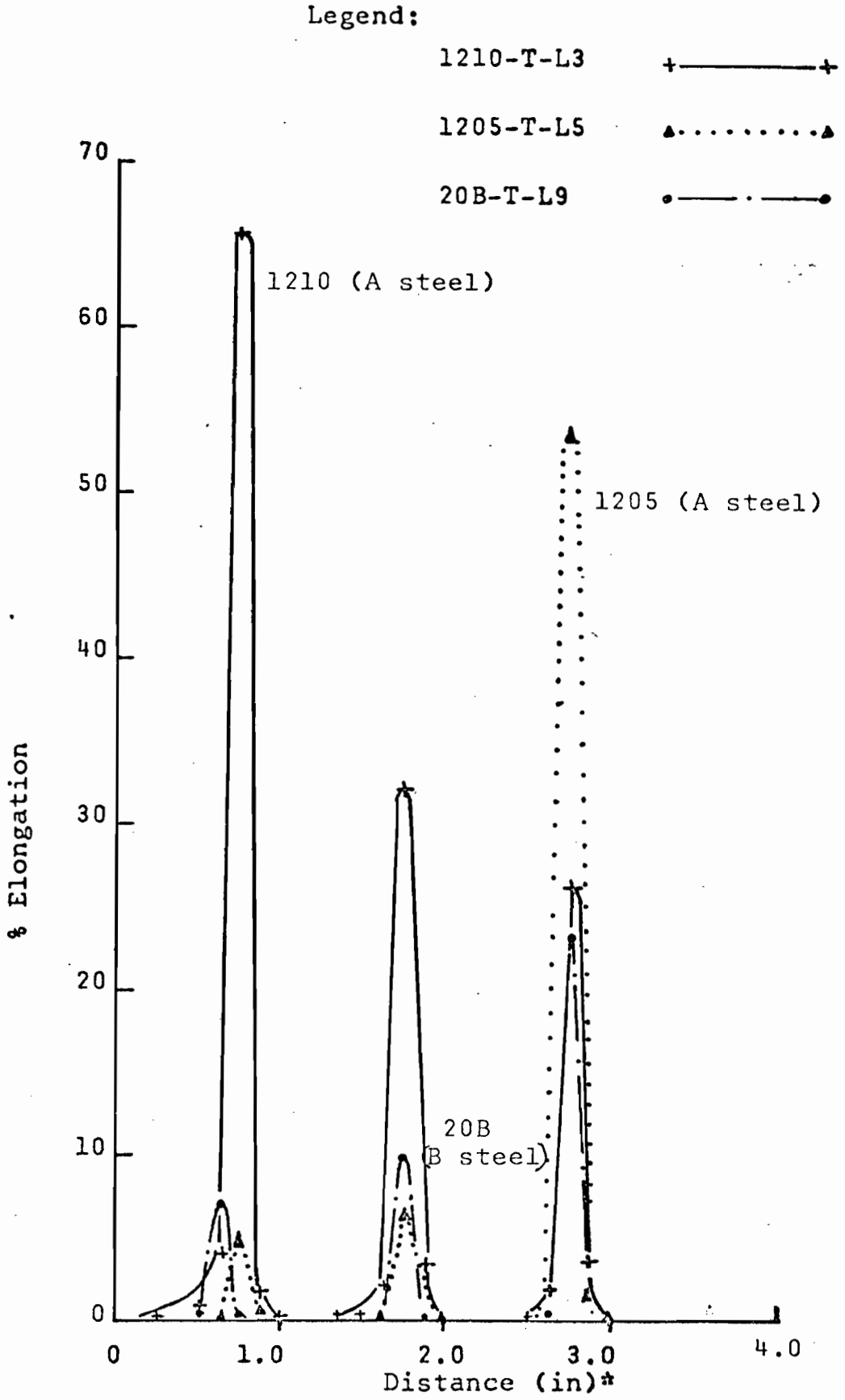

FIG. 5d. LONGITUDINAL STRAIN DISTRIBUTION (AFTER FRACTURE)

* Distance measured from Line A-A (Fig. 5b)

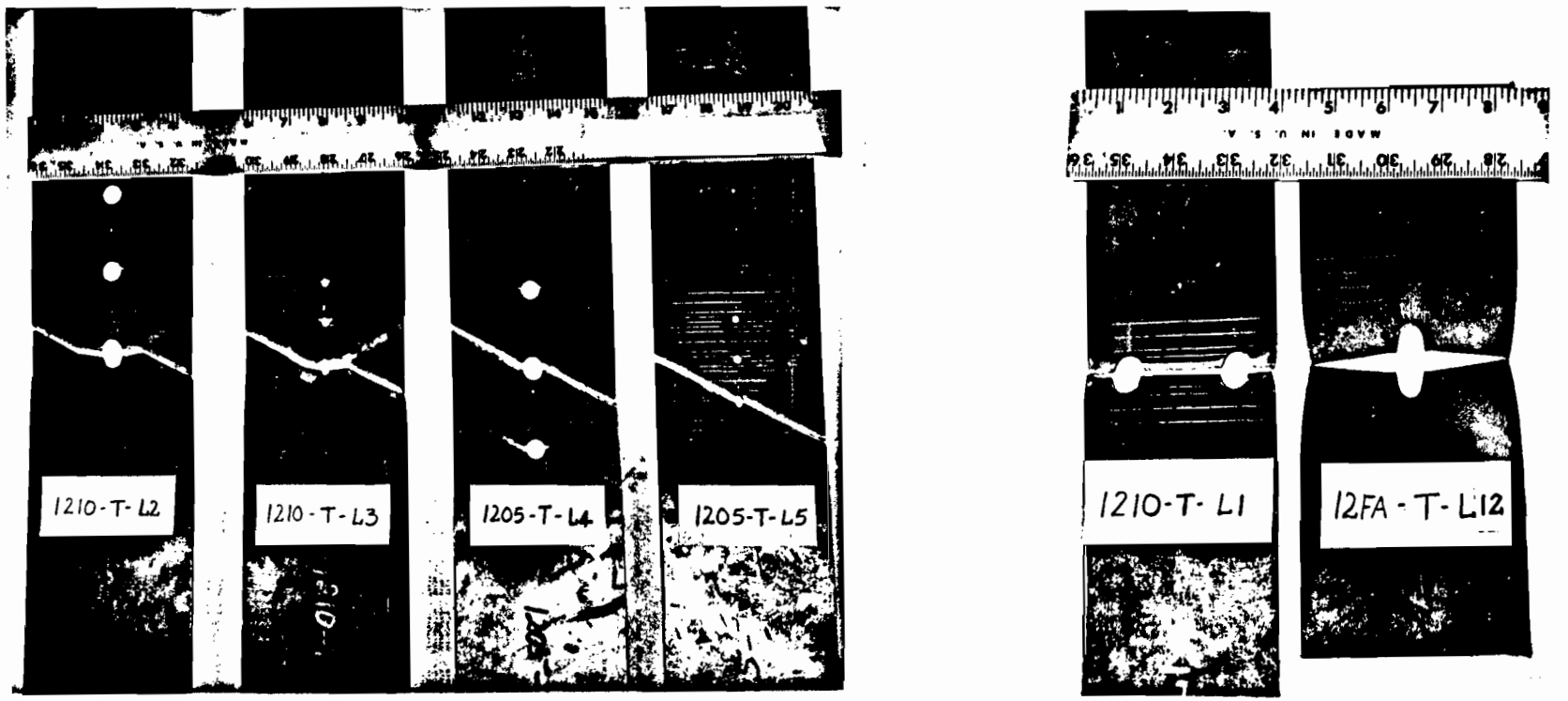

Fig. 6a. Rectangular Plate Specimens After Fracture (A Steel)

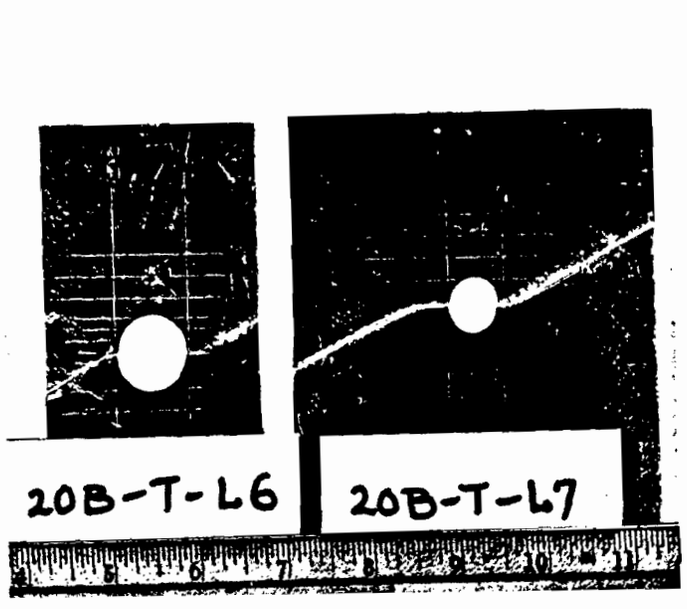

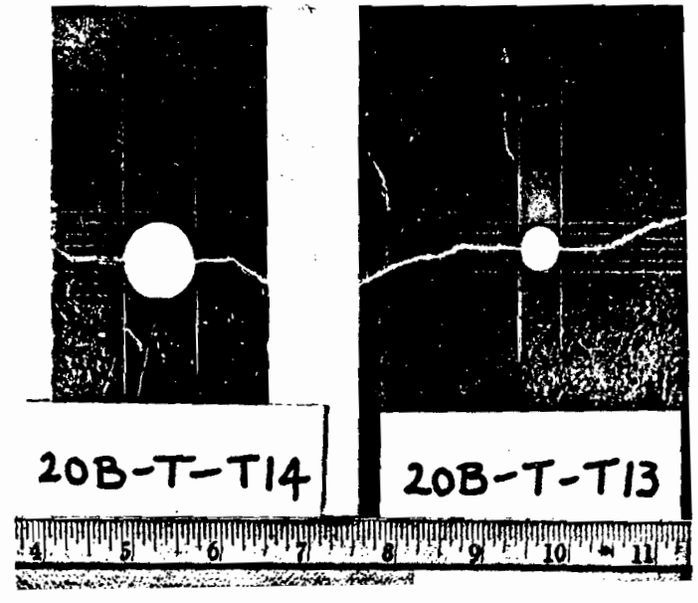

Fig. 6b. Rectangular Plate Specimens After Fracture (B Steel)

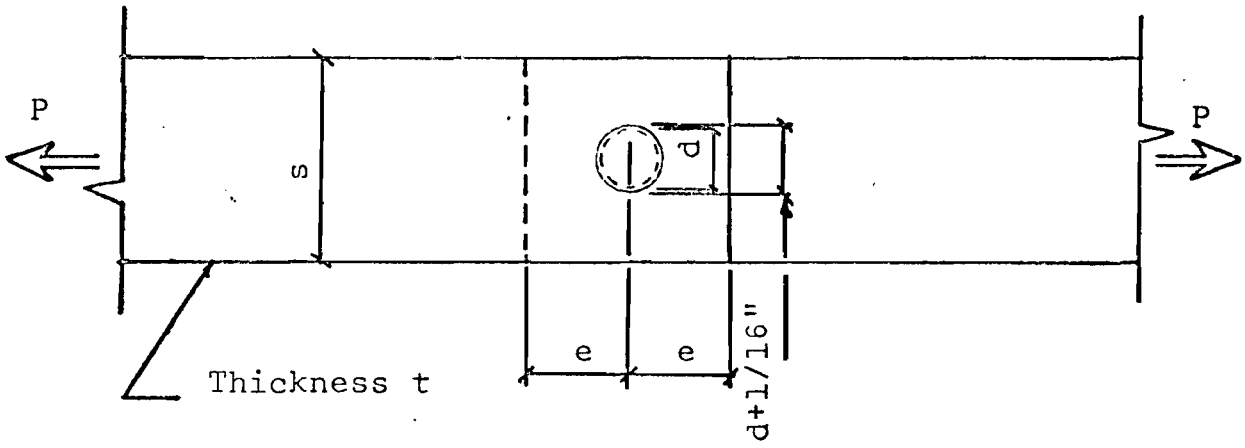

FIG. 7a. SKETCH OF A SINGLE BOLTED CONNECTION

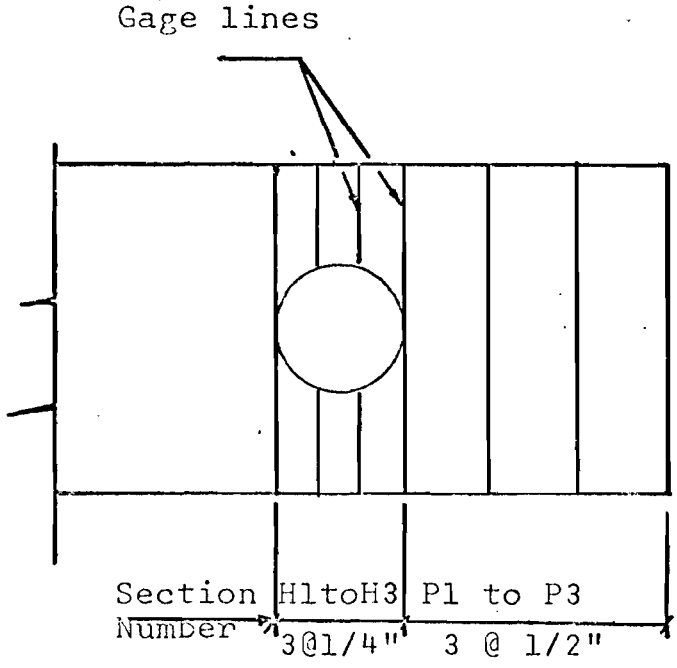

FIG. 7b. SKETCH OF A SCRIBED PLATE

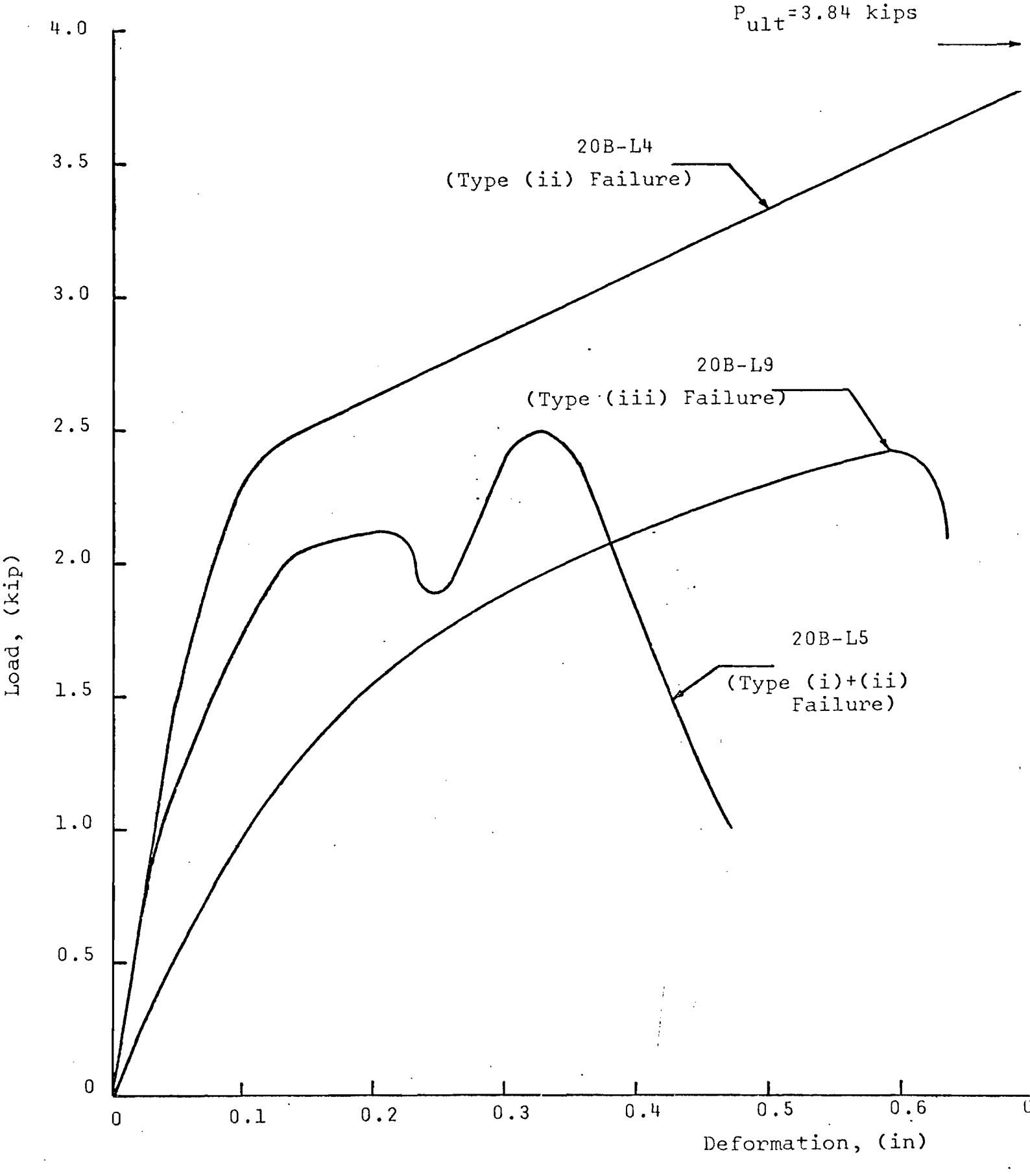

FIG. 8a. LOAD-DEFORMATION CURVES FOR LONGITUDINAL 20 GAGE B STEEL SINGLE-BOLTED CONNECTION SPECIMENS

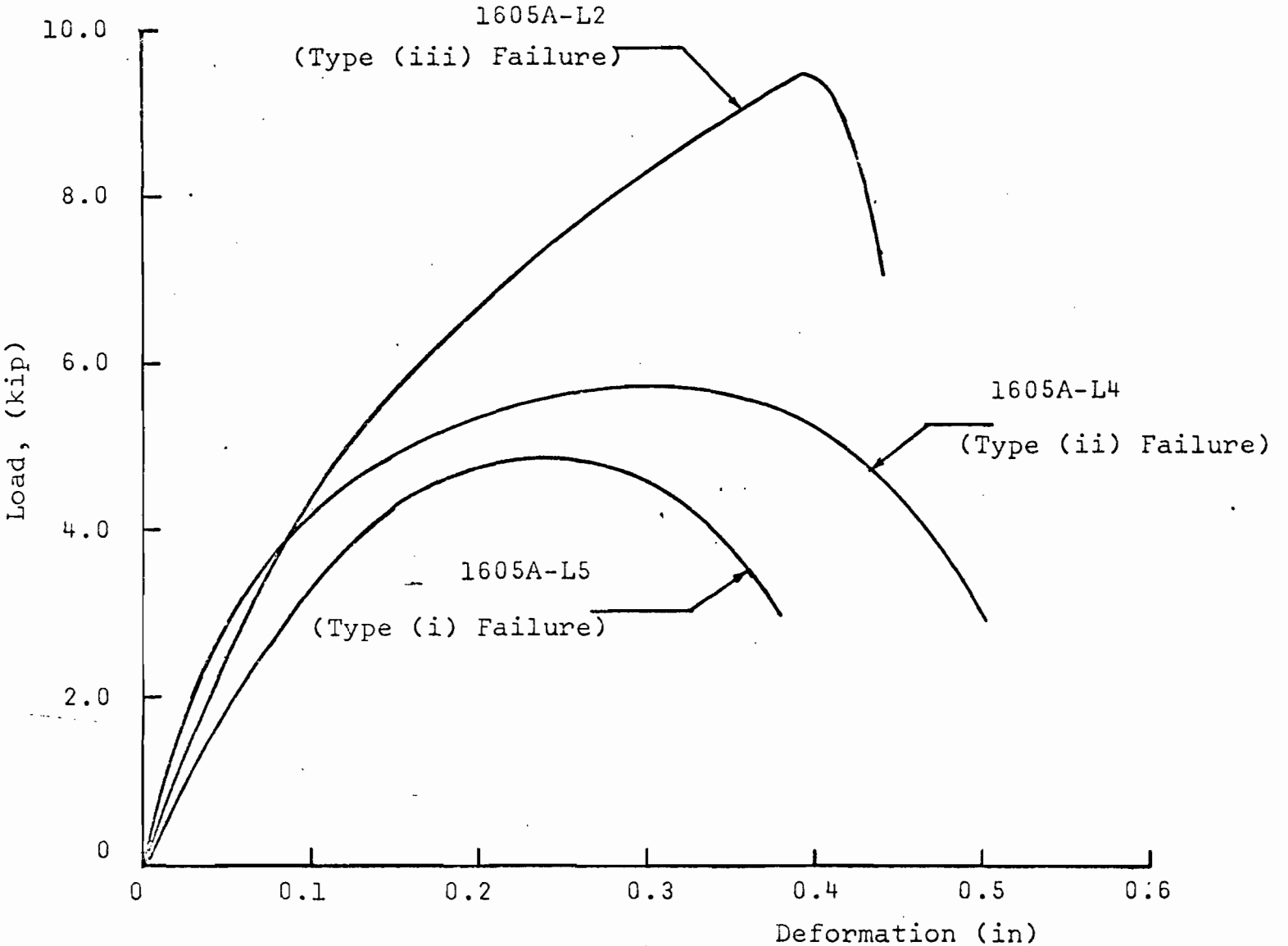

FIG. 8b. LOAD-DEFORMATION CURVES FOR 16 GAGE LOW DUCTILITY A STEEL SINGLE BOLTED CONNECTIONS

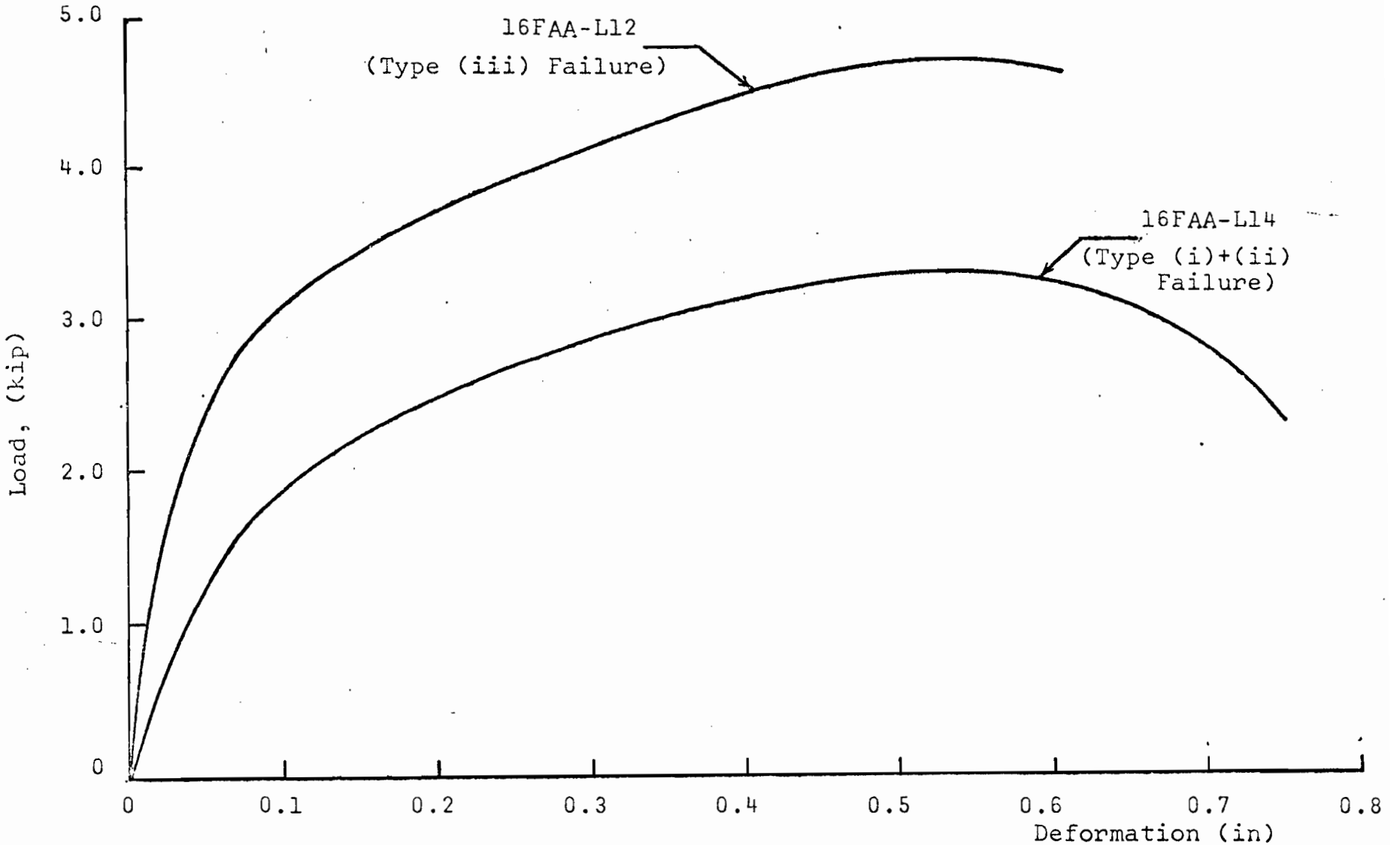

FIG. 8c. LOAD-DEFORMATION CURVES FOR 16 GAGE FULL ANNEALED A STEEL SINGLE BOLTED CONNECTIONS

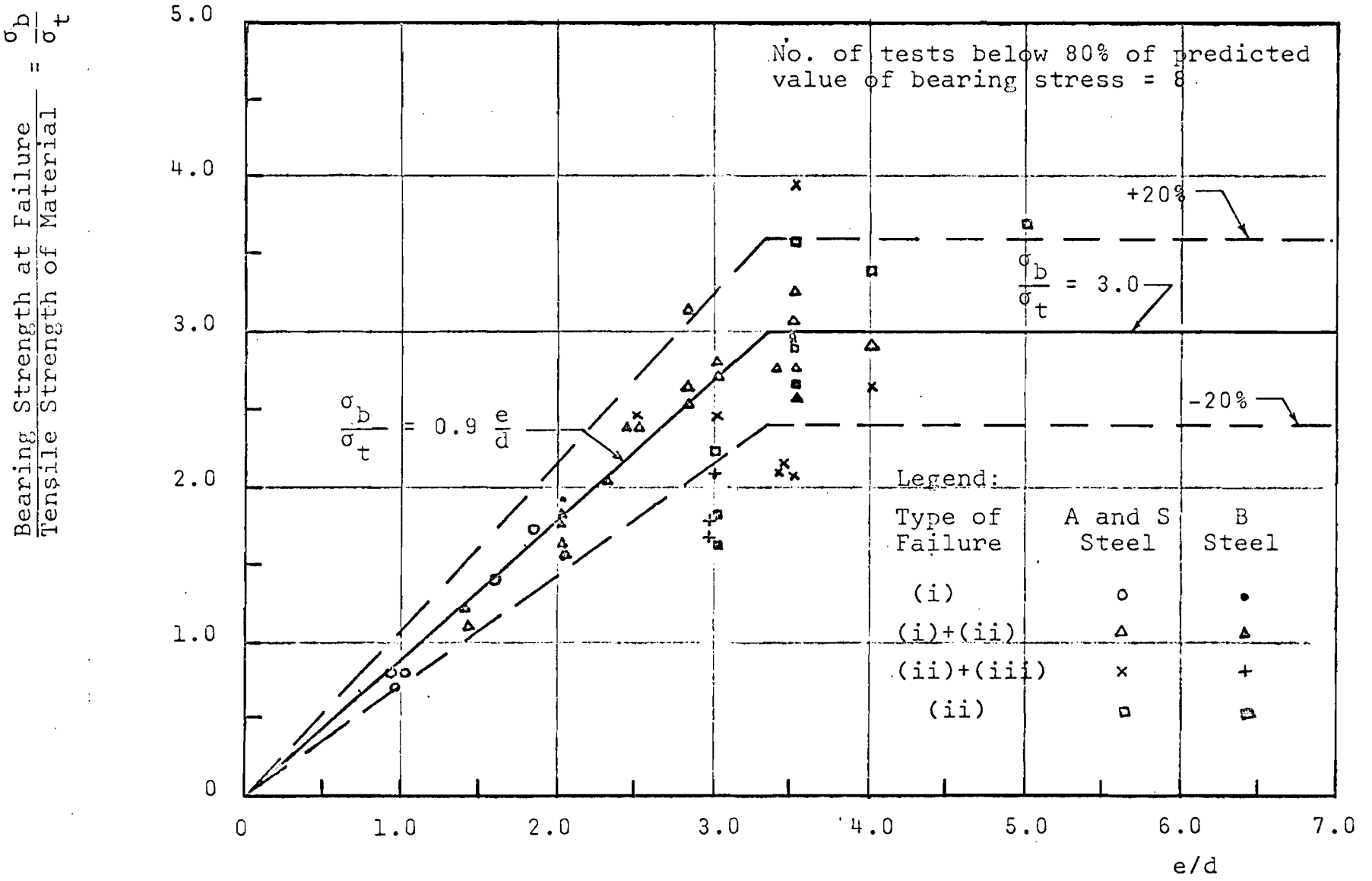

FIG. 9: BEARING AND SHEAR ON COMBINED FAILURES (LOW DUCTILITY STEEL)

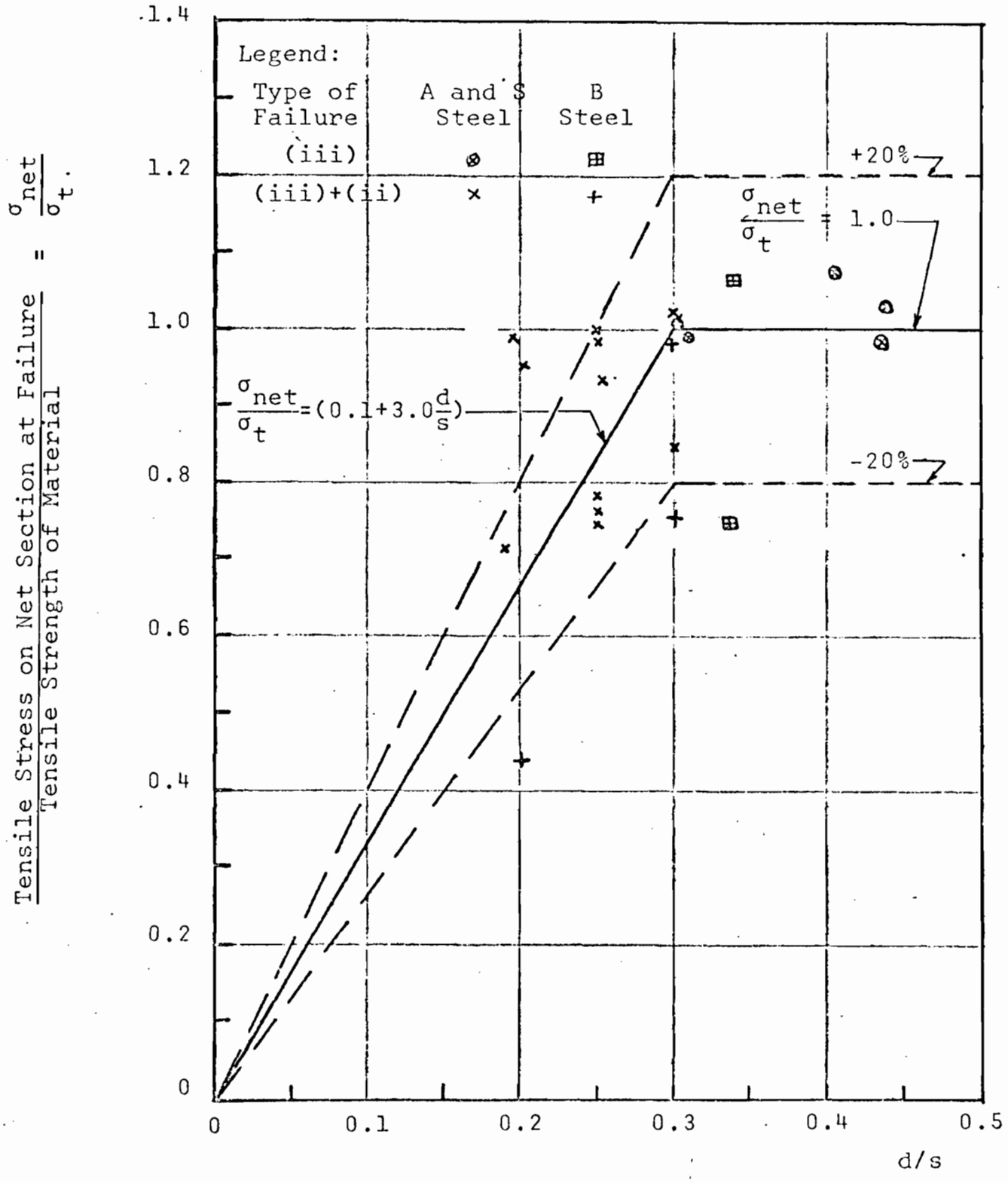

FIG. 10. TRANSVERSE TEARING OR COMBINATION OF BEARING AND TENSION FAILURES (LOW DUCTILITY STEEL)

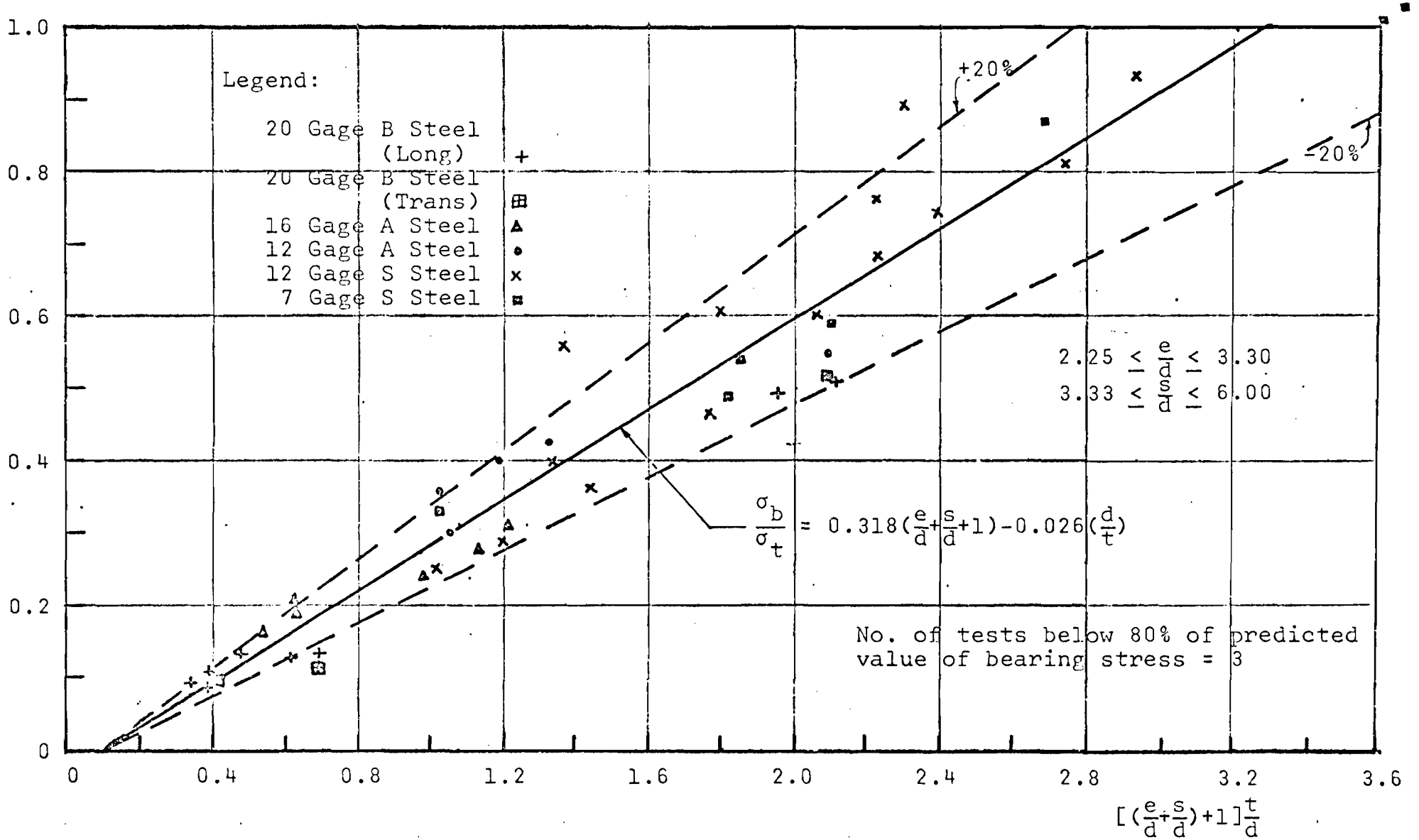

FIG. 11. ALTERNATE REPRESENTATION OF BEARING AND COMBINATION OF SHEAR AND BEARING OR TENSION AND BEARING TYPE OF FAILURE (LOW DUCTILITY STEEL)

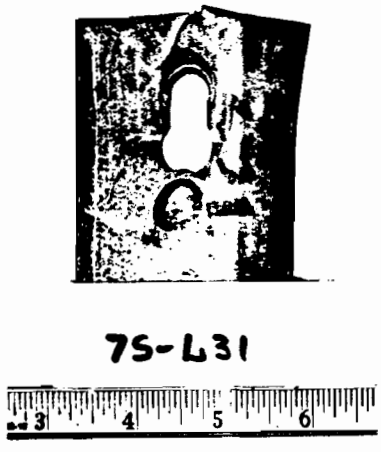

Fig. 12a. Longitudinal Shearing [Type (i) Failure (low Ductility S Steel)

Fig. 12b. Predominantly Bearing [Type (ii)] Failure (low Ductility A Steel)

Fig. 12c. Combination of Bearing and Transverse Tearing [Type (ii) + (iii)] Failure (Low Ductility A and B Steels)

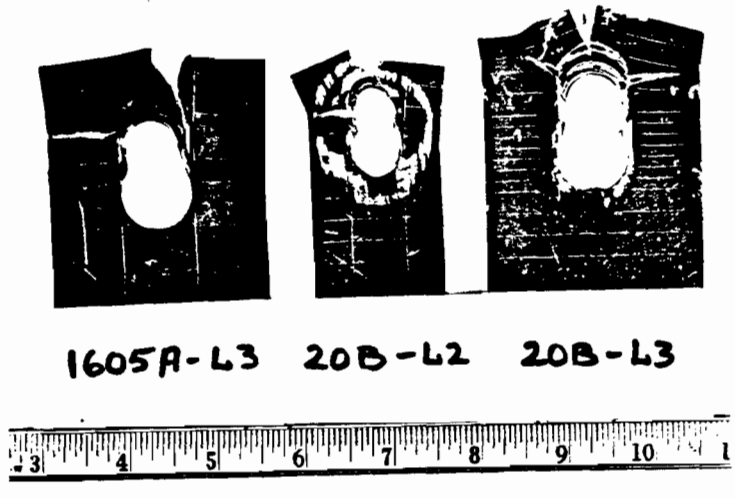

Fig. 12d. Combination of Bearing, Shear and Transverse Tearing [Type (ii) + (i) + (iii)] Failure (Low Ductility A and B Steels)

Fig. 12e. Transverse Tearing [Type (iii)] Failure (Low Ductility A and B Steels)

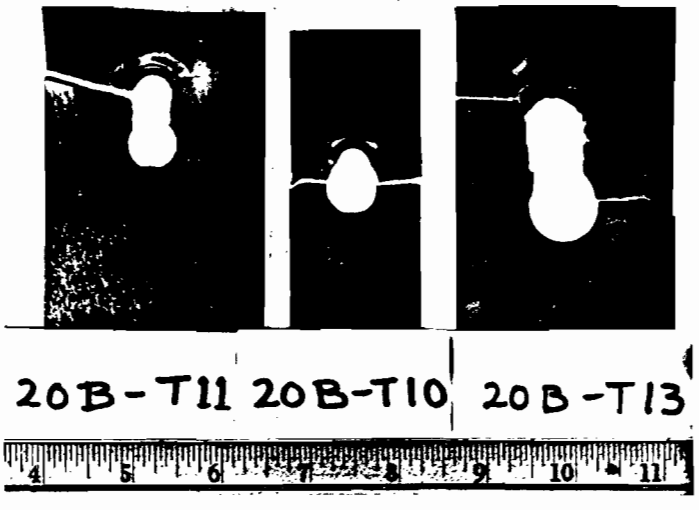

Fig. 12f. Tearing and Combination of Bearing Shear and Tearing in B Steel Specimens in the Transverse Direction

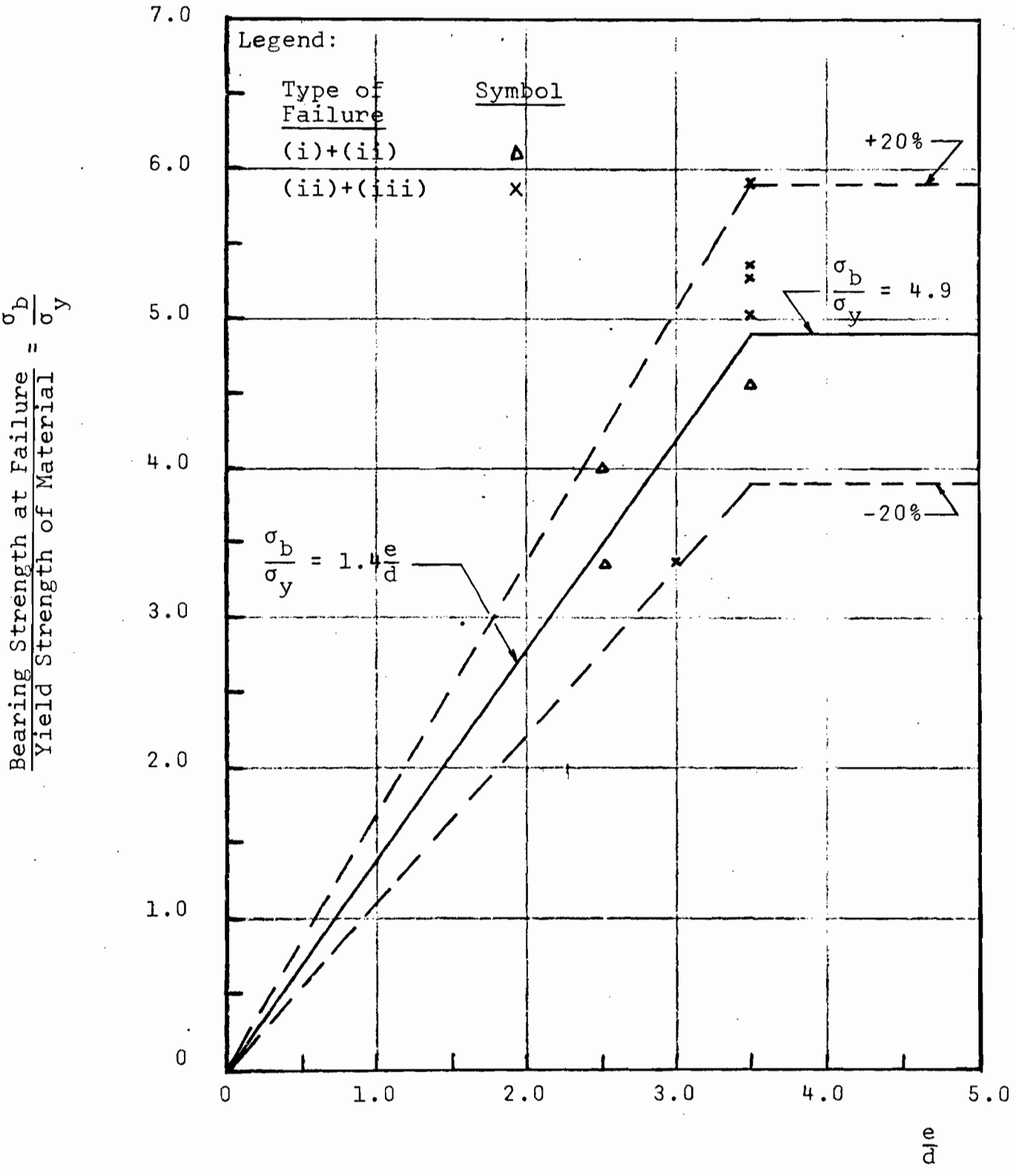

FIG. 13. BEARING AND SHEAR OR COMBINATION FAILURES (FULL ANNEALED A STEEL)

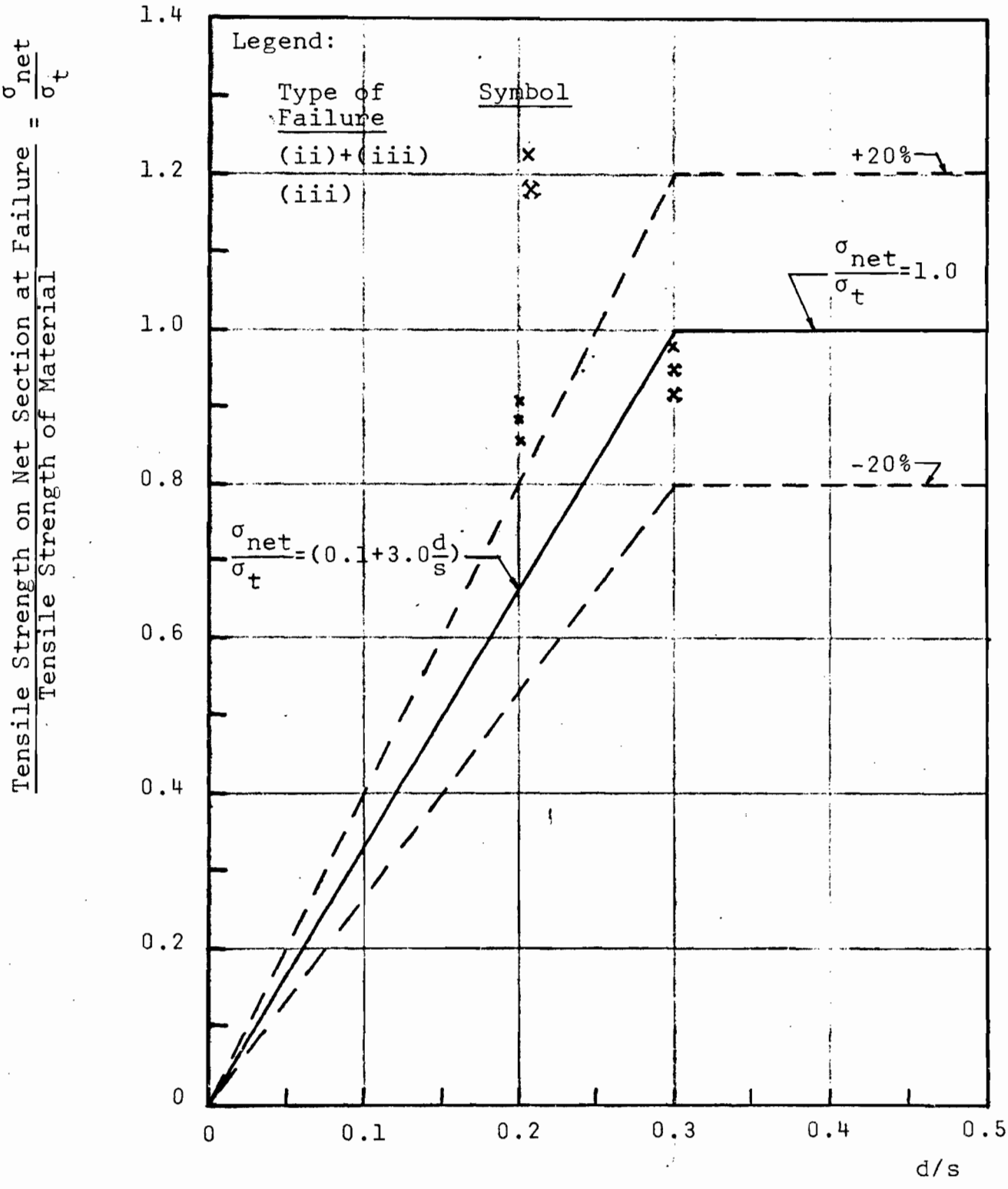

FIG. 14. TRANSVERSE TEARING OR COMBINATION OF BEARING AND TENSION FAILURES (FULL ANNEALED A STEEL)

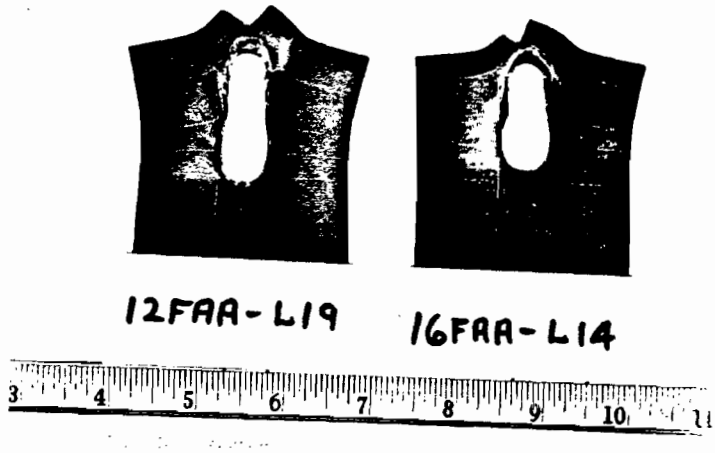

Fig. 15a. Combination of Bearing and Longitudinal Shear [Type (ii) + (i)] Failure (Full Annealed A Steel)

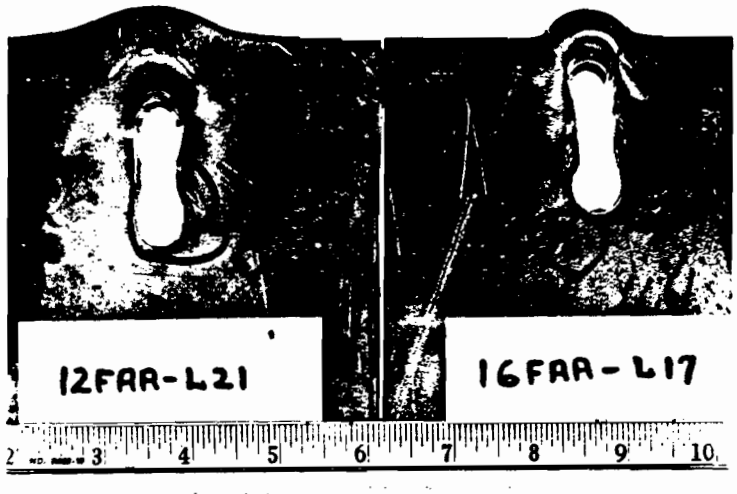

Fig. 15b. Predominantly Bearing [Type (ii)] Failure (Full Annealed A Steel)

Fig. 15c. Combination of Bearing and Transverse Tearing [Type (ii) + (iii)] Failure (Full Annealed A Steel)

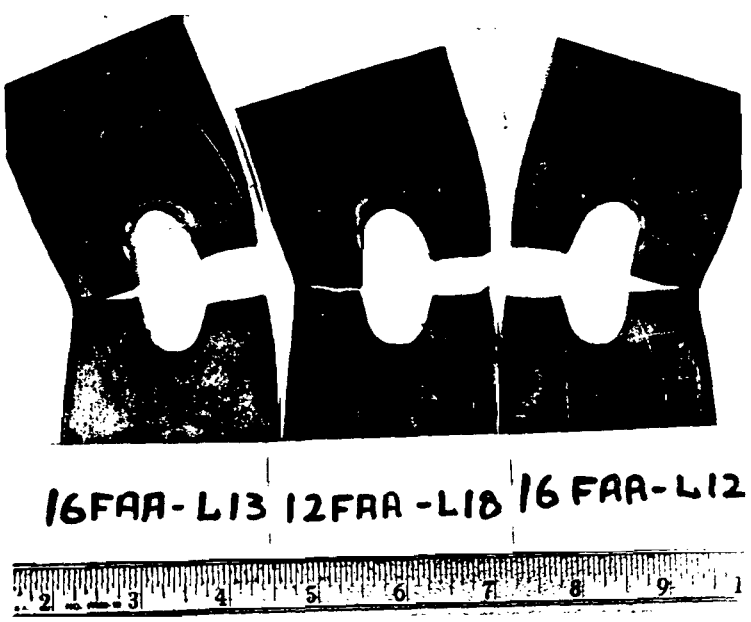

Fig. 15d. Transverse Tearing [Type (iii)] Failure (Full Annealed A Steel)

APPENDIX A

TABLES A1 to A4

TABLE A1

LENGTHWISE INELASTIC STRAIN* DISTRIBUTION AFTER FRACTURE IN RECTANGULAR PLATE WITH HOLES (TENSION SPECIMENS)

$$\% \text{ Strain} = \frac{\text{Original G.L.} - \text{Final G.L.}}{\text{Original G.L.}} \times 100$$

Section No.	Approx. Length of Section	Spec. 1210-T-L2	Spec. 1205-T-L4	Spec. 20B-T-L8
	(in)	%	%	%
P1	1/4	0.0	0.0	0.0
P2	1/4	0.5	0.0	0.0
H1	1/8	1.5	0.0	0.0
H2	1/8	5.0	0.0	0.0
H3	1/8	66.5	10.7	11.2
H4	1/8	7.9	2.6	1.0
H5	1/8	0.8	0.0	0.0
H6	1/8	0.8	0.0	0.0
P3	1/4	0.0	0.0	0.2
P4	1/4	0.5	0.0	0.0
P5	1/4	0.0	0.0	0.2
P6	1/4	0.0	0.0	0.0
P7	1/4	0.2	0.4	0.0
H7	1/8	0.4	0.0	0.0
H8	1/8	0.5	1.6	0.0
H9	1/8	23.6	54.0	9.4
H10	1/8	6.4	3.2	1.7
H11	1/8	0.4	0.8	0.0
H12	1/8	0.0	0.0	0.0
P8	1/4	0.6	0.0	0.0
P9	1/4	0.0	0.0	0.0
P10	1/4	0.0	0.0	0.1
P11	1/4	0.0	0.0	0.0
P12	1/4	0.0	0.0	0.4
H13	1/8	1.6	0.0	0.3
H14	1/8	4.0	0.4	1.7
H15	1/8	21.4	9.2	22.4
H16	1/8	2.4	1.6	0.1
H17	1/8	0.0	0.0	0.0
P13	1/4	0.0	0.0	0.2
P14	1/4	0.2	0.0	0.2

* Gage distances measured before and after the test under a travelling microscope. (Least count .0001").

Underlined values indicate maximum elongation occurring near each hole. (1/8 inch gage length).

TABLE A2

LENGTHWISE INELASTIC STRAIN* DISTRIBUTION AFTER FRACTURE IN RECTANGULAR PLATE WITH HOLES (TENSION SPECIMENS)

$$\% \text{ Strain} = \frac{\text{Original G.L.} - \text{Final G.L.}}{\text{Original G.L.}} \times 100$$

Section No.	Approx. Length of Section	Spec. 1210-T-L3	Spec. 1205-T-L5	Spec. 20B-T-18
	(in)	%	%	%
P1	1/4	0.0	0.0	0.1
P2	1/4	0.8	0.3	0.0
H1	1/8	4.0	0.4	0.0
H2	1/8	65.7	4.0	7.3
H3	1/8	1.6	0.0	0.2
H4	1/8	0.0	0.0	0.0
P3	1/4	0.2	0.0	0.0
P4	1/4	0.2	0.0	0.0
H5	1/8	2.0	0.4	0.0
H6	1/8	32.0	6.4	10.6
H7	1/8	3.2	0.4	0.0
H8	1/8	0.4	0.4	0.2
P5	1/4	0.0	0.0	0.2
P6	1/4	0.0	0.0	0.1
H9	1/8	1.6	1.2	0.0
H10	1/8	26.0	52.4	20.4
H11	1/8	3.2	1.2	0.0
P7	1/4	0.0	0.0	0.0
P8	1/4	0.0	0.0	0.0

* Gage distances measured before and after the test under a travelling microscope. (Least count .0001").

Underlined values indicate maximum elongation occurring near each hole. (1/8 inch gage length).

TABLE A3

LENGTHWISE INELASTIC STRAIN* DISTRIBUTION (AFTER FAILURE) IN SINGLE BOLTED CONNECTION SPECIMENS

(LOW DUCTILITY A AND B STEEL)

$$\% \text{ Strain} = \frac{\text{Original G.L.} - \text{Final G.L.}}{\text{Original G.L.}} \times 100$$

Section No.	Approx. Length of Section (in)	Spec. 20B-L1 (%) B Steel	Spec. 20B-L9 (%) B Steel	Spec. 1605A-L3 (%) A Steel	Spec. 1605A-L5 (%) A Steel	Spec. 1605A-L2 A Steel	Spec. 1205A-11 A Steel
H1	0.25	0.0	0.0	0.0	——	0.0	0.0
H2	0.25	12.4	11.5	5.2	0.6	19.8	26.0
H3	0.25	1.0	3.6	3.2	1.1	1.1	1.8
P1	0.50	0.0	0.5	21.4	1.4	0.0	1.5
P2	0.50	0.0	0.1	-1.8	16.2	0.0	-0.3
P3	0.50	0.4	-0.2	——	——	-0.2	0
P4	0.50	——	0	——	——	-0.4	0

* Gage distances measured before and after the test under a travelling microscope.

Underlining indicates maximum elongation occurring in the plate (1/4 inch gage length).

TABLE A4

LENGTHWISE INELASTIC STRAIN* DISTRIBUTION (AFTER FRACTURE) IN SINGLE BOLTED CONNECTION SPECIMENS

(HIGH DUCTILITY A STEEL)

$$\% \text{ Strain} = \frac{\text{Original G.L.} - \text{Final G.L.}}{\text{Original G.L.}} \times 100$$

Section No.	Approx. Length of Section (in)	Spec. 16FAA-L15 (%)	Spec. 12FAA-L18 (%)	Spec. 12FAA-L19 (%)
H1	0.25	——	11.9	——
H2	0.25	22.2	<u>131.0</u>	16.9
H3	0.25	<u>46.2</u>	22.0	<u>49.5</u>
P1	0.50	26.1	1.7	17.9
P2	0.50	-13.9	-3.2	-7.0
P3	0.50	-8.8	——	——

* Gage distances measured before and after the test under a travelling microscope.

Underlining indicates maximum elongation occurring in the plate (1/4 inch gage length).

APPENDIX B

Processing and Metallurgical History of A, S and B Steels

S Steel

7 Gage S steel was temper rolled from a coil of aluminum killed steel, AISI 1006 of original thickness of 0.281 inches to a final thickness of 0.183 inches. Approximate cold reduction was 33.8 percent. 12 gage S steel was temper rolled from a coil of rimmed steel, AISI 1005 of original thickness of 0.156 inches to a final one of 0.106 inches. Approximate cold reduction was 32.0 percent. Hardness Rockwell B for 7 gage and 12 gage steels are 90 and 79 respectively. Chemical composition by ladle analysis for the two gages is as follows:

	C	Mn	P	S	Cu	Ni	Cr	Mo	Sn	Aℓ
7 gage	0.06	.34	0.008	0.019	0.13	0.02	0.07	0.01	0.008	0.038
12 gage	0.07	.40	0.007	0.014	0.06	0.04	0.03	0.02	0.01	-

A Steel

12 gage and 16 gage A steels were cold reduced by 41 and 52 percent respectively, from a low carbon rimmed steel SAE 1008. Different annealing temperatures were used to arrive at different elongation and strength characteristics of the material used in this project. 1205A steel did not receive any annealing treatment while 1210, 12FA, 1605, 1610 and 16FA A steels were annealed at 780, 1300, 650, 900 and 1300 degrees respectively. Annealing time was one hour, while heating and cooling rates were about 50 degrees per hour. For low ductility A steels (1205, 1210, 1605 and 1610) hardness Rockwell B was 90 while for full annealed A steels (12FA and 16FA)

hardness Rockwell B was 43. Typical chemical composition of SAE 1008 steel by ladle analysis is as follows: 0.06% C, 0% S and 0.30% Mn.

B Steel

B steel is a commercial galvanized E grade low ductility steel of structural quality, and it is described in detail in ASTM specifications A446-65T. Chemical composition by ladle analysis is as prescribed below:

	C	P	S
Grade E	0.15%	0.04%	0.05%

The above percentages are the maximum permissible by ladle analysis.

CONNECTIONS IN THIN LOW-DUCTILITY STEELS

by A. K. Dhalla[1], S. J. Errera[2], M.ASCE
and G. Winter[3], F.ASCE

INTRODUCTION

The current "Specification for the Design of Cold-Formed Steel Structural Members" (1)[4] permits the use of any steel whose "properties and suitability" have been established by a recognized specification or appropriate tests. A problem exists, however, in defining what constitutes a "suitable steel" for cold-formed construction. A research program is in progress at Cornell University aimed at establishing criteria which will be helpful in solving this problem. The investigation is limited to determining the influence of two factors, (a) ductility and (b) the spread between the yield strength and tensile strength, on the behavior of cold-formed members and connections under static loading.

Ductility is the ability of a material to undergo plastic deformations without fracture. It reduces the harmful effects of stress concentrations, permits large local strains without serious damage, and helps achieve uniform stress or load distribution in members or connections. Some codes presently impose restrictions or penalties on allowable design stresses for steels which do not conform to minimum required values of ductility and tensile-yield strength ratios that have been established considering standardized materials that were readily available, and a history of satisfactory performance of those materials. With the increased availability and use of higher strength steels with lower ductility and lower tensile-yield strength ratios, there is need for more definitive information on this subject.

---

[1]Research Assistant, Department of Structural Engineering, Cornell University, Ithaca, N. Y.

[2]Associate Professor of Structural Engineering, Cornell University, Ithaca, N. Y.

[3]Professor of Engineering (Class of 1912 Chair), Cornell University, Ithaca, N. Y.

[4]Numerals in parentheses refer to the corresponding items in the Appendix. - References.

It was felt that connections may be one of the most critical problem areas for low-ductility steels. This report is concerned primarily with an investigation of bolted and welded connections which were fabricated from flat sheet and tested as part of the research program on low-ductility steels.

MATERIAL PROPERTIES

Three types of low carbon steels, designated A, B and S, were obtained for this research. Steels A and S were specially produced for the program; Steel A was cold-reduced an average of 45% in the thickness direction, to produce 12 gage (0.106") and 16 gage (0.062") material and then annealed to arrive at the desired elongation requirements in 2 inches, while S Steel was cold reduced an average of 33% to obtain 7 gage (0.183") and 12 gage (0.106") material, and received no annealing treatment. B Steel is an ASTM A446 Grade E commercial product which was obtained in 20 gage (0.038").

It is important to distinguish between the ductility of a material and the ductility of a member as fabricated and subjected to an imposed system of stresses (3). There are a number of standard tests to measure ductility of a material. Of these, the tension coupon test has special significance to a structural engineer since it supplies values for the yield and tensile strength and indicates stress-strain characteristics for static load conditions. A measure of ductility in a coupon test is the elongation at fracture in a specified gage length, usually 2 or 8 inches.

Preliminary standard coupon tests on the steels used in this investigation indicated that although the elongation in a 2-inch gage length was only 4 to 8 percent, the elongation in a 1/4-inch length ranged from 15 to 50 percent. Hence, while ductility as measured by elongation in 2" was "low", some of the materials exhibited very good local ductility.

Many years ago Unwin (7) suggested that total elongation in a bar of gage length L is made up of two parts: the first part is the uniform elongation along the bar and therefore proportional to the gage length, and the other is due to local stretching and contraction of the section which occurs at later stages of the tension coupon test. To include size effects, Unwin used Barba's Law of Similarity and suggested the following equation for strain, ε, in gage length L,

$$\varepsilon = \frac{c\sqrt{A}}{L} + b \qquad (1)$$

where b and c are constants, and A is the cross-sectional area of the specimen. To extend the range of applicability, Oliver (5) suggested the following modified form of Eq. 1:

$$\varepsilon = K\left[\frac{L}{\sqrt{A}}\right]^{\alpha} \qquad (2)$$

Eq. 2 is a straight line when plotted on a log-log scale; K is the value of strain when $L/\sqrt{A} = 1$, and α is the slope of the line. The relationship suggested by Oliver has the advantage that elongation of various size and shape tension specimens can be compared for specified $L/\sqrt{A}$; it is valid for steel as well as other materials, and the constants K and α are indicative of the physical properties of the material tested. K is the indicator of local ductility of the material, while α is a function of the strain hardening property and therefore governs the uniform ductility.

Coupons for standard tension tests were prepared as per ASTM-A370-68 specifications. Initial test speed was 0.005 in/min, which was increased to 0.02 in/min at approximately 1% strain. Load strain curves were plotted by an autographic recorder using a 2-inch gage length extensometer. Typical complete stress-strain curves are shown in Fig. 1. Curves are plotted for 12 gage A steel (1205A-L2), 16 gage A steel (1605A-L2), 20 gage B steel (20B-L5) and 12 gage S steel (12S-L2), all in the longitudinal direction; that is, for load applied parallel to the direction of rolling. The curve for 20 gage B steel in the transverse direction (20B-T2) is shown in the same figure, because it is the lowest ductility steel used in the investigation, and because the shape of the stress-strain curve is quite different from that of the same B steel in the longitudinal direction. It can be observed from Fig. 1 that the major portion of the strain in a 2-inch gage length in A or S steel occurs after ultimate load is reached, in contrast to the behavior of B steel. That is, before the necking process starts, a small amount of plastic strain is uniformly distributed over the length of A or S steel specimens, but afterwards the strain recorded in 2 inches is in effect localized at the eventual fracture zone.

Table 1 presents ductility parameters obtained from representative standard tension coupon tests on A, B and S steel, wherein reduction of area, elongation in 1/4-inch gage length (including the fracture), and K are indicators

TABLE 1

DUCTILITY CHARACTERISTICS OF A, B AND S STEELS

Ductility Parameters	2CB-L-Av. B Steel (Long.)	20B-T-Av. B Steel (Trans.)	12S-L3 S Steel (Long)	1205-L2 A Steel (Long.)	1605-L3 A Steel (Long.)	16FAA-L1 A-Annealed Steel (Long.)
Elongation in 2" (%)	4.38	1.51	5.13	5.58	6.84	52.20
Reduction in Area (%)	56.10	33.50	65.20	69.40	59.00	83.80
Tensile/Yield Ratio	1.08	1.00	1.01	1.00	1.00	1.48
Elongation in 1/4" Including Neck (%)	15.55	6.09	38.40	44.40	35.20	85.60
Elongation in 2 1/2" Excluding Neck (%)	2.74[a]	0.48	0.33	0.40	1.28	38.00
K	20.50	12.10	45.00	46.00	45.00	120.00
a	-0.579	-0.834	-0.974	-0.983	-0.795	-0.335

[a] This value is for elongation in 2", excluding neck.

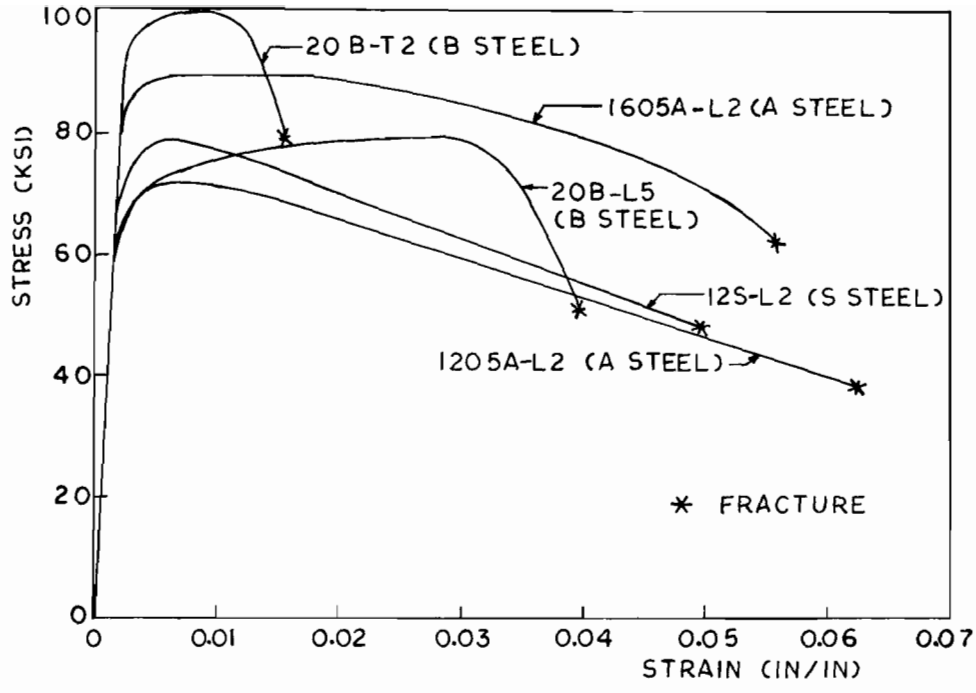

FIG. 1. COMPLETE STRESS STRAIN CURVES OF A, B AND S STEELS (2" G.L.)

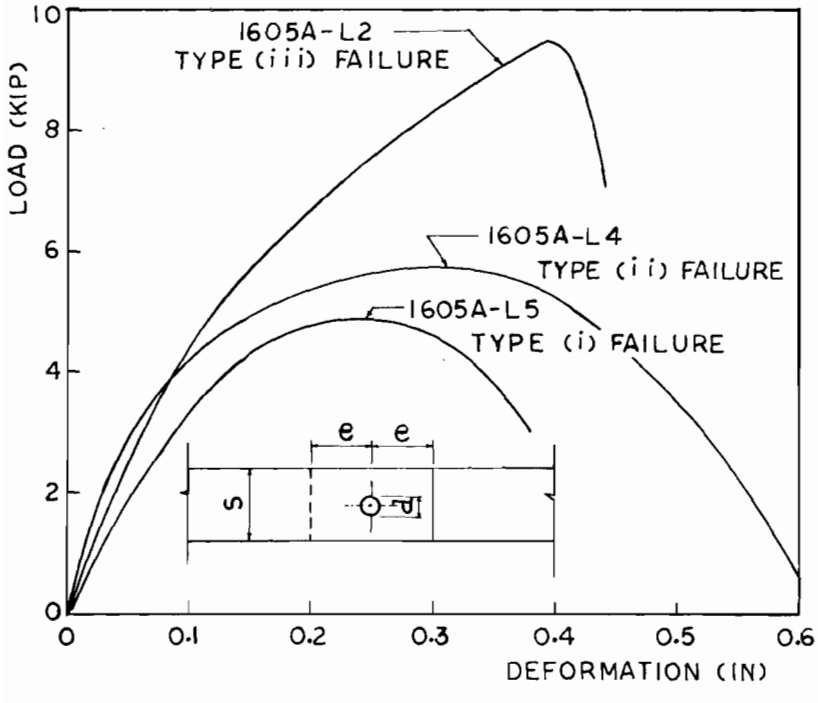

FIG. 2. LOAD-DEFORMATION CURVES, 16 GAGE 'A' STEEL BOLTED CONNECTIONS

of local ductility of the material, while tensile-to-yield strength ratio, elongation in 2 1/2-inch gage length (excluding the fracture), and α are indicators of uniform ductility. Higher algebraic values given in Table 1 indicate greater local or uniform ductility. For example, comparison of the tabulated values indicates that A and S steels have more local ductility and less uniform ductility than that observed for B steel in the longitudinal direction, as confirmed by the stress-strain curves.

Strain hardenability in a material (correlating with significant uniform ductility) can distribute yielding to areas other than where it was initiated, while sufficient local ductility can wipe out the effect of stress concentration.

PLATES WITH HOLES

To determine the behavior of the project steels under stress concentrations, tests were conducted on rectangular plates with holes. From these tests it was concluded that, except for B steel in the transverse direction, all the project steels were able to develop their full tensile strength as calculated on the net cross-sectional area; that is:

$$\frac{\sigma_{tt}}{\sigma_t} \geq 1.0 \qquad (3)$$

where σ_{tt} is the average tensile stress at P_{ult} calculated on the net area of the plate and σ_t is the tensile strength determined from a standard tension coupon. Eq. 3 indicates that for A and S steel and B steel in the longitudinal direction, the effect of the stress concentration near the hole is wiped out and the entire net section is able to fully plastify. For the two tests of B steel in the transverse direction σ_{tt}/σ_t measured 0.94, a relatively minor reduction from the full tensile strength.

BOLTED CONNECTIONS

The bolted connection is one of the critical problem areas for low ductility steels under static loading. Force is applied at the hole through the contact pressure between the bolt and the plate. This is a more severe stress concentration than that occurring in a rectangular plate with a central hole, wherein the load is applied at the ends of the plate.

A total of 59 single-bolt connection tests were conducted on low ductility steels using both single and double shear

assemblies. Specimens were made from 7 and 12 gage S steel, 12 and 16 gage A steel and 20 gage B steel. Holes were drilled 1/16" larger than the bolt diameter, and the bolt was finger tightened with washers under the head and nut. Holes were punched in a few specimens, while in some others the bolts were hand torqued; however, no significant difference in the carrying capacity of the connection was observed due to these variations. Hence all tests were combined to arrive at prediction equations for the failure load. To compare the behavior of low ductility steels with that of high ductility steels, 9 single-bolt connection tests were conducted on 12 and 16 gage full annealed A steel.

Variables considered in the program in addition to the type of steel used were: edge distance, e; bolt diameter, d; sheet thickness, t; plate width, s; and coupon tensile strength, σ_t.

All connections were tested in an hydraulic testing machine. Some selected plates were scribed at 1/4-inch intervals, and measured before and after test under a traveling microscope. All tests were conducted using an autographic recorder with an extensometer gage length of (2e + 1) inches. A sketch of a connection specimen and typical load-deformation curves are presented in Fig. 2.

Ultimate Load Formulas. Observed failure modes of both the low and high ductility steel specimens were the same as previously described by Winter (8). These are:

Type (i) -- Longitudinal shearing of the plate along two nearly parallel planes whose distance is equal to the bolt diameter

Type (ii) -- Bearing failure with considerable elongation of the hole and material "piling up" in front of the bolt

Type (iii) -- Transverse tension-tearing across the net section of the sheet.

Experimental results plotted in Fig. 3 represent shear, bearing or combinations of bearing with either shear or tension modes of failure. The ordinate is the ratio of the computed bearing stress at failure (σ_b) to the tensile strength of the material as determined from a coupon test (σ_t), and the abscissa is the ratio of the edge distance, e, to bolt diameter, d. Up to about e/d = 3.33 the bearing stress ratio increases with increasing e/d and is satisfactorily predicted

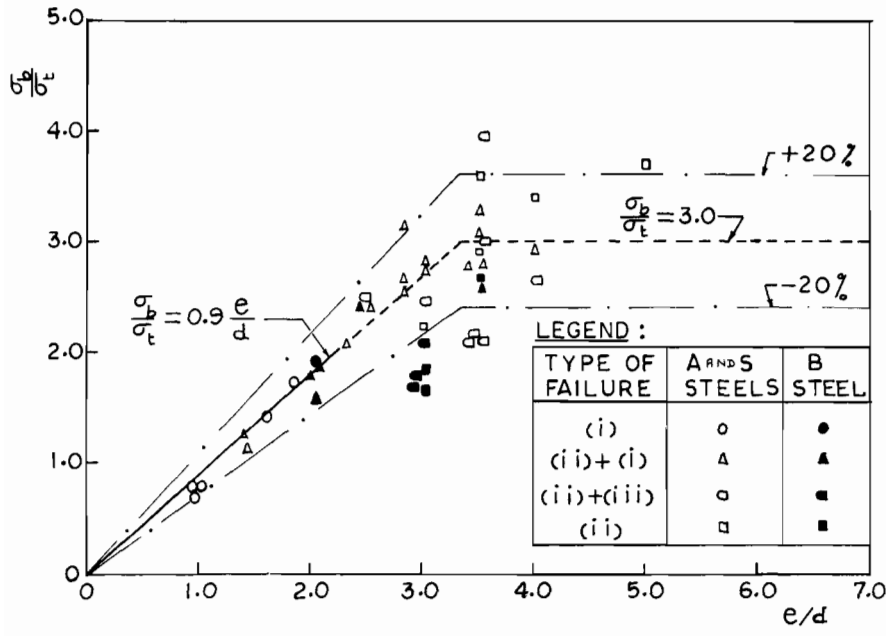

FIG. 3. BEARING AND SHEAR OR COMBINED FAILURES

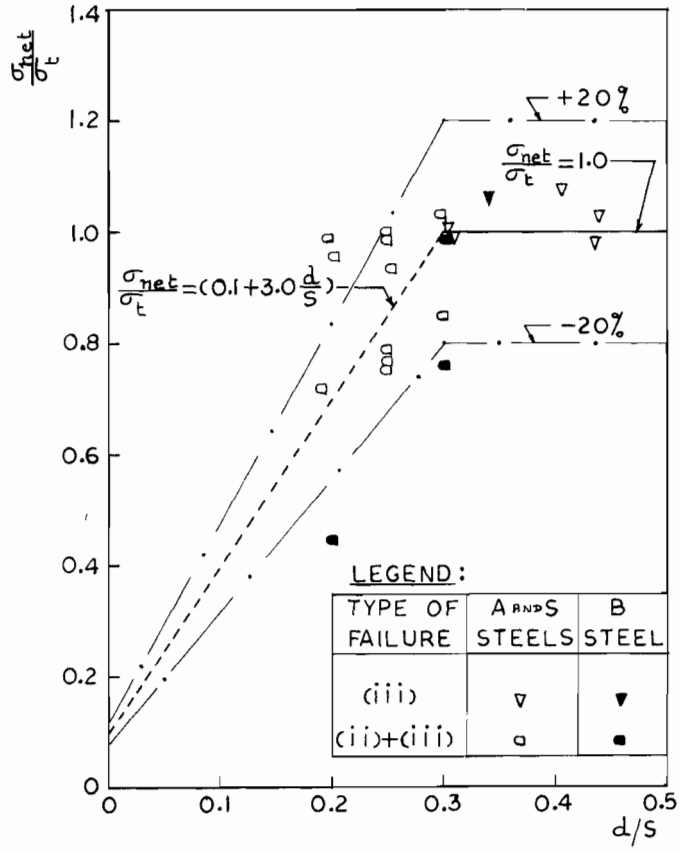

FIG. 4. TRANSVERSE TEARING OR COMBINATION FAILURES

by the equation

$$\frac{\sigma_b}{\sigma_t} = 0.9\ \frac{e}{d} \qquad (4)$$

However, for e/d greater than 3.33, the scatter of experimental values increases, and there is a greater tendency toward bearing type failures, rather than predominantly shear type, with little or no increase in bearing stress ratio. Therefore, an upper limit of 3.0 can be placed on Eq. 4. These relationships can be expressed in terms of failure loads for shear (P_s) and bearing (P_b), respectively, as

$$P_s = 0.9\ e\ t\ \sigma_t \qquad (5)$$

and

$$P_b = 3.0\ d\ t\ \sigma_t \qquad (6)$$

In Fig. 4 experimental results are plotted for tension and combined bearing and tension modes of failure. Not enough tension failures occurred in the low ductility specimens to develop an expression for the tension failure load (P_t), but the results are in fair agreement with Winter's (8) expression for high ductility steels, i.e.,

$$\frac{\sigma_{net}}{\sigma_t} = (0.1 + 3.0\ \frac{d}{s}) \leq 1.0 \qquad (7)$$

or,

$$P_t = (0.1 + 3.0\ \frac{d}{s})\ A_{net}\ \sigma_t \leq A_{net}\ \sigma_t \qquad (8)$$

where σ_{net} is the average tensile stress at failure, calculated on the net area (A_{net}) of the cross-section. In both Figs. 3 and 4 it is noted that connections using B steel, which is the thinnest material and has the lowest local ductility, tend to give lower results than the others. The maximum shear, bearing or tensile stresses according to Eqs. 5, 6 and 8 are

$$(\tau_s)_{max} = P_s/2\ e\ t = 0.45\ \sigma_t \qquad (9)$$

$$(\sigma_b)_{max} = P_b/dt = 3.0\ \sigma_t \qquad (10)$$

$$(\sigma_{net})_{max} = P_t/A_{net} = (0.1 + 3.0\ \frac{d}{s})\ \sigma_t \leq \sigma_t \qquad (11)$$

Comparison with High Ductility Steels. Results of tests of the nine full annealed A Steel connection specimens agreed with Winter's prediction equations for high ductility

steels, and are not presented here. Winter's expressions for failure stresses are recorded below for comparison with the low-ductility steel test results.

$$(\tau_s)_{max} = 0.70\ \sigma_y \tag{12}$$

$$(\sigma_b)_{max} = 4.9\ \sigma_y \tag{13}$$

$$(\sigma_{net})_{max} = (0.1 + 3.0\ \frac{d}{s})\ \sigma_t \leq \sigma_t \tag{14}$$

where σ_y is the yield stress of the material in tension. Eqs. 12 and 13 predict failure stresses in shear and bearing in terms of yield stress of the material, because this property gave best correlation with the test results. The tensile-yield strength ratio for the steels in those tests averaged about 1.35. Applying this factor to Eqs. 12 and 13, the shear and bearing failure stresses for the high ductility steels can be expressed as $\tau_s = 0.52\ \sigma_t$ and $\sigma_b = 3.6\ \sigma_t$. In contrast, for low ductility steels Eqs. 9 and 10 show $\tau_s = 0.45\ \sigma_t$ and $\sigma_b = 3.0\ \sigma_t$. Thus, the shear and bearing strength of low ductility steel, in terms of σ_t, is somewhat lower than for high ductility steel, while the tensile strength in the net section seems unaffected by the lower ductility.

Comparisons of high and low ductility steel also have been made for connections with two or three bolts in line with the applied stress (6). Here too it was found that the tensile strength of the connection was unaffected by the ductility of the steel.

Alternate Prediction of Ultimate Load (2). There is a fair amount of scatter in the test results shown in Fig. 3, particularly when combined failure modes are involved; hence alternate predictions of the failure load were sought. Functional dependence of the ultimate load, P_{ult}, on the variables considered can be obtained using dimensional analysis (4). For a single-bolt connection, the relationship can be expressed as

$$\frac{P_{ult}}{\sigma_t d^2} = f_1\left(\frac{\sigma_b}{\sigma_t}, \frac{\tau_s}{\sigma_t}, \frac{e}{d}, \frac{s}{d}, \frac{t}{d}\right) \tag{15}$$

If the bearing stress σ_b and the shear stress τ_s are assumed to be proportional to the tensile strength σ_t of the material, then Eq. 15 reduces to

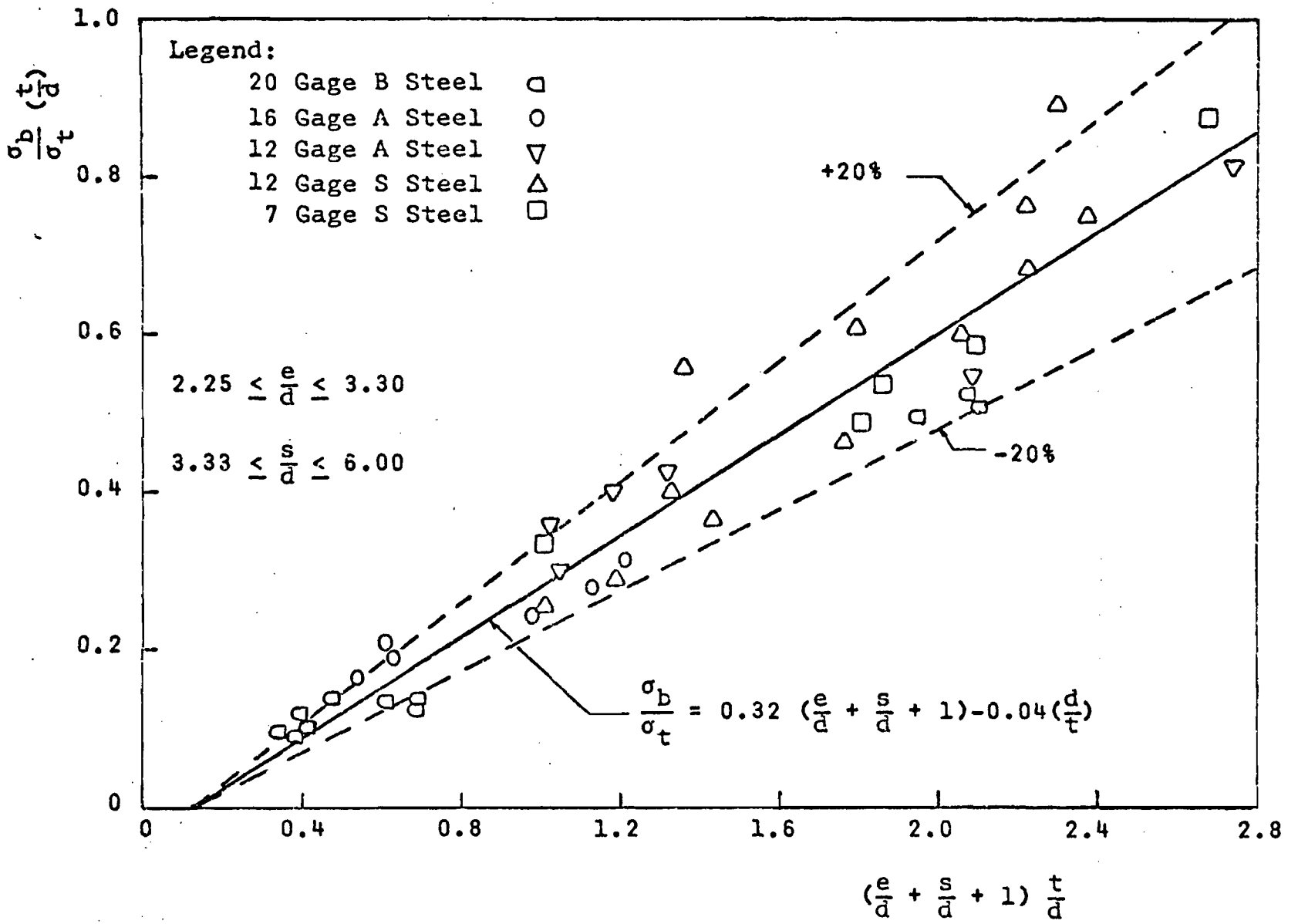

FIG. 5. ALTERNATE REPRESENTATION OF BEARING OR COMBINATION OF SHEAR AND BEARING OR TENSION AND BEARING TYPE OF FAILURES.

$$\frac{P_{ult}}{(td)} \frac{(td)}{\sigma_t d^2} = \frac{\sigma_b}{\sigma_t} \left(\frac{t}{d}\right) = f_2 \left(\frac{e}{d}, \frac{s}{d}, \frac{t}{d}\right) \qquad (16)$$

This expression can be modified further, with due recognition of limiting conditions, to obtain predictions of the form presented earlier for shear or tension failures. In addition, using a trial and error approach to provide a best fit to the data and to evaluate numerical coefficients, the following expression for bearing or combined failures was obtained:

$$P_c = 0.32 \left(\frac{e}{d} + \frac{s}{d} + 1\right) - 0.04 \frac{d}{t} \qquad (17)$$

provided $2.25 \leq \frac{e}{d} \leq 3.30$

and $3.33 \leq \frac{s}{d} \leq 6.00$

This prediction is plotted in non-dimensional form along with the pertinent data in Fig. 5. The prediction error is reduced an average of about 25% compared to Eqs. 5 and 6, at the cost of additional complexity.

FILLET WELDED CONNECTIONS

Variables considered in the tests of longitudinal and transverse fillet weld connections included: length of weld, L; thickness of material, t; and type of steel. For the low ductility steel specimens where the tensile strength of the material ranged from 75 to 100 ksi, low hydrogen welding electrode E-10018 (ASTM designation A-316) was used. A few tests were made on full annealed A steel specimens (12FAA) using low hydrogen E-7018 electrodes. To facilitate the welding process the connection specimens were clamped on a steel table, which also served as a heat sink. Voltage was held constant at 25 volts, and current input was varied for the different sheet thicknesses to obtain a satisfactory weld without undercutting the material. The current as recorded by an ammeter was 120, 120, 85 and 60 amps, respectively, for 7, 12, 16 and 20 gage sheets.

LONGITUDINAL FILLET WELD CONNECTIONS

Fig. 6 shows a sketch of the longitudinal fillet weld connections. The width of the narrower plate, b_n, was 3.0" for all except the 7S and 12FAA specimens, where b_n was 2.5" and 4.0" respectively. The width of the other plate, b_w, was 1

inch greater than b_n to facilitate welding. Table 2 gives the weld lengths along with the average mechanical properties of the material. The eighteen specimens were divided into three groups: Group I specimens were designed to fail in tension in the plate, called type "a" failure. Group II specimens were designed to produce shear failure in the weld, called type "b" failure. Group III specimens were designed so that either type of failure was equally likely.

Tension tests were conducted in an hydraulic testing machine, and load-deformation curves were autographically recorded for a gage length of (L + 3) inches. The results are presented in Table 2. The following observations are made:

(1) All the specimens in Group I, which had the longest weld length, failed by transverse tearing of the narrower plate (type "a" failure). Group II specimens which had the shortest weld length, failed by shearing of the weld (type "b"), except for the full annealed specimen which exhibited a combined type failure. In Group III, the failures were about evenly divided.

(2) For the low ductility steel specimens that failed in tension, the ratio of the tensile strength developed by the plate, σ_{tt}, to the tensile strength of the coupon, σ_t, ranges from 0.89 to 1.05, and averages 0.96. This compares favorably with the corresponding value of 0.88 for the specimen of full annealed material (12FAA-L6) which failed in tension, and indicates that connections made with low ductility steel were able to develop almost the full strength of the narrower plate. Considerable out-of-plane deformation occurred in Specimen 12FAA-L6 (and other full-annealed specimens) after the yield load was reached; this may have reduced the resulting ultimate carrying capacity.

(3) For type "b" failures, comparison can be made between the computed shear strength of the weld and the expected shear strength of the weld, where the expected shear strength is assumed to be 0.577 times the minimum tensile strength of the weld metal as specified by ASTM. This ratio ranges from 0.99 to 1.05 for Group II specimens of low ductility steel except for 1205A-L9 which may have had a defective weld. The same ratio for Type "b" failures in Group III specimens ranges from 0.94 to 0.98. That is, the shorter welds of Group II apparently had more uniform stress distribution, and thus higher average stresses, than the longer welds of Group III.

(4) For Group I specimens which failed in tension, the local ductility parameter (elongation in 1/4-inch gage

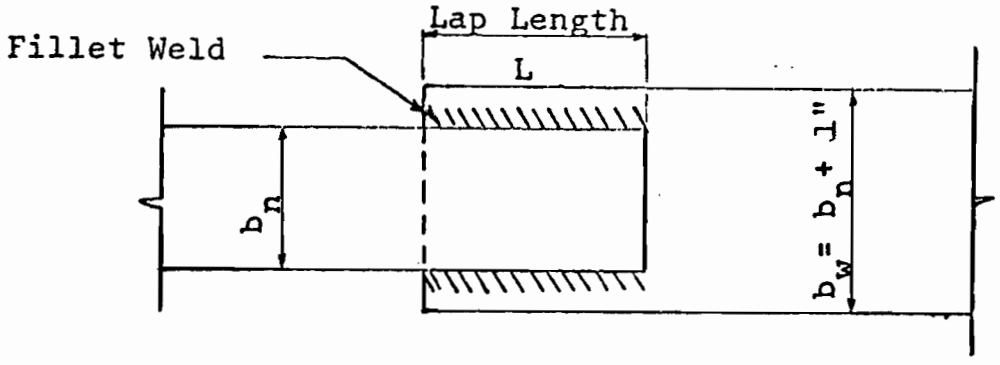

FIG. 6. SINGLE LAP LONGITUDINAL FILLET WELD CONNECTION.

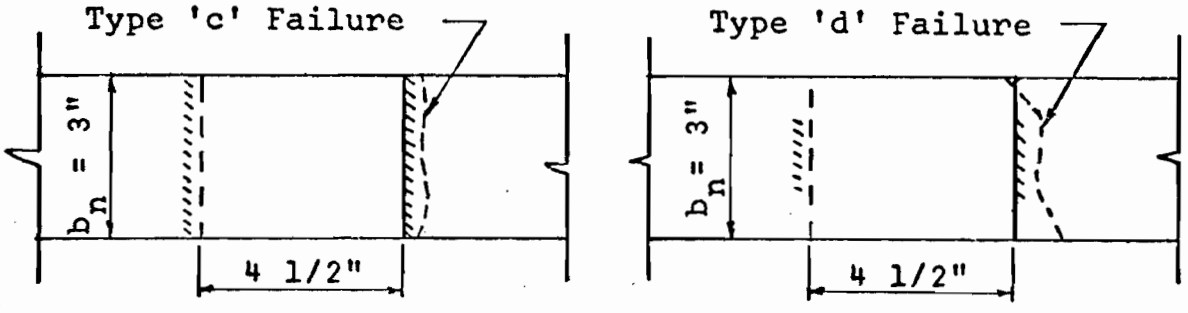

a. Single Lap, Full Length Weld (TF).

b. Single Lap, Partial Width Weld (TP).

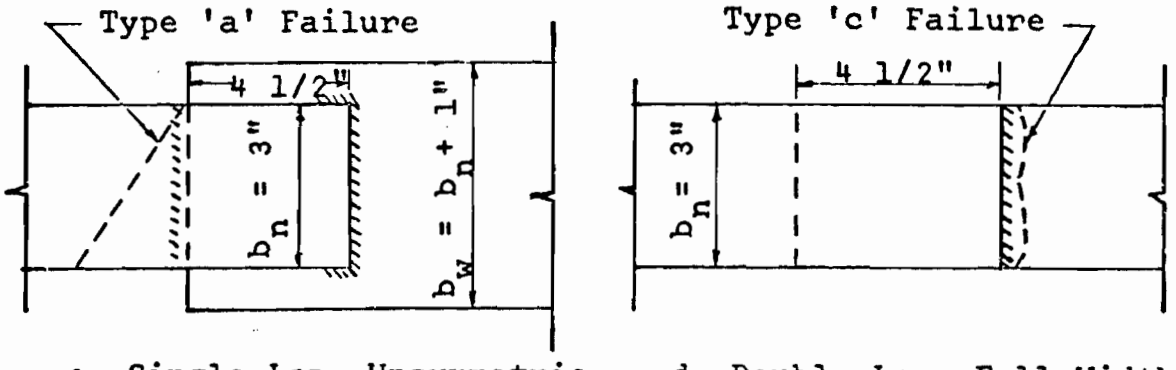

c. Single Lap, Unsymmetric Weld (TU).

d. Double Lap, Full Width Weld (TD).

FIG. 7. TRANSVERSE FILLET WELD SPECIMENS.

TABLE 2
LONGITUDINAL FILLET WELD CONNECTIONS

1	2	3	4	5	6	7	8	9	10	11
		Avg. Mat'l Properties			Experimental Results					
Spec. Designation**	Lap Length L in	Tensile Str. of Coupon σ_t ksi	Elong in 1/4" G. L. %	Shear Str.of Electrode* τ_{sa} ksi	Tensile Str.of Plate σ_{tt} ksi	Shear Str.of Weld τ_{su} ksi	$\frac{\sigma_{tt}}{\sigma_t}$	$\frac{\tau_{su}}{\tau_{sa}}$	Elong. in 1/4" G. L. %	Mode of Failure type
GROUP I SPECIMENS										
7S-L-L1	3.25	83.3	47.0	57.7	83.7	45.5	1.00	0.78	49.8	a
12S-L-L2	3.25	82.5	31.4	57.7	78.8	51.0	0.96	0.88	27.6	a
1205A-L-L3	3.25	84.1	29.9	57.7	79.0	51.6	0.94	0.89	32.4	a
1605A-L-L4	3.75	98.0	26.6	57.7	87.8	50.2	0.89	0.87	21.7	a
20B-L-L5	3.50	81.7	15.5	57.7	86.0	52.2	1.05	0.90	12.0	a
12FAA-L-L6	3.75	45.0	105.0	40.4	39.9	29.5	0.88	0.73	102.0	a
GROUP II SPECIMENS										
7S-L-L7	2.25	83.3	47.0	57.7	73.8	58.4	0.88	1.01	16.8	b
12S-L-L8	2.25	82.5	31.4	57.7	60.8	57.5	0.74	0.99	8.8	b
1205A-L-L9	2.25	84.1	29.9	57.7	50.2	47.6	0.60	0.82	38.8	b
1605A-L-L10	2.75	98.0	26.6	57.7	75.7	58.8	0.77	1.02	--	b
20B-L-L11	2.50	81.7	15.5	57.7	62.2	53.0	0.76	0.92	--	b
12FAA-L-L12	1.50	45.0	105.0	40.4	22.7	42.8	0.51	1.06	25.6	a+b
GROUP III SPECIMENS										
7S-L-L13	2.75	83.3	47.0	57.7	82.0	52.6	0.98	0.91	20.2	a
12S-L-L14	2.75	82.5	31.4	57.7	70.0	54.1	0.85	0.94	--	b
1205A-L-L15	2.75	84.1	29.9	57.7	70.5	56.6	0.84	0.98	--	b
1605A-L-L16	3.25	98.0	26.6	57.7	85.7	56.4	0.87	0.97	5.6	b
20B-L-L17	2.85	81.7	15.5	57.7	74.3	55.4	0.91	0.95	--	a
12FAA-L-L18	2.00	44.6	105.0	40.4	28.2	38.6	0.63	0.95	24.6	a+b

*Computed as 0.577 x ASTM specified minimum tensile strength.

**Load was applied parallel to the direction of rolling.

length, Col. 10) is in satisfactory agreement with the values obtained in the tension coupon tests (Col. 4).

TRANSVERSE FILLET WELD CONNECTIONS

The high strength of the low carbon A, B and S steels was achieved by cold working. Therefore, it was anticipated that partial annealing of these low ductility steels due to weld heat would reduce the tension strength of the transverse fillet weld connections shown in Fig. 7. Unlike a longitudinally welded specimen, the whole cross-section of a full width transverse weld specimen is partially annealed. For a partial width weld, only the part of the cross-section that is welded would be affected. The reduction in strength would depend upon the length of weld on the critical cross-section and the details of the welding procedure.

The transverse fillet weld specimens were divided into four groups as indicated below and in Table 3 and Fig. 7.

Group IV: single lap, full width welds

Group V: single lap, partial width welds

Group VI: single lap, full width unsymmetrical welds

Group VII: double lap, full width welds

Seventeen transverse fillet weld specimens were designed using 7 and 12 gage S steel, 12 and 16 gage A steel, and 20 gage B steel. Duplicate specimens were made; but for brevity, only 7 gage S, 12 gage A and 20 gage B tests are presented in Table 3. However, the observations made subsequently apply to all 34 specimens tested. The test procedure for the transverse weld specimens was the same as for the longitudinally welded connections.

All specimens in Groups IV, VI and VII failed by transverse tearing of the connected plate. Tension failure in these specimens is designated by types "a", "c" and "d" in Fig. 7 and Table 3, to differentiate between the different modes of tension tearing. Type "a" failure gives an inclined fracture, which is the same as that observed in longitudinally welded specimens. Type "c" failure follows the contour of the fillet weld toe. Type "d" failure occurred in some of the partial width weld specimens; it follows the contour of the toe for the length of the weld, and is inclined in the unwelded portions of the plate. Three

TABLE 3
TRANSVERSE FILLET WELD CONNECTIONS[1]

1	2	3	4	5	6
Specimen Designation[p]	Total Length of Weld L in	Tensile Str. of Coupon σ_t ksi	Experimental Results: Tensile Str. of Plate σ_{tt} ksi	$\frac{\sigma_{tt}}{\sigma_t}$	Mode of Failure Type[m]
GROUP IV - FULLY WELDED SPECIMENS					
20B-TF-L11	6.04	81.7	70.0	0.86	c
20B-TF-L12	6.02	81.7	68.3	0.84	c
1205A-TF-L31	6.02	74.6	66.5	0.89	c
1205A-TF-L32	6.02	74.6	67.2	0.91	c
7S-TF-L51	6.00	86.3	80.9	0.94	c
7S-TF-L52	6.00	86.3	80.9	0.94	a
GROUP V - PARTIALLY WELDED SPECIMENS					
20B-TP-L11	3.50	81.7	75.1	0.92	d
20B-TP-L12	3.60	81.7	77.0	0.94	d
1205A-TP-L31	3.64	74.6	73.7	0.99	d
1205A-TP-L32	3.08	74.6	73.1	0.98[n]	b
7S-TP-L51	3.60	86.3	73.4	0.85[n]	b
7S-TP L52	3.44	86.3	71.8	0.83[n]	b
GROUP VI - UNSYMMETRICALLY WELDED SPECIMENS					
20B-TU-L11	6.02	81.7	71.5	0.87	c
20B-TU-L12	6.02	81.7	72.3	0.88	c
1205A-TU-L31	6.02	74.6	70.3	0.94	c
1205A-TU-L32	6.02	74.6	70.9	0.95	c
7S-TU-L51	6.00	86.3	82.0	0.95	a
7S-TU-L52	6.00	86.3	82.5	0.96	a
GROUP VII - DOUBLY LAPPED SPECIMENS					
20B-TD-L11	6.02	81.7	70.3	0.86	c
20B-TD-L12	6.02	81.7	69.0	0.84	c
7S-TD-L51	6.00	86.3	82.0	0.95	a
7S-TD-L52	6.00	86.3	81.5	0.94	c

[1] Geometry of the specimens is shown in Fig. 7.

[m] Modes of failure are indicated by dotted lines in Fig. 7.

[n] $\frac{\tau_{su}}{\tau_{sa}}$ ratios for specimens 1205A-TP-L32, 7S-TP-L51 and and L-52 are 1.73, 1.48, and 1.55 respectively.

[p] Load was applied parallel to the direction of rolling.

of the partial width weld specimens included in Table 3 failed in the weld (type "b" failure), and three had type "d" failures.

The predicted maximum load for a plate of thickness t and width b_n is given by

$$P_{max} = b_n \, t \, \sigma_t \qquad (18)$$

where σ_t is the tensile coupon strength of the material. The ratio of the tensile strength developed by the connected plate, σ_{tt}, to the tensile coupon strength σ_t is given in Col. 5 of Table 3. This ratio is between 0.84 and 0.96 for all of the Group IV, VI and VII specimens (full width welds) which failed by tension tearing. Within any one group, the ratio increases with increasing thickness of the material. The double lap specimens of Group VII have about the same strength ratio as Group IV and VI specimens, indicating that the small strength reduction of approximately 10% due to some annealing is caused by only one pass of the welding electrode, and subsequent welding on the same cross-section does not reduce the tension strength any further.

The partial width weld specimens of Group V which failed in tension had σ_{tt}/σ_t ratios of 0.92 to 0.99, averaging slightly higher than the full width weld specimens. Apparently only that part of the cross section which was welded had its strength somewhat reduced by partial annealing, while the part which was not welded developed tensile strength close to that obtained in the coupons.

Two high-ductility A steel transverse fillet weld specimens in Groups IV and V were tested to compare their behavior with low ductility specimens. There was no reduction in the strength of these connections due to the welding process.

SUMMARY AND CONCLUSIONS

Bolted and fillet welded connections in thin low-ductility steels were tested as part of a research program investigating the influence of ductility on the behavior of cold-formed members under static loading. In dealing with such steels it appears necessary to distinguish between uniform ductility and local ductility. Uniform ductility is characterized by the ability of a member made of the subject material to undergo sizeable plastic deformations over significant portions of its length, prior to failure. Such ductility is attained if a material possesses a significant strain hardening range. On the other hand, local ductility is the ability to

undergo plastic deformation in a localized area. Most of the "low ductility" steels investigated herein showed significant local ductility.

The modes of failure and simplified formulas obtained for single-bolt connections are similar for low and high ductility steels. In terms of coupon tensile strength σ_t, maximum shear and bearing stress values for low ductility steels are 0.45 σ_t and 3.0 σ_t, respectively. Corresponding values for high ductility steels are 0.52 σ_t and 3.6 σ_t respectively, indicating that the low ductility of these special steels lowered the strength of the tested bolted connections only by about 15% in terms of the coupon tensile strength. Bolted connections of low ductility steel showed adequate elongation capability.

The low ductility steels were weldable; that is, no special welding process was used in fabricating the specimens, nor were any noticeable defects observed. In longitudinal fillet weld specimens with adequate weld length, the connections developed almost the full predicted load based on coupon tensile strength. Both plate failure and weld failure of longitudinal fillet weld connections in these low ductility steels can be predicted using the same methods as for high ductility steel.

Transverse fillet weld specimens showed some effect of partial annealing, but still developed an average stress of more than 90% of the coupon tensile strength.

ACKNOWLEDGMENTS

This research was sponsored by the American Iron and Steel Institute. The cooperation of the cognizant research committee, and of the companies who furnished the steels for the investigation, is gratefully acknowledged.

APPENDIX - REFERENCES

1. American Iron and Steel Institute, "Specification for the Design of Cold-Formed Steel Structural Members," 1968 Edition, N. Y.

2. Dhalla, A. K., "Influence of Ductility on the Structural Behavior of Cold-Formed Steel Members", Dept. of Structural Engineering Report No. 336, Cornell University, Ithaca, N.Y. (to be published).

3. Frankland, J. M., "Physical Metallurgy and Mechanical Properties of Materials: Ductility and the Strength of Metallic Structures," Proc. ASCE, Vol. 86, No. EM6, Dec. 1960.

4. Murphy, G., "Similitude in Engineering," The Ronald Press Co., N. Y., 1950.

5. Oliver, D. A., "Proposed New Criteria of Ductility from a New Law Connecting the Percentage Elongation to the Size of Test Piece," Inst. of Mech. Engineers, Vol. II, 1928.

6. Popowich, D. W., "Tension Capacity of Bolted Connections in Light Gage Cold-Formed Steel," thesis presented to Cornell University, in 1969, in partial fulfillment for the requirements of the degree of Master of Science.

7. Unwin, W. C., "Tensile Tests of Mild Steel, and the Relation of Elongation to the Size of the Test Bar," Proc. Inst. of Civil Engineers, 1903.

8. Winter, G., "Tests on Bolted Connections in Light Gage Steel," Proc. ASCE, Vol. 82, Paper No. 920, March 1956.

THE EFFECTIVE UTILIZATION OF YIELD STRENGTH

by

J. H. Gross

Applied Research Laboratory
U. S. Steel Corporation
Monroeville, Pennsylvania

For presentation at a Seminar sponsored by the West Scotland Iron and Steel Institute, to be held in Glasgow, Scotland, on May 15, 1970, and for subsequent publication by the Institute.

Introduction

Any comprehensive discussion of high-yield-strength steels must include consideration of designs that are based on the yield strength. This arises because the ratio of the yield strength to the tensile strength increases from about 0.65 at a tensile strength of 60 ksi to about 0.95 at a tensile strength of 260 ksi, Figure 1. Consequently, a design stress based on some percentage of the yield strength would be almost 50 percent greater (0.95/0.65) for the 260-ksi steel than that based on a similar percentage of the tensile strength. The increase would be less for lower strength steels (about 30 and 45 percent, respectively, for 100-ksi and 200-ksi yield-strength steels), but would still be extremely attractive.

The advantage that could be realized is illustrated in Figure 2, which compares the design stress for various design criteria that are in use or have been considered for the ASME Boiler and Pressure-Vessel Code. For the most commonly used criterion, Curve A, the design stress is based on 5/8 of the yield strength for yield-tensile ratios less than 0.4, and on 1/4 of the tensile strength for yield-tensile ratios greater than 0.4. The dividing ratio of 0.4 is determined by equating the yield-strength and tensile-strength criteria as follows:

$$5/8\ YS = 1/4\ TS$$

$$\frac{YS}{TS} = \frac{1}{4} \times \frac{8}{5} = 0.40$$

As shown by Curve A, this criterion is based entirely on tensile strength, and permits no advantage for an increase in the yield-tensile ratio be-

cause the yield-tensile ratio never falls below 0.4, even for the lowest strength steels, Figure 1. The criterion described by Curve B, Figure 2 (2/3 of the yield strength or 1/3 of the tensile strength, whichever is less) extends yield strength as the controlling criterion to a yield-tensile ratio of 0.5. However, this criterion also permits no advantage for an increase in the yield-tensile ratio because the yield-tensile ratio falls below 0.5 only for steels with tensile strengths less than 40 ksi, which are unimportant for structural applications. Curve C, Figure 2 illustrates the advantage in design stress that would result if the yield strength and tensile strength were equally weighted over the full range of yield-tensile ratios. Even more attractive would be a design stress based entirely on yield strength, Curves D and E. Compared with design stresses based on the Curve C criterion, the design stresses are higher for Curve D for yield-tensile ratios greater than 0.67, and for Curve E for yield-tensile ratios greater than 0.60, which correspond to tensile strengths greater than 60 and 50 ksi, respectively, both of which cover essentially the range of interest for structural steels.

The practicality of effectively utilizing the increasing yield-tensile ratio of structural steels with increasing tensile strength depends upon the ability of the steels to be satisfactorily fabricated and to perform satisfactorily in service. The present paper summarizes studies on the effect of the yield-tensile ratio on the fabricability (forming and welding) of high-yield-strength steels and on the service performance

of these steels (their resistance to failure by bursting, brittle fracture, fatigue, or stress corrosion), with particular emphasis on plate steels and on applications such as pressure vessels.

Fabricability

Formability

The ability to form plates or other structural products into useful configurations, usually under plane-strain conditions (width more than eight times thickness), is an important requisite for structural materials. In assessing the effect of yield strength on plane-strain ductility, Clausing[1)]* showed that the true strain at cracking in a plane-strain bend test decreases continuously as the yield strength increases, Figure 3. If the values of true strain corresponding to the average curve are converted to the ratio of bend diameter to plate thickness (D/t), the bend diameter at cracking is seen to increase from about 1t at a yield strength of 50 ksi, to about 1.5t, 2t, and 3t at 100, 150, and 200 ksi, respectively. To form these materials without danger of cracking, the minimum bend diameter should be about double that at cracking. Thus, an increase in bend diameter from about 2t to 6t would appear to be appropriate for an increase in yield strength from 50 to 200 ksi. Although this is a significant increase in bend diameter with yield strength, it should not unduly limit the use of high-strength steels as long as the requirement is recognized.

Weldability

The yield strength of ferritic steels influences their weldability through effects on both the heat-affected zone (HAZ) and the weld

*See References.

metal. However, the effects on weld metal are considered beyond the scope of this paper. Thus, comments will be confined to the effect of yield strength on the soundness and mechanical properties of the HAZ.

Defects in the HAZ usually occur when the HAZ has transformed to martensite and when the hydrogen content of the HAZ is relatively high. Under these conditions, cracks (called cold cracks) can occur in the HAZ and subsequently propagate to cause failure. The most important factor contributing to HAZ cold cracking is the carbon and alloy content of the steel. This combined effect can be expressed quantitatively in terms of the carbon equivalent (CE). As the CE increases, the susceptibility to cold cracking increases. One of the more common equations for calculating the CE is as follows:

$$CE = \%C + \frac{\%Mn}{4} + \frac{\%Ni}{20} + \frac{\%Cr}{10} - \frac{\%Mo}{50} - \frac{\%V}{10} + \frac{\%Cu}{40}$$

In general, an increase in yield strength is achieved by increasing the carbon and alloy content, which usually increases the CE, and therefore, the susceptibility to HAZ cold cracking, Table I. However, further examination of the table indicates that the CE does not necessarily rise directly with yield strength. Moreover, a very low carbon content, such as that for HY-130 steel, results in the formation of a lower-hardness martensite in the HAZ that is relatively resistant to cracking. Thus, while susceptibility to HAZ cold cracking generally increases with yield strength, compositions can be optimized to minimize the effect. Moreover, cold cracking can be essentially eliminated through proper design and welding practice.

Because the HAZ undergoes a variety of thermal cycles during welding, its mechanical properties can differ markedly from those of the unaffected base plate. In the region just below the fusion line, the grains are very coarse and may exhibit poor toughness, particularly if a high carbon and alloy content result in transformation to high-carbon martensite. In the region that is heated subcritically, tempering may result in a low-strength region. In general, the higher carbon and alloy content of the high-strength steels results in greater changes in the mechanical properties of the HAZ during welding. The same measures that are employed to minimize HAZ cracking can be employed to ensure satisfactory HAZ mechanical properties. Thus, welding need not be a significant deterrent to the use of steels of increasing yield strength. For a more complete discussion of the subject, the reader is referred to the book entitled Welding High-Strength Steels, published by the American Society for Metals.

Service Performance

In general, steels of increasing yield strength are used because of an increase in the operating stress. Therefore, the suitability of a higher strength steel for a particular application usually depends on its ability to resist stress-induced failures, such as overload, brittle fracture, fatigue, or stress corrosion. The effect of increasing yield strength on these failure modes is discussed in the following sections.

Resistance to Failure by Overload

As previously noted, the design stress is most commonly based on some fraction of the resistance to failure by ductile overload. In pressure vessels, for example, this corresponds to the resistance to bursting. Because burst strength has been correlated with the ultimate tensile strength of the material, the design stress established by the ASME Boiler and Pressure Vessel Committee has been based primarily on the ultimate tensile strength, and as previously noted, does not recognize any effect of yield strength above a yield-tensile ratio of 0.5.

In his comparison of bursting-strength formulas, Langer[2] has recommended a formula developed by Svensson[3] as the best compromise between simplicity and accuracy. The Svensson equation is based on the tensile strength, but also incorporates a factor based on the strain-hardening exponent, n, which is equal to the true uniform elongation ε_u. The value of n or ε_u is incorporated in such a way that the bursting strength increases as n or ε_u decreases, for designs based on the tensile strength. This is illustrated in Figure 4, which shows that the relative bursting strength based on the tensile strength increases with tensile strength, and at a tensile strength of 200 ksi, the bursting strength is more than 20 percent higher than that calculated by means of the ASME formula. The curve was obtained by calculating the bursting strength by using Svensson's formula and the ε_u values shown in Figure 1, and comparing it with that calculated by using the ASME formula. Because the yield strength and the yield-tensile ratio increase with decreasing ε_u,

the comparison indicates that the relative resistance to bursting increases as the yield strength increases. Thus, an increase in the yield-tensile ratio is desirable with respect to bursting strength.

Figure 4 also shows, however, that the bursting-strength index decreases with tensile strength for designs based on the yield strength.* This comparison shows that the increase in resistance to bursting with yield strength is not as great as the increase in design stress when the design stress is based on the yield strength rather than on the tensile strength. These results indicate that the design stress based on tensile strength can be increased with increasing tensile strength with no loss in safety, but that the design stress should not be based directly on the yield strength unless a reduction in the bursting-strength index can be tolerated.

Even though the resistance to bursting increases with tensile strength, the increase is based on failure in the membrane region and assumes no increase in notch sensitivity with tensile strength that would cause failure at stress raisers and thus negate the greater resistance to bursting in the membrane region. To test this possibility, the Pressure Vessel Research Committee (PVRC) is investigating the bursting strength of the specimen shown in Figure 5. The diaphragm is loaded to failure hydraulically in a special fixture, and the bursting pressure and failure location (edge or center) are recorded for various edge radii

---

*The yield strength corresponding to a given tensile strength was obtained from Figure 1.

and diaphragm thicknesses. The data for edge failures obtained for steels with yield strengths from 34 to 250 ksi were analyzed by Langer,[2] who compared the limit pressure, P_O $\left[P_O = 2.71(\frac{t}{R})^2 \sigma_y\right]$, for a fixed-edge disc with the experimental bursting pressure, P_B, observed in the tests. The comparison, Figure 5, clearly shows that the ratio of P_O to P_B, which is a measure of the resistance to edge failure, increases with the uniform true strain, ε_u. Thus, steels with increased yield strength (decreased ε_u and n) have a lesser resistance to edge failures or a greater susceptibility to failure at notches or strain raisers. Accordingly, design and fabrication must be controlled so that failure will occur in the membrane region rather than at strain raisers if advantage is to be taken of increased bursting pressure with increasing strength. PVRC is investigating the improvement in design and fabrication with increasing strength that is required to ensure failure in the membrane region and avoid failure at strain raisers.

Resistance to Brittle Fracture

The resistance to brittle fracture must be considered on the basis of the temperature at which the behavior changes from ductile to brittle and on the basis of the adequacy of the shelf energy absorption. Figure 6 compares transition-temperature curves for conventionally melted steels (primarily open-hearth) of yield strengths in the range 30 to 200 ksi. In general, the quenched and tempered martensitic-type steels (A517-F 140(X), and 4320) have lower transition temperatures than the remaining pearlitic-type steels. In contrast, however, the shelf energy absorption of the pearlitic steels is much higher than that of the martensitic steels.

Consequently, the major problem in utilizing steels of increasing yield strength in structural applications is concerned with ensuring resistance to rapid crack propagation at any temperature up to and including the shelf temperature.

The typical reduction in shelf energy that occurs with increasing strength is illustrated in Figure 7 for conventionally melted steels. To a limited extent, the data were selected to illustrate the point in question, and the slope of the line and its displacement with respect to energy could be significantly varied if other data were selected. Nevertheless, the curve demonstrates the typical loss in shelf energy that must be considered in utilizing increased yield strength. The effect of this decrease could not be properly assessed in the past because only the temperature at which the fracture changed from ductile to brittle was normally considered. However, with the advent of linear elastic fracture mechanics, reasonable estimates of the effect of shelf energy on susceptibility to rapid crack propagation can be made.

The ability of materials to resist unstable rapid crack propagation can be measured in terms of the plane-strain stress-intensity factor, K_{Ic}, which relates the stress and flaw size for unstable rapid propagation. In general, failure occurs by plane strain when the toughness factor

$$\left[\frac{K_{Ic}}{\sigma_y}\right]^2 \frac{1}{t} \leq 0.4$$

Thus, unstable rapid crack propagation is avoided if the toughness factor is greater than 0.4. A significantly greater resistance to crack propa-

gation obtains when the toughness factor is about equal to 1.0, which corresponds to through-thickness yielding of the plate.

When the toughness factors are combined with an empirical equation[4]* relating K_{Ic} to Charpy V-notch (CVN) energy absorption, the following equations result:

$$CVN = \frac{\sigma_y}{5} \quad (0.4t + 0.25) \text{ for } \left[\frac{K_{Ic}}{\sigma_y}\right]^2 \frac{1}{t} = 0.4$$

and $$CVN = \frac{\sigma_y}{5} \quad (t + 0.25) \text{ for } \left[\frac{K_{Ic}}{\sigma_y}\right]^2 \frac{1}{t} = 1.0$$

The change in CVN energy-absorption requirements with yield strength for both equations is shown in Figure 8. A comparison of these requirements with the typical shelf energy for conventionally melted steels from Figure 7 indicates that plane-strain behavior of 1-inch-thick plates can be avoided up to a yield strength of about 180 ksi and that through-thickness yielding can be obtained up to a yield strength of 150 ksi. The yield strength at which these respective behaviors can be achieved can be significantly increased through appropriate control of metallurgical factors, as discussed later.

Resistance to Fatigue

Most structures are loaded repeatedly; therefore, resistance to failure by fatigue can be important to service performance. The number of loading cycles varies widely for different structural appli-

---

* $\left[\frac{K_{Ic}}{\sigma_y}\right]^2 = \frac{5}{\sigma_y}\left[CVN - \frac{\sigma_y}{20}\right]$.

cations. Thus, both low-cycle and high-cycle fatigue must be considered. In addition, the type of loading may vary from tension-tension ($0 < R \leq 1$), to zero to tension ($R = 0$), to tension-compression ($0 > R \geq -1$).

The effect of increasing yield strength on fatigue life at various cycle lives and for various types of loading is shown in Figure 9 for A36 and A517-F steels. For the most important loading conditions, $R \leq \frac{1}{2}$, the comparison shows that the stress range decreases rapidly with increasing cycles to failure, particularly for A517-F steel, and the effect of changing R value is small. This effect is illustrated in Figure 10 with respect to yield strength and tensile strength. The plotted values were obtained by calculating the ratio of the stress range to the minimum specified yield strength for A36 (36 ksi) and A517-F (100 ksi) steels and to the typical tensile strength (62 and 120 ksi, respectively). The ratio for A36 steel was then compared with the corresponding value for A517-F steel.

The results indicate that at 10^5 cycles, the stress ranges for A36 and A517-F steels are about equal proportions of the tensile strength, but that the stress range for A517-F steel is only about 70 percent of that for the A36 steel on a yield-strength proportion basis. For longer cycle lives (6×10^5 and $\sim 2 \times 10^6$), the stress range for A517-F steel is only about 70 and 65 percent, respectively, of that for A36 steel on a tensile-strength basis, and about 46 and 48 percent, respectively, on a yield-strength basis. The percentages cited are an average for the various R values and do not vary much with R value. These results show

that fatigue strength decreases with increasing tensile strength, except for short cycle lives, and decreases even more with increasing yield strength at all cycle lives.

The preceding data are based on the failure of a relatively large specimen without regard to the initiation or propagation parts of the failure. Thus, the data cannot be readily applied to the prediction of failure on the basis of the rate at which cracks propagate. Such studies have been in progress at U. S. Steel for some time, and preliminary results were recently reported by Barsom, et al.[5] These studies indicate that the fatigue-crack growth rate, da/dn, depends primarily on the stress-intensity-factor range, ΔK_I ($\Delta K_I = \Delta\sigma\sqrt{a}$), Figure 11, and thus the crack-growth rate is independent of yield strength. Consequently, cracks of a given size do not propagate any more rapidly in high-yield-strength steels than in low-yield-strength steels, as has been reported.

Although crack-growth rate is independent of yield strength, the rate increases with yield strength if the stress range is increased in proportion to the yield strength. In addition, crack propagation terminates in failure when the critical crack size is reached. Because the critical flaw size, a_{cr}, decreases with increased yield strength for a given K_{Ic} value, failure will occur in fewer cycles for high-yield-strength steels than for low-yield-strength steels. Thus, appropriate care must be taken in the design of structures to be fabricated from high-yield-strength steels to minimize the probability of crack formation, and in the inspection of such structures to eliminate the propagation of cracks to critical size.

Resistance to Stress Corrosion

Traditionally, resistance to stress corrosion has been equated to the strength of ferritic steels. When conventional smooth bend specimens or unnotched tension specimens were tested in sea water, failure by stress corrosion was seldom observed below a yield strength of about 180 ksi, Figure 12. However, the use in recent years of fatigue-cracked test specimens, such as the NRL fatigue-cracked cantilever-beam specimen, has significantly reduced the yield strength at which stress corrosion in sea water has been observed, probably because resistance to pitting by corrosion and to subsequent crack formation is essentially eliminated from fatigue-cracked specimens. Thus, materials that were considered immune to stress corrosion because they did not pit in a particular environment, or pitted at an extremely slow rate, may exhibit a susceptibility when the test specimen is fatigue-cracked. Additionally, if the fatigue-cracked specimen is of the fracture-mechanics type, the specimen can be failed in air to determine the plane-strain stress-intensity factor, K_{Ic}, and similar specimens can be exposed in a corrosive environment to determine how much the K_I value is reduced because of crack growth by stress corrosion. At some reduced stress, the fatigue crack does not extend by stress corrosion, and the K_I value corresponding to the reduced stress is referred to as the K_{Iscc} value, or the K_I value below which stress corrosion does not occur for the material and corrosion environment in question. The relative susceptibility to stress corrosion can thus be expressed as the difference between the K_{Ic} and the K_{Iscc} values. This difference indicates the amount the design stress

must be reduced to avoid growth of cracks by stress corrosion to the critical size at which unstable rapid crack propagation will occur.

The reduction in yield strength at which stress corrosion occurs in fatigue-cracked specimens is illustrated in Figure 13, which indicates that stress corrosion can occur in sea water in ferritic materials at yield strengths down to about 110 ksi. However, the figure also shows that the degree of susceptibility, as measured by the decrease in the K_I value, varies over a wide range. This variation suggests that some material factor other than strength must also influence susceptibility to stress corrosion. Inspection of the data indicated that, at a given strength level, steels with the highest fracture toughness were the most resistant to stress corrosion. For example, the factor that would account for the wide difference in stress-corrosion susceptibility among the 180-ksi yield-strength steels, Figure 13, was their fracture toughness (the data were observed to range from 44 to 92 ft-lb for the CVN energy absorption and from 85 to 231 ksi $\sqrt{\text{inch}}$ for the K_{Ic}, both measured at room temperature). When the stress-corrosion susceptibility was plotted against the fracture toughness, the correlation with CVN energy absorption was found to be reasonably good, whereas the correlation with K_{Ic} was poor, Figure 14.

Because fracture toughness depends on yield strength, the stress-corrosion susceptibility was plotted against the CVN energy absorption and the K_{Ic} normalized for the effect of yield strength, (CVN/σ_y) and $(K_{Ic}/\sigma_y)^2$, respectively, Figure 15. The correlation with both fracture-

toughness factors improved significantly, and indicates that in the yield-strength range 100 to 200 ksi, susceptibility to stress corrosion is influenced by the strength and fracture toughness of the steel. Moreover, the fracture toughness required to minimize susceptibility at a particular strength level can probably be estimated from correlations such as that shown in Figure 15. For the conditions concerned, Figure 15 indicates that susceptibility to stress corrosion in sea water can be minimized if the CVN energy absorption (in ft-lb) is about 0.7 of the yield strength (in ksi). Similarly, the square of the ratio of the K_{Ic} (in ksi $\sqrt{\text{inch}}$) to the yield strength (in ksi) should be about 1.6, and thus, the ratio of the K_{Ic} to σ_y should be about 1.25. This suggests that the susceptibility to stress corrosion can be minimized if the K_{Ic} value (in ksi $\sqrt{\text{inch}}$) is 1.25 times the yield strength (in ksi). The (CVN/σ_y) value corresponding to a $(K_{Ic}/\sigma_y)^2$ value of 1.6 is 0.37,* which is significantly less than the value of 0.7 that was obtained directly from the (CVN/σ_y) curve in Figure 15. These differences indicate the present limitation of quantitatively determining resistance to stress corrosion on the basis of strength and fracture toughness, and the need for additional experimentation to confirm the validity of such an approach. Nevertheless, the data strongly suggest that yield strength is not the only factor influencing susceptibility to stress corrosion, that fracture

---

*Determined from the previously cited equation:[4)]

$$\left[\frac{K_{Ic}}{\sigma_y}\right]^2 = \frac{5}{\sigma_y}\left[CVN - \frac{\sigma_y}{20}\right]$$

toughness also influences this susceptibility, and that steels with adequately high fracture toughness may be resistant to stress corrosion regardless of strength. Thus, the use of high-strength steels need not necessarily be limited with respect to the maximum usable strength by susceptibility to stress corrosion.

General Discussion

For the various stress-dependent modes of failure, increasing the design stress in proportion to the yield strength increased the probability of failure. However, the propagation of cracks to critical size by fatigue or stress corrosion was observed to depend on the fracture toughness of the steel. Thus, the probability of failure by modes except overload can be decreased by increasing the fracture toughness of the steel. Although fracture toughness as measured by energy absorption generally decreases with yield strength, as previously shown (Figure 7), practices are available through which the fracture toughness can be very significantly increased. For example, the shelf energy absorption of about 40 ft-lb for the 140-ksi yield-strength steel can be increased to 100 ft-lb by appropriate control of metallurgical factors. Under special circumstances, an energy absorption as high as 175 ft-lb at a yield strength of 200 ksi has been obtained by special metallurgical control, and the ability to apply such control is improving continuously. For these and related reasons, the possibility of more effectively utilizing the yield strength of steel should be re-examined.

Summary

The present paper is intended to review the effect of yield strength on fabricability and stress-dependent modes of failure to determine the feasibility of utilizing the yield strength of steel more effectively. The results of the review may be summarized as follows:

1. The bendability of plates can be predicted from the plane-strain ductility. Because plane-strain ductility decreases with increasing yield strength, bendability decreases with yield strength. However, the loss in bendability with yield strength does not appear to be unduly restrictive.

2. The care required to weld steels increases with yield strength. However, the welding practices required are in common use and are not a significant deterrent to the use of high-yield-strength steels.

3. Resistance to failure by simple overload increases with tensile strength and is believed to increase more rapidly as the yield-to-tensile ratio increases. However, this effect of the yield strength may be limited by susceptibility to localized failure outside the membrane region.

4. In general, the transition-temperature characteristics of high-yield-strength steels are more attractive than those for lower-strength steels.

5. If design stress is based directly on yield strength, the safety factor against failure because of low shear energy absorption, or because cracks grow to critical size by fatigue or stress corrosion, decreases with increasing yield strength. However, this tendency can be reduced by increasing the fracture toughness.

In recent years, the fracture toughness of steel has been continuously rising because control of metallurgical factors is continuously improving. For this and other reasons that suggest beneficial effects of yield strength, the possibility of more effectively utilizing the yield strength of steel should be re-examined.

References

1. D. P. Clausing, "Effect of Plastic Strain State on Ductility and Toughness," presented at WESTEC Conference, Los Angeles, California, March 12, 1969; to be published in International Journal of Fracture Mechanics, March 1970.

2. B. F. Langer, "PVRC Interpretive Report on Pressure Vessel Research: Section 1—Design Considerations," Welding Research Council Bulletin No. 95, April 1964.

3. N. L. Svensson, "Bursting Pressure of Cylindrical and Spherical Vessels," Journal of Applied Mechanics, ASME, 25 (1), 89-96 (March 1958).

4. S. T. Rolfe, J. M. Barsom, and M. Gensamer, "Fracture-Toughness Requirements for Steels," Proceedings of the First Offshore Technology Conference, held in Houston, Texas, May 18-21, 1969 (Paper No. OTC 1045).

5. J. M. Barsom, E. J. Imhof, and S. T. Rolfe, "Fatigue-Crack Propagation in High-Yield-Strength Steels," submitted for publication in the Journal of Engineering Fracture Mechanics.

Table I

Carbon Equivalent for Five Steels of Different Yield Strengths

Steel	Yield Strength, ksi	Carbon Equivalent*	Chemical Composition,** percent						
			C	Mn	Ni	Cr	Mo	V	Cu
ABS-C	40	0.35	0.20	0.60	—	—	—	—	—
A302-B	56	0.53	0.19	1.40	—	—	0.49	—	—
HY-80	81	0.49	0.16	0.28	2.26	1.46	0.30	—	—
A517-F	121	0.45	0.17	0.78	0.88	0.56	0.42	0.036	0.26
HY-130	140	0.61	0.11	0.85	4.91	0.58	0.58	0.050	—

*Calculated from $CE = \%C + \frac{\%Mn}{4} + \frac{\%Ni}{20} + \frac{\%Cr}{10} - \frac{\%Mo}{50} - \frac{\%V}{10} + \frac{\%Cu}{40}$.

**Check chemical analysis only for elements included in above CE equation.

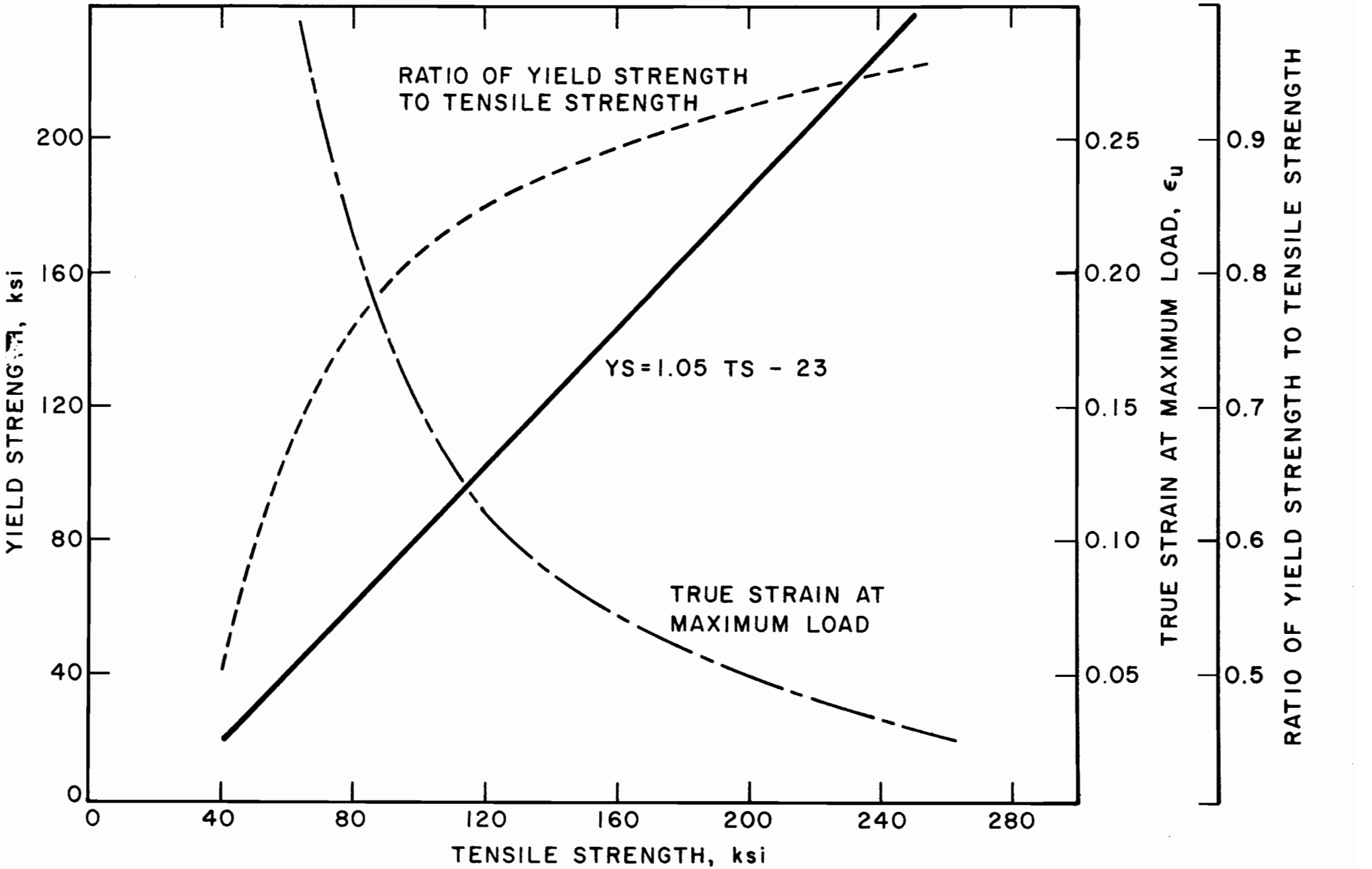

FIG. 1
VARIATION IN YIELD STRENGTH WITH TENSILE STRENGTH OF STRUCTURAL STEELS

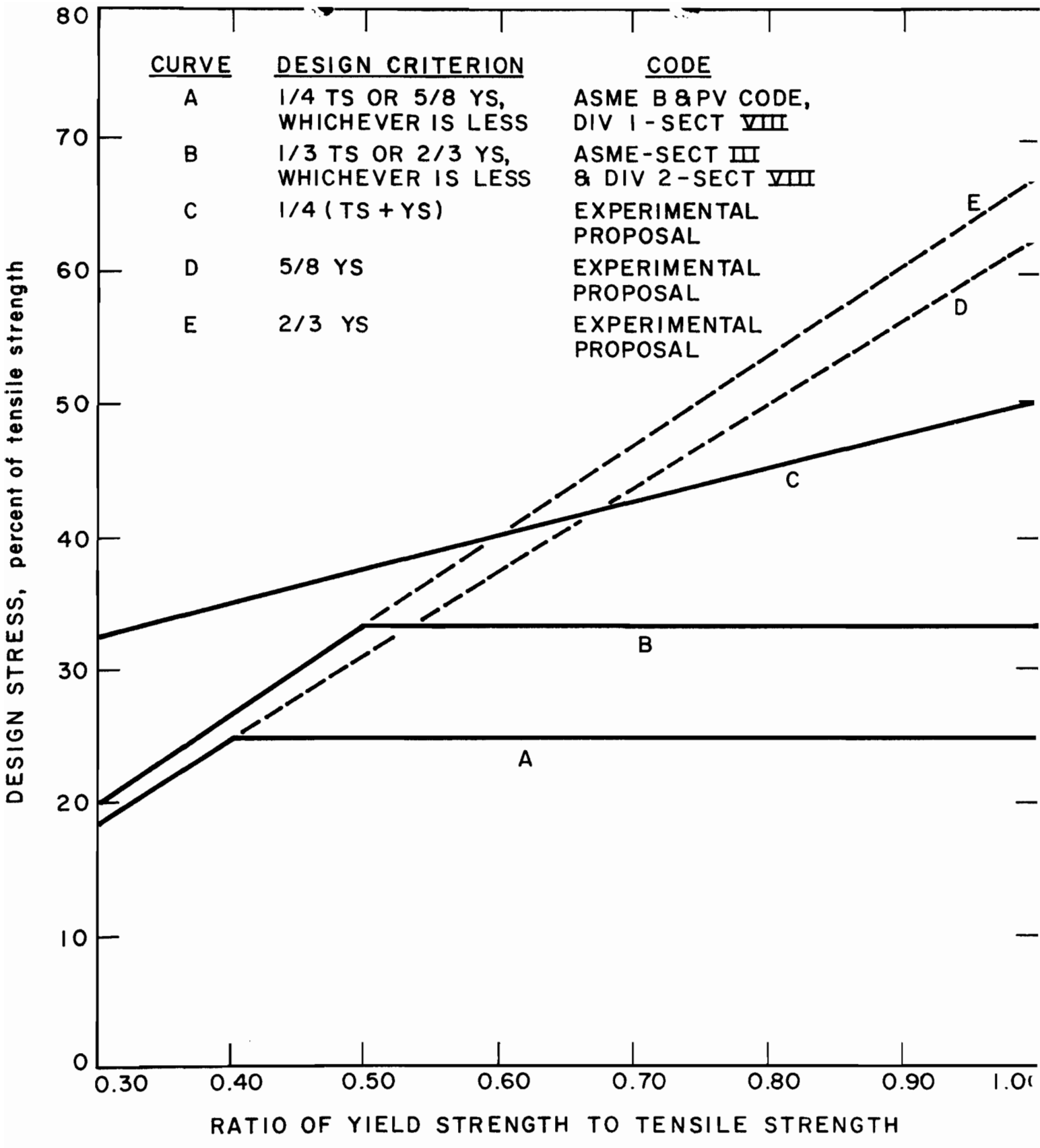

FIG. 2
VARIATION IN DESIGN STRESS WITH YIELD-TENSILE RATIO FOR VARIOUS DESIGN CRITERIA

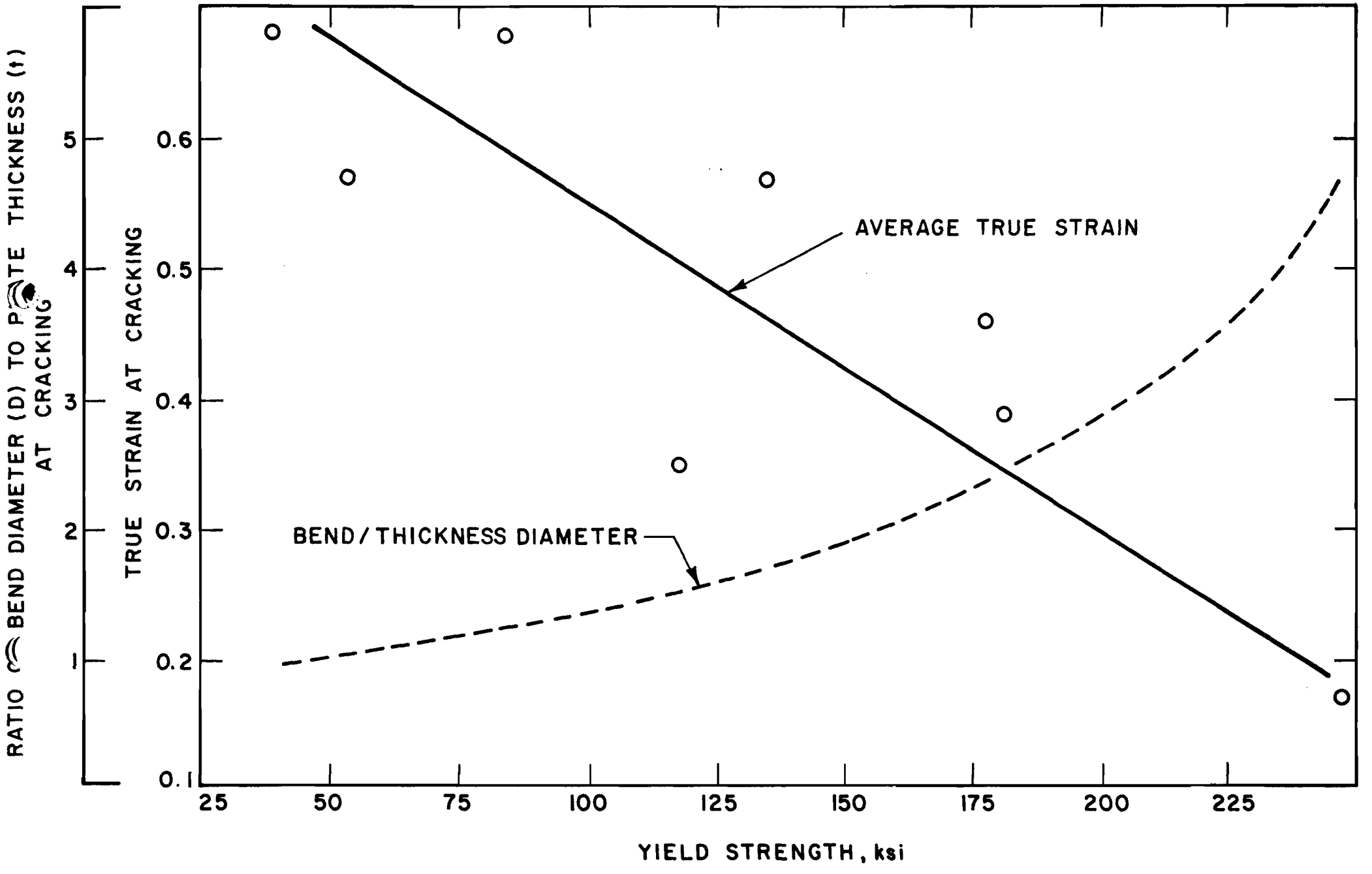

FIG. 3
EFFECT OF YIELD STRENGTH ON CRACKING DURING PLANE-STRAIN BENDING

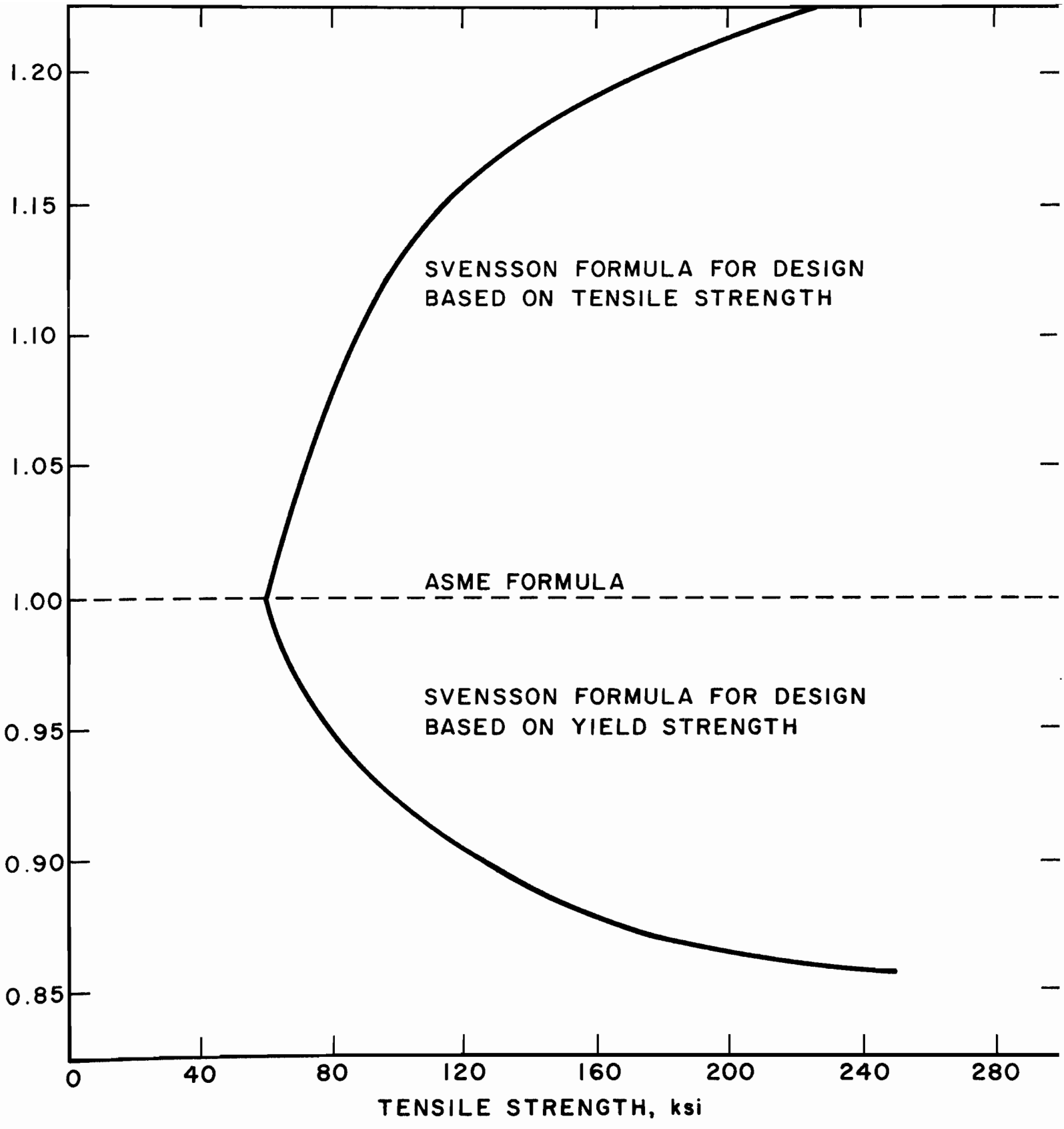

FIG. 4
BURSTING STRENGTH CALCULATED BY SVENSSON FORMULA COMPARED WITH THAT FOR ASME FORMULA FOR DESIGNS BASED ON TENSILE STRENGTH AND ON YIELD STRENGTH

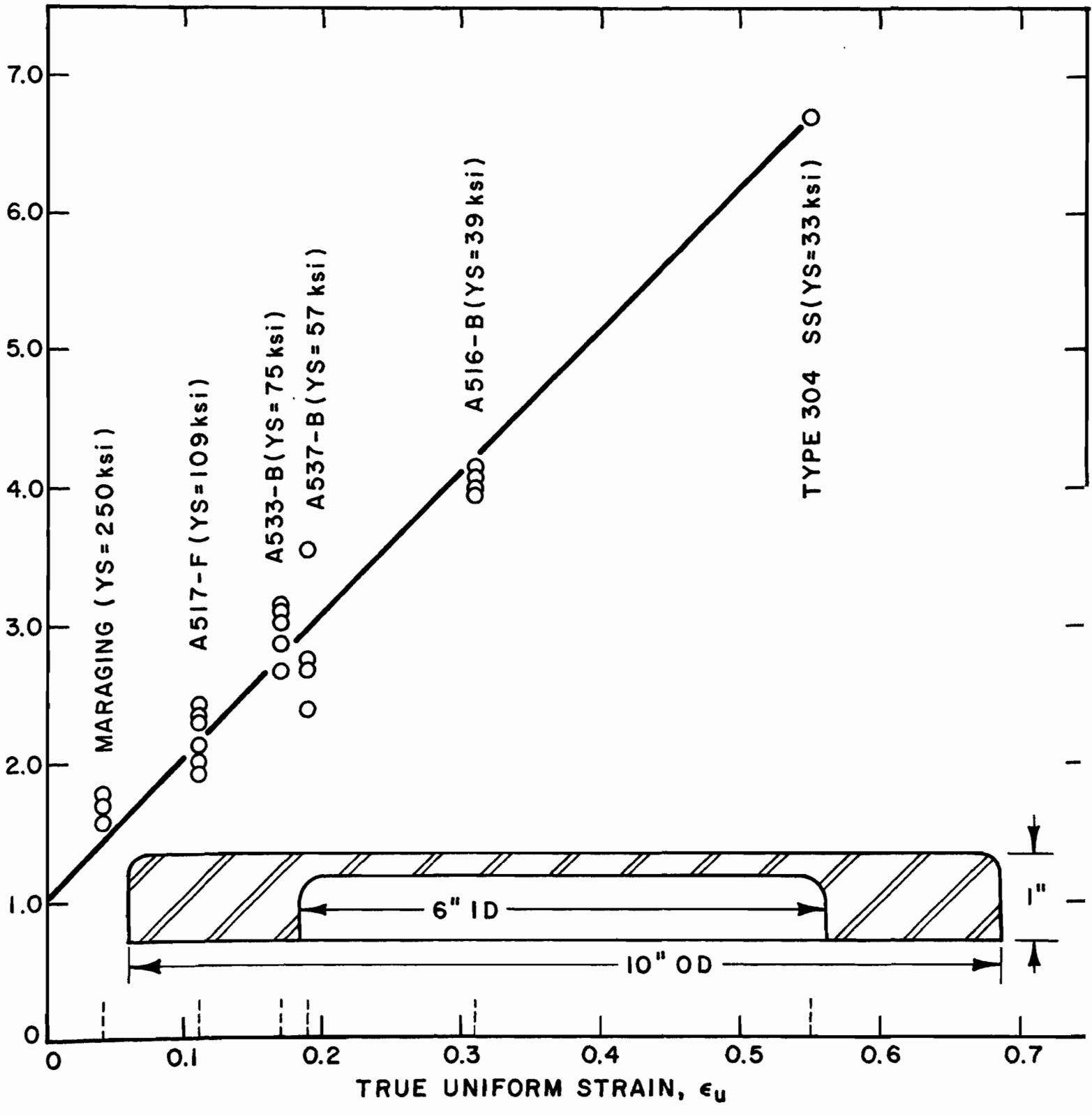

FIG. 5
CHANGE IN RESISTANCE TO EDGE FAILURE FOR VARIOUS STEELS

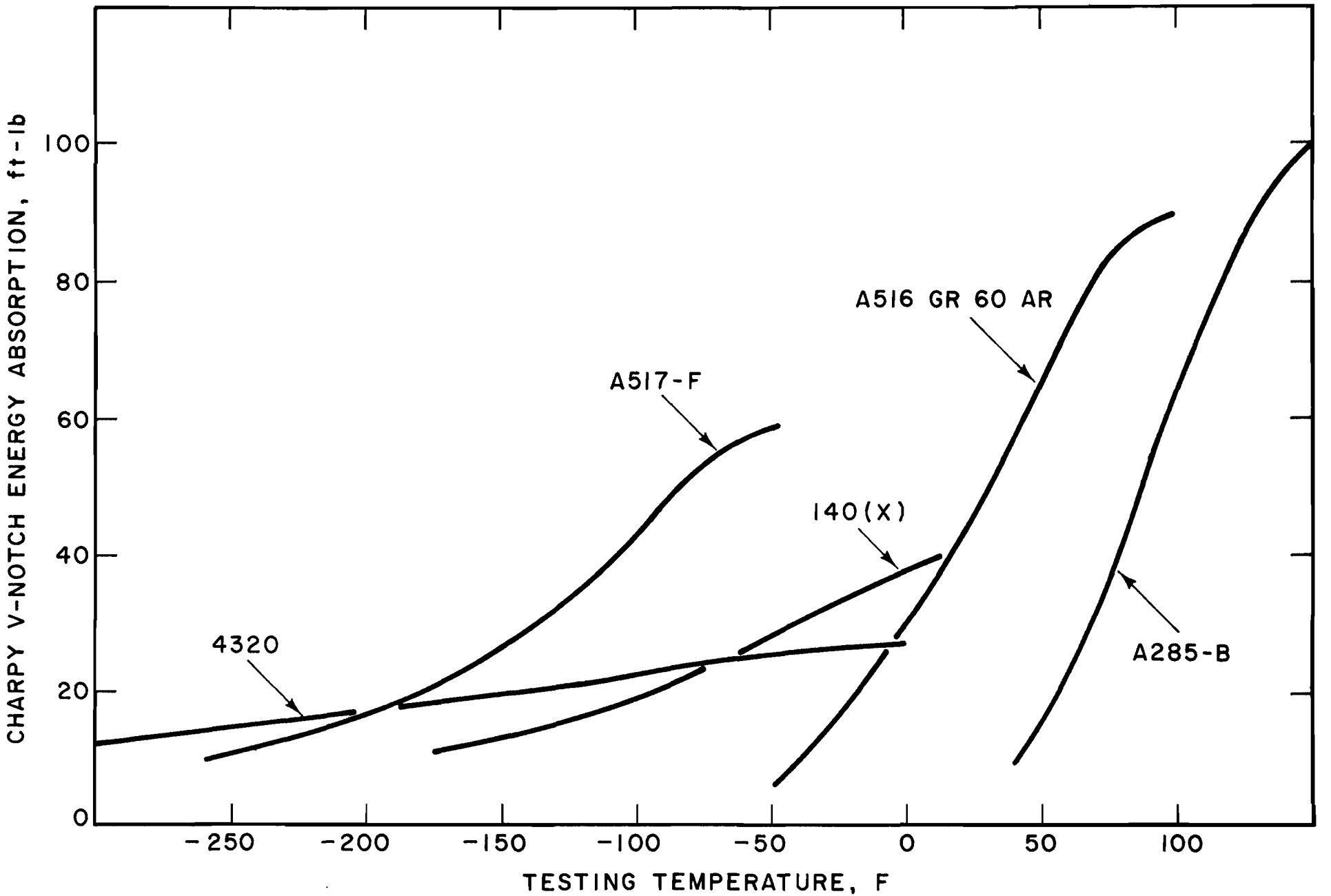

FIG. 6
TRANSITION-TEMPERATURE CURVES FOR CONVENTIONALLY MELTED STEELS AT VARIOUS STRENGTH LEVELS

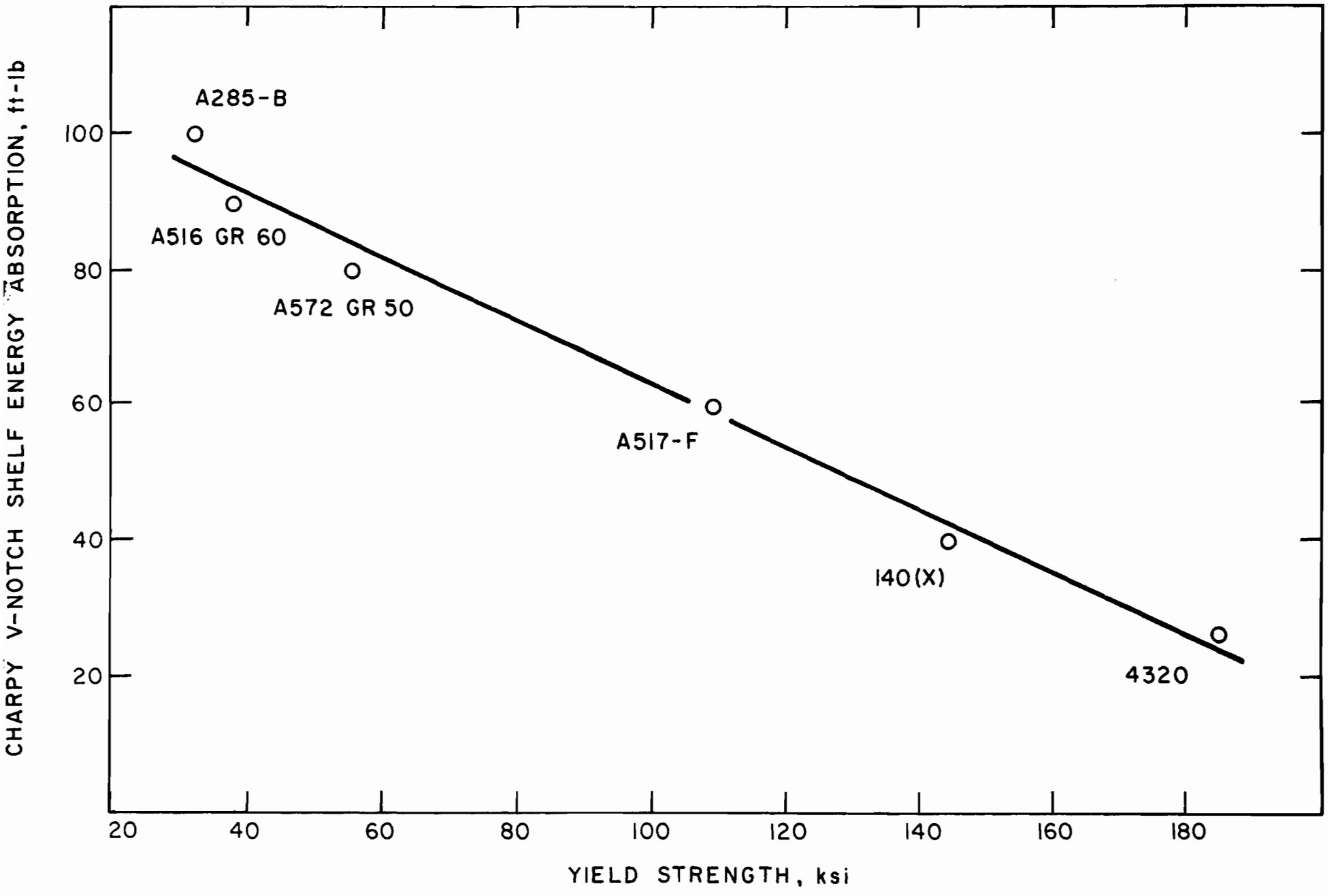

FIG. 7

EFFECT OF YIELD STRENGTH ON SHELF ENERGY ABSORPTION OF CONVENTIONALLY MELTED STEELS

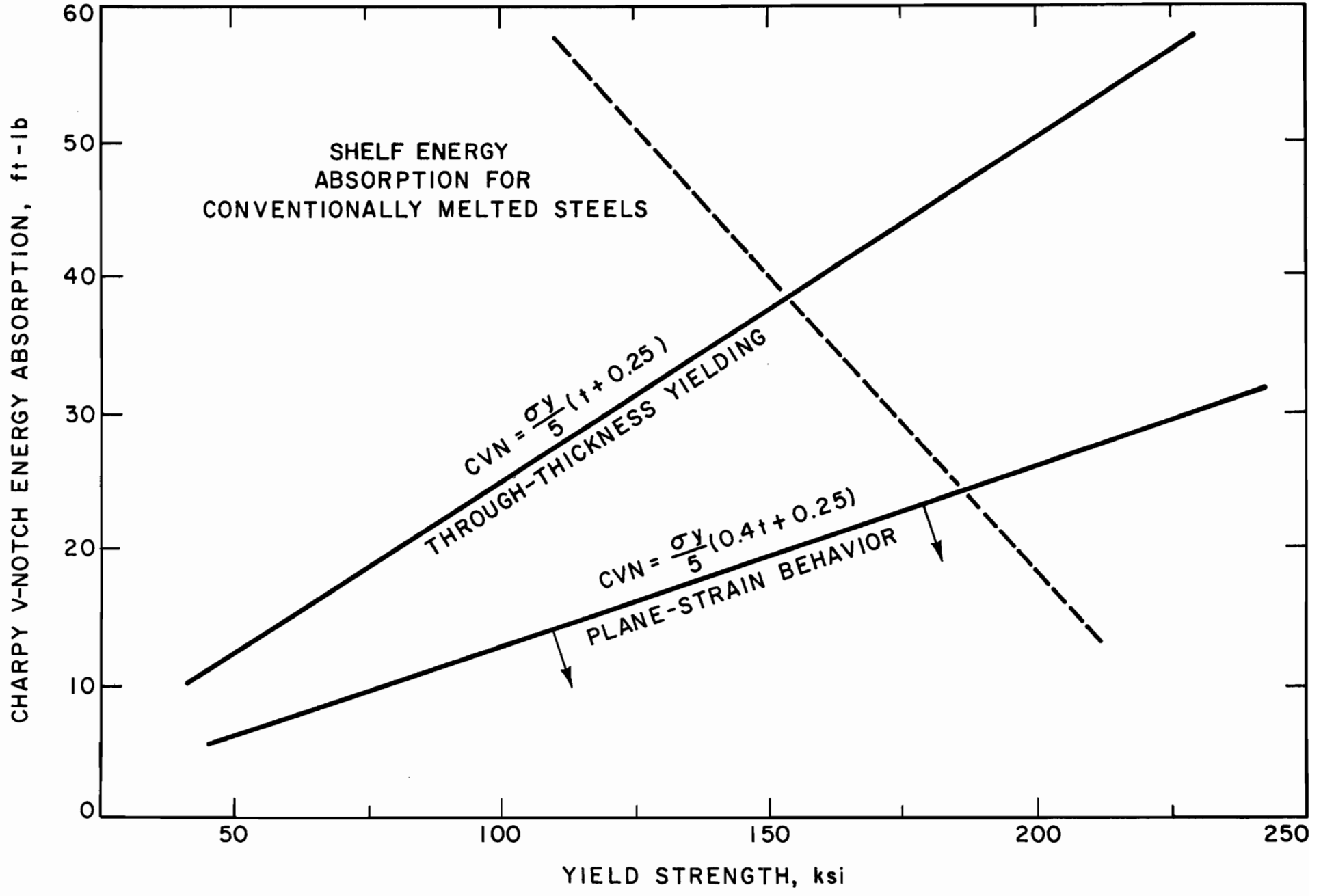

FIG. 8

EFFECT OF YIELD STRENGTH ON CHARPY V-NOTCH ENERGY ABSORPTION FOR PLANE-STRAIN BEHAVIOR AND FOR THROUGH-THICKNESS YIELDING FOR 1-INCH-THICK PLATE

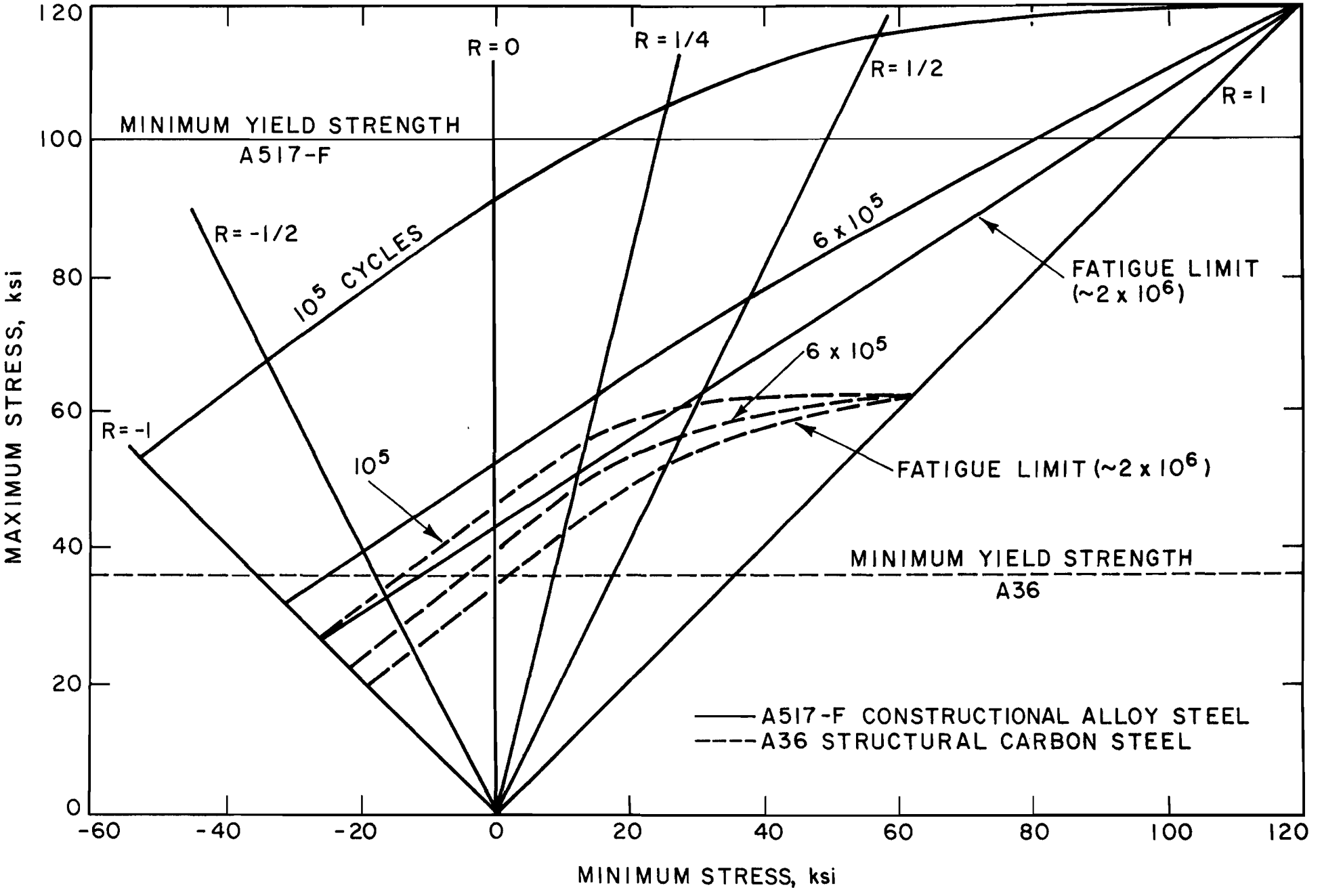

FIG. 9
COMPARISON OF FATIGUE STRENGTH OF A36 AND A517-F STEEL PLATES

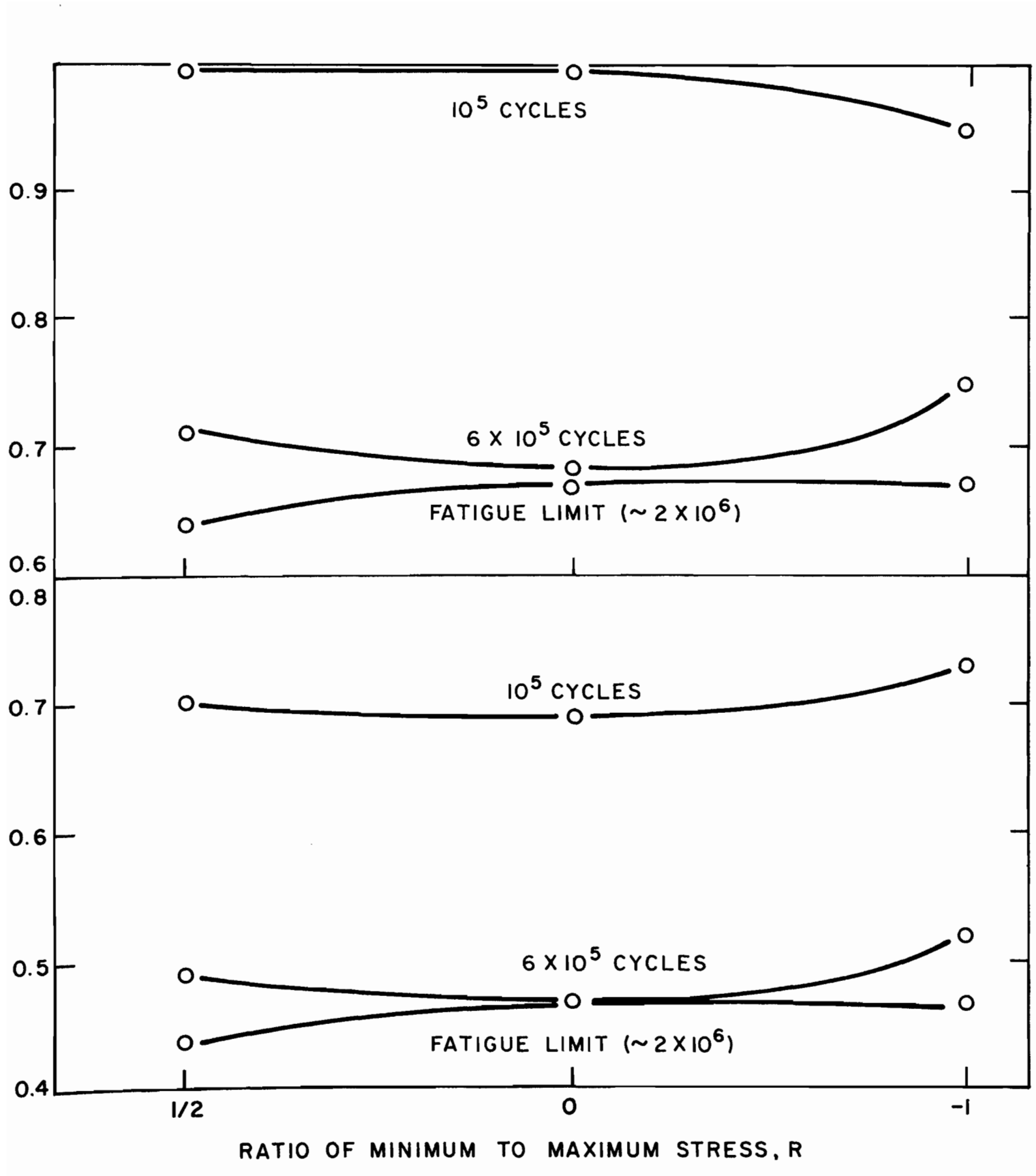

FIG. 10
COMPARISON OF FATIGUE LIFE FOR A36 AND A517-F STEELS

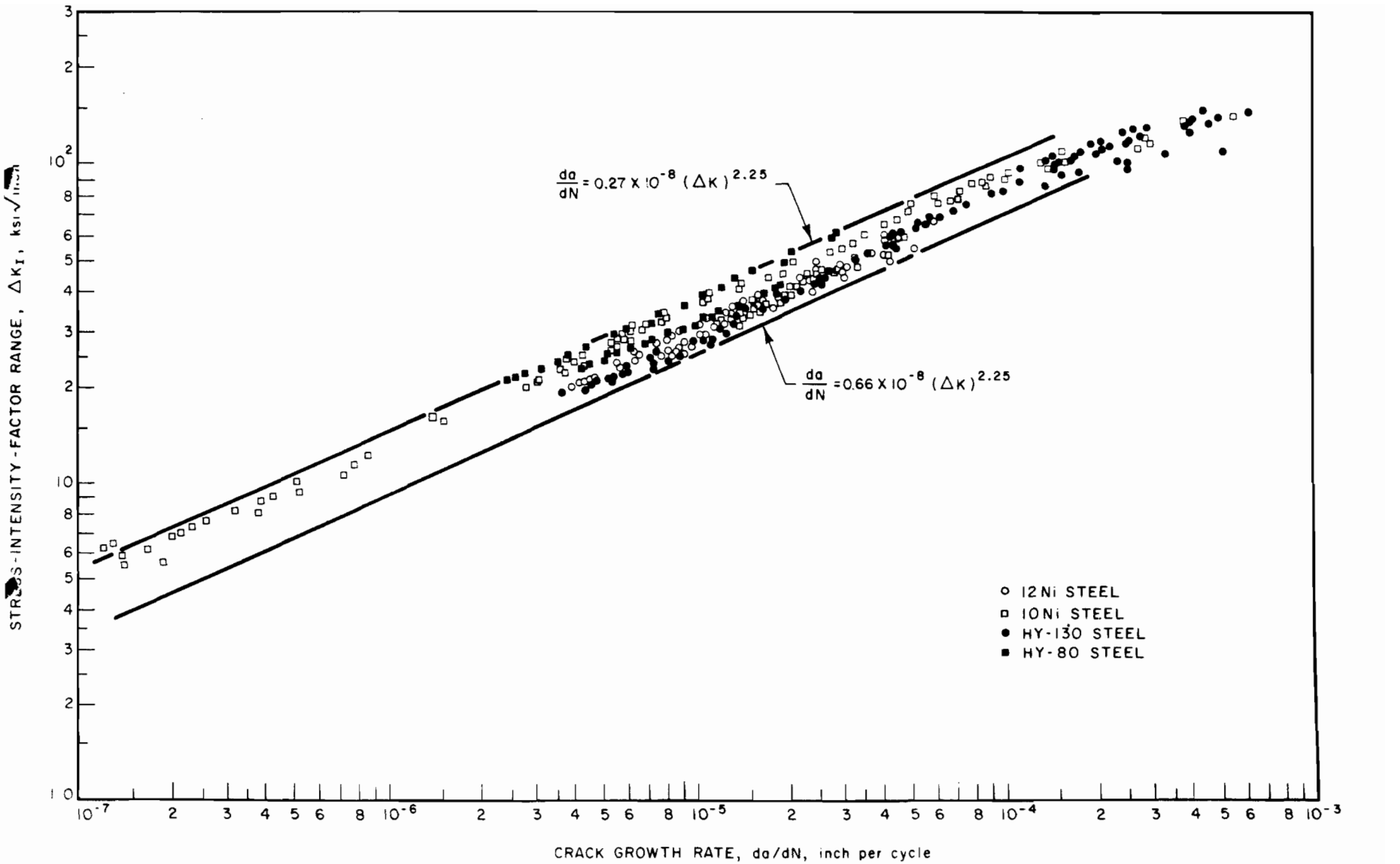

SUMMARY OF FATIGUE-CRACK-GROWTH DATA FOR HIGH-STRENGTH STEELS

Figure 11

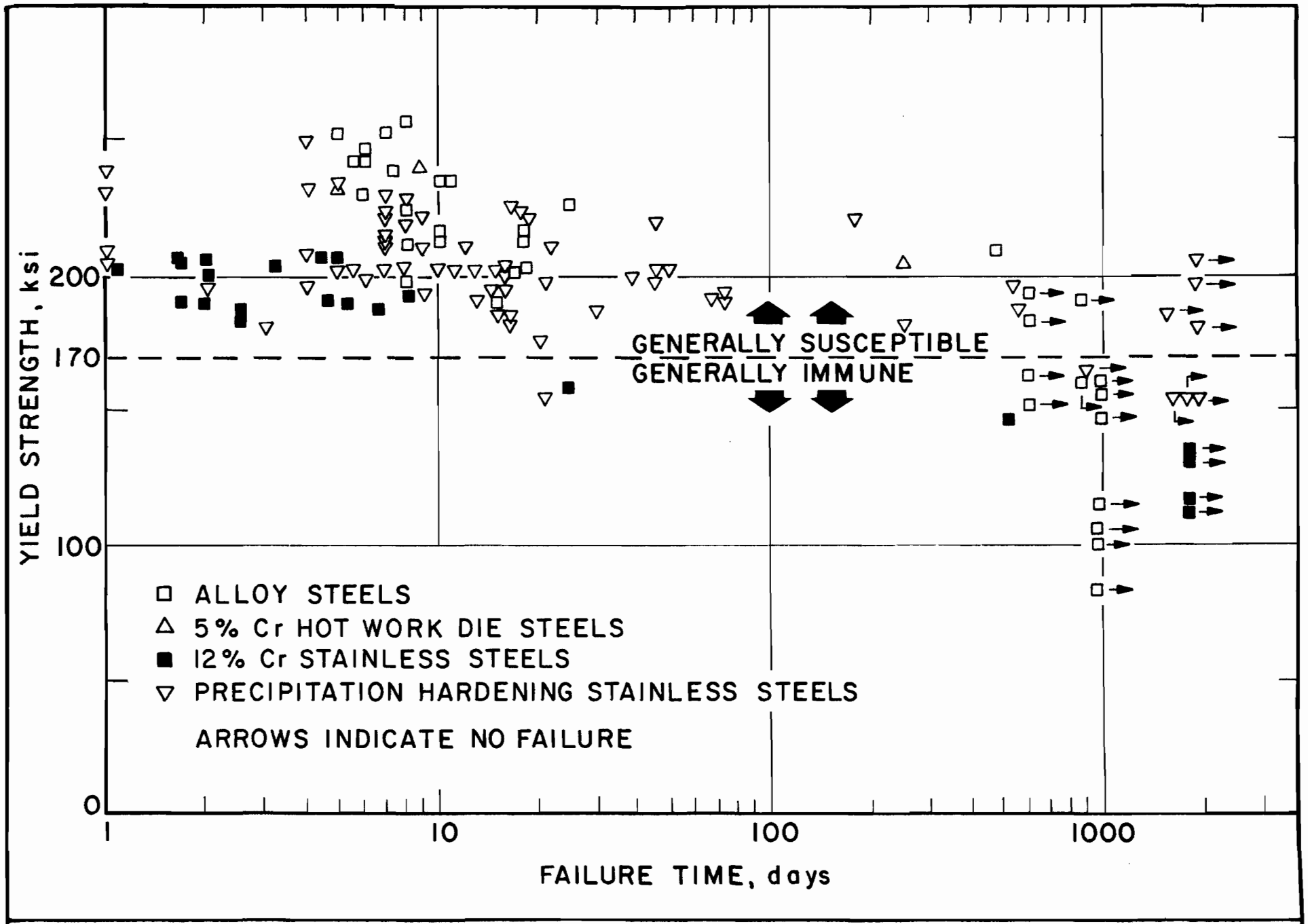

STRESS-CORROSION RESULTS OF ALLOY AND STAINLESS STEELS EXPOSED TO MARINE ATMOSPHERE AT 75 PERCENT OF THE YIELD STRENGTH

FIGURE NO. 12

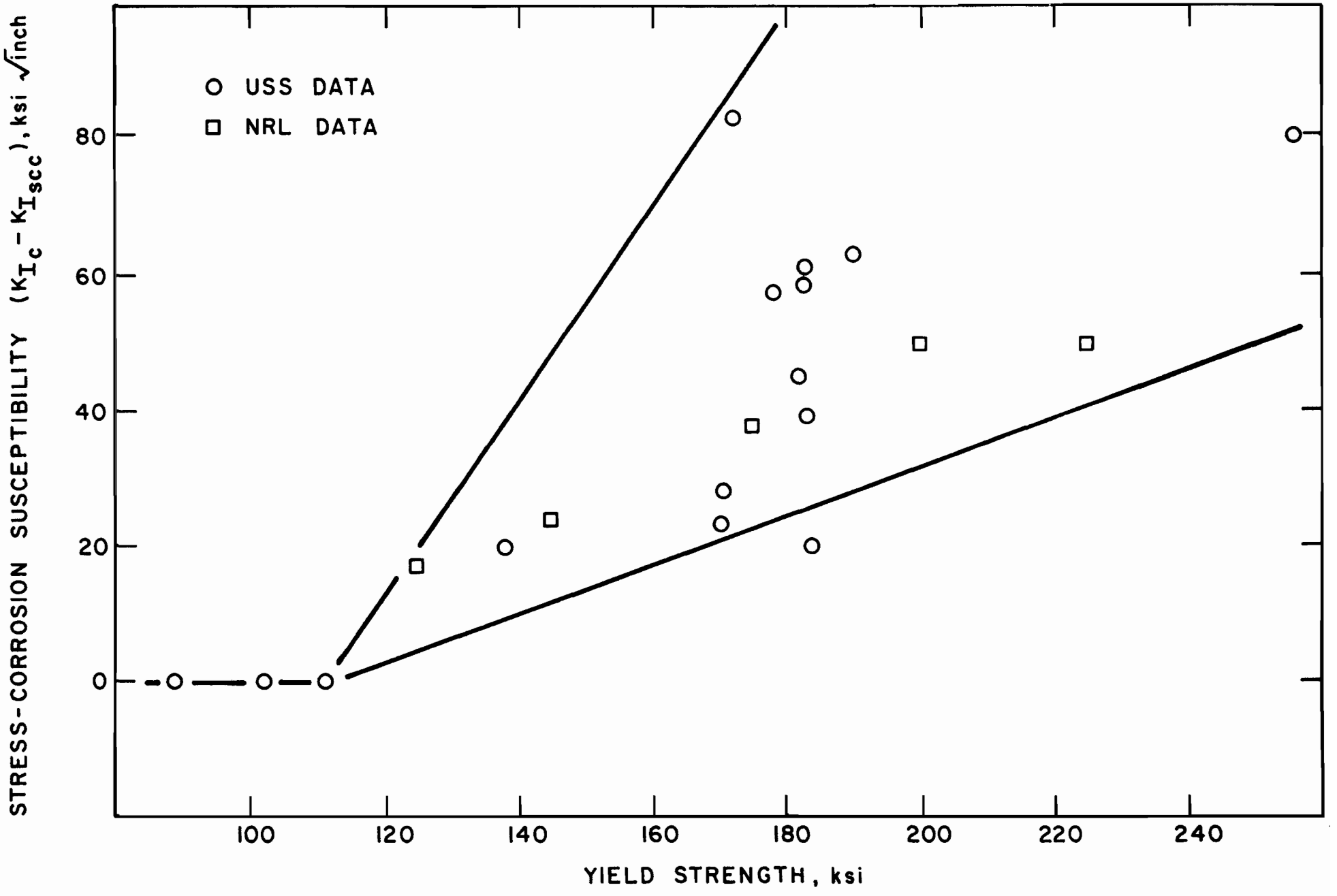

FIG. 13
EFFECT OF YIELD STRENGTH ON SUSCEPTIBILITY TO STRESS-CORROSION IN SEA WATER

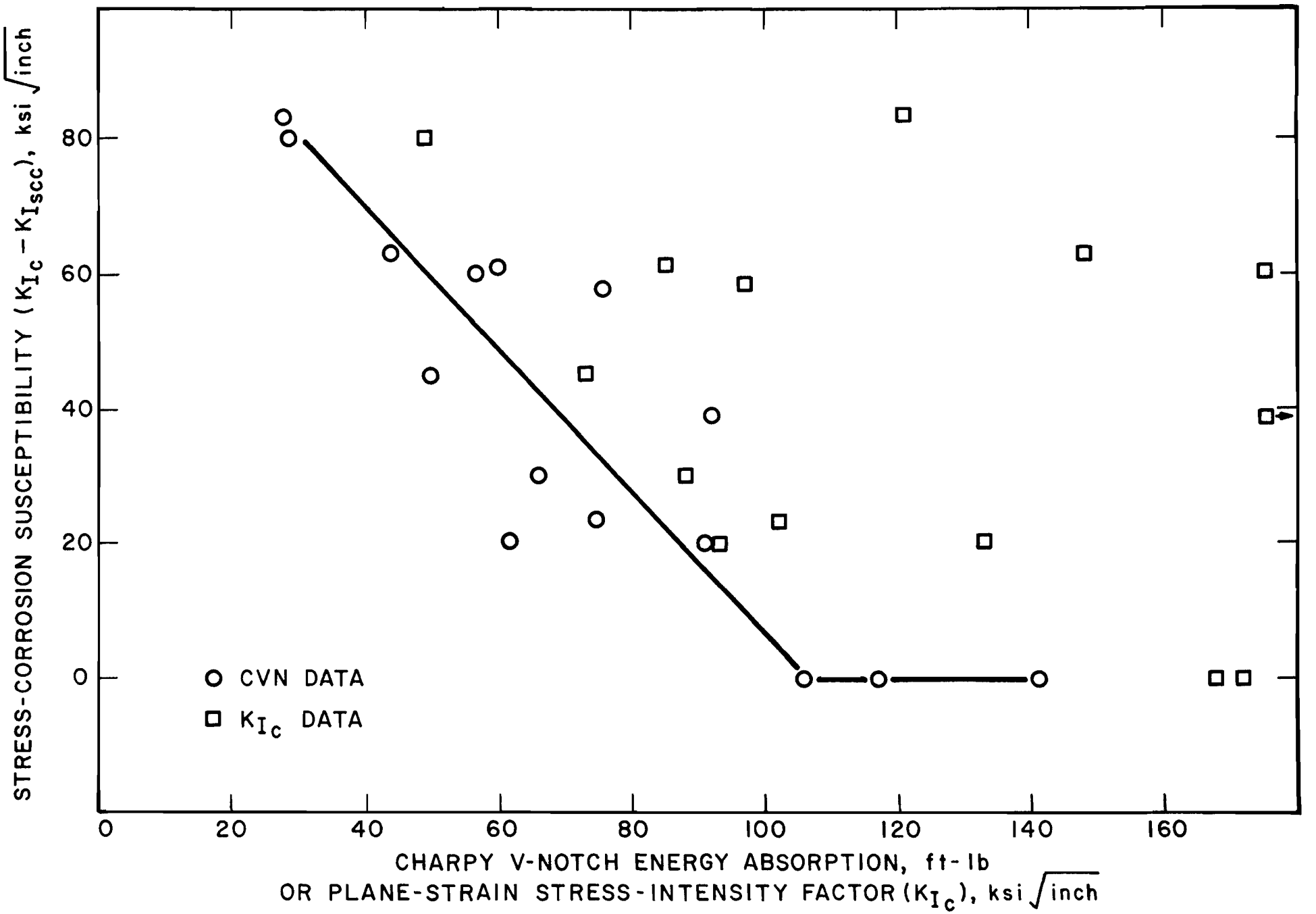

FIG. 14
EFFECT OF TOUGHNESS ON SUSCEPTIBILITY TO STRESS CORROSION IN SEA WATER

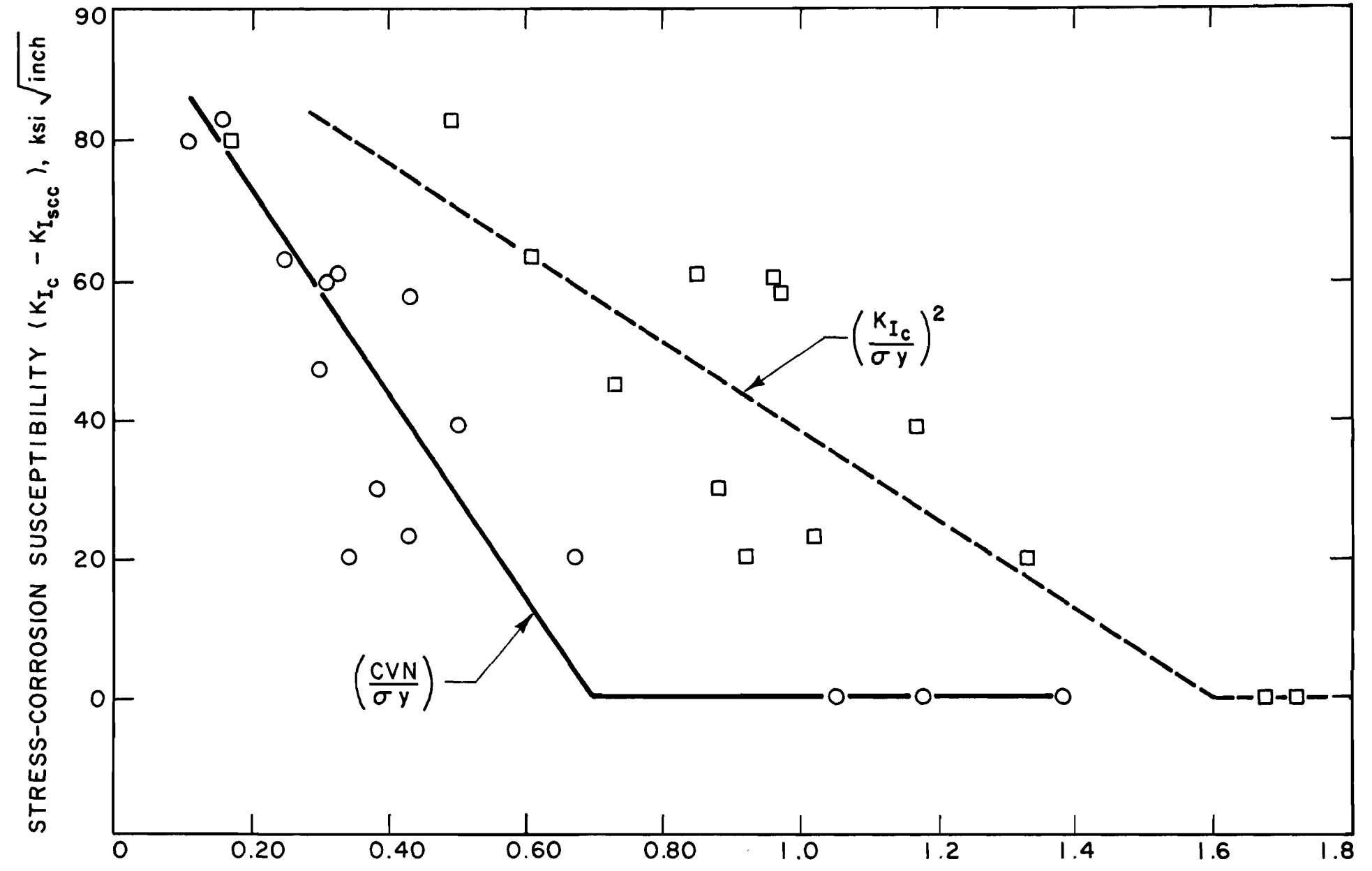

FIG. 15
EFFECT OF FRACTURE-TOUGHNESS-STRENGTH RATIO ON SUSCEPTIBILITY TO STRESS CORROSION IN SEA WATER

CONNECTIONS IN THIN LOW-DUCTILITY STEELS

by A. K. Dhalla[1], S. J. Errera[2], M.ASCE
and G. Winter[3], F.ASCE

INTRODUCTION

The current American Iron and Steel Institute "Specification for the Design of Cold-Formed Steel Structural Members" (1)[4] permits the use of any steel whose "properties and suitability" have been established by a recognized specification or appropriate tests. A problem exists, however, in defining what constitutes a "suitable steel" for cold-formed construction. A research program is in progress at Cornell University aimed at establishing criteria which will be helpful in solving this problem. The investigation is limited to determining the influence of two factors, (a) ductility and (b) the spread between the yield strength and tensile strength, on the behavior of cold-formed members and connections under static loading.

Ductility is the ability of a material to undergo plastic deformations without fracture. It reduces the harmful effects

---

[1]Research Assistant, Department of Structural Engineering, Cornell University, Ithaca, N. Y.

[2]Associate Professor of Structural Engineering Cornell University, Ithaca, N. Y.

[3]Professor of Engineering (Class of 1912 Chair), Cornell University, Ithaca, N. Y.

[4]Numerals in parentheses refer to the corresponding items in Appendix I. - References.

of stress concentrations, permits large local strains without serious damage, and helps achieve uniform stress or load distribution in members or connections. Some codes presently impose restrictions or penalties on allowable design stresses for steels which do not conform to minimum required values of ductility and tensile-yield strength ratios that have been established considering standardized materials that were readily available, and a history of satisfactory performance of those materials. With the increased availability and use of higher strength steels with lower ductility and lower tensile-yield strength ratios, there is need for more definitive information on this subject.

It was felt that connections may be one of the most critical problem areas for low-ductility steels. This report is concerned primarily with an investigation of bolted and welded connections which were fabricated from flat sheet and tested as part of the research program on low-ductility steels.

MATERIAL PROPERTIES

Three types of low carbon steels, designated X, Y and Z, were obtained for this research. Steels X and Y were specially produced for the program; Steel X was cold-reduced an average of 45% in the thickness direction, to produce 12 gage (0.106") and 16 gage (0.062") material and then annealed to arrive at the desired elongation requirements in 2 inches, while Y Steel was cold reduced an average of 33% to obtain 7 gage (0.183") and 12 gage (0.106") material, and received no annealing treatment. Z Steel is an ASTM A446 Grade E commercial product which was obtained in 20 gage (0.038").

It is important to distinguish between the ductility of a material and the ductility of a member as fabricated and subjected to an imposed system of stresses (3). There are a number of standard tests to measure ductility of a material. Of these, the tension coupon test has special significance to a structural engineer since it supplies values for the yield and tensile strength and indicates stress-strain characteristics for static load conditions. A measure of ductility in a coupon test is the elongation at fracture in a specified gage length, usually 2 or 8 inches.

Preliminary standard coupon tests on the steels used in this investigation indicated that although the elongation in a 2-inch gage length was only 4 to 8 percent, the elongation in a 1/4-inch length ranged from 15 to 50 percent. Hence, while ductility as measured by elongation in 2" was "low", some of the materials exhibited very good local ductility.

Many years ago Unwin (7) suggested that total elongation in a bar of gage length L is made up of two parts: the first part is the uniform elongation along the bar and therefore proportional to the gage length, and the other is due to local stretching and contraction of the section which occurs at later stages of the tension coupon test. To include size effects, Unwin used Barba's Law of Similarity and suggested the following equation for strain, ε, in gage length L,

$$\varepsilon = \frac{c\sqrt{A}}{L} + b \qquad (1)$$

where b and c are constants, and A is the cross-sectional area

of the specimen. To extend the range of applicability, Oliver (5) suggested the following modified form of Eq. 1:

$$\varepsilon = K\left[\frac{L}{\sqrt{A}}\right]^{\alpha} \qquad (2)$$

Eq. 2 is a straight line when plotted on a log-log scale; K is the value of strain when $L/\sqrt{A} = 1$, and α is the slope of the line. The relationship suggested by Oliver has the advantage that elongation of various size and shape tension specimens can be compared for specified $L/\sqrt{A}$; it is valid for steel as well as other materials, and the constants K and α are indicative of the mechanical properties of the material tested. K is the indicator of local ductility of the material, while α is a function of the strain hardening property and therefore governs the uniform ductility.

Coupons for standard tension tests were prepared as per ASTM-A370-68 specifications. Initial test speed was 0.005 in/min, which was increased to 0.02 in/min at approximately 1% strain. Load-strain curves were plotted by an autographic recorder using a 2-inch gage length extensometer. Typical complete stress-strain curves are shown in Fig. 1. Curves are plotted for 12 gage X steel (1205X-L2), 16 gage X steel (1605X-L2), 20 gage Z steel (20Z-L5) and 12 gage Y steel (12Y-L2), all in the longitudinal direction; that is, for load applied parallel to the direction of rolling. The curve for 20 gage Z steel in the transverse direction (20Z-T2) is shown in the same figure, because it is the lowest ductility steel used in the investigation, and because the shape of the stress-

strain curve is quite different from that of the same Z steel in the longitudinal direction. It can be observed from Fig. 1 that the major portion of the strain in a 2-inch gage length in X or Y steel occurs after ultimate load is reached, in contrast to the behavior of Z steel. That is, before the necking process starts, a small amount of plastic strain is uniformly distributed over the length of X or Y steel specimens, but afterwards the strain recorded in 2 inches is in effect localized at the eventual fracture zone.

Table 1 presents ductility parameters obtained from representative standard tension coupon tests on X, Y and Z steel, wherein reduction of area, elongation in 1/4-inch gage length (including the fracture), and K are indicators of local ductility of the material, while tensile-to-yield strength ratio, elongation in 2 1/2-inch gage length (excluding the fracture), and α are indicators of uniform ductility. Higher algebraic values given in Table 1 indicate greater local or uniform ductility. For example, comparison of the tabulated values indicates that X and Y steels have more local ductility and less uniform ductility than that observed for Z steel in the longitudinal direction, as confirmed by the stress-strain curves.

Strain hardenability in a material (correlating with significant uniform ductility) can distribute yielding to areas other than where it was initiated, while sufficient local ductility can wipe out the effect of stress concentration.

PLATES WITH HOLES

To determine the behavior of the project steels under stress concentrations, tests were conducted on rectangular plates with holes. From these tests it was concluded that, except for Z steel in the transverse direction, all the project steels were able to develop their full tensile strength as calculated on the net cross-sectional area; that is:

$$\frac{\sigma_{tt}}{\sigma_t} \geq 1.0 \qquad (3)$$

where σ_{tt} is the average tensile stress at P_{ult} calculated on the net area of the plate and σ_t is the tensile strength determined from a standard tension coupon. Eq. 3 indicates that for X and Y steel and Z steel in the longitudinal direction, the effect of the stress concentration near the hole is wiped out and the entire net section is able to fully plastify. For the two tests of Z steel in the transverse direction σ_{tt}/σ_t measured 0.94, a relatively minor reduction from the full tensile strength.

BOLTED CONNECTIONS

The bolted connection is one of the critical problem areas for low ductility steels under static loading. Force is applied at the hole through the contact pressure between the bolt and the plate. This is a more severe stress concentration than that occurring in a rectangular plate with a central hole, wherein the load is applied at the ends of the plate.

A total of 59 single-bolt connection tests were conducted on low ductility steels using both single and double shear

assemblies. Specimens were made from 7 and 12 gage Y steel, 12 and 16 gage X steel and 20 gage Z steel. Holes were drilled 1/16" larger than the bolt diameter, and the bolt was finger tightened with washers under the head and nut. Holes were punched in a few specimens, while in some others the bolts were hand torqued; however, no significant difference in the carrying capacity of the connection was observed due to these variations. Hence all tests were combined to arrive at prediction equations for the failure load. To compare the behavior of low ductility steels with that of high ductility steels, 9 single-bolt connection tests were conducted on 12 and 16 gage full annealed X steel.

Variables considered in the program in addition to the type of steel used were: edge distance, e; bolt diameter, d; sheet thickness, t; plate width, s; and coupon tensile strength, σ_t.

All connections were tested in an hydraulic testing machine. Some selected plates were scribed at 1/4-inch intervals, and measured before and after test under a traveling microscope. All tests were conducted using an autographic recorder with an extensometer gage length of (2e + 1) inches. A sketch of a connection specimen and typical load-deformation curves are presented in Fig. 2.

Ultimate Load Formulas. Observed failure modes of both the low and high ductility steel specimens were the same as previously described by Winter (8). These are:

Type (i) -- Longitudinal shearing of the plate along two nearly parallel planes whose distance is equal to the bolt diameter

Type (ii) -- Bearing failure with considerable elongation of the hole and material "piling up" in front of the bolt

Type (iii) -- Transverse tension-tearing across the net section of the sheet.

Experimental results plotted in Fig. 3 represent shear, bearing or combinations of bearing with either shear or tension modes of failure. The ordinate is the ratio of the computed bearing stress at failure (σ_b) to the tensile strength of the material as determined from a coupon test (σ_t), and the abscissa is the ratio of the edge distance, e, to bolt diameter, d. Up to about e/d = 3.33 the bearing stress ratio increases with increasing e/d and is satisfactorily predicted by the equation

$$\frac{\sigma_b}{\sigma_t} = 0.9 \frac{e}{d} \tag{4}$$

However, for e/d greater than 3.33, the scatter of experimental values increases, and there is a greater tendency toward bearing type failures, rather than predominantly shear type, with little or no increase in bearing stress ratio. Therefore, an upper limit of 3.0 can be placed on Eq. 4. These relationships can be expressed in terms of failure loads for shear (P_s) and bearing (P_b), respectively, as

$$P_s = 0.9 \; e \; t \; \sigma_t \tag{5}$$

and

$$P_b = 3.0\ d\ t\ \sigma_t \tag{6}$$

In Fig. 4 experimental results are plotted for tension and combined bearing and tension modes of failure. Not enough tension failures occurred in the low ductility specimens to develop an expression for the tension failure load (P_t), but the results are in fair agreement with Winter's (8) expression for high ductility steels, i.e.,

$$\frac{\sigma_{net}}{\sigma_t} = (0.1 + 3.0\ \frac{d}{s}) \leq 1.0 \tag{7}$$

or,

$$P_t = (0.1 + 3.0\ \frac{d}{s})\ A_{net}\ \sigma_t \leq A_{net}\ \sigma_t \tag{8}$$

where σ_{net} is the average tensile stress at failure, calculated on the net area (A_{net}) of the cross-section. In both Figs. 3 and 4 it is noted that connections using Z steel, which is the thinnest material and has the lowest local ductility, tend to give lower results than the others. The maximum shear, bearing or tensile stresses according to Eqs. 5, 6 and 8 are

$$(\tau_s)_{max} = P_s/2\ e\ t = 0.45\ \sigma_t \tag{9}$$

$$(\sigma_b)_{max} = P_b/dt = 3.0\ \sigma_t \tag{10}$$

$$(\sigma_{net})_{max} = P_t/A_{net} = (0.1 + 3.0\ \frac{d}{s})\ \sigma_t \leq \sigma_t \tag{11}$$

Comparison with High Ductility Steels. Results of tests of the nine full annealed X Steel connection specimens agreed with Winter's prediction equations for high ductility steels, and are not presented here. Winter's expressions for failure stresses are recorded below for comparison with the low-ductility

steel test results.

$$(\tau_s)_{max} = 0.70\ \sigma_y \tag{12}$$

$$(\sigma_b)_{max} = 4.9\ \sigma_y \tag{13}$$

$$(\sigma_{net})_{max} = (0.1 + 3.0\ \frac{d}{s})\ \sigma_t \leq \sigma_t \tag{14}$$

where σ_y is the yield stress of the material in tension. Eqs. 12 and 13 predict failure stresses in shear and bearing in terms of yield stress of the material, because this property gave best correlation with the test results. The tensile-yield strength ratio for the steels in those tests averaged about 1.35. Applying this factor to Eqs. 12 and 13, the shear and bearing failure stresses for the high ductility steels can be expressed as $\tau_s = 0.52\ \sigma_t$ and $\sigma_b = 3.6\ \sigma_t$. In contrast, for low ductility steels Eqs. 9 and 10 show $\tau_s = 0.45\ \sigma_t$ and $\sigma_b = 3.0\ \sigma_t$. Thus, the shear and bearing strength of low ductility steel, in terms of σ_t, is somewhat lower than for high ductility steel, while the tensile strength in the net section seems unaffected by the lower ductility.

Comparisons of high and low ductility steel also have been made for connections with two or three bolts in line with the applied stress (6). Here too it was found that the tensile strength of the connection was unaffected by the ductility of the steel.

Alternate Prediction of Ultimate Load (2). There is a fair amount of scatter in the test results shown in Fig. 3, particularly when combined failure modes are involved; hence alternate predictions of the failure load were sought. Function-

al dependence of the ultimate load, P_{ult}, on the variables considered can be obtained using dimensional analysis (4). For a single-bolt connection, the relationship can be expressed as

$$\frac{P_{ult}}{\sigma_t d^2} = f_1 \left(\frac{\sigma_b}{\sigma_t} , \frac{\sigma_s}{\sigma_t} , \frac{e}{d} , \frac{s}{d} , \frac{t}{d} \right) \tag{15}$$

If the bearing stress σ_b and the shear stress τ_s are assumed to be proportional to the tensile strength σ_t of the material, then Eq. 15 reduces to

$$\frac{P_{ult}}{(td)} \frac{(td)}{\sigma_t d^2} = \frac{\sigma_b}{\sigma_t} \left(\frac{t}{d}\right) = f_2 \left(\frac{e}{d} , \frac{s}{d} , \frac{t}{d}\right) \tag{16}$$

This expression can be modified further, with due recognition of limiting conditions, to obtain predictions of the form presented earlier for shear or tension failures. In addition, using a trial and error approach to provide a best fit to the data and to evaluate numerical coefficients, the following expression for bearing or combined failures was obtained:

$$P_c = 0.32 \left(\frac{e}{d} + \frac{s}{d} + 1\right) - 0.04 \frac{d}{t} \tag{17}$$

provided $\quad 2.25 \leq \frac{e}{d} \leq 3.30$

and $\quad 3.33 \leq \frac{s}{d} \leq 6.00$

This prediction is plotted in non-dimensional form along with the pertinent data in Fig. 5. The prediction error is reduced an average of about 25% compared to Eqs. 5 and 6, at the cost of additional complexity.

FILLET WELDED CONNECTIONS

Variables considered in the tests of longitudinal and transverse fillet weld connections included: length of weld, L; thickness of material, t; and type of steel. For the low ductility steel specimens where the tensile strength of the material ranged from 75 to 100 ksi, low hydrogen welding electrode E-10018 (ASTM designation A-316) was used. A few tests were made on full annealed X steel specimens (12FAX) using low hydrogen E-7018 electrodes. To facilitate the welding process the connection specimens were clamped on a steel table, which also served as a heat sink. Voltage was held constant at 25 volts, and current input was varied for the different sheet thicknesses to obtain a satisfactory weld without undercutting the material. The current as recorded by an ammeter was 120, 120, 85 and 60 amps, respectively, for 7, 12, 16 and 20 gage sheets.

LONGITUDINAL FILLET WELD CONNECTIONS

Fig. 6 shows a sketch of the longitudinal fillet weld connections. The width of the narrower plate, b_n, was 3.0" for all except the 7Y and 12FAX specimens, where b_n was 2.5" and 4.0" respectively. The width of the other plate, b_w, was 1 inch greater than b_n to facilitate welding. Table 2 gives the weld lengths along with the average mechanical properties of the material. The eighteen specimens were divided into three groups: Group I specimens were designed to fail in tension in the plate, called type "a" failure. Group II specimens were designed to produce shear failure in the weld, called type "b"

failure. Group III specimens were designed so that either type of failure was equally likely.

Tension tests were conducted in an hydraulic testing machine, and load-deformation curves were autographically recorded for a gage length of (L + 3) inches. The results are presented in Table 2. The following observations are made:

(1) All the specimens in Group I, which had the longest weld length, failed by transverse tearing of the narrower plate (type "a" failure). Group II specimens which had the shortest weld length, failed by shearing of the weld (type "b"), except for the full annealed specimen which exhibited a combined type failure. In Group III, the failures were about evenly divided.

(2) For the low ductility steel specimens that failed in tension, the ratio of the tensile strength developed by the plate, σ_{tt}, to the tensile strength of the coupon, σ_t, ranges from 0.89 to 1.05, and averages 0.96. This compares favorably with the corresponding value of 0.88 for the specimen of full annealed material (12FAX-L6) which failed in tension, and indicates that connections made with low ductility steel were able to develop almost the full strength of the narrower plate. Considerable out-of-plane deformation occurred in Specimen 12FAX-L6 (and other full-annealed specimens) after the yield load was reached; this may have reduced the resulting ultimate carrying capacity.

(3) For type "b" failures, comparison can be made between the computed shear strength of the weld and the expected shear strength of the weld, where the expected shear strength is

assumed to be 0.577 times the minimum tensile strength of the weld metal as specified by ASTM. This ratio ranges from 0.99 to 1.05 for Group II specimens of low ductility steel except for 1205X-L9 which may have had a defective weld. The same ratio for Type "b" failures in Group III specimens ranges from 0.94 to 0.98. That is, the shorter welds of Group II apparently had more uniform stress distribution, and thus higher average stresses, than the longer welds of Group III.

(4) For Group I specimens which failed in tension, the local ductility parameter (elongation in 1/4-inch gage length, Col. 10) is in satisfactory agreement with the values obtained in the tension coupon tests (Col. 4).

TRANSVERSE FILLET WELD CONNECTIONS

The high strength of the low carbon X, Y and Z steels was achieved by cold working. Therefore, it was anticipated that partial annealing of these low ductility steels due to weld heat would reduce the tension strength of the transverse fillet weld connections shown in Fig. 7. Unlike a longitudinally welded specimen, the whole cross-section of a full width transverse weld specimen is partially annealed. For a partial width weld, only the part of the cross-section that is welded would be affected. The reduction in strength would depend upon the length of weld on the critical cross-section and the details of the welding procedure.

The transverse fillet weld specimens were divided into four groups as indicated below and in Table 3 and Fig. 7.

Group IV: single lap, full width welds

Group V: single lap, partial width welds

Group VI: single lap, full width unsymmetrical welds

Group VII: double lap, full width welds

Seventeen transverse fillet weld specimens were designed using 7 and 12 gage Y steel, 12 and 16 gage X steel, and 20 gage Z steel. Duplicate specimens were made; but for brevity, only 7 gage Y , 12 gage X and 20 gage Z tests are presented in Table 3. However, the observations made subsequently apply to all 34 specimens tested. The test procedure for the transverse weld specimens was the same as for the longitudinally welded connections.

All specimens in Groups IV, VI and VII failed by transverse tearing of the connected plate. Tension failure in these specimens is designated by types "a", "c" and "d" in Fig. 7 and Table 3, to differentiate between the different modes of tension tearing. Type "a" failure gives an inclined fracture, which is the same as that observed in longitudinally welded specimens. Type "c" failure follows the contour of the fillet weld toe. Type "d" failure occurred in some of the partial width weld specimens; it follows the contour of the toe for the length of the weld, and is inclined in the unwelded portions of the plate. Three of the partial width weld specimens included in Table 3 failed in the weld (type "b" failure), and three had type "d" failures.

The predicted maximum load for a plate of thickness t and width b_n is given by

$$P_{max} = b_n \, t \, \sigma_t \qquad (18)$$

where σ_t is the tensile coupon strength of the material. The ratio of the tensile strength developed by the connected plate, σ_{tt}, to the tensile coupon strength σ_t is given in Col. 5 of Table 3. This ratio is between 0.84 and 0.96 for all of the Group IV, VI and VII specimens (full width welds) which failed by tension tearing. Within any one group, the ratio increases with increasing thickness of the material. The double lap specimens of Group VII have about the same strength ratio as Group IV and VI specimens, indicating that the small strength reduction of approximately 10% due to some annealing is caused by only one pass of the welding electrode, and subsequent welding on the same cross-section does not reduce the tension strength any further.

The partial width weld specimens of Group V which failed in tension had σ_{tt}/σ_t ratios of 0.92 to 0.99, averaging slightly higher than the full width weld specimens. Apparently only that part of the cross section which was welded had its strength somewhat reduced by partial annealing, while the part which was not welded developed tensile strength close to that obtained in the coupons.

Two high-ductility X steel transverse fillet weld specimens in Groups IV and V were tested to compare their behavior with low ductility specimens. There was no reduction in the strength of these connections due to the welding process.

CONCLUSIONS

Bolted and fillet welded connections in thin low-ductility

steels were tested as part of a research program investigating the influence of ductility on the behavior of cold-formed members under static loading. In dealing with such steels it appears necessary to distinguish between uniform ductility and local ductility. Uniform ductility is characterized by the ability of a member made of the subject material to undergo sizeable plastic deformations over significant portions of its length, prior to failure. Such ductility is attained if a material possesses a significant strain hardening range. On the other hand, local ductility is the ability to undergo plastic deformation in a localized area. Most of the "low ductility" steels investigated herein showed significant local ductility.

The modes of failure and simplified formulas obtained for single-bolt connections are similar for low and high ductility steels. In terms of coupon tensile strength σ_t, maximum shear and bearing stress values for low ductility steels are 0.45 σ_t and 3.0 σ_t, respectively. Corresponding values for high ductility steels are 0.52 σ_t and 3.6 σ_t respectively, indicating that the low ductility of these special steels lowered the strength of the tested bolted connections only by about 15% in terms of the coupon tensile strength. Bolted connections of low ductility steel showed adequate elongation capability.

The low ductility steels were weldable; that is, no special welding process was used in fabricating the specimens, nor were any noticeable defects observed. In longitudinal

fillet weld specimens with adequate weld length, the connections developed almost the full predicted load based on coupon tensile strength. Both plate failure and weld failure of longitudinal fillet weld connections in these low ductility steels can be predicted using the same methods as for high ductility steel.

Transverse fillet weld specimens showed some effect of partial annealing, but still developed an average stress of more than 90% of the coupon tensile strength.

ACKNOWLEDGMENTS

This research was sponsored by the American Iron and Steel Institute. The cooperation of the cognizant research committee, and of the companies who furnished the steels for the investigation, is gratefully acknowledged.

APPENDIX I. - REFERENCES

1. American Iron and Steel Institute, "Specification for the Design of Cold-Formed Steel Structural Members," 1968 Edition, N. Y.

2. Dhalla, A. K., "Influence of Ductility on the Structural Behavior of Cold-Formed Steel Members", Dept. of Structural Engineering Report No. 336, Cornell University, Ithaca, N. Y. (to be published).

3. Frankland, J. M., "Physical Metallurgy and Mechanical Properties of Materials: Ductility and the Strength of Metallic Structures,", Proc. ASCE, Vol. 86, No. EM6, Dec. 1960.

4. Murphy, G., "Similitude in Engineering," The Ronald Press Co., N. Y., 1950.

5. Oliver, D. A., "Proposed New Criteria of Ductility from a New Law Connecting the Percentage Elongation to the Size of Test Piece," Inst. of Mech. Engineers, Vol. II, 1928.

6. Popowich, D. W., "Tension Capacity of Bolted Connections in Light Gage Cold-Formed Steel," thesis presented to Cornell University, in 1969, in partial fulfillment for the requirements of the degree of Master of Science.

7. Unwin, W. C., "Tensile Tests of Mild Steel, and the Relation of Elongation to the Size of the Test Bar," Proc. Inst. of Civil Engineers, 1903.

8. Winter, G., "Tests on Bolted Connections in Light Gage Steel," Proc. ASCE, Vol. 82, Paper No. 920, March 1956.

APPENDIX II. - NOTATION

The following symbols are used in this paper:

A = Gross cross-sectional area of coupon or tension member.

A_{net} = Net cross-sectional area of a tension member or connection.

b = Constant used in Eq. 1.

b_n = Width of the narrower plate in fillet welded connections.

b_w = Width of the wider plate in fillet welded connections.

c = Constant used in Eq. 1.

d = Diameter of the bolt.

e = Edge distance in bolted connection.

K = Constant which indicates local ductility of the material.

L = Gage Length.

P_b = Bearing failure load in bolted connection.

P_c = Combination failure load in bolted connection.

P_{max} = Predicted maximum load.

P_s = Shear failure load in bolted connection.

P_t = Tension failure load in bolted connection.

P_{ult} = Ultimate load.

S = Width of plate.

t = Thickness of plate.

α = Constant which indicates strain hardening capacity of the material.

ϵ = Elongation in gage length L in coupon test.

σ_t = Tensile strength of the material.

σ_{tt} = Average tensile stress at P_{ult} calculated on net area of the connected plate.

σ_y = Yield strength of the material.

τ_{sa} = Shear strength of the electrode.

τ_{su} = Shear strength of fillet weld.

TABLE 1

DUCTILITY CHARACTERISTICS OF X, Y AND Z STEELS

Ductility Parameters	20Z-L-Av. Z Steel (Long.)	20Z-T-Av. Z Steel (Trans.)	12Y-L3 Y Steel (Long.)	1205X-L2 X Steel (Long.)	1605X-L3 X Steel (Long.)	16FAX-L1 X-Annealed Steel (Long.)
Elongation in 2" (%)	4.38	1.51	5.13	5.58	6.84	52.20
Reduction in Area (%)	56.10	33.50	65.20	69.40	59.00	83.80
Tensile/ Yield Ratio	1.08	1.00	1.01	1.00	1.00	1.48
Elongation in 1/4" Including Neck (%)	15.55	6.09	38.40	44.40	35.20	85.60
Elongation in 2 1/2" Excluding Neck (%)	2.74[a]	0.48	0.33	0.40	1.28	38.00
K	20.50	12.10	45.00	46.00	45.00	120.00
α	-0.579	-0.834	-0.974	-0.983	-0.795	-0.335

[a]This value is for elongation in 2", excluding neck.

TABLE 2
LONGITUDINAL FILLET WELD CONNECTIONS

1	2	3	4	5	6	7	8	9	10	11
		Avg. Mat'l Properties			Experimental Results					
Spec. Designation**	Lap Length L in	Tensile Str. of Coupon σ_t ksi	Elong. in 1/4" G. L. %	Shear Str.of Electrode* τ_{sa} ksi	Tensile Str.of Plate σ_{tt} ksi	Shear Str.of Weld τ_{su} ksi	$\frac{\sigma_{tt}}{\sigma_t}$	$\frac{\tau_{su}}{\tau_{sa}}$	Elong. in 1/4" G. L. %	Mode of Failure type
GROUP I SPECIMENS										
7Y-L-L1	3.25	83.3	47.0	57.7	83.7	45.5	1.00	0.78	49.8	a
12Y-L-L2	3.25	82.5	31.4	57.7	78.8	51.0	0.96	0.88	27.6	a
1205X-L-L3	3.25	84.1	29.9	57.7	79.0	51.6	0.94	0.89	32.4	a
1605X-L-L4	3.75	98.0	26.6	57.7	87.8	50.2	0.89	0.87	21.7	a
20Z-L-L5	3.50	81.7	15.5	57.7	86.0	52.2	1.05	0.90	12.0	a
12FAX-L-L6	3.75	45.0	105.0	40.4	39.9	29.5	0.88	0.73	102.0	a
GROUP II SPECIMENS										
7Y-L-L7	2.25	83.3	47.0	57.7	73.8	58.4	0.88	1.01	16.8	b
12Y-L-L8	2.25	82.5	31.4	57.7	60.8	57.5	0.74	0.99	8.8	b
1205X-L-L9	2.25	84.1	29.9	57.7	50.2	47.6	0.60	0.82	38.8	b
1605X-L-L10	2.75	98.0	26.6	57.7	75.7	58.8	0.77	1.02	--	b
20Z-L-L11	2.50	81.7	15.5	57.7	62.2	53.0	0.76	0.92	--	b
12FAX-L-L12	1.50	45.0	105.0	40.4	22.7	42.8	0.51	1.06	25.6	a+b
GROUP III SPECIMENS										
7Y-L-L13	2.75	83.3	47.0	57.7	82.0	52.6	0.98	0.91	20.2	a
12Y-L-L14	2.75	82.5	31.4	57.7	70.0	54.1	0.85	0.94	--	b
1205X-L-L15	2.75	84.1	29.9	57.7	70.5	56.6	0.84	0.98	--	b
1605X-L-L16	3.25	98.0	26.6	57.7	85.7	56.4	0.87	0.97	5.6	b
20Z-L-L17	2.85	81.7	15.5	57.7	74.3	55.4	0.91	0.95	--	a
12FAX-L-L18	2.00	44.6	105.0	40.4	28.2	38.6	0.63	0.95	24.6	a+b

*Computed as 0.577 x ASTM specified minimum tensile strength.

**Load was applied parallel to the direction of rolling.

TABLE 3
TRANSVERSE FILLET WELD CONNECTIONS[1]

Specimen Designation[p]	Total Length of Weld L in	Tensile Str. of Coupon σ_t ksi	Experimental Results: Tensile Str. of Plate σ_{tt} ksi	$\frac{\sigma_{tt}}{\sigma_t}$	Mode of Failure Type[m]
GROUP IV - FULLY WELDED SPECIMENS					
20Z-TF-L11	6.04	81.7	70.0	0.86	c
20Z-TF-L12	6.02	81.7	68.3	0.84	c
1205X-TF-L31	6.02	74.6	66.5	0.89	c
1205X-TF-L32	6.02	74.6	67.2	0.91	c
7Y-TF-L51	6.00	86.3	80.9	0.94	c
7Y-TF-L52	6.00	86.3	80.9	0.94	a
GROUP V - PARTIALLY WELDED SPECIMENS					
20Z-TP-L11	3.50	81.7	75.1	0.92	d
20Z-TP-L12	3.60	81.7	77.0	0.94	d
1205X-TP-L31	3.64	74.6	73.7	0.99	d
1205X-TP-L32	3.08	74.6	73.1	0.98[n]	b
7Y-TP-L51	3.60	86.3	73.4	0.85[n]	b
7Y-TP-L52	3.44	86.3	71.8	0.83[n]	b
GROUP VI - UNSYMMETRICALLY WELDED SPECIMENS					
20Z-TU-L11	6.02	81.7	71.5	0.87	c
20Z-TU-L12	6.02	81.7	72.3	0.88	c
1205X-TU-L31	6.02	74.6	70.3	0.94	c
1205X-TU-L32	6.02	74.6	70.9	0.95	c
7Y-TU-L51	6.00	86.3	82.0	0.95	a
7Y-TU-L52	6.00	86.3	82.5	0.96	a
GROUP VII - DOUBLY LAPPED SPECIMENS					
20Z-TD-L11	6.02	81.7	70.3	0.86	c
20Z-TD-L12	6.02	81.7	69.0	0.84	c
7Y-TD-L51	6.00	86.3	82.0	0.95	a
7Y-TD-L52	6.00	86.3	81.5	0.94	c

[1] Geometry of the specimens is shown in Fig. 7.

[m] Modes of failure are indicated by dotted lines in Fig. 7.

[n] $\frac{\tau_{su}}{\tau_{sa}}$ ratios for specimens 1205X-TP-L32, 7Y-TP-L51 and L-52 are 1.73, 1.48, and 1.55 respectively.

[p] Load was applied parallel to the direction of rolling.

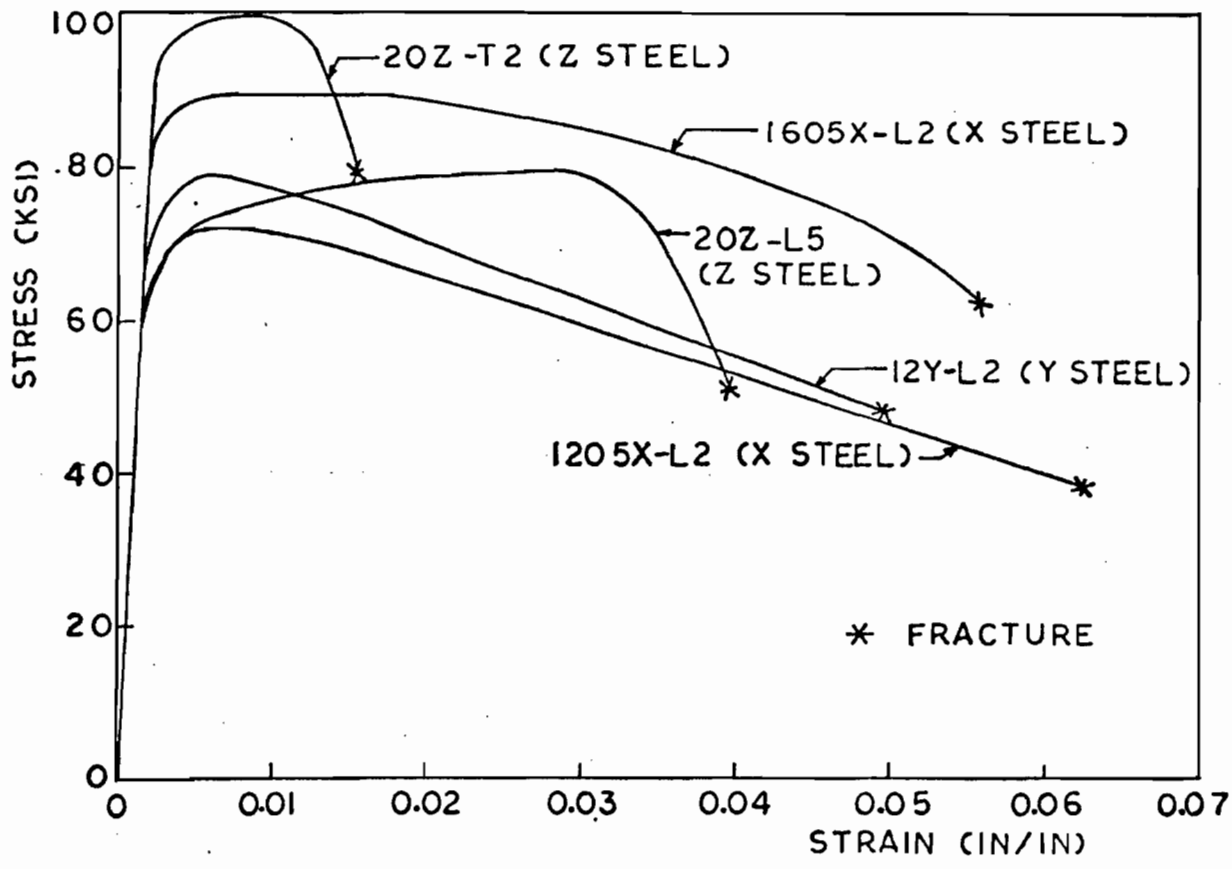

FIG. 1. COMPLETE STRESS STRAIN CURVES OF X, Y AND Z STEELS (2" G.L.)

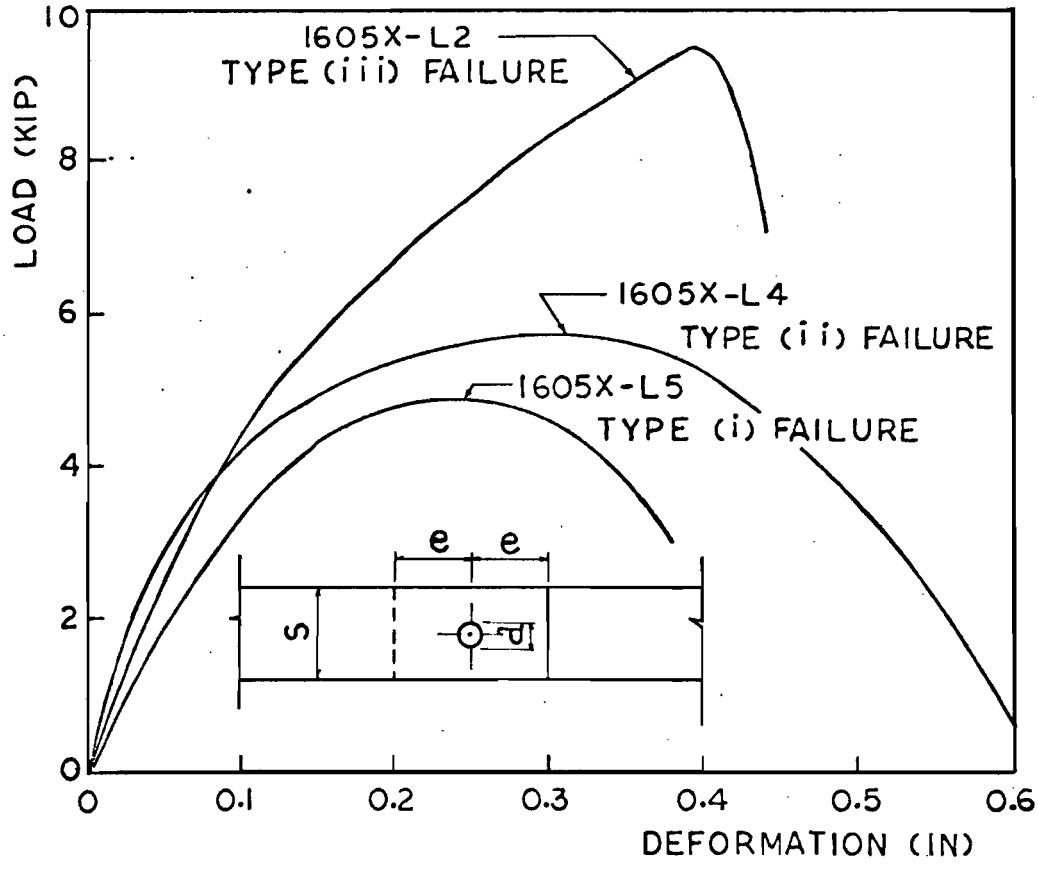

FIG.2. LOAD-DEFORMATION CURVES, 16 GAGE 'X' STEEL BOLTED CONNECTIONS

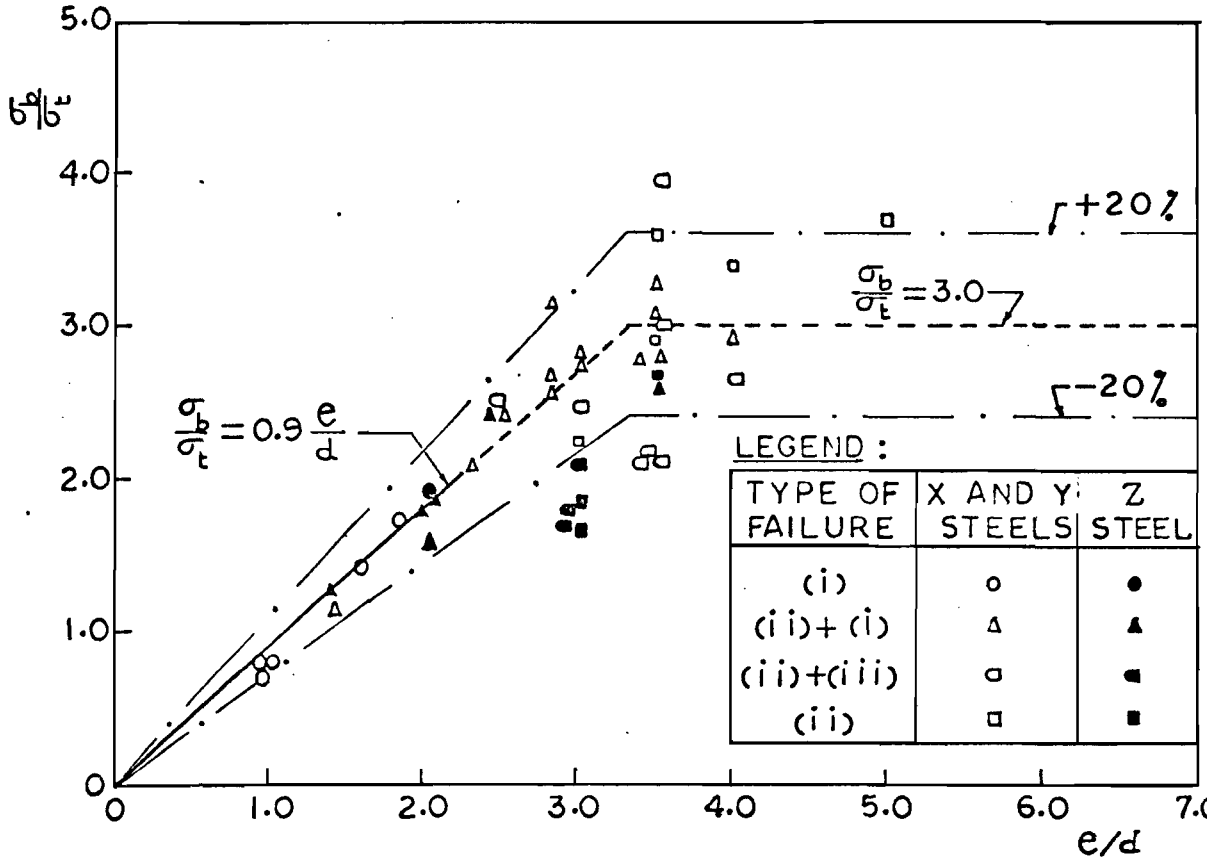

FIG. 3. BEARING AND SHEAR OR COMBINED FAILURES

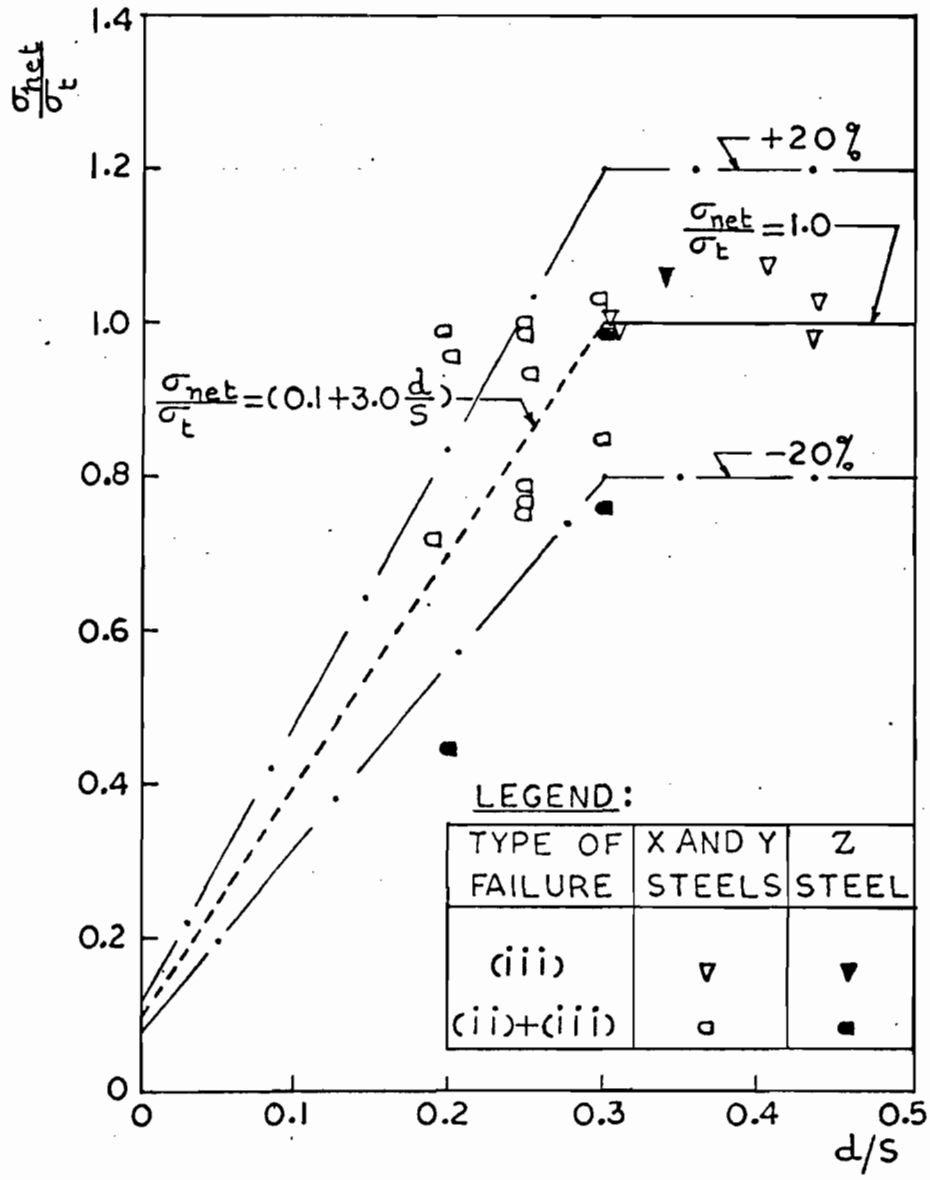

FIG. 4. TRANSVERSE TEARING OR COMBINATION FAILURES

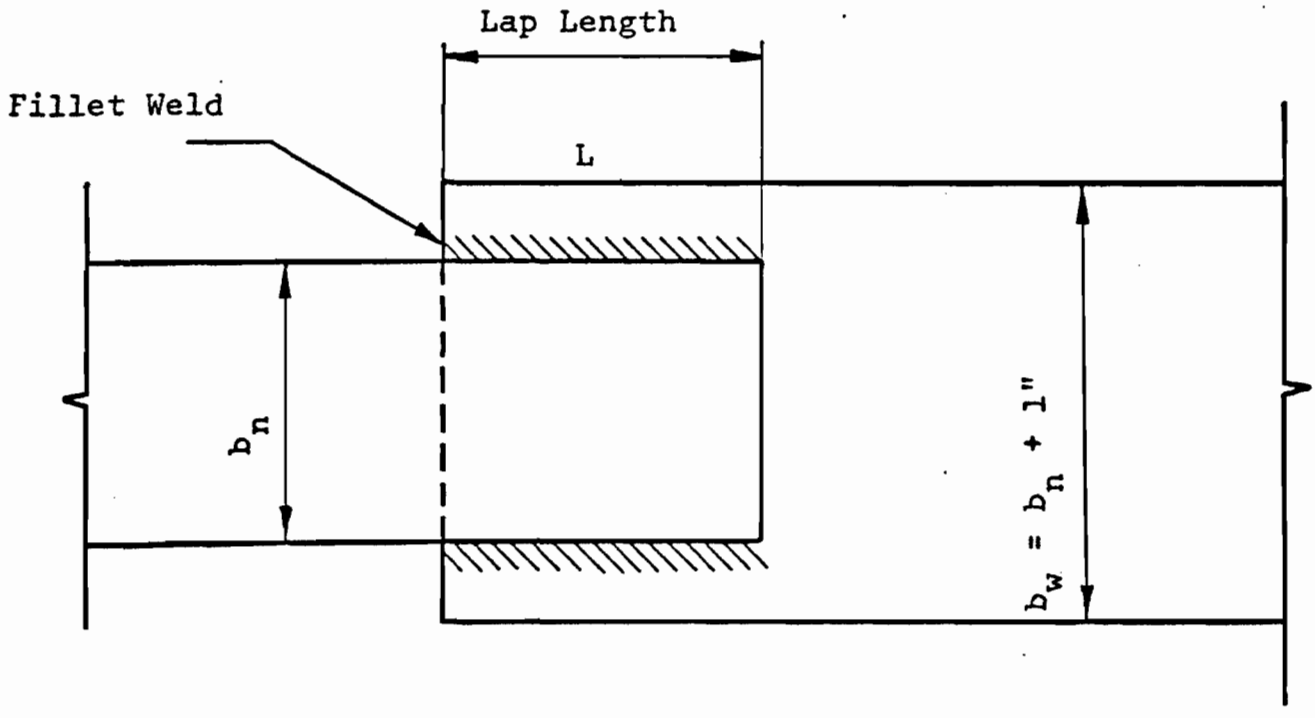

FIG. 6. SINGLE LAP LONGITUDINAL FILLET WELD CONNECTION.

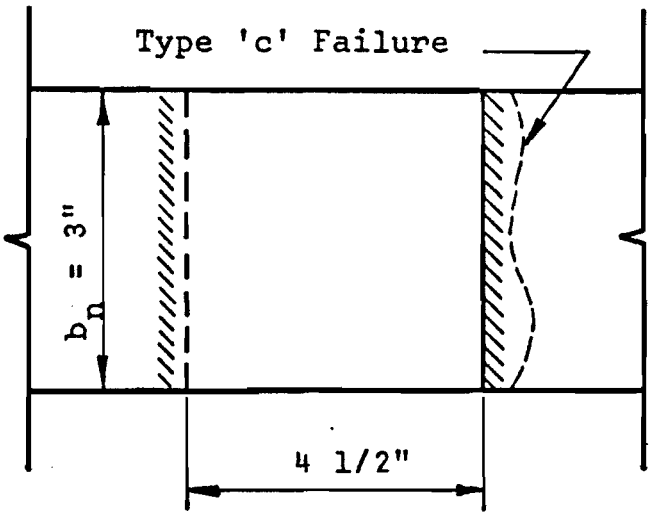

a. Single Lap, Full Length Weld (TF).

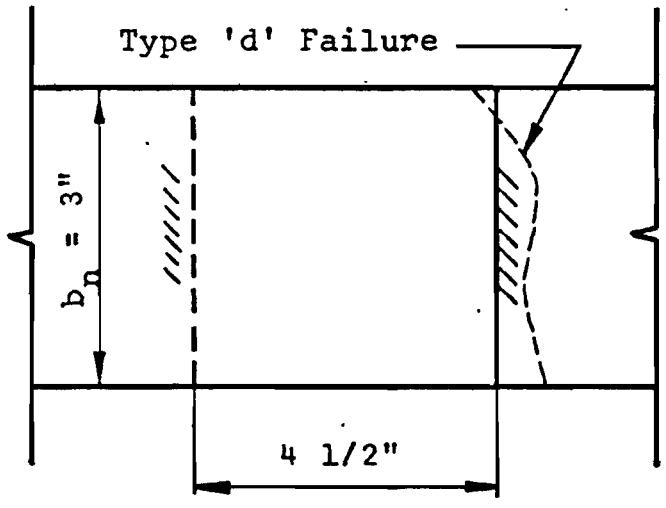

b. Single Lap, Partial Width Weld (TP).

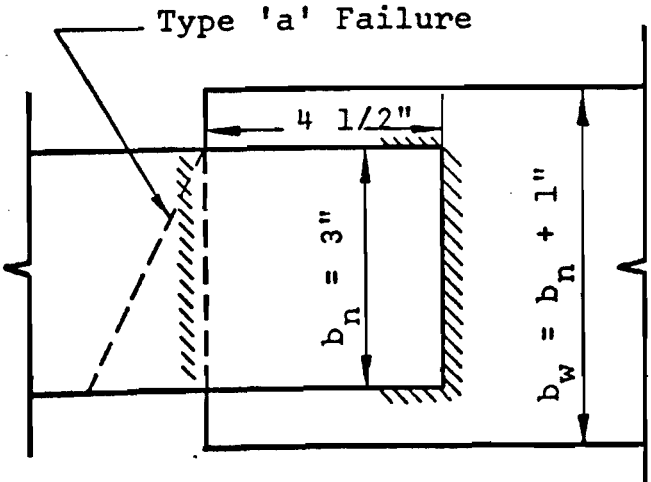

c. Single Lap, Unsymmetric Weld (TU).

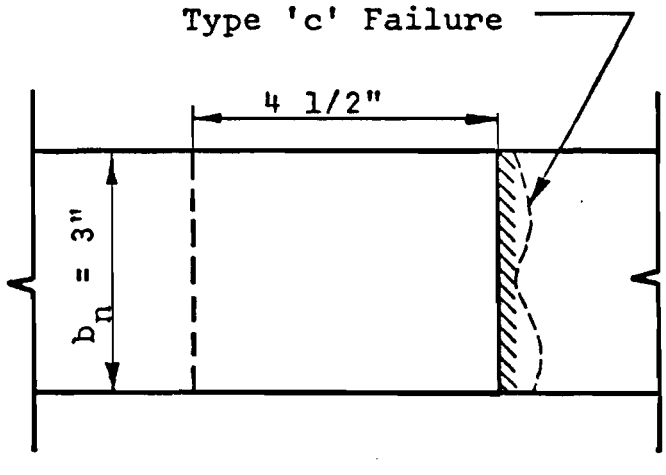

d. Double Lap, Full Width Weld (TD).

FIG. 7. TRANSVERSE FILLET WELD SPECIMENS.

SUMMARY

Tests were made on bolted and fillet welded connections in thin low-ductility low carbon steels. Material elongation in a 2-inch gage length ranged from 4% to 8%, while the tensile to yield strength ratio ranged from 1.0 to 1.1. The load carrying capacity of the connections can be predicted by equations similar to those for high ductility steels.

ABSTRACT

Bolted and fillet welded connections fabricated from flat sheets of thin low-ductility low carbon steels were tested as part of a research program investigating the influence of ductility on the behavior of cold-formed members under static loading. Material elongation in a 2-inch gage length ranged from 4% to 8%, while the tensile to yield strength ratio ranged from 1.0 to 1.1. Standard tension coupon test procedures were modified to distinguish between local and uniform ductility of the material. The load carrying capacity of the connections can be predicted by equations similar to those for high ductility steels.

KEY WORDS

Bolted Connection

Cold Formed

High Ductility

High Strength

Local Ductility

Longitudinal Fillet Weld

Low Carbon Steel

Low Ductility

Plane Stress

Structural Engineering

Tension Coupon

Transverse Fillet Weld

Uniform Ductility

CONNECTIONS IN THIN LOW-DUCTILITY STEELS

by A. K. Dhalla[1], S. J. Errera[2], M.ASCE
and G. Winter[3], F.ASCE

INTRODUCTION

The current American Iron and Steel Institute "Specification for the Design of Cold-Formed Steel Structural Members" (1)[4] permits the use of any steel whose "properties and suitability" have been established by a recognized specification or appropriate tests. A problem exists, however, in defining what constitutes a "suitable steel" for cold-formed construction. A research program is in progress at Cornell University aimed at establishing criteria which will be helpful in solving this problem. The investigation is limited to determining the influence of two factors, (a) ductility and (b) the spread between the yield strength and tensile strength, on the behavior of cold-formed members and connections under static loading.

Ductility is the ability of a material to undergo plastic deformations without fracture. It reduces the harmful effects

---

[1]Research Assistant, Department of Structural Engineering, Cornell University, Ithaca, N. Y.

[2]Associate Professor of Structural Engineering Cornell University, Ithaca, N. Y.

[3]Professor of Engineering (Class of 1912 Chair), Cornell University, Ithaca, N. Y.

[4]Numerals in parentheses refer to the corresponding items in Appendix I. - References.

of stress concentrations, permits large local strains without serious damage, and helps achieve uniform stress or load distribution in members or connections. Some codes presently impose restrictions or penalties on allowable design stresses for steels which do not conform to minimum required values of ductility and tensile-yield strength ratios that have been established considering standardized materials that were readily available, and a history of satisfactory performance of those materials. With the increased availability and use of higher strength steels with lower ductility and lower tensile-yield strength ratios, there is need for more definitive information on this subject.

It was felt that connections may be one of the most critical problem areas for low-ductility steels. This report is concerned primarily with an investigation of bolted and welded connections which were fabricated from flat sheet and tested as part of the research program on low-ductility steels.

MATERIAL PROPERTIES

Three types of low carbon steels, designated X, Y and Z, were obtained for this research. Steels X and Y were specially produced for the program; Steel X was cold-reduced an average of 45% in the thickness direction, to produce 12 gage (0.106") and 16 gage (0.062") material and then annealed to arrive at the desired elongation requirements in 2 inches, while Y Steel was cold reduced an average of 33% to obtain 7 gage (0.183") and 12 gage (0.106") material, and received no annealing treatment. Z Steel is an ASTM A446 Grade E commercial product which was obtained in 20 gage (0.038").

It is important to distinguish between the ductility of a material and the ductility of a member as fabricated and subjected to an imposed system of stresses (3). There are a number of standard tests to measure ductility of a material. Of these, the tension coupon test has special significance to a structural engineer since it supplies values for the yield and tensile strength and indicates stress-strain characteristics for static load conditions. A measure of ductility in a coupon test is the elongation at fracture in a specified gage length, usually 2 or 8 inches.

Preliminary standard coupon tests on the steels used in this investigation indicated that although the elongation in a 2-inch gage length was only 4 to 8 percent, the elongation in a 1/4-inch length ranged from 15 to 50 percent. Hence, while ductility as measured by elongation in 2" was "low", some of the materials exhibited very good local ductility.

Many years ago Unwin (7) suggested that total elongation in a bar of gage length L is made up of two parts: the first part is the uniform elongation along the bar and therefore proportional to the gage length, and the other is due to local stretching and contraction of the section which occurs at later stages of the tension coupon test. To include size effects, Unwin used Barba's Law of Similarity and suggested the following equation for strain, ϵ, in gage length L,

$$\epsilon = \frac{c\sqrt{A}}{L} + b \qquad (1)$$

where b and c are constants, and A is the cross-sectional area

of the specimen. To extend the range of applicability, Oliver (5) suggested the following modified form of Eq. 1:

$$\varepsilon = K\left[\frac{L}{\sqrt{A}}\right]^{\alpha} \qquad (2)$$

Eq. 2 is a straight line when plotted on a log-log scale; K is the value of strain when $L/\sqrt{A} = 1$, and α is the slope of the line. The relationship suggested by Oliver has the advantage that elongation of various size and shape tension specimens can be compared for specified $L/\sqrt{A}$; it is valid for steel as well as other materials, and the constants K and α are indicative of the mechanical properties of the material tested. K is the indicator of local ductility of the material, while α is a function of the strain hardening property and therefore governs the uniform ductility.

Coupons for standard tension tests were prepared as per ASTM-A370-68 specifications. Initial test speed was 0.005 in/min, which was increased to 0.02 in/min at approximately 1% strain. Load-strain curves were plotted by an autographic recorder using a 2-inch gage length extensometer. Typical complete stress-strain curves are shown in Fig. 1. Curves are plotted for 12 gage X steel (1205X-L2), 16 gage X steel (1605X-L2), 20 gage Z steel (20Z-L5) and 12 gage Y steel (12Y-L2), all in the longitudinal direction; that is, for load applied parallel to the direction of rolling. The curve for 20 gage Z steel in the transverse direction (20Z-T2) is shown in the same figure, because it is the lowest ductility steel used in the investigation, and because the shape of the stress-

strain curve is quite different from that of the same Z steel in the longitudinal direction. It can be observed from Fig. 1 that the major portion of the strain in a 2-inch gage length in X or Y steel occurs after ultimate load is reached, in contrast to the behavior of Z steel. That is, before the necking process starts, a small amount of plastic strain is uniformly distributed over the length of X or Y steel specimens, but afterwards the strain recorded in 2 inches is in effect localized at the eventual fracture zone.

Table 1 presents ductility parameters obtained from representative standard tension coupon tests on X, Y and Z steel, wherein reduction of area, elongation in 1/4-inch gage length (including the fracture), and K are indicators of local ductility of the material, while tensile-to-yield strength ratio, elongation in 2 1/2-inch gage length (excluding the fracture), and α are indicators of uniform ductility. Higher algebraic values given in Table 1 indicate greater local or uniform ductility. For example, comparison of the tabulated values indicates that X and Y steels have more local ductility and less uniform ductility than that observed for Z steel in the longitudinal direction, as confirmed by the stress-strain curves.

Strain hardenability in a material (correlating with significant uniform ductility) can distribute yielding to areas other than where it was initiated, while sufficient local ductility can wipe out the effect of stress concentration.

PLATES WITH HOLES

To determine the behavior of the project steels under stress concentrations, tests were conducted on rectangular plates with holes. From these tests it was concluded that, except for Z steel in the transverse direction, all the project steels were able to develop their full tensile strength as calculated on the net cross-sectional area; that is:

$$\frac{\sigma_{tt}}{\sigma_t} \geq 1.0 \qquad (3)$$

where σ_{tt} is the average tensile stress at P_{ult} calculated on the net area of the plate and σ_t is the tensile strength determined from a standard tension coupon. Eq. 3 indicates that for X and Y steel and Z steel in the longitudinal direction, the effect of the stress concentration near the hole is wiped out and the entire net section is able to fully plastify. For the two tests of Z steel in the transverse direction σ_{tt}/σ_t measured 0.94, a relatively minor reduction from the full tensile strength.

BOLTED CONNECTIONS

The bolted connection is one of the critical problem areas for low ductility steels under static loading. Force is applied at the hole through the contact pressure between the bolt and the plate. This is a more severe stress concentration than that occurring in a rectangular plate with a central hole, wherein the load is applied at the ends of the plate.

A total of 59 single-bolt connection tests were conducted on low ductility steels using both single and double shear

assemblies. Specimens were made from 7 and 12 gage Y steel, 12 and 16 gage X steel and 20 gage Z steel. Holes were drilled 1/16" larger than the bolt diameter, and the bolt was finger tightened with washers under the head and nut. Holes were punched in a few specimens, while in some others the bolts were hand torqued; however, no significant difference in the carrying capacity of the connection was observed due to these variations. Hence all tests were combined to arrive at prediction equations for the failure load. To compare the behavior of low ductility steels with that of high ductility steels, 9 single-bolt connection tests were conducted on 12 and 16 gage full annealed X steel.

Variables considered in the program in addition to the type of steel used were: edge distance, e; bolt diameter, d; sheet thickness, t; plate width, s; and coupon tensile strength, σ_t.

All connections were tested in an hydraulic testing machine. Some selected plates were scribed at 1/4-inch intervals, and measured before and after test under a traveling microscope. All tests were conducted using an autographic recorder with an extensometer gage length of (2e + 1) inches. A sketch of a connection specimen and typical load-deformation curves are presented in Fig. 2.

Ultimate Load Formulas. Observed failure modes of both the low and high ductility steel specimens were the same as previously described by Winter (8). These are:

Type (i) -- Longitudinal shearing of the plate along two nearly parallel planes whose distance is equal to the bolt diameter

Type (ii) -- Bearing failure with considerable elongation of the hole and material "piling up" in front of the bolt

Type (iii) -- Transverse tension-tearing across the net section of the sheet.

Experimental results plotted in Fig. 3 represent shear, bearing or combinations of bearing with either shear or tension modes of failure. The ordinate is the ratio of the computed bearing stress at failure (σ_b) to the tensile strength of the material as determined from a coupon test (σ_t), and the abscissa is the ratio of the edge distance, e, to bolt diameter, d. Up to about e/d = 3.33 the bearing stress ratio increases with increasing e/d and is satisfactorily predicted by the equation

$$\frac{\sigma_b}{\sigma_t} = 0.9 \frac{e}{d} \qquad (4)$$

However, for e/d greater than 3.33, the scatter of experimental values increases, and there is a greater tendency toward bearing type failures, rather than predominantly shear type, with little or no increase in bearing stress ratio. Therefore, an upper limit of 3.0 can be placed on Eq. 4. These relationships can be expressed in terms of failure loads for shear (P_s) and bearing (P_b), respectively, as

$$P_s = 0.9 \; e \; t \; \sigma_t \qquad (5)$$

and

$$P_b = 3.0\ d\ t\ \sigma_t \tag{6}$$

In Fig. 4 experimental results are plotted for tension and combined bearing and tension modes of failure. Not enough tension failures occurred in the low ductility specimens to develop an expression for the tension failure load (P_t), but the results are in fair agreement with Winter's (8) expression for high ductility steels, i.e.,

$$\frac{\sigma_{net}}{\sigma_t} = (0.1 + 3.0\ \frac{d}{s}) \leq 1.0 \tag{7}$$

or,

$$P_t = (0.1 + 3.0\ \frac{d}{s})\ A_{net}\ \sigma_t \leq A_{net}\ \sigma_t \tag{8}$$

where σ_{net} is the average tensile stress at failure, calculated on the net area (A_{net}) of the cross-section. In both Figs. 3 and 4 it is noted that connections using Z steel, which is the thinnest material and has the lowest local ductility, tend to give lower results than the others. The maximum shear, bearing or tensile stresses according to Eqs. 5, 6 and 8 are

$$(\tau_s)_{max} = P_s/2\ e\ t = 0.45\ \sigma_t \tag{9}$$

$$(\sigma_b)_{max} = P_b/dt = 3.0\ \sigma_t \tag{10}$$

$$(\sigma_{net})_{max} = P_t/A_{net} = (0.1 + 3.0\ \frac{d}{s})\ \sigma_t \leq \sigma_t \tag{11}$$

Comparison with High Ductility Steels. Results of tests of the nine full annealed X Steel connection specimens agreed with Winter's prediction equations for high ductility steels, and are not presented here. Winter's expressions for failure stresses are recorded below for comparison with the low-ductility

steel test results.

$$(\tau_s)_{max} = 0.70\ \sigma_y \tag{12}$$

$$(\sigma_b)_{max} = 4.9\ \sigma_y \tag{13}$$

$$(\sigma_{net})_{max} = (0.1 + 3.0\ \frac{d}{s})\ \sigma_t \leq \sigma_t \tag{14}$$

where σ_y is the yield stress of the material in tension. Eqs. 12 and 13 predict failure stresses in shear and bearing in terms of yield stress of the material, because this property gave best correlation with the test results. The tensile-yield strength ratio for the steels in those tests averaged about 1.35. Applying this factor to Eqs. 12 and 13, the shear and bearing failure stresses for the high ductility steels can be expressed as $\tau_s = 0.52\ \sigma_t$ and $\sigma_b = 3.6\ \sigma_t$. In contrast, for low ductility steels Eqs. 9 and 10 show $\tau_s = 0.45\ \sigma_t$ and $\sigma_b = 3.0\ \sigma_t$. Thus, the shear and bearing strength of low ductility steel, in terms of σ_t, is somewhat lower than for high ductility steel, while the tensile strength in the net section seems unaffected by the lower ductility.

Comparisons of high and low ductility steel also have been made for connections with two or three bolts in line with the applied stress (6). Here too it was found that the tensile strength of the connection was unaffected by the ductility of the steel.

Alternate Prediction of Ultimate Load (2). There is a fair amount of scatter in the test results shown in Fig. 3, particularly when combined failure modes are involved; hence alternate predictions of the failure load were sought. Function-

al dependence of the ultimate load, P_{ult}, on the variables considered can be obtained using dimensional analysis (4). For a single-bolt connection, the relationship can be expressed as

$$\frac{P_{ult}}{\sigma_t d^2} = f_1 \left(\frac{\sigma_b}{\sigma_t} , \frac{\sigma_s}{\sigma_t} , \frac{e}{d} , \frac{s}{d} , \frac{t}{d} \right) \tag{15}$$

If the bearing stress σ_b and the shear stress τ_s are assumed to be proportional to the tensile strength σ_t of the material, then Eq. 15 reduces to

$$\frac{P_{ult}}{(td)} \frac{(td)}{\sigma_t d^2} = \frac{\sigma_b}{\sigma_t} \left(\frac{t}{d}\right) = f_2 \left(\frac{e}{d} , \frac{s}{d} , \frac{t}{d}\right) \tag{16}$$

This expression can be modified further, with due recognition of limiting conditions, to obtain predictions of the form presented earlier for shear or tension failures. In addition, using a trial and error approach to provide a best fit to the data and to evaluate numerical coefficients, the following expression for bearing or combined failures was obtained:

$$P_c = 0.32 \left(\frac{e}{d} + \frac{s}{d} + 1\right) - 0.04 \frac{d}{t} \tag{17}$$

provided $2.25 \leq \frac{e}{d} \leq 3.30$

and $3.33 \leq \frac{s}{d} \leq 6.00$

This prediction is plotted in non-dimensional form along with the pertinent data in Fig. 5. The prediction error is reduced an average of about 25% compared to Eqs. 5 and 6, at the cost of additional complexity.

FILLET WELDED CONNECTIONS

Variables considered in the tests of longitudinal and transverse fillet weld connections included: length of weld, L; thickness of material, t; and type of steel. For the low ductility steel specimens where the tensile strength of the material ranged from 75 to 100 ksi, low hydrogen welding electrode E-10018 (ASTM designation A-316) was used. A few tests were made on full annealed X steel specimens (12FAX) using low hydrogen E-7018 electrodes. To facilitate the welding process the connection specimens were clamped on a steel table, which also served as a heat sink. Voltage was held constant at 25 volts, and current input was varied for the different sheet thicknesses to obtain a satisfactory weld without undercutting the material. The current as recorded by an ammeter was 120, 120, 85 and 60 amps, respectively, for 7, 12, 16 and 20 gage sheets.

LONGITUDINAL FILLET WELD CONNECTIONS

Fig. 6 shows a sketch of the longitudinal fillet weld connections. The width of the narrower plate, b_n, was 3.0" for all except the 7Y and 12FAX specimens, where b_n was 2.5" and 4.0" respectively. The width of the other plate, b_w, was 1 inch greater than b_n to facilitate welding. Table 2 gives the weld lengths along with the average mechanical properties of the material. The eighteen specimens were divided into three groups: Group I specimens were designed to fail in tension in the plate, called type "a" failure. Group II specimens were designed to produce shear failure in the weld, called type "b"

failure. Group III specimens were designed so that either type of failure was equally likely.

Tension tests were conducted in an hydraulic testing machine, and load-deformation curves were autographically recorded for a gage length of (L + 3) inches. The results are presented in Table 2. The following observations are made:

(1) All the specimens in Group I, which had the longest weld length, failed by transverse tearing of the narrower plate (type "a" failure). Group II specimens which had the shortest weld length, failed by shearing of the weld (type "b"), except for the full annealed specimen which exhibited a combined type failure. In Group III, the failures were about evenly divided.

(2) For the low ductility steel specimens that failed in tension, the ratio of the tensile strength developed by the plate, σ_{tt}, to the tensile strength of the coupon, σ_t, ranges from 0.89 to 1.05, and averages 0.96. This compares favorably with the corresponding value of 0.88 for the specimen of full annealed material (12FAX-L6) which failed in tension, and indicates that connections made with low ductility steel were able to develop almost the full strength of the narrower plate. Considerable out-of-plane deformation occurred in Specimen 12FAX-L6 (and other full-annealed specimens) after the yield load was reached; this may have reduced the resulting ultimate carrying capacity.

(3) For type "b" failures, comparison can be made between the computed shear strength of the weld and the expected shear strength of the weld, where the expected shear strength is

assumed to be 0.577 times the minimum tensile strength of the weld metal as specified by ASTM. This ratio ranges from 0.99 to 1.05 for Group II specimens of low ductility steel except for 1205X-L9 which may have had a defective weld. The same ratio for Type "b" failures in Group III specimens ranges from 0.94 to 0.98. That is, the shorter welds of Group II apparently had more uniform stress distribution, and thus higher average stresses, than the longer welds of Group III.

(4) For Group I specimens which failed in tension, the local ductility parameter (elongation in 1/4-inch gage length, Col. 10) is in satisfactory agreement with the values obtained in the tension coupon tests (Col. 4).

TRANSVERSE FILLET WELD CONNECTIONS

The high strength of the low carbon X, Y and Z steels was achieved by cold working. Therefore, it was anticipated that partial annealing of these low ductility steels due to weld heat would reduce the tension strength of the transverse fillet weld connections shown in Fig. 7. Unlike a longitudinally welded specimen, the whole cross-section of a full width transverse weld specimen is partially annealed. For a partial width weld, only the part of the cross-section that is welded would be affected. The reduction in strength may depend upon the length of weld at the critical cross-section, the details of the welding procedure and to what extent contiguous cold metal serves as a heat sink.

The transverse fillet weld specimens were divided into four groups as indicated below and in Table 3 and Fig. 7.

Group IV: single lap, full width welds

Group V: single lap, partial width welds

Group VI: single lap, full width unsymmetrical welds

Group VII: double lap, full width welds

Seventeen transverse fillet weld specimens were designed using 7 and 12 gage Y steel, 12 and 16 gage X steel, and 20 gage Z steel. Duplicate specimens were made; but for brevity, only 7 gage Y , 12 gage X and 20 gage Z tests are presented in Table 3. However, the observations made subsequently apply to all 34 specimens tested. The test procedure for the transverse weld specimens was the same as for the longitudinally welded connections.

All specimens in Groups IV, VI and VII failed by transverse tearing of the connected plate. Tension failure in these specimens is designated by types "a", "c" and "d" in Fig. 7 and Table 3, to differentiate between the different modes of tension tearing. Type "a" failure gives an inclined fracture, which is the same as that observed in longitudinally welded specimens. Type "c" failure follows the contour of the fillet weld toe. Type "d" failure occurred in some of the partial width weld specimens; it follows the contour of the toe for the length of the weld, and is inclined in the unwelded portions of the plate. Three of the partial width weld specimens included in Table 3 failed in the weld (type "b" failure), and three had type "d" failures.

The predicted maximum load for a plate of thickness t and width b_n is given by

$$P_{max} = b_n \, t \, \sigma_t \qquad (18)$$

where σ_t is the tensile coupon strength of the material. The ratio of the tensile strength developed by the connected plate, σ_{tt}, to the tensile coupon strength σ_t is given in Col. 5 of Table 3. This ratio is between 0.84 and 0.96 for all of the Group IV, VI and VII specimens (full width welds) which failed by tension tearing. Within any one group, the ratio increases with increasing thickness of the material. The double lap specimens of Group VII have about the same strength ratio as Group IV and VI specimens, indicating that the small strength reduction of approximately 10% due to some annealing is caused by only one pass of the welding electrode, and subsequent welding on the same cross-section does not reduce the tension strength any further.

The partial width weld specimens of Group V which failed in tension had σ_{tt}/σ_t ratios of 0.92 to 0.99, averaging slightly higher than the full width weld specimens. Apparently only that part of the cross section which was welded had its strength somewhat reduced by partial annealing, while the part which was not welded developed tensile strength close to that obtained in the coupons.

Two high-ductility X steel transverse fillet weld specimens in Groups IV and V were tested to compare their behavior with low ductility specimens. There was no reduction in the strength of these connections due to the welding process.

INFLUENCE OF DUCTILITY ON CONNECTION BEHAVIOR

This investigation of connection behavior is part of an overall study undertaken at Cornell University, on the influence of ductility on cold-formed members under static loading(2). Therefore the observed connection behavior should be interpreted against the background of the overall observations made on these specially rolled, low ductility project steels. In dealing with such steels it appears necessary to distinguish between uniform ductility and local ductility. Uniform ductility is characterized by the ability of a member made of the subject material to undergo sizeable plastic deformations over significant portions of its length, prior to failure. Such ductility is attained if a material possesses a significant strain hardening range. On the other hand, local ductility is the ability to undergo plastic deformation in a localized area. Most of the "low ductility" steels investigated herein showed significant local ductility, but very limited uniform ductility.

The modes of failure and simplified formulas obtained for single-bolt connections are similar for low and high ductility steels. In terms of coupon tensile strength σ_t, maximum shear and bearing stress values for low ductility steels are 0.45 σ_t and 3.0 σ_t, respectively. Corresponding values for high ductility steels are 0.52 σ_t and 3.6 σ_t respectively, indicating that the low ductility of these special steels lowered the strength of the tested bolted connections only by about 15% in terms of the coupon tensile strength. Bolted connections of

low ductility steel showed adequate elongation capability.

The low ductility steels were weldable; that is, no special welding process was used in fabricating the specimens, nor were any noticeable defects observed. In longitudinal fillet weld specimens with adequate weld length, the connections developed almost the full predicted load based on coupon tensile strength. Both plate failure and weld failure of longitudinal fillet weld connections in these low ductility steels can be predicted using the same methods as for high ductility steel.

Transverse fillet weld specimens showed some effect of partial annealing, but still developed a stress no less than about 83% of the coupon tensile strength. This reduction may vary depending on the welding procedure, and the rate of heat dissipation.

ACKNOWLEDGMENTS

This research was sponsored by the American Iron and Steel Institute. The cooperation of the cognizant research committee, and of the companies who furnished the steels for the investigation, is gratefully acknowledged.

APPENDIX I. - REFERENCES

1. American Iron and Steel Institute, "Specification for the Design of Cold-Formed Steel Structural Members," 1968 Edition, N. Y.

2. Dhalla, A. K., "Influence of Ductility on the Structural Behavior of Cold-Formed Steel Members", Dept. of Structural Engineering Report No. 336, Cornell University, Ithaca, N. Y. (to be published).

3. Frankland, J. M., "Physical Metallurgy and Mechanical Properties of Materials: Ductility and the Strength of Metallic Structures,", Proc. ASCE, Vol. 86, No. EM6, Dec. 1960.

4. Murphy, G., "Similitude in Engineering," The Ronald Press Co., N. Y., 1950.

5. Oliver, D. A., "Proposed New Criteria of Ductility from a New Law Connecting the Percentage Elongation to the Size of Test Piece," Inst. of Mech. Engineers, Vol. II, 1928.

6. Popowich, D. W., "Tension Capacity of Bolted Connections in Light Gage Cold-Formed Steel," thesis presented to Cornell University, in 1969, in partial fulfillment for the requirements of the degree of Master of Science.

7. Unwin, W. C., "Tensile Tests of Mild Steel, and the Relation of Elongation to the Size of the Test Bar," Proc. Inst. of Civil Engineers, 1903.

8. Winter, G., "Tests on Bolted Connections in Light Gage Steel," Proc. ASCE, Vol. 82, Paper No. 920, March 1956.

APPENDIX II. - NOTATION

The following symbols are used in this paper:

A = Gross cross-sectional area of coupon or tension member.

A_{net} = Net cross-sectional area of a tension member or connection.

b = Constant used in Eq. 1.

b_n = Width of the narrower plate in fillet welded connections.

b_w = Width of the wider plate in fillet welded connections.

c = Constant used in Eq. 1.

d = Diameter of the bolt.

e = Edge distance in bolted connection.

K = Constant which indicates local ductility of the material.

L = Gage Length.

P_b = Bearing failure load in bolted connection.

P_c = Combination failure load in bolted connection.

P_{max} = Predicted maximum load.

P_s = Shear failure load in bolted connection.

P_t = Tension failure load in bolted connection.

P_{ult} = Ultimate load.

S = Width of plate.

t = Thickness of plate.

α = Constant which indicates strain hardening capacity of the material.

ϵ = Elongation in gage length L in coupon test.

σ_t = Tensile strength of the material.

σ_{tt} = Average tensile stress at P_{ult} calculated on net area of the connected plate.

σ_y = Yield strength of the material.

τ_{sa} = Shear strength of the electrode.

τ_{su} = Shear strength of fillet weld.

TABLE 1

DUCTILITY CHARACTERISTICS OF X, Y AND Z STEELS

Ductility Parameters	20Z-L-Av. Z Steel (Long.)	20Z-T-Av. Z Steel (Trans.)	12Y-L2 Y Steel (Long.)	1205X-L2 X Steel (Long.)	1605X-L2 X Steel (Long.)	16FAX-L1 X-Annealed Steel (Long.)
Elongation in 2" (%)	4.38	1.51	5.13	5.58	6.84	52.20
Reduction in Area (%)	56.10	33.50	65.20	69.40	59.00	83.80
Tensile/ Yield Ratio	1.08	1.00	1.01	1.00	1.00	1.48
Elongation in 1/4" Including Neck (%)	15.55	6.09	38.40	44.40	35.20	85.60
Elongation in 2 1/2" Excluding Neck (%)	2.74[a]	0.48	0.33	0.40	1.28	38.00
K	20.50	12.10	45.00	46.00	45.00	120.00
α	-0.579	-0.834	-0.974	-0.983	-0.795	-0.335

[a]This value is for elongation in 2", excluding neck.

TABLE 2
LONGITUDINAL FILLET WELD CONNECTIONS

1	2	3	4	5	6	7	8	9	10	11
		Avg. Mat'l Properties			Experimental Results					
Spec. Designation**	Lap Length L in	Tensile Str. of Coupon σ_t ksi	Elong. in 1/4" G. L. %	Shear Str.of Electrode* τ_{sa} ksi	Tensile Str.of Plate σ_{tt} ksi	Shear Str.of Weld τ_{su} ksi	$\frac{\sigma_{tt}}{\sigma_t}$	$\frac{\tau_{su}}{\tau_{sa}}$	Elong. in 1/4" G. L. %	Mode of Failure type
GROUP I SPECIMENS										
7Y-L-L1	3.25	83.3	47.0	57.7	83.7	45.5	1.00	0.78	49.8	a
12Y-L-L2	3.25	82.5	31.4	57.7	78.8	51.0	0.96	0.88	27.6	a
1205X-L-L3	3.25	84.1	29.9	57.7	79.0	51.6	0.94	0.89	32.4	a
1605X-L-L4	3.75	98.0	26.6	57.7	87.8	50.2	0.89	0.87	21.7	a
20Z-L-L5	3.50	81.7	15.5	57.7	86.0	52.2	1.05	0.90	12.0	a
12FAX-L-L6	3.75	45.0	105.0	40.4	39.9	29.5	0.88	0.73	102.0	a
GROUP II SPECIMENS										
7Y-L-L7	2.25	83.3	47.0	57.7	73.8	58.4	0.88	1.01	16.8	b
12Y-L-L8	2.25	82.5	31.4	57.7	60.8	57.5	0.74	0.99	8.8	b
1205X-L-L9	2.25	84.1	29.9	57.7	50.2	47.6	0.60	0.82	38.8	b
1605X-L-L10	2.75	98.0	26.6	57.7	75.7	58.8	0.77	1.02	--	b
20Z-L-L11	2.50	81.7	15.5	57.7	62.2	53.0	0.76	0.92	--	b
12FAX-L-L12	1.50	45.0	105.0	40.4	22.7	42.8	0.51	1.06	25.6	a+b
GROUP III SPECIMENS										
7Y-L-L13	2.75	83.3	47.0	57.7	82.0	52.6	0.98	0.91	20.2	a
12Y-L-L14	2.75	82.5	31.4	57.7	70.0	54.1	0.85	0.94	--	b
1205X-L-L15	2.75	84.1	29.9	57.7	70.5	56.6	0.84	0.98	--	b
1605X-L-L16	3.25	98.0	26.6	57.7	85.7	56.4	0.87	0.97	5.6	b
20Z-L-L17	2.85	81.7	15.5	57.7	74.3	55.4	0.91	0.95	--	a
12FAX-L-L18	2.00	44.6	105.0	40.4	28.2	38.6	0.63	0.95	24.6	a+b

*Computed as 0.577 x ASTM specified minimum tensile strength.

**Load was applied parallel to the direction of rolling.

TABLE 3
TRANSVERSE FILLET WELD CONNECTIONS[1]

Specimen Designation[p]	Total Length of Weld L in	Tensile Str. of Coupon σ_t ksi	Experimental Results: Tensile Str. of Plate σ_{tt} ksi	$\frac{\sigma_{tt}}{\sigma_t}$	Mode of Failure Type[m]
GROUP IV - FULLY WELDED SPECIMENS					
20Z-TF-L11	6.04	81.7	70.0	0.86	c
20Z-TF-L12	6.02	81.7	68.3	0.84	c
1205X-TF-L31	6.02	74.6	66.5	0.89	c
1205X-TF-L32	6.02	74.6	67.2	0.91	c
7Y-TF-L51	6.00	86.3	80.9	0.94	c
7Y-TF-L52	6.00	86.3	80.9	0.94	a
GROUP V - PARTIALLY WELDED SPECIMENS					
20Z-TP-L11	3.50	81.7	75.1	0.92	d
20Z-TP-L12	3.60	81.7	77.0	0.94	d
1205X-TP-L31	3.64	74.6	73.7	0.99[n]	d
1205X-TP-L32	3.08	74.6	73.1	0.98[n]	b
7Y-TP-L51	3.60	86.3	73.4	0.85[n]	b
7Y-TP-L52	3.44	86.3	71.8	0.83[n]	b
GROUP VI - UNSYMMETRICALLY WELDED SPECIMENS					
20Z-TU-L11	6.02	81.7	71.5	0.87	c
20Z-TU-L12	6.02	81.7	72.3	0.88	c
1205X-TU-L31	6.02	74.6	70.3	0.94	c
1205X-TU-L32	6.02	74.6	70.9	0.95	c
7Y-TU-L51	6.00	86.3	82.0	0.95	a
7Y-TU-L52	6.00	86.3	82.5	0.96	a
GROUP VII - DOUBLY LAPPED SPECIMENS					
20Z-TD-L11	6.02	81.7	70.3	0.86	c
20Z-TD-L12	6.02	81.7	69.0	0.84	c
7Y-TD-L51	6.00	86.3	82.0	0.95	a
7Y-TD-L52	6.00	86.3	81.5	0.94	c

[1] Geometry of the specimens is shown in Fig. 7.

[m] Modes of failure are indicated by dotted lines in Fig. 7.

[n] $\frac{\tau_{su}}{\tau_{sa}}$ ratios for specimens 1205X-TP-L32, 7Y-TP-L51 and L-52 are 1.73, 1.48, and 1.55 respectively.

[p] Load was applied parallel to the direction of rolling.

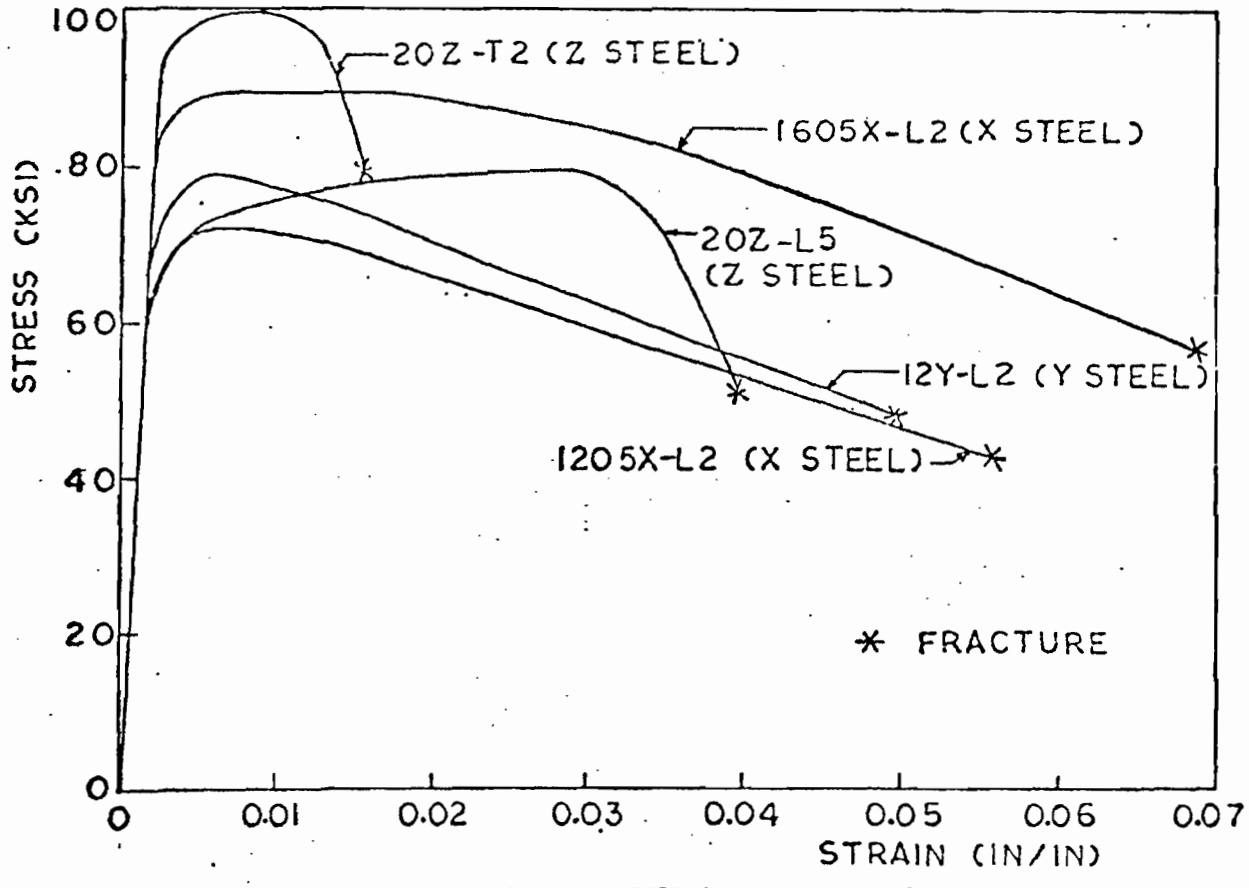

FIG. 1. COMPLETE STRESS STRAIN CURVES OF X, Y AND Z STEELS (2" G.L.)

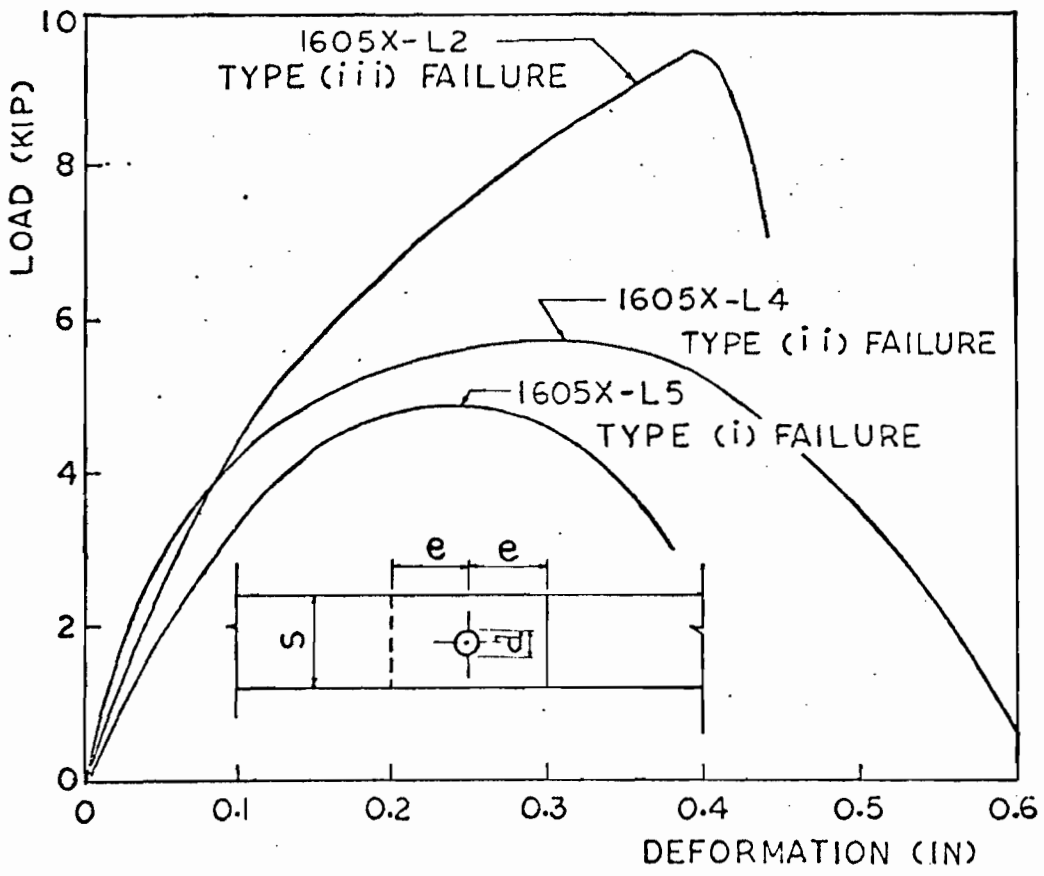

FIG. 2. LOAD-DEFORMATION CURVES, 16 GAGE 'X' STEEL BOLTED CONNECTIONS

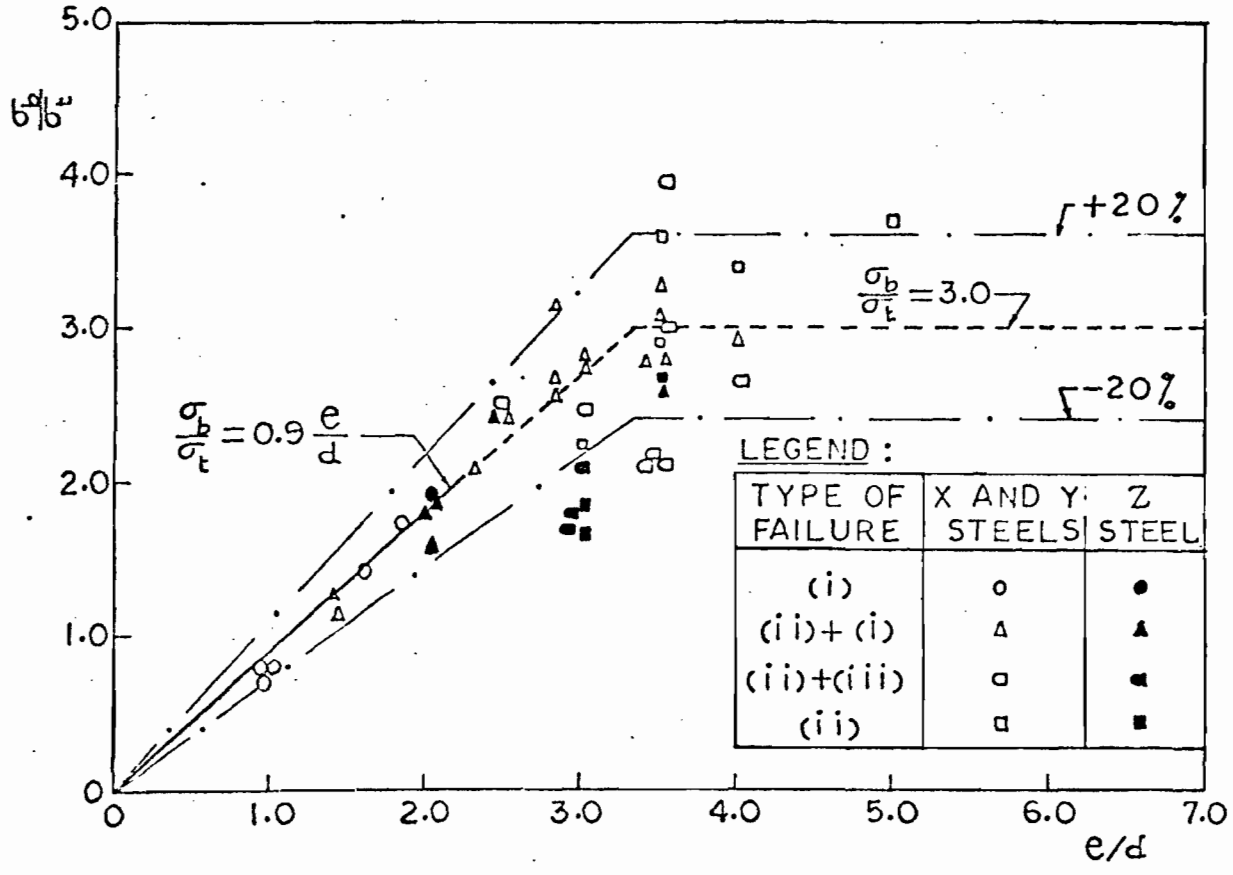

FIG. 3. BEARING AND SHEAR OR COMBINED FAILURES

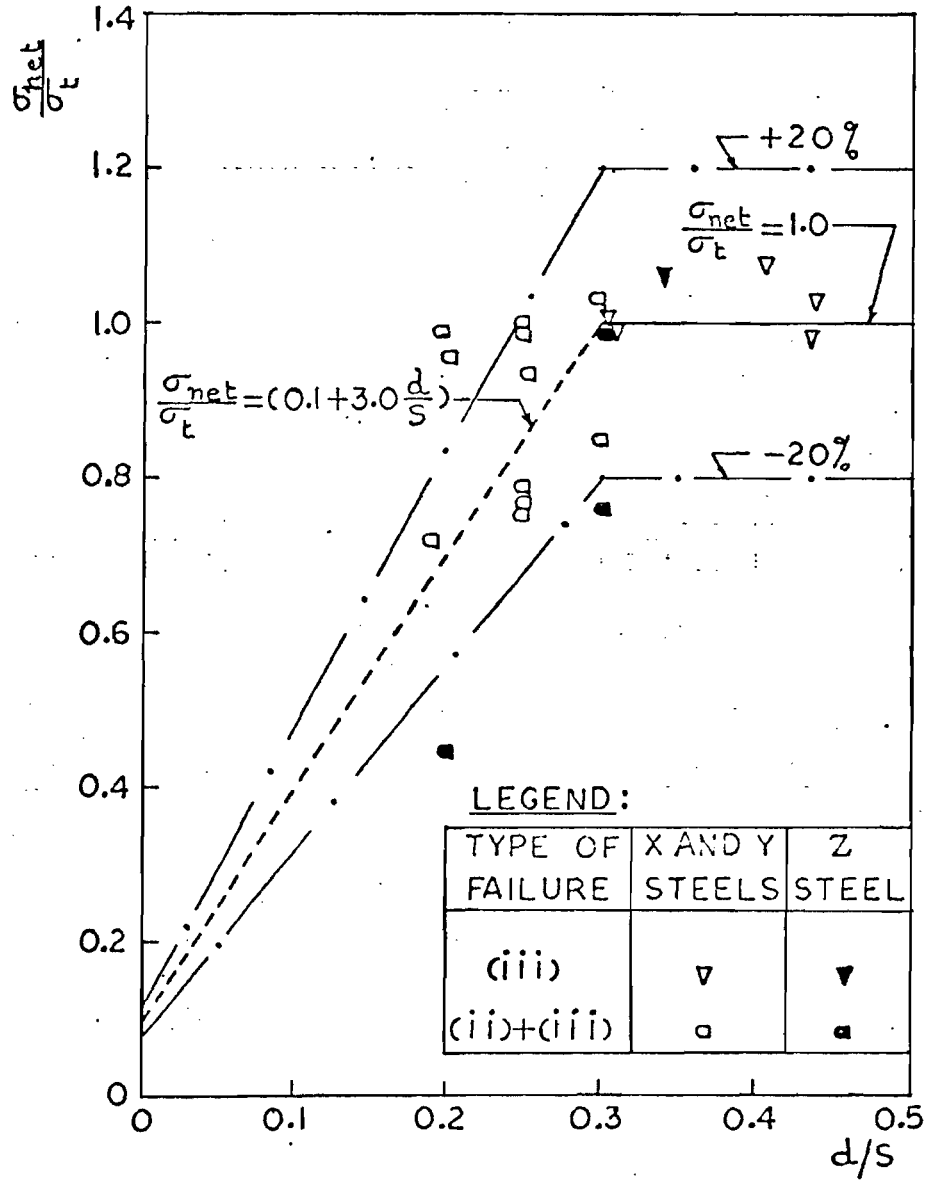

FIG. 4. TRANSVERSE TEARING OR COMBINATION FAILURES

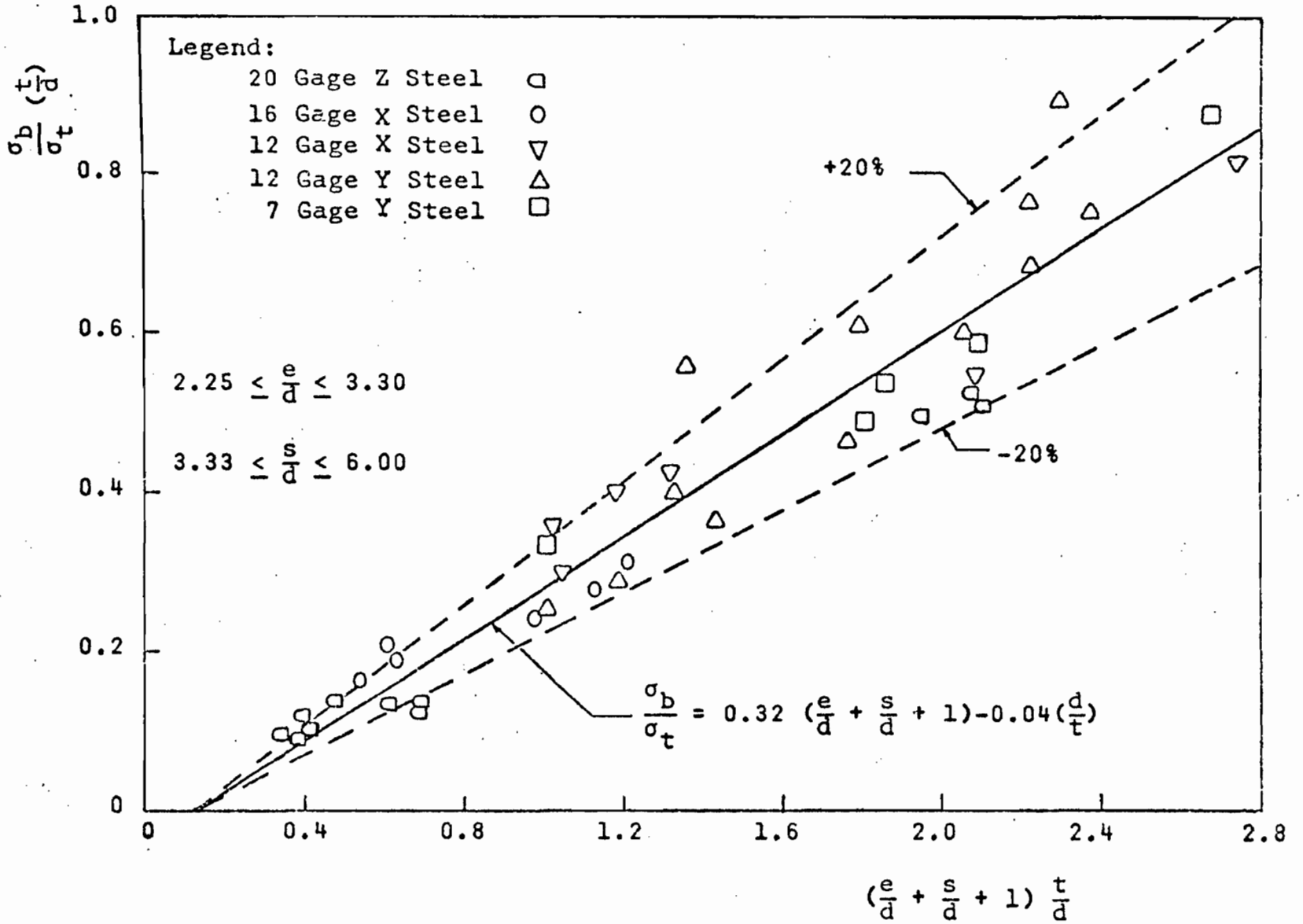

FIG. 5. ALTERNATE REPRESENTATION OF BEARING OR COMBINATION OF SHEAR AND BEARING OR TENSION AND BEARING TYPE OF FAILURES.

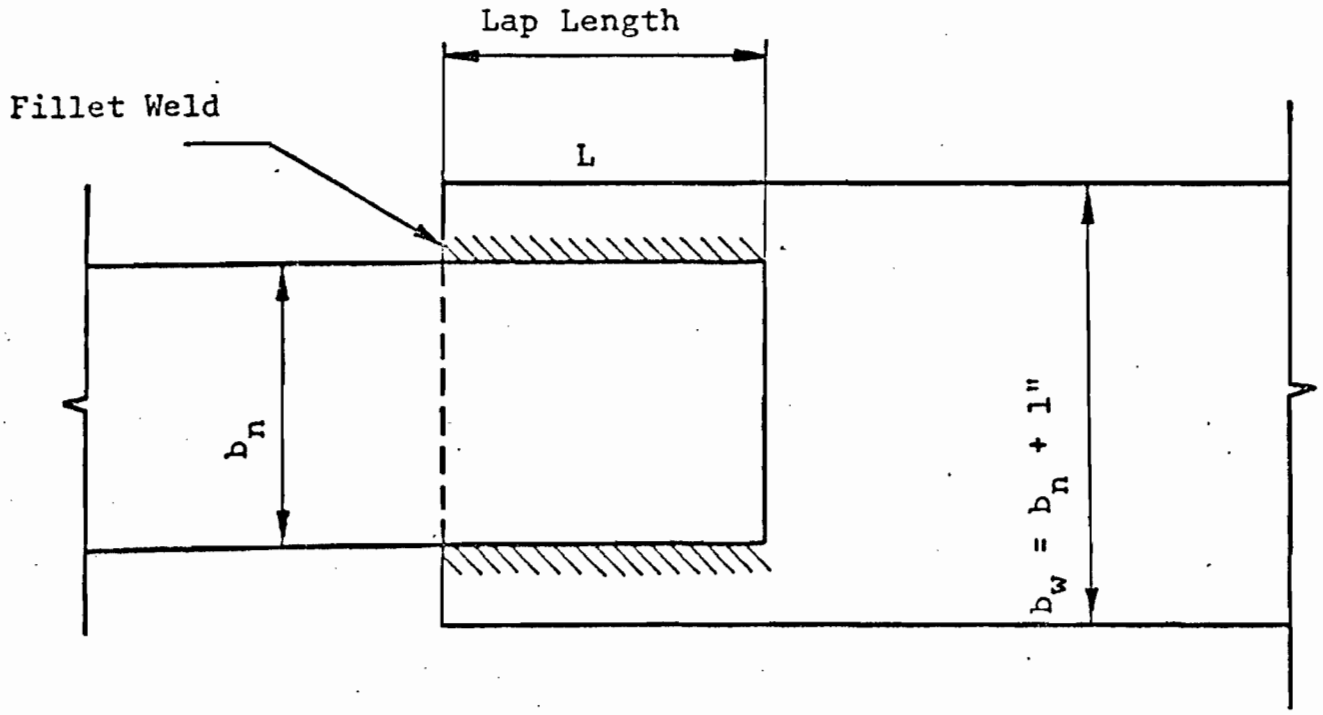

FIG. 6. SINGLE LAP LONGITUDINAL FILLET WELD CONNECTION.

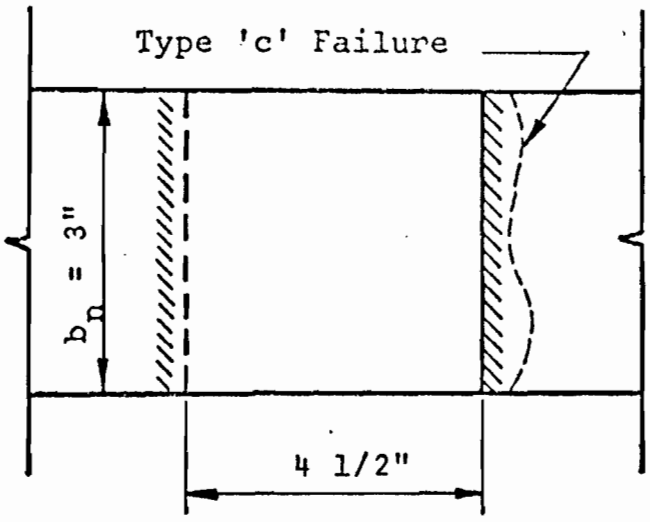

a. Single Lap, Full Length Weld (TF).

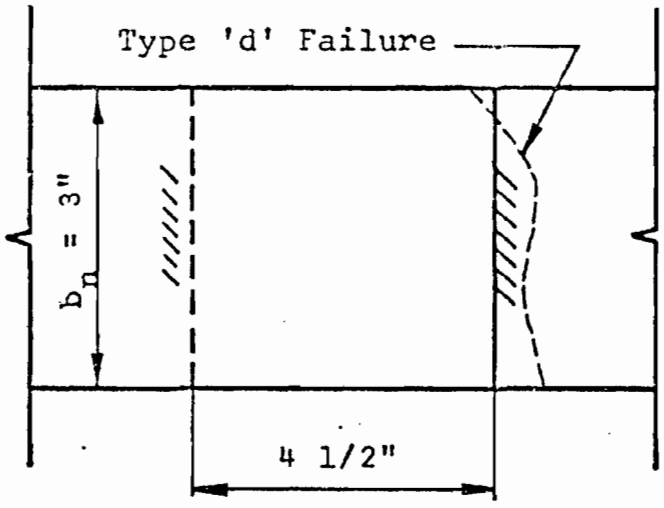

b. Single Lap, Partial Width Weld (TP).

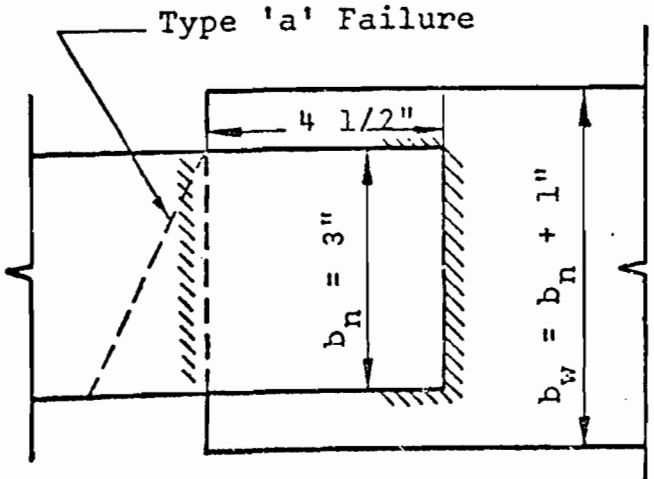

c. Single Lap, Unsymmetric Weld (TU).

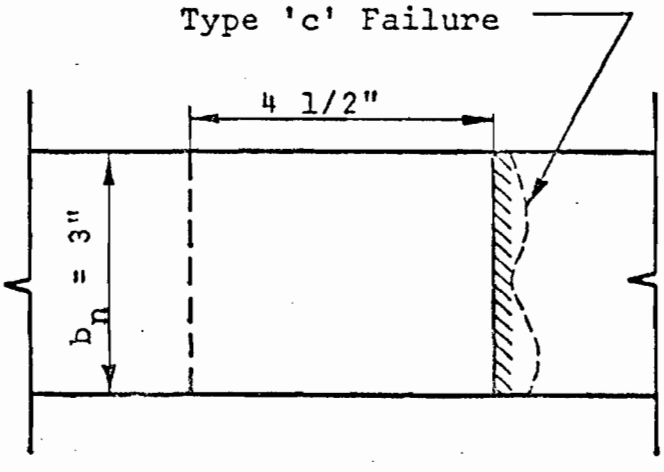

d. Double Lap, Full Width Weld (TD).

FIG. 7. TRANSVERSE FILLET WELD SPECIMENS.

SUMMARY

Tests were made on bolted and fillet welded connections in thin low-ductility low carbon steels. Material elongation in a 2-inch gage length ranged from 4% to 8%, while the tensile to yield strength ratio ranged from 1.0 to 1.1. The load carrying capacity of the connections can be predicted by equations similar to those for high ductility steels.

ABSTRACT

Bolted and fillet welded connections fabricated from flat sheets of thin low-ductility low carbon steels were tested as part of a research program investigating the influence of ductility on the behavior of cold-formed members under static loading. Material elongation in a 2-inch gage length ranged from 4% to 8%, while the tensile to yield strength ratio ranged from 1.0 to 1.1. Standard tension coupon test procedures were modified to distinguish between local and uniform ductility of the material. The load carrying capacity of the connections can be predicted by equations similar to those for high ductility steels.

KEY WORDS

Bolted Connection

Cold Formed

High Ductility

High Strength

Local Ductility

Longitudinal Fillet Weld

Low Carbon Steel

Low Ductility

Plane Stress

Structural Engineering

Tension Coupon

Transverse Fillet Weld

Uniform Ductility

5/28/71

DUCTILITY CRITERIA AND PERFORMANCE OF LOW DUCTILITY STEELS FOR COLD-FORMED MEMBERS

by A. K. Dhalla[1] and G. Winter[2], F.ASCE

INTRODUCTION

The cold-working of low carbon steel or the higher carbon contents in medium carbon steels increase the yield and the ultimate strengths while decreasing the elongation capability or ductility. The present investigation was undertaken to study the feasibility of effectively utilizing these high strength, low ductility steels in structural members.

The current Specification for the Design of Cold-Formed Steel Structural Members (1)[3] permits the use of any steel whose properties and suitability have been established by a recognized specification or appropriate tests. A problem exists, however, in defining what constitutes a suitable steel for cold-formed construction. The yield strength and tensile strength can be varied over a wide range, while the modulus of elasticity is nearly constant. In addition to these mechanical properties, ductility, formability and weldability are among the desirable performance attributes of a steel for cold-formed members.

---

[1]Research Assistant, Department of Structural Engineering, Cornell University, Ithaca, N. Y.

[2]Professor of Engineering (Class of 1912 Chair), Cornell University, Ithaca, N. Y.

[3]Numerals in parentheses refer to the corresponding items in Appendix I. - References.

An extensive investigation was carried out at Cornell University (Reference 2) to study the effects of ductility and of the spread between the yield and the ultimate tensile strength, on the behavior of thin cold-formed members and connections under essentially static loading. A limited study of performance attributes such as formability, and weldability of low ductility steels was also undertaken in the same investigation (2). In this paper only, the ductility parameters and the minimum ductility requirements for thin members are briefly reported.

Ductility is the ability of a material to undergo plastic deformations without fracture. It reduces the harmful effects of stress concentrations, and helps achieve uniform stress or load distribution in members or connections. A conventional measure of ductility, as per ASTM specifications (A370-68), is the elongation in a 2 inch gage length, ε_2, of a standard tension coupon. The minimum ε_2, specified for various grades and thicknesses of structural steel varies from 18 to 24%. Based on these specified minimum values and on ultimate tensile to yield strength ratios, σ_t/σ_y, established somewhat arbitrarily in the same ASTM specifications, some building codes presently impose restrictions or penalties on allowable design stresses for lower ductility steels. With the increased availability and use of higher strength steels possessing lower ductility and lower σ_t/σ_y ratios there is a need for more definitive information on such requirements.

Various standard tests which measure ductility of a material were evaluated from a survey of the pertinent literature. There

are a number of standard tests such as the tension test (9), bend test (14), or notch test (7), to measure the ductility of a material. The standard tension coupon test was chosen for investigation because it is widely used and has special significance to structural engineers. It supplies values of the yield and tensile strength, and indicates stress-strain characteristics of a material for static load conditions (9), (12).

Significance of Ductility. - There is an essential difference between the tensile strength of a structural member and the tensile strength of the material (5). This difference is associated with the presence of stress concentrations in the structure, e.g., at structural discontinuities, connections, holes, etc. The relative importance of stress concentrations for structural tensile strength depends strongly upon ductility. Qualitatively, the greater the ductility the greater the reduction of stress concentration from its elastic value. Because of the fact that stress concentrations provide a weak link in a structure, it appears that strains associated with a localized region of elastic stress concentrations may provide some meaningful estimate of the structural significance of ductility. Stowell (15) showed that the stress concentration factor in a tension member loaded into the plastic range decreases from its elastic value, while the strain concentration factor increases. Thus the strain concentration factor at impending complete plastification of a critical net section of a tension member can be correlated to the ductility requirements of the material.

In terms of the usual tension coupon test parameters, i.e. the elongation in a 2 inch G.L., ε_2, and the σ_t/σ_y ratio, the following criteria are suggested to distinguish roughly between low, medium and high ductility steels. That is:

Low ductility ..... $\varepsilon_2 \leq 10.0\%$ or $\sigma_t/\sigma_y \leq 1.1$

Medium ductility .... $10.0\% < \varepsilon_2 \leq 25.0\%$ and $\sigma_t/\sigma_y > 1.1$

High ductility ..... $\varepsilon_2 > 25.0\%$ and $\sigma_t/\sigma_y > 1.1$

The significance of the above differentiation of various ductility steels will become apparent in the section on "Uniform Ductility".

For this research three types of low carbon steels, designated X, Y, and Z, were made available by three different manufacturers. Steels X and Y were specially produced for the program; steel X was cold-reduced an average of 45% in the thickness direction, to produce 12 gage (0.106") and 16 gage (0.062") material and then annealed to arrive at the desired elongation requirements in 2 inches; while steel Y was cold reduced an average of 33% to obtain 7 gage (0.183") and 12 gage (0.106") material, and received no annealing treatment. Steel Z is an ASTM A446 Grade E commercial product which was obtained in 20 gage (0.038").

To distinguish between different types of steels used in this investigation, the following typical specimen designations will be used, (all "percent elongations" are nominal elongations in a 2 inch G.L. of a standard tension coupon test).

708Y - 7 gage Y steel, 8 percent elongation.

1205Y - 12 gage Y steel, 5 percent elongation.

1205X - 12 gage X steel, 5 percent elongation.

1610X - 16 gage X steel, 10 percent elongation.

16FAX - 16 gage fully annealed X steel, 50 percent elongation.

2004Z - 20 gage Z steel, 4 percent elongation.

Specimens loaded perpendicular to the rolling direction (transverse) are designated by the letter "T"; those loaded parallel to the direction of rolling (longitudinal) by the letter "L"; the average material properties are designated by AV.

MATERIAL PROPERTIES

There are two basic aims in material testing:

(i) To distinguish and compare various deformations and strength characteristics of different materials.

(ii) To correlate the results of material tests with the structural behavior of members made from the subject material.

Compression members are not affected by lower steel ductility (e.g. Ref. 2, Chapter 6). Therefore in this paper, attention will be focused on the elongation capability of tension members or tension components of members.

Preliminary Tension Coupon Test Results and Observations. - Coupons for standard tension tests were prepared as per ASTM specifications A370-68. Load strain curves were plotted by an autographic recorder using a 2 inch G.L. extensometer. Initial test speed was 0.005 in/min which was increased to 0.02 in/min at approximately 1% strain. The average mechanical properties of a few steels, as obtained from the coupon test, are reported in Table 1. All coupon specimens, except for 2004Z-T-AV1 material, were taken

in a direction parallel to rolling (i.e. longitudinal). The mechanical properties of Z steel (2004Z-T-AV1) perpendicular to the rolling direction (transverse) have been included because this is the lowest ductility steel investigated in this project. To compare the stress-strain characteristics, typical complete stress-strain curves of a few low ductility steel specimens are plotted in Fig. 1.

The elongations in a 2 inch G.L. (ε_2) for longitudinal specimens 2004Z-L5, 1205Y-L2, 1205X-L2 and 1605X-L2 are about 4, 5, 6, and 7% respectively. Although the values of ε_2 for steels X, Y, and longitudinal Z are in the same range the shapes of the stress-strain curves are quite different. For example, longitudinal Z steel specimen shows a noticeable strain hardening capacity; indicated by the spread between the yield strength σ_y, and the ultimate strength σ_t. Furthermore, the major portion (73%) of the total strain in a 2 inch G.L. in 2004Z-L5 coupon is incurred before the ultimate load is reached, i.e. before necking. On the other hand the major portion of the strain in a 2 inch G.L. in X or Y steel occurs after the ultimate load is reached. That is, before the necking process starts, only a small amount of plastic strain is uniformly distributed over the length of the coupon, while the larger strains occur in the descending branch and are in effect localized at the neck in the eventual fracture zone.

The above comparison suggests that the distribution of strain for nearly the same elongation in a 2 inch G.L. may be

different for coupon specimens of different steels.

Thus the qualitative examination of stress-strain curves seems to indicate that it is essential to have at least two ductility parameters to describe the total elongation capability of a material. One would characterize the uniform straining in the strain hardening portion of the stress-strain curve, while the other that would identify the localized elongation in the neck, i.e. the downward branch of the stress-strain curve.

ELONGATION EQUATION

In a standard tension coupon test, at successive load increments, the change in length ΔL, is accompanied by a reduction of the cross-sectional area ΔA. MacGregor (10) showed that by measuring the reduction in area of a coupon at various stages of loading in a tension test, true uniform strain, and the true necking strain can be obtained in terms of the reduction in area. However, for thin rectangular coupon specimens it is difficult to measure accurately the reduction in area at fracture (2). Therefore an alternate method was sought to represent the longitudinal strain distribution along the length of the coupon.

In 1903, Unwin (17) suggested that the total elongation of a tension coupon of gage length L is made up of two parts: The first part is the uniform elongation along the bar and therefore proportional to the gage length; the second is due to local stretching and contraction in the neck which occurs at later stages of the tension test. To include size effects, Unwin used Barba's Law of Similarity and suggested the following

equation for strain, ε_L, in gage length L,

$$\varepsilon_L = \frac{c\sqrt{A}}{L} + b \qquad (1)$$

where "b" and "c" are constants obtained from $[\varepsilon_L - \frac{L}{\sqrt{A}}]$ plots, and A is the cross-sectional area of the specimen.

To extend the range of applicability Oliver (11) proposed the following modified form of Eq. 1:

$$\varepsilon_L = K\,[\frac{L}{\sqrt{A}}]^{\alpha} \qquad (2)$$

Eq. 2 is a straight line when plotted on a logarithmic scale; K is the value of strain when $L/\sqrt{A} = 1$, and α is the slope of the line.

Since Eq. 2 takes into account the length "L" as well as the cross-sectional area "A" of a coupon specimen, Oliver (11) indicated that the constants K and α are material constants independent of specimen shape. Furthermore the constants K and α, can be determined from a few extra observations (i.e. measuring elongations in 2 or 3 different gage lengths including the fractured portion) in any of the usual tension tests.

Thus, for the present investigation the relationship between percent elongation ε_L and $L/\sqrt{A}$ indicated by Eq. 2 offers a viable alternative in identification of ductility parameters instead of the measurement of reduction in area suggested by MacGregor (10).

To obtain the longitudinal strain distribution the central 3 inch length of tension coupons were scribed at 1/4 inch intervals (Fig. 2a). These gage lines were measured before and after the tension test under a travelling microscope (least count =

0.0001"). The longitudinal strain distribution along the length of a few low ductility steel specimens is shown in Fig. 2b. Fig. 3 gives a typical $[\varepsilon_L - \frac{L}{\sqrt{A}}]$ plot for 16 gage X steel. For steels presented in Table 1, the constants K and α were obtained from similar $[\varepsilon_L - \frac{L}{\sqrt{A}}]$ plots and are recorded in rows 3 and 7 respectively of Table 2.

Comments on Elongation Equation: - Rectangular coupons according to ASTM specifications A370-68 have a constant gage length (usually 2 or 8 inches) and 1/2 inch width. Thus the elongation equation (Eq. 2) can be rewritten as:

$$\varepsilon_L = K \left[\frac{L}{\sqrt{t/2}}\right]^{\alpha} \qquad (3)$$

where t = thickness of the specimen

The conventional measure of ductility is the elongation in a 2 inch (or 8 inch) gage length. For example, to obtain the elongation in a 2 inch G.L. ε_2, for low ductility steel 1205X-L-AV1 (in Table 2), one can substitute K = 50.0, α = -1.0 and L = 2.0 in Eq. 3.

i.e. $$\varepsilon_2 = \frac{50}{2\sqrt{2}} [\sqrt{t}] \qquad (4)$$

Thus Eq. 4 shows that ε_2, which is one of the conventional measures of ductility, varies with the thickness of the material. For this reason the elongation in a fixed gage length of rectangular tension coupons is not a valid measure of ductility. In contrast, for circular cylindrical ASTM tension coupons of specified constant cross-sectional area A, the elongation in a constant G.L. "L" (usually 8 inches) would be the same for

the coupons machined from different thickness materials.

Recognizing the above difficulty, in the German Code (8) DIN 50 125, the total elongation of a material is computed for a variable gage length which is proportional to the area of the rectangular specimen, instead of using a constant G.L. as is done in the ASTM specifications.

In addition, as will be noted in the next section even the elongation in one fixed gage length of cylindrical bar of fixed diameter, is not sufficient to differentiate between the local and the uniform elongation capabilities of the material.

DUCTILITY PARAMETERS

An earlier comparison of different characteristics of the stress-strain curves of steels Y and longitudinal Z (in Fig. 1), had indicated that for the same elongation in a 2 inch G.L. Y steel had greater local elongation capability but less strain hardening ability than longitudinal Z steel specimen. In the next two sections the same two steels Y and longitudinal Z will be compared to show that K and α are local and uniform ductility parameters of a material.

Local Ductility. - In Table 2, it can be observed that the average values of percent reduction in area and of K (in rows 2 and 3 respectively), are greater for Y steel (1205Y-L-AV2) than for Z steel (2004Z-L-AV1). Reduction in area identifies the local elongation capability of the material. Hence, it is concluded that K, also called specific elongation in Ref. 11, identifies the local ductility of the material. For project steels X, Y and Z, the average reduction in area is plotted

against the average specific elongation K in Fig. 4. The experimental points obtained from tension coupon test indicate that K increases with the increasing reduction in area. Because of scatter no attempt is made to fit a curve through the points plotted in Fig. 4. This scatter may very well be due to the inaccuracy in the measurement of final area after fracture in thin rectangular specimens.

Thus K and reduction area are local ductility parameters of a material. However, the evaluation of these quantities involve a considerable amount of work in routine practical application of tension test. Therefore, for simplicity the elongation measured in a 1/2 inch G.L. (row 4, Table 2), which includes the fractured portion, is suggested as a local ductility parameter. This 1/2 inch length is large enough to include the necked portion of various thicknesses and types of steel used, and is small enough to give valid comparison for different types of steels.

Uniform Ductility. - In Table 2, it can be observed that the average algebraic values of elongation ε_{un}, in a 2 1/2 inch G.L. excluding the neck (i.e. elongation in a 3 inch G.L. minus elongation in 1/2 inch of the necked portion), α, and the σ_t/σ_y ratio for Z steel (2004Z-L-AV1) are greater than those for Y steel (1205Y-L-AV2). Note that σ_t/σ_y identifies the strainhardening ability of a material and ε_{un} indicates the uniform elongation capability of a material excluding neck. Hence it is construed that α, which is the slope of $[\varepsilon_L - \frac{L}{\sqrt{A}}]$

plot on a lagarithmic scale, identifies the uniform ductility of the material. For example, in Fig. 3 (or in row 7 in Table 2) α increases from -0.82 for 1605X low ductility steel to -0.32 for 16FAX fully annealed steel, and their respective σ_t/σ_y ratios are 1.00 and 1.51 (row 5, Table 2).

For various project steels ε_{un} is plotted against α in Fig. 5. The equations of the linear least square fits for the experimental values are also plotted and are given by:

$$\varepsilon_{un} = 10.8 + 10.8\ \alpha \qquad \text{for } \alpha \leq -0.46 \qquad (5)$$

and

$$\varepsilon_{un} = 111.0 + 228.0\ \alpha \qquad \text{for } \alpha > -0.46 \qquad (6)$$

In Fig. 5 there is a distinct break at $\alpha = -0.46$ and $\varepsilon_{un} = 5.8\%$. Furthermore, the overall experimental observations indicated that the uniform ductility parameters for the medium and high ductility X steels (i.e. for $\varepsilon_2 > 10.0\%$, and $\sigma_t/\sigma_y > 1.1$), are $\varepsilon_{un} > 5.8\%$ and $\alpha > -0.46$. In contrast, for low ductility steels X, Y, and Z (i.e. for $\varepsilon_2 \leq 10.0\%$ or $\sigma_t/\sigma_y \leq 1.1$) the uniform ductility parameters are $\varepsilon_{un} < 5.8\%$ and $\alpha < -0.46$. Therefore it is construed that the values of the uniform ductility parameters at the break in the ε_{un} versus α plot differentiate the low ductility steels from the higher ductility steels.

In practice and for simplicity a conservative measure of uniform ductility can be obtained from a coupon test by measuring elongation in a 3 inch G.L. and subtracting from it the elongation in one inch G.L. This difference gives the percent elongation in a 2 inch G.L. not containing the fractured portion; hence it is a measure of the uniform ductility of a material.

MINIMUM DUCTILITY REQUIREMENTS

The establishment of minimum ductility requirements, for thin cold-formed members under static loading is part of the present study. In the subsequent sections the experimental and analytical results on member behavior will be discussed briefly and interpreted against the background of observations on materials behavior made on these low ductility project steels.

Summary of Experimental Investigation. - Elastic stress concentrations represent weak links in a structure. Therefore, to provide meaningful estimates of the structural significence of ductility, simple tension members were tested under static loading. Tests were made on rectangular plates with holes, followed by a detailed experimental investigation of the bolted and welded connections (Ref. 3).

From tension tests on perforated plates, it was concluded that, except for Z steel loaded transversely, all the project steels were able to develop the full tensile strength of the member $P_{ult} = \sigma_t A_{net}$ on the net cross-sectional area. Expressed differently, for all steels

$$\frac{\sigma_{tt}}{\sigma_t} \geq 1.0 \qquad (7)$$

where σ_{tt} = the average stress on the net area A_{net} at ultimate load,

and σ_t = material tensile strength determined from coupon test.

Eq. 7 indicates that the effect of the elastic stress concentration near the hole is wiped out and the material is able to

redistribute stresses in the plastic range and develop the full tension capacity of the member. For the two tests on transverse Z steel specimens which failed in a semi-brittle manner the average σ_{tt}/σ_t was 0.94.

In bolted connections failure in low ductility steels X, Y and longitudinal Z occurred in a ductile manner. However, a few transverse Z steel specimens again failed in a semi-brittle manner. That is, the net section of transverse Z steel specimens developed an average of 75% of the predicted ultimate strength, and showed a transverse cleavage type fracture, rather than the inclined shear type of fracture observed in ductile failure of all other steels.

The ductile failure of connections made of steels X, Y, and longitudinal Z, which failed in tension tearing, was accompanied by localized plastic deformations. Furthermore these low ductility steel connection specimens showed considerable plastic deformations in bearing failure of bolted connections, and in weld shear failure in fillet weld connections. These two failure modes were similar to those obtained for high ductility steels (2). Therefore the experimental observations suggest that steels X, Y, and longitudinal Z, in spite of their conventionally low ductility had sufficient ductility to prevent premature brittle fracture at elastic stress concentrations in perforated plates and in connections. The significance of the above observations will be evaluated in the section "Evaluation of Experimental and Analytical Results".

Summary of Analytical Results. - Ductility requirements should ensure that for a steel with ductilities greater than the required minimum a ductile fracture will occur when such a steel is used as a conventional structural member under static loading. To complement the experimental results and to help in establishing minimum ductility requirements, perforated and notched plates were analyzed in the elastic-plastic range utilizing a finite element computer program (13). In order to develop the full tensile strength of a member with a stress raiser, and to avoid premature brittle fracture it is necessary to achieve full plastification of a "critical" section. For example, in the case of a perforated plate (Fig. 6a), when the plastic zones initiated at the points of elastic stress concentration (A) travel to the free edge (B-B), a ductile fracture is obtained and the member is able to develop its full ultimate tension capacity. In the case of a notched plate (Fig. 6b), the plastic zones initiated at the points of elastic stress concentration (A) would have to meet at the centerline (B-B) to cause a ductile fracture.

Consequently, if the strain at "A" (Fig. 6), is less than the elongation capability of the material, just when the plastic zone initiated at "A" reaches the line B-B, then it can be said that the critical section is able to plastify. Thus, the minimum straining capacity ε_{min} which the material should possess for a ductile failure under static loading is given by:

$$\varepsilon_{min} \geq (\varepsilon_A)_{pl} \qquad (8)$$

where $(\varepsilon_A)_{p\ell}$ = the strain at the point of largest elastic stress concentration at impending complete plastification. $(\varepsilon_A)_{p\ell}$ can be obtained either experimentally or analytically. In the present study, perforated and notched plates were examined in the elastic-plastic range using an available computer program developed by Salmon et al (13). At first, the stress and strain distributions in the elastic range at the net section of a perforated plate were compared with the analytical results given by Howland (6), and in the plastic range with the experimental results of Theocaris and Marketos (16). These comparisons showed satisfactory correlation hence the finite element computer program was used to solve elasto-plastically six rectangular plates with different elastic stress concentrations. $(\varepsilon_A)_{p\ell}$ was obtained for three perforated plates, with d/s ratios of 1/2, 1/3 and 1/5, and three notched plates with flank angles of 0°, 60° and 90°, (see Fig. 6). Typical finite element idealizations for perforated plate with d/s = 1/3 is shown in Fig. 7b.

A bilinear idealized stress-strain curve of longitudinal Z steel (shown in Fig. 8) was used. The material properties of this Z steel are:

$$E = 30{,}000 \text{ ksi} \quad ; \quad E_{str} = 250.0 \text{ ksi}$$

$$\sigma_y = 70.0 \text{ ksi} \quad ; \quad \mu = 0.30.$$

The spread of the plastic enclaves for various (σ_{mean}/σ_y) ratios, calculated on the net section of the perforated plate (d/s = 1/3), is given in Fig. 7a.

The load at which the plastic zone reaches the boundary of the perforated plate or meets at the center in a notched

plate is designated as the impending complete plastification load level. The maximum strains $(\varepsilon_A)_{p\ell}$ directly at the stress raisers, for these loads are recorded in Table 3. The computed values of $(\varepsilon_A)_{p\ell}$ range from 1.1 to 2.6 percent. From the practical viewpoint of establishing minimum ductility requirements these values of minimum strains, necessary for complete plastification of the critical section, are the important findings of this study.

It was discussed earlier that ductility of a material is made up of local and uniform elongation capabilities. Local ductility is characterized by the descending branch of the stress-strain curve. Unfortunately, as postulated by Drucker (4), the classical "Theory of Plasticity" (on which the finite element program is based), cannot utilize this unstable falling branch of the stress-strain curve. Therefore, the ductility requirement (ε_{min}) cannot be correlated explicitly with the ductility parameters of the material.

Evaluation of Experimental and Analytical Results. - As noted earlier, low ductility X, Y, and longitudinal Z steel failed in a ductile manner in all tension tests. Steels X and Y (i.e. 1205Y, 1205X, and 1605X in Table 2) had very little strain hardening capacity (average $\sigma_t/\sigma_y = 1.01$), and consequently a very small amount of uniform ductility (average ε_{un} of about 0.6%). However, these steels had significant local ductility; i.e. the average elongation $\varepsilon_{1/2}$, in a 1/2 inch G.L. including fracture, was about 24%. According to the results presented in Table 3, $\varepsilon_{un} = 0.6\%$ is much lower than $(\varepsilon_A)_{p\ell} = 1.1$ to 2.6%,

the minimum ductility at the stress concentration required for complete plastification of the critical section. This suggests that in conjunction with uniform ductility of the order of 0.6%, the additional local ductility $\varepsilon_{1/2}$ of about 24% in these X and Y steels was sufficient to wipe out the effects of elastic stress concentrations, and completely plastify the critical section.

Thus, in X and Y steels, local ductility was needed in addition to uniform ductility, to avoid premature brittle fracture at stress concentrations. Unfortunately, it is difficult to quantify the required local ductility for the following reasons:

(a) Local ductility, when measured in a 1/2 inch G.L. in rectangular tension coupons, is dependent on the thickness of the material.

(b) Significant member ductility (i.e. plastification of sections other than the critical one) is obtained only if the material possesses definite strain hardening ability or uniform ductility.

(c) $(\varepsilon_A)_{p\ell}$ in Table 3 was derived according to the classical "Theory of Plasticity". However the theoretical plasticity calculations do not admit the descending unstable branch of the stress-strain curve (4), which accounts for the local ductility of the material.

For these reasons $(\varepsilon_A)_{p\ell}$ will be correlated with the uniform ductility of the material to establish minimum ductility requirements; the additionally required local ductility will be regarded as a ductility reserve. As discussed earlier, longi-

tudinal Z eteel which had a conventional elongation capability in a 2 inch G.L. of about 4.4% had fractured in a ductile manmer in all tension member tests. This steel had very low local ductility ($\varepsilon_{1/2}$ of about 10%), but had significant strain hardening capacity (average $\sigma_t/\sigma_y = 1.08$), and consequently significant uniform ductility, $\varepsilon_{un} = 2.7\%$. The finite element computer program utilized in this paper incorporated the idealized stress-strain curve of longitudinal Z steel (Fig. 8). From this computer program the required uniform ductility $\varepsilon_{un} = (\varepsilon_A)_{p\ell}$ was computed to be between 1 and 3 percent, for complete plastification of the critical section in various tension members with stress raisers (see Table 3). Therefore, from the analytical as well as experimental investigation it is concluded that a material possessing an ε_{un} of about 3 percent along with σ_t/σ_y of about 1.1, has sufficient ductility to wipe out the effects of elastic stress concentrations and completely plastify the critical section in thin rectangular plates with geometric discontinuities, or in bolted or welded connections.

On the other hand, Z steel in the transverse direction had a uniform ductility ε_{un} of only 0.5 percent and $\sigma_t/\sigma_y = 1.0$, which, by analysis, should be insufficient to fully plastify the critical section in a tension member with stress raiser. In addition transverse Z steel had $\varepsilon_{1/2} = 4\%$ which too was considerably lower than the 25% possessed by steels X and Y. In fact, in tension tests on perforated plates and some bolted connections the failure in transverse Z steel occurred in a semi-brittle manner, because the material did not have sufficient

elongation capability (neither local nor uniform) to completely plastify the critical section. In transverse Z steel tension members, the failure loads, based on complete plastification of net section, ranged from 73 to 94 percent, i.e. they were smaller than those for full plastification.

Thus, to ensure a ductile fracture of a thin-walled tension member with the usual stress concentrations, the analytical and experimental investigations indicate that the uniform ductility of a material, ε_{un}, should be greater than about 3% along with $\sigma_t/\sigma_y \geq 1.1$ and $\varepsilon_{1/2} \geq 25\%$.

CONCLUSIONS

The following conclusions arrived at in this investigation have been interpreted against the background of overall observations made on the low ductility project steels (2).

(1) In dealing with the problem of ductility measurement in a standard tension coupon it appears necessary to distinguish between (a) local ductility, and (b) uniform ductility, which when added together, give total ductility of the material.

(2) For a given material, the elongation as measured in a fixed gage length (usually 2 or 8 inches) varies with the thickness of the rectangular standard tension coupon specimen (Eq. 4). Therefore the conventional elongation in a 2 inch G.L. cannot be used as a reliable measure of ductility for comparing elongation capabilities of materials with different sheet thicknesses. Furthermore over the range of different ductility steels investigated herein, elongation in a 2 inch G.L. did not correlate satisfactorily with either the local

or the uniform ductility of the material.

(3) Localized elongation at the eventual fracture zone is designated as local ductility, and is identified in the elongation equation (Eq. 2) by the constant K. Other measures for local ductility are the reduction in area or the elongation in a small gage length across the neck. Uniform ductility is the ability of a tension coupon to undergo sizeable plastic deformations along its entire length prior to necking, and is identified by the elongation equation constant α in Eq. 2, as well as by the strain, ε_{un}, in a tension coupon excluding fracture, or by the σ_t/σ_y ratio.

(4) From an analytical investigation of plates with geometric discontinuities, and from observations on tension tests on perforated plates, and bolted and welded connections, approximate minimum ductility requirements have been established for thin tension members under a monotonically increasing static load. To redistribute the stresses in the plastic range so as to avoid premature brittle fracture, and achieve full net-section strength in a tension member with stress concentrations, it is suggested that the minimum elongation in a 1/2 inch gage length of a standard tension coupon including the neck be at least 25 percent; the minimum uniform elongation in a 3 inch gage length minus the elongation in a 1 inch length containing neck and fracture be at least 3 percent; and the σ_t/σ_y ratio be at least 1.1.

ACKNOWLEDGMENTS

This research was sponsored by the American Iron and Steel Institute. The cooperation of the cognizant research committee, and of the companies who furnished the steels for the investigation, is gratefully acknowledged. So are the contributions, in the early phases of this work, of Dr. S. J. Errera, then associate professor of structural engineering at Cornell University.

APPENDIX I. - REFERENCES

1. Anon., "Specification for the Design of Cold-Formed Steel Structural Members", American Iron and Steel Institute, New York, N.Y., 1968 Edition.

2. Dhalla, A. K., "Influence of Ductility on the Structural Behavior of Cold-Formed Steel Members", Dept. of Structural Engineering, Report No. 336, Cornell University, Ithaca, N.Y.

3. Dhalla, A. K., Errera, S. J., and Winter, G., "Connections in Thin Low-Ductility Steels", Proc. of Speciality Conference on Steel Structures, ASCE, June 8-12, 1970, pp. 119-125.

4. Drucker, D. C., "A More Fundamental Approach to Plastic Stress-Strain Relations", Proc. of the first U.S. National Congress of Applied Mechanics, ASME, 1951, pp. 487-491.

5. Gerrard, G., "Structural Significance of Ductility", Journal of Metals, March 1961.

6. Howland, R. C. J., "On the Stresses in the Neighbourhood of a Circular Hole in a Strip Under Tension", Phil. Trans. Roy. Soc., A, Vol. 229, 1930, pp 48-86.

7. Hoyt, S. L., "Notched Bar Testing and Impact Testing", Symposium on Impact Testing, Proc. ASTM, Vol. 38, Part II, 1938.

8. Körber, F. and Krisch, A., "Festigkeitsprüfung bei ruhender Beanspruchung", pp 73 and 81-88, Chapter I, Vol. II of "Handbuch der Werkstoffprüfung" Edited by Siebel, E., Springer-Verlag, 1955.

9. MacGregor, C. W., "The Tension Test", Symposium on Significance of the Tension Test, Proc. ASTM, Vol. 40, 1940, pp. 508-534.

10. MacGregor, C. W., "Relations Between Stress and Reduction in Area for Tensile Tests of Metals", Tech. Publ. 805, Am. Inst. of Mining and Mat. Engs., 1937, pp 208-228.

11. Oliver, D. A., "Proposed New Criteria of Ductility From a New Law Connecting the Percentage Elongation with Size of Test Piece", Inst. of Mech. Engineers, Vol. II, 1928.

12. Parker, E. R., Davis, H. E., and Flanigan, A. E., "A Study of the Tension Test", Proc. ASTM, Vol. 46, 1946.

13. Salmon, M., Berke, L., and Sandhu, R., "An Application of the Finite Element Method to Elastic Plastic Problems of Plane Stress", Tech. Rept. AFFDL-TR-68-39, May 1970.

14. Schuster, L. W., "The Bend Test and its Value as a Guide to Ductility", Engineering, April 5, 1935, pp 372 and 400.

15. Stowell, E. Z., "Stress and Strain Concentration at a Circular Hole in an Infinite Plate", NACA T.N. 2073, 1950.

16. Theocaris, P. S. and Marketos, E., "Elastic Plastic Analysis of Perforated Thin Strips of Strain Hardening Material", Jn. of the Mech. and Phy. of Solids, Vol. 12, 1964, pp 377-390.

17. Unwin, W. C., "Tensile Tests of Mild Steel, and the Relation of Elongation to the Size of the Test Bar", Proc. Inst. of Civil Engineers, 1903.

APPENDIX II. - NOTATION

The following symbols are used in this paper:

A = Gross cross-sectional area of coupon or tension member.

A_{net} = Net cross-sectional area of a tension member or connection.

b = Constant used in Eq. 1.

c = Constant used in Eq. 1.

d = Diameter of hole in a perforated plate.

K = Elongation equation constant which indicates local ductility of the material.

L = Gage length of standard tension coupon.

P_{ult} = Ultimate load.

s = Width of plate.

t = Thickness of a coupon specimen or a tension member

α = Elongation equation constant which indicates strain hardening capacity of the material.

ε_L = Elongation in gage length L in standard tension coupon test.

$(\varepsilon_A)_{p\ell}$ = The strain at the point of largest elastic stress-concentration at impending complete plastification.

ε_{un} = Uniform elongation in a tension coupon excluding 1/2 inch of the central fractured portion.

ε_{min} = Minimum straining capacity the material should possess for a ductile failure of tension members with stress concentrations under static loading.

σ_t = Ultimate tensile strength of the material.

σ_{tt} = Average tensile stress at P_{ult} calculated on the net area, A_{net}, of the tension member.

σ_y = 0.2% offset tensile yield strength of the material.

TABLE 1

AVERAGE MECHANICAL PROPERTIES OF STEELS X, Y AND Z, AS OBTAINED FROM STANDARD TENSION COUPON TESTS

Average Values of Various Steels	Thickness t (in)	0.2% Offset Yield Strength σ_y (ksi)	Tensile Strength σ_t (ksi)	Tensile Yield Ratio σ_t/σ_y	Elongation in a 2" G.L. ε_2 (%)	Reduction in Area (%)	Reduction in Thickness (%)
2004Z-L-AV1	0.039	75.5	81.7	1.08	4.38	56.1	55.8
2004Z-T-AV1	0.039	99.4	99.8	1.00	1.34	37.3	-
1205Y-L-AV2	0.106	78.3	79.2	1.01	5.20	65.2	61.0
1205X-L-AV1	0.106	72.2	72.2	1.00	6.00	71.4	67.6
1605X-1-AV1	0.062	88.7	88.9	1.00	5.30	60.9	57.4
1225X-L-AV1	0.108	36.6	50.0	1.37	36.50	79.2	70.2
1625X-L-AV1	0.065	38.5	49.1	1.28	39.20	81.9	74.0
16FAX-L-AV1	0.064	29.9	45.4	1.51	49.8	84.4	72.7

TABLE 2

COMPARISON OF DUCTILITY PARAMETERS*

Ductility Parameters	Low Ductility					Medium Ductility		High Ductility
	Z Steel 2004Z-L-AV1	Z Steel 2004Z-T-AV1	Y Steel 1205Y-L-AV2	X Steel 1205X-L-AV1	X Steel 1605X-L-AV1	X Steel 1225X-L-AV1	X Steel 1625X-L-AV1	X Steel 16FAX-L-AV1
Elongation in a 2" G.L.(incl. neck),(%)	4.4	1.3	5.2	6.0	5.3	36.5	39.1	49.8
Reduction in Area,(%)...	56.1	37.3	65.2	71.4	60.9	70.1	74.0	84.4
K, (%)...	22.0	10.0	44.0	50.0	39.0	80.0	88.0	114.0
Elongation in a ½" G.L.(incl.neck),(%)	9.9	4.2	20.5	23.6	17.0	60.0	59.9	78.1
Tensile-Yield Strength Ratio ...	1.08	1.00	1.01	1.00	1.00	1.37	1.28	1.51
Elongation in a 2½" G.L.(excl.neck),(%)	2.7	0.5	0.2	0.4	1.1	26.5	30.6	36.1
α , ...	-0.60	-0.78	-0.98	-0.97	-0.82	-0.36	-0.34	-0.32

* The values reported in this Table are the average values for different sheets of the corresponding steel reported in Table 1.

TABLE 3

MAXIMUM STRAIN $(\varepsilon_A)_{p\ell}$ AT THE POINT OF ELASTIC STRESS CONCENTRATION AT IMPENDING COMPLETE PLASTIFICATION IN PERFORATED AND NOTCHED PLATES

Rectangular Plate	Elastic Stress Concentration Factor		$(\varepsilon_A)_{p\ell}$ (%)
	K_{appl}*	K_{net}**	
Perforated Plates			
$\frac{d}{s} = \frac{1}{5}$	2.68	2.14	1.16
$\frac{d}{s} = \frac{1}{3}$	3.09	2.06	1.07
$\frac{d}{s} = \frac{1}{2}$	3.99	1.99	1.21
Notched Plates			
Flank Angle=90°	3.75	2.03	1.11
Flank Angle=60°	4.58	2.68	2.58
Flank Angle=0°	5.93	2.96	2.34

* K_{appl} based on applied stress = $(\frac{\sigma_{max}}{\sigma_{appl}})$

** K_{net} based on net section mean stress = $(\frac{\sigma_{max}}{\sigma_{mean}})$

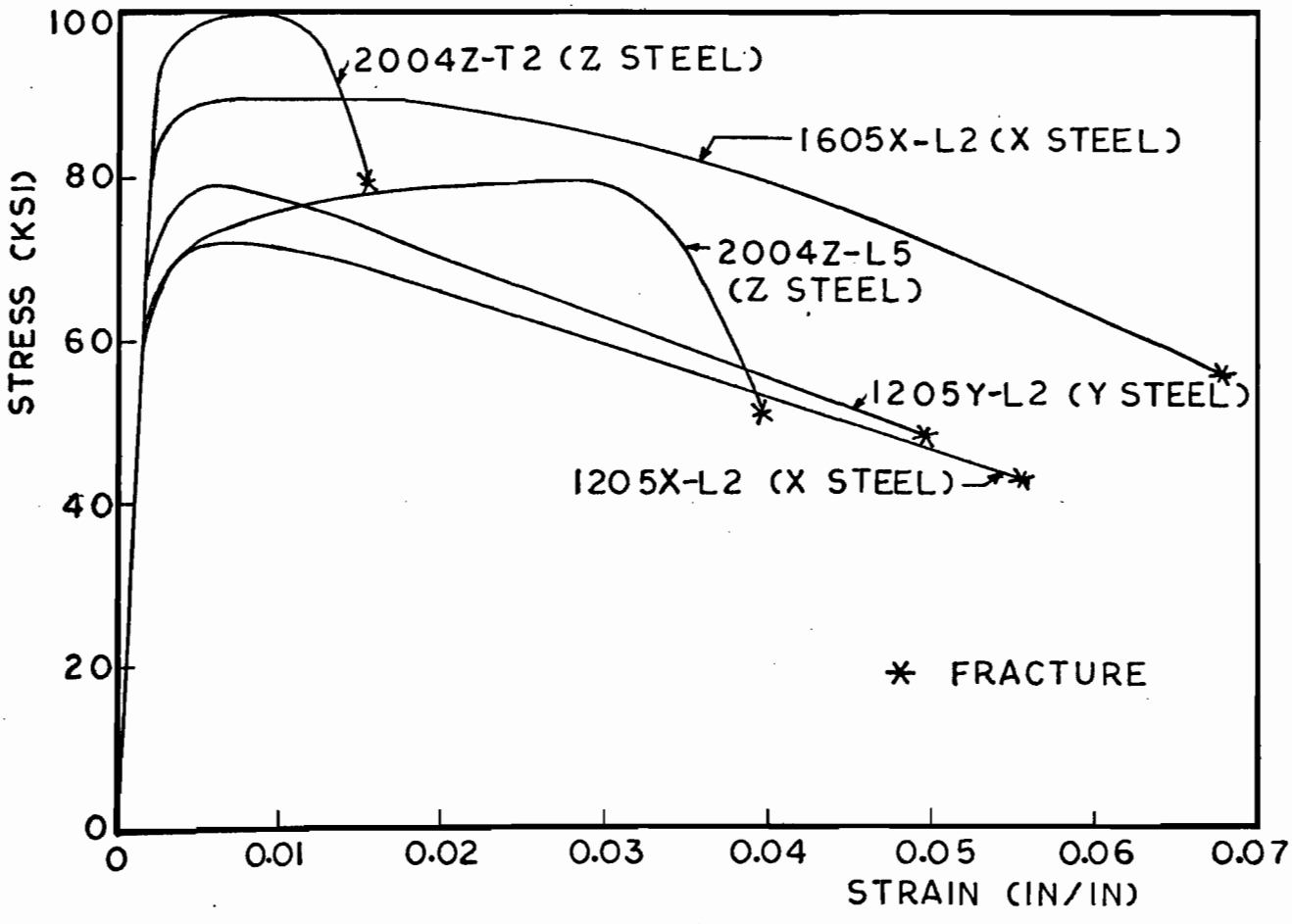

FIG. 1. COMPLETE STRESS STRAIN CURVES OF X, Y AND Z STEELS (2" G.L.)

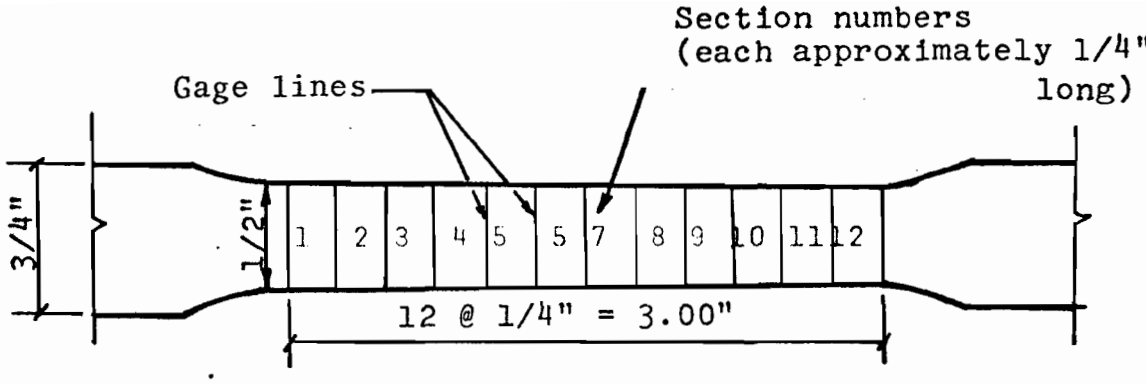

Fig. 2a. Sketch of a standard tension coupon.

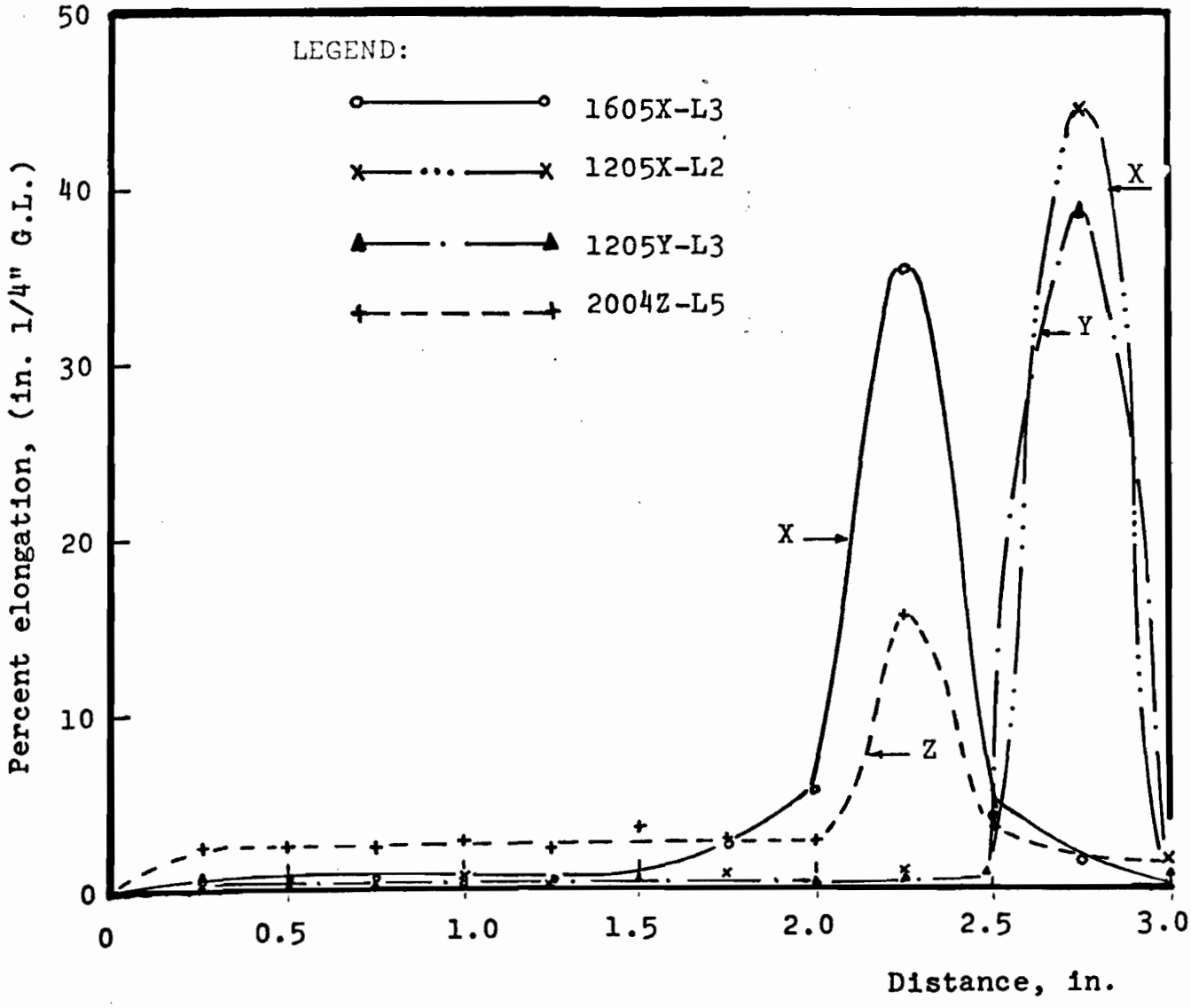

Fig. 2b. Distribution of longitudinal strain in tension coupon, (after fracture).

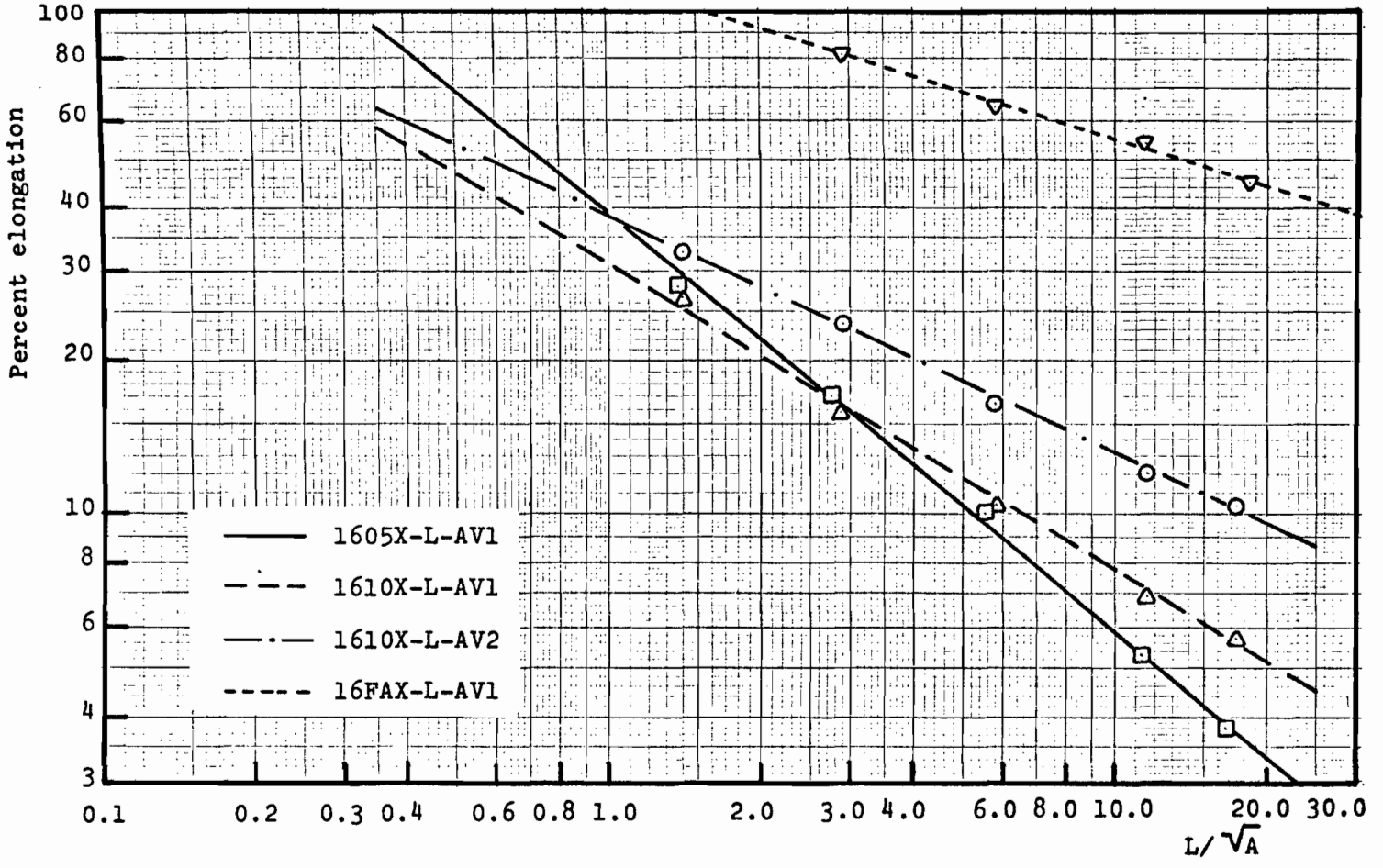

Fig. 3. Elongation - L/ $\sqrt{A}$ curves for 16 gage X steel.

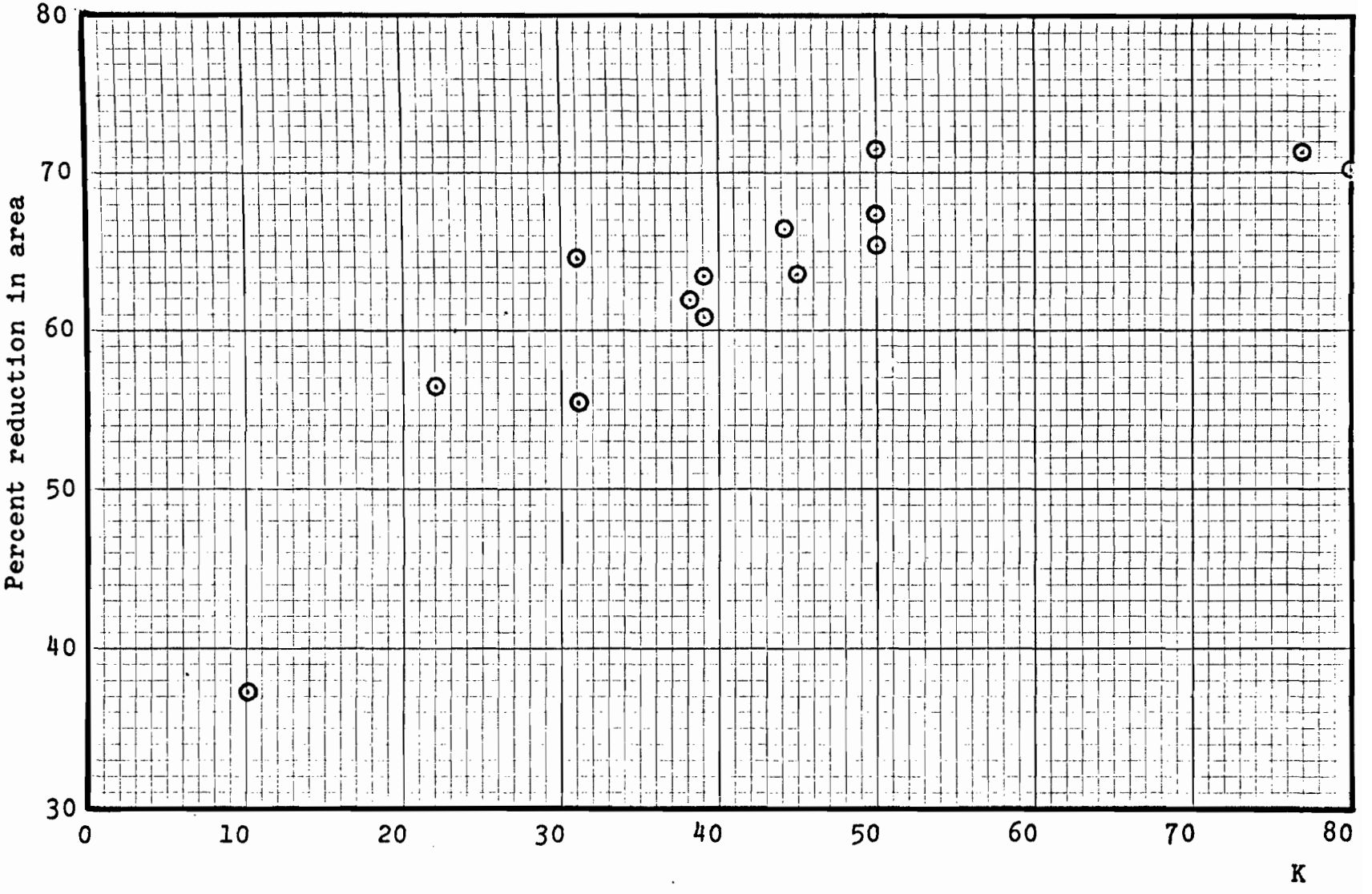

Fig. 4. Percent reduction in area plotted against elongation equation parameter K.

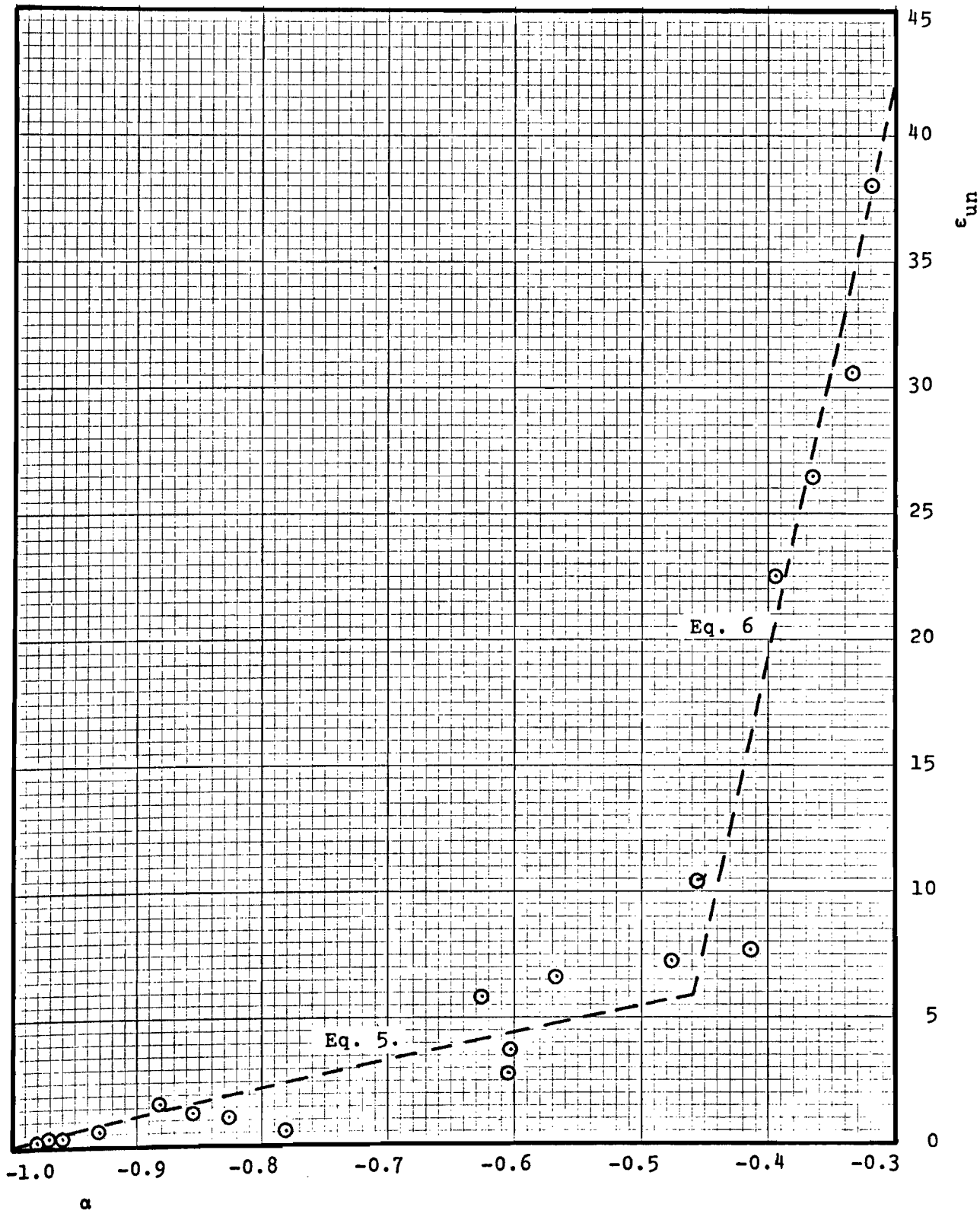

Fig. 5. Relationship between uniform strain ε_{un}, and α for steels X, Y and Z.

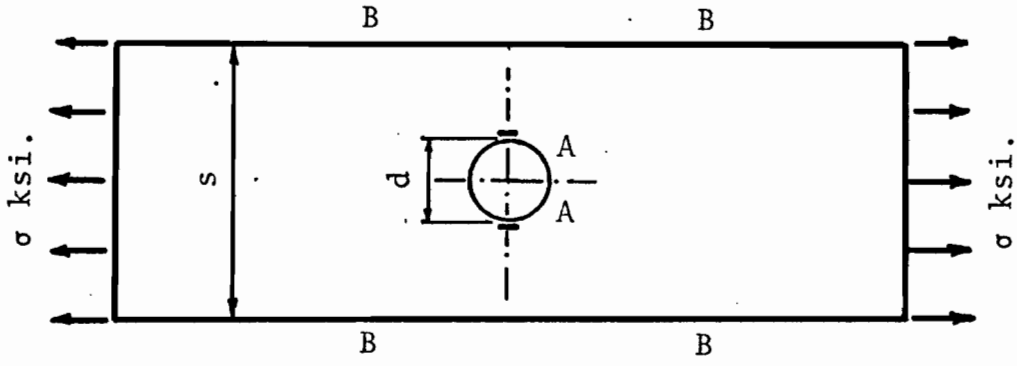

(a) Perforated Plate

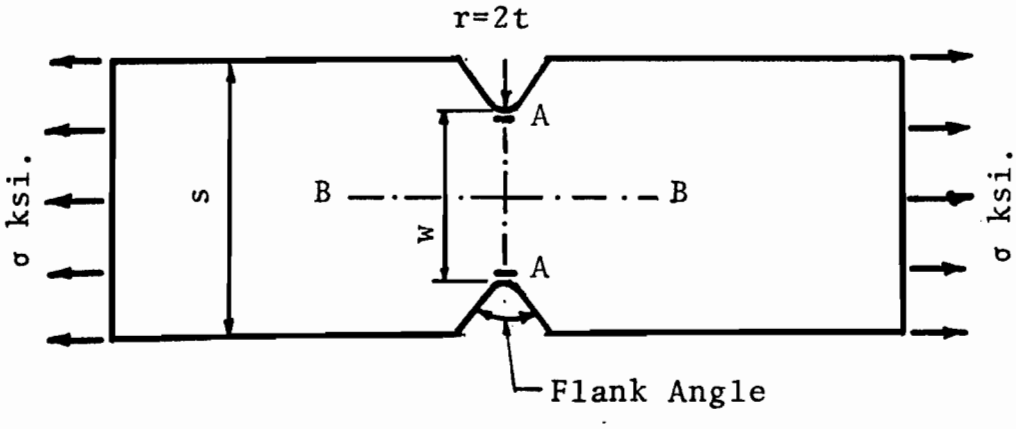

(b) Notched Plate

Fig. 6. Tension Members with Elastic Stress Concentrations at A.

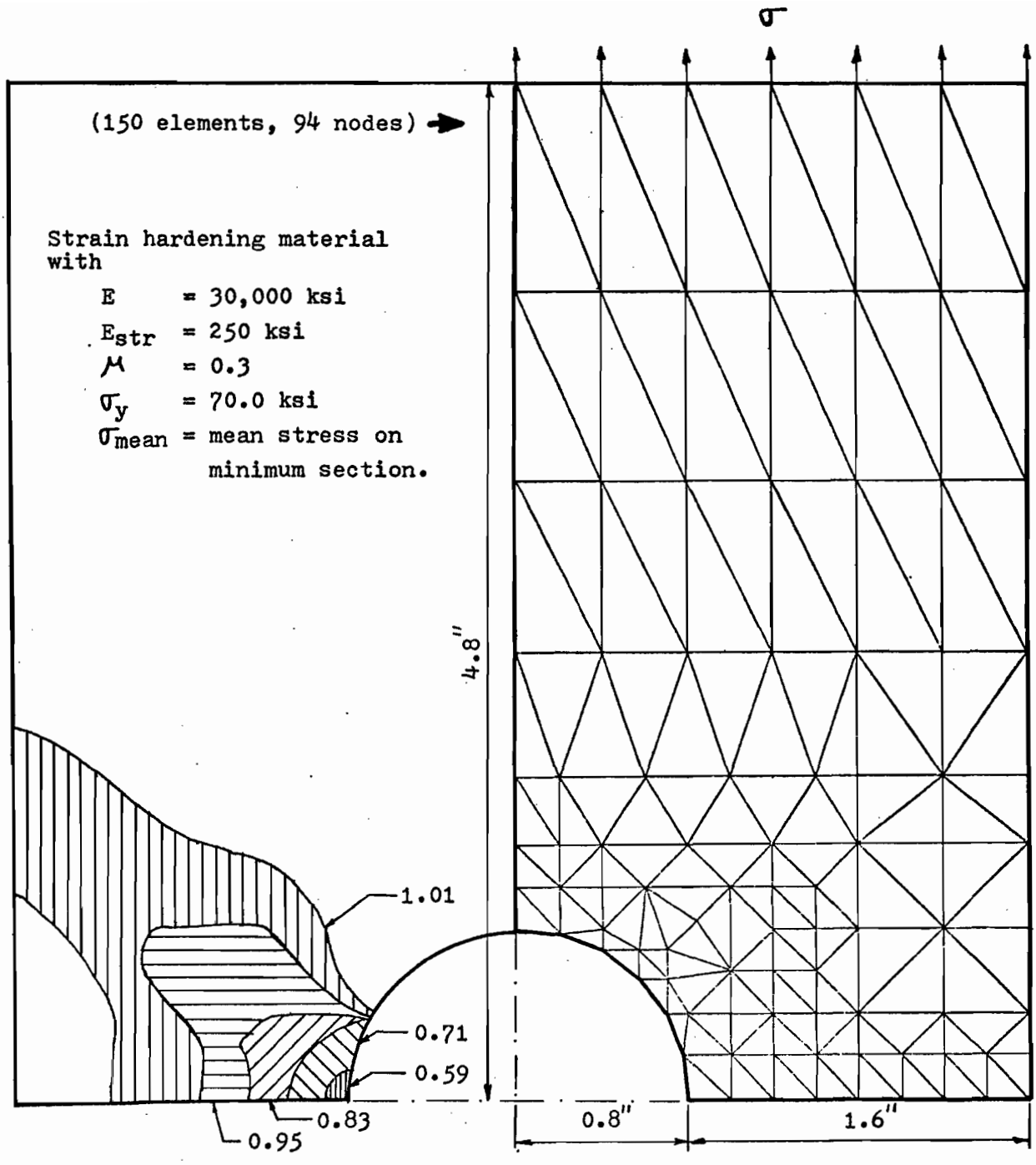

(a) Spread of plastic zones for various ratios of σ_{mean}/σ_y.

(b) Finite element idealization.

Fig. 7. Perforated tension strip (d/s = 0.33), plane stress.

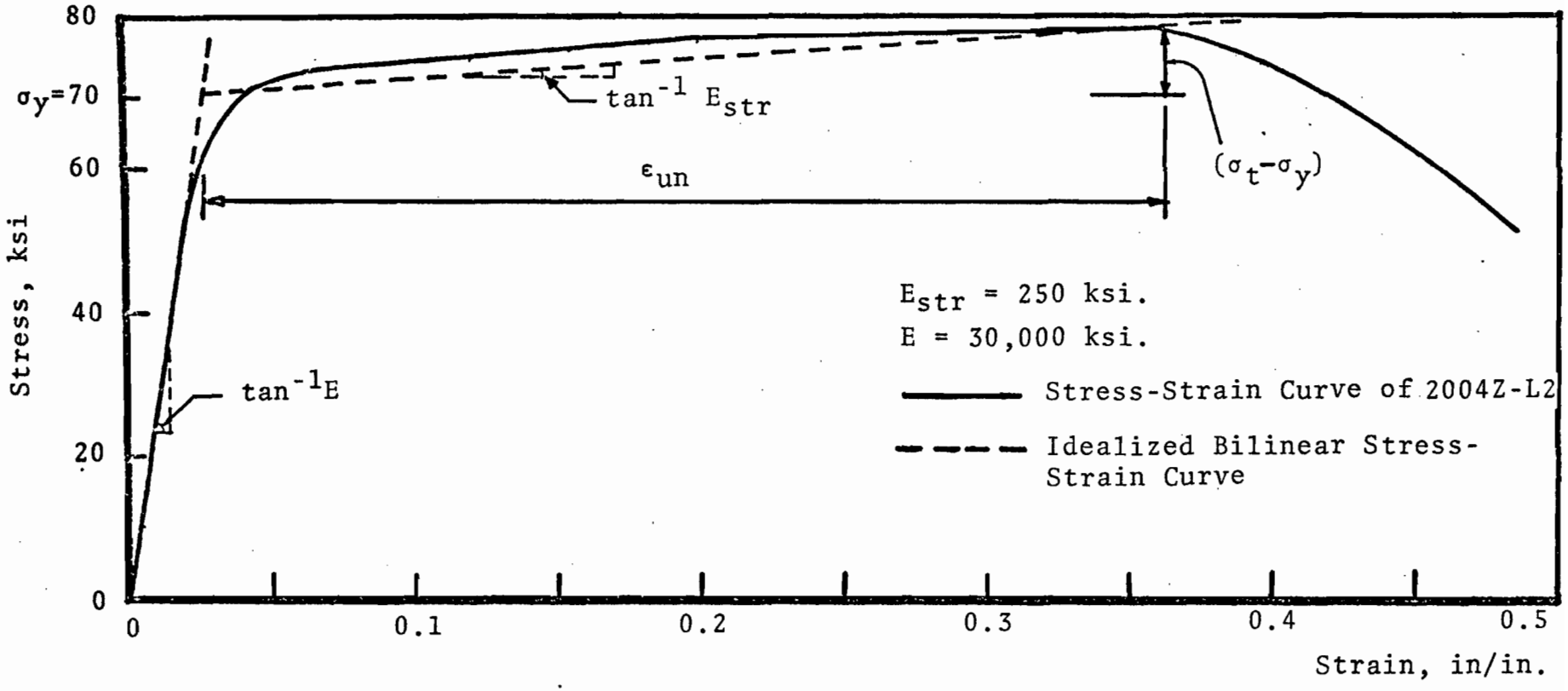

Fig. 8. Idealized Stress-Strain Curve of Z Steel (2" Gage Length)

SUMMARY

Low ductility high strength steels have been investigated to determine the influence of ductility on the behavior of cold-formed members with stress concentrations under static loading. A modified tension coupon test is used to measure the local and uniform elongation capabilities of the material. Based on experimental and analytical investigation of members with stress concentrations minimum ductility requirements are suggested.